

Chemical and Biochemical Physics, Kinetics and Thermodynamics

New Perspectives

Contributors

M. Akbari	Yu. G. Medvedevskikh
A. V. Alessenko	A. K. Mikitaev
A. Farjad Bastani	M. A. Mikitaev
L. I. Bazylyak	K. Mohammadi
A. Y. Bedanokov	E. M. Molochkina
V. A. Borisov	L. A. Mosolova
E. B. Burlakova	G. A. Nikiforov
L. A. Chernozatonskii	P. H. Pardo
E. Ya. Davydov	G. B. Pariiskii
E. Efremenko	T. V. Pokholok
I. S. Gaponova	A. A. Popov
F. Greulich	Pavel G. Pronkin
D. Gudkov	F. Raeesi
H. Haftchenary	A. Sadrumontazi
A. K. Haghi	P. B. Sorokin
I. Lyagin	O. N. Sorokina
A. L. Kovarski	Alexander S. Tatikolov
B. E. Krisyuk	V. Verkhusha
Vladimir A. Kuzmin	G. E. Zaikov
L. I. Matienko	M. Ziabari

Paul E. Stott ■ G. E. Zaikov
Viktor F. Kablov

Editors

NOVA

CHEMICAL AND BIOCHEMICAL PHYSICS, KINETICS AND THERMODYNAMICS: NEW PERSPECTIVES

No part of this digital document may be reproduced, stored in a retrieval system or transmitted in any form or by any means. The publisher has taken reasonable care in the preparation of this digital document, but makes no expressed or implied warranty of any kind and assumes no responsibility for any errors or omissions. No liability is assumed for incidental or consequential damages in connection with or arising out of information contained herein. This digital document is sold with the clear understanding that the publisher is not engaged in rendering legal, medical or any other professional services.

**CHEMICAL AND BIOCHEMICAL
PHYSICS, KINETICS AND
THERMODYNAMICS:
NEW PERSPECTIVES**

**PAUL E. STOTT
G. E. ZAIKOV
AND
VIKTOR F. KABLOV
EDITORS**

Nova Science Publishers, Inc.
New York

Copyright © 2007 by Nova Science Publishers, Inc.

All rights reserved. No part of this book may be reproduced, stored in a retrieval system or transmitted in any form or by any means: electronic, electrostatic, magnetic, tape, mechanical photocopying, recording or otherwise without the written permission of the Publisher.

For permission to use material from this book please contact us:
Telephone 631-231-7269; Fax 631-231-8175
Web Site: <http://www.novapublishers.com>

NOTICE TO THE READER

The Publisher has taken reasonable care in the preparation of this book, but makes no expressed or implied warranty of any kind and assumes no responsibility for any errors or omissions. No liability is assumed for incidental or consequential damages in connection with or arising out of information contained in this book. The Publisher shall not be liable for any special, consequential, or exemplary damages resulting, in whole or in part, from the readers' use of, or reliance upon, this material.

Independent verification should be sought for any data, advice or recommendations contained in this book. In addition, no responsibility is assumed by the publisher for any injury and/or damage to persons or property arising from any methods, products, instructions, ideas or otherwise contained in this publication.

This publication is designed to provide accurate and authoritative information with regard to the subject matter covered herein. It is sold with the clear understanding that the Publisher is not engaged in rendering legal or any other professional services. If legal or any other expert assistance is required, the services of a competent person should be sought. FROM A DECLARATION OF PARTICIPANTS JOINTLY ADOPTED BY A COMMITTEE OF THE AMERICAN BAR ASSOCIATION AND A COMMITTEE OF PUBLISHERS.

LIBRARY OF CONGRESS CATALOGING-IN-PUBLICATION DATA

Chemical and biochemical physics, kinetics, and thermodynamics : new perspectives / Paul Edwin Stott, Gennady Efremovich Zaikov and Viktor Fedorovich Kablov (editors).

p. cm.

ISBN 978-1-60692-528-7

1. Chemical kinetics. 2. Chemical reactions. 3. Thermochemistry. 4. Antioxidants. 5. Nanotubes. I. Stott, Paul Edwin II. Zaikov, Gennady Efremovich III. Kablov, Viktor Fedorovich. QD502.C466 2008

541'.394--dc22

2007036465

Published by Nova Science Publishers, Inc. ✦ New York

CONTENTS

Preface		vii
Chapter 1	Hybrid Antioxidants <i>E. B. Burlakova, E. M. Molochkina and G. A. Nikiforov</i>	1
Chapter 2	Oxidative Radical Generation via Nitrogen Dioxide Dimer Conversions Induced by Amide Groups of Macromolecules <i>E. Ya. Davydov, I. S. Gaponova, T. V. Pokholok, G. B. Pariiskii and G. E. Zaikov</i>	19
Chapter 3	Addition of Ozone to Multiple Bonds: Competition of the Reaction Pathways <i>B. E. Krisyuk and A. A. Popov</i>	31
Chapter 4	Peculiarities of Electron Magnetic Resonance Spectra of the Linear Aggregates of Ferromagnetic Nanoparticles <i>O. N. Sorokina and A. L. Kovarski</i>	49
Chapter 5	Theoretical Investigation of Structure of Boron Carbonitride Nanotubes <i>P. B. Sorokin, P. H. Pardo and L. A. Chernozatonskii</i>	57
Chapter 6	Effect of Steric Factor on the Triplet State Quenching of Meso-Substituted Thiocarbocyanine Dyes in Complexes with DNA <i>Pavel G. Pronkin, Alexander S. Tatikolov and Vladimir A. Kuzmin</i>	65
Chapter 7	Heme Oxygenase Activity in Rat Liver Depending on Action of CoCl ₂ , ANIT and Tween <i>F. Greulich and A. V. Alessenko</i>	75
Chapter 8	Genetic Construct Encoding the Biosynthesis of N-His ₆ -e-pHluorin _s -OPH in E.Coli Cells <i>I. Lyagin, D. Gudkov, V. Verkhusha and E. Efremenko</i>	83

Chapter 9	Microwave Heat Treatment of Textiles and a Review on Mathematical Model of Drying <i>A. K. Haghi</i>	91
Chapter 10	Electrospun Nanofibers: A Fiber Digest for Beginners <i>A. K. Haghi and M. Akbari</i>	111
Chapter 11	Experimental Study on Application of Waste Rubber in Bitumen Composite <i>A. K. Haghi</i>	147
Chapter 12	Thermodynamics of Osmotic Pressure of Polymeric Solutions <i>Yu. G. Medvedevskikh, L. I. Bazilyak and G. E. Zaikov</i>	157
Chapter 13	Experimental Survey on a Polymeric Stabilizer Material <i>A. K. Haghi</i>	169
Chapter 14	Polymers in Electronic Devices: New Trends and Achievements <i>M. Ziabari, F. Raeesi and A. K. Haghi</i>	179
Chapter 15	Selective Ethylbenzene Oxidation into α -Phenylethylhydroperoxide with Dioxygen in the Presence of Triple Catalytic Systems Including Bis (Acetylacetonate) Ni(II) and Additives of Electron-Donor Compound L^2 and Phenol as Exo Ligands <i>L. I. Matienko and L. A. Mosolova</i>	195
Chapter 16	Application of Polypropylene Fiber and Recycled Glass in Component of Cement-Based Composite <i>A. Sadrmomtazi and A. K. Haghi</i>	205
Chapter 17	A New Approach for Prediction of Failure in Unidirectional Glass/Epoxy Composites <i>A. Farjad Bastani, H. Haftchenary, K. Mohammadi and A. K. Haghi</i>	221
Chapter 18	Properties of Polymer Nanocomposites Based on Organomodified Na^+ -Montmorillonite <i>A. Y. Bedanokov, A. K. Mikitaev, V. A. Borisov and M. A. Mikitaev</i>	235
Index		243

PREFACE

"I like work; it fascinates me.
I can sit and look at it for hours
when somebody is working"
Jerome K. Jerome

"If you are eaten, it means that
somebody needed you".
Emperor Bokassa I
Central African Empire,
Cavaliere of Honorary Legionary Order of France

We hope that these epigraphs do not relate to the editors and the authors of this volume; our aim is only to attract attention and arouse the interest of the reader for the book.

Czar Peter I (the Great) of Russia issued a decree on January 31, 1696, according to which children of nobles could not marry unless they got an adequate education. There is a lot of sense in this. Knowledge is an absolute necessity for all people. We believe that this book is a brick laid in the World Science Building.

You know, "jurists hide their mistakes in jails; physicians, in graves." Chemists are in a privileged position. Our mistakes inflict no great damages to humans (except for those to the Environment).

Once, U.S. President Warren G. Harding lost at cards a Chinese porcelain set owned by the White House in Washington, DC. We hope that our book will cause no similar loss to either the USA or to Russia.

This book is a collection of articles on polymers in electronic devices, experimental surveys on stabilized polymer materials, the application of waste rubber in bitumen composites, nanofibers, the interaction between nitrogen oxides and organic compounds, textile materials, selective oxidation processes, peculiarities of electron magnetic resonance spectra of the linear aggregates of ferromagnetic nanoparticles, a theoretical investigation of the structure of boron carbonitride nanotubes, heme oxygenase activity in rat liver depending on the action of different components, the effect of the steric factor on the triplet state quenching of meso-substituted thiocarbocyanine dyes in complexes with DNA, the genetic construct encoding biosynthesis in cells, the effect of super low doses on biological activity, the interaction between ozone and organic compounds, hybrid antioxidants, etc.

It is well known that the Emperor Diocletian of the Ancient Rome resigned from power of his own free will, quit for the countryside and was happy to grow cabbage. We believe that it is too early for us (the editors and the authors) to grow cabbage and we will work for the good of science.

We would like to know the opinion of the readers about this.

Dr. Paul Edwin Stott
Chemtura Corp., Middlebury, CT, USA

Prof. Gennady Efremovich Zaikov
Institute of Biochemical Physics,
Russian Academy of Sciences,
Moscow, Russia

Prof. Viktor Fedorovich Kablov
Volzhsky Polytechnical Institute
(Branch of Volgograd State University)
Volzsky, Volgograd region, Russia

Chapter 1

HYBRID ANTIOXIDANTS

E. B. Burlakova, E. M. Molochkina and G. A. Nikiforov

Emanuel Institute of Biochemical Physics,
Russian Academy of Sciences, Moscow, Russia

PREFACE

In 1954, the book by Professor B.N. Tarusov "Principles of Biological Effects of Radioactive Emissions" was published [1]; the book made a great impression on me. The author, an outstanding Soviet biophysicist, Head of the Biophysics Department at the Faculty of Biology of the Moscow State University, put forward a hypothesis that the development of radiation-induced disease is associated with the induction of ramified chain reaction of oxidation of fats of cellular shells (membranes), the oxidation products are very toxic for the cell.

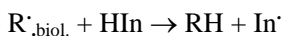
I had dreamed of studying the mechanism of radiation-induced disease but nobody at the Faculty of Chemistry dealt with these subjects then. Now two areas of my scientific interests have converged – chain reactions that had always been the main subject of investigation at the Chemical Kinetics Department of the Faculty of Chemistry (headed by N.N. Semenov, Nobel Prize Laureate) at the Moscow State University, where I wrote my diploma work, and radiation-induced disease, that was of interest at the Biophysics Department. I was permitted to write my diploma work on biology under the guidance of Academician N.M. Emanuel and Professors B.G. Dzantiev and G.B. Sergeev. The aim of my work was to find out what biologically toxic products are formed upon irradiation of lipids. A model substrate chosen for radiolytic oxidation of fat was natural cod-liver oil. The oil was exposed to radiation, its composition was investigated, and then the oil was oxidized. The investigation results showed that even after high-dose exposures no detectable quantities of specifically new products are formed and the toxicity of the exposed oil depended only on a degree of oxidation. The higher the oxidation degree, the more the deep-oxidation products (aldehydes, ketones, peracids, etc.) and the higher the oil toxicity. At equal oxidation degrees, the toxicity of exposed and unexposed oil was equal [2-4]. The main irradiation effect was reduced to decomposition of natural antioxidants in oil. Generally speaking, this result (a decrease in the quantity of

antioxidants upon exposure) was not unexpected: the effect had been determined previously in in vitro experiments with irradiation of various fats.

However, this result interested us in view of its significance with respect to radiation-involved reactions. A simultaneous investigation of toxic effects of irradiation on plant and animal fats made it possible to conclude that toxicity of irradiated fat is not associated with the formation of new products of oxidation but rather with acceleration of oxidation of exposed fat because of decomposition of natural antioxidants in fat. Hence, an unambiguous practical conclusion was drawn: if animals could be administered with antioxidants before exposure, we could slow down processes associated with acceleration of oxidation of lipids and formation of oxidized toxic products. Therefore, we should introduce compounds that could fulfill functions of antioxidants decomposed upon exposure. We started with introduction of natural antioxidant – tocopherol and found out that we can increase the average life-span of irradiated animals. Then, by analogy with works on preventing fats from oxidative decay, we introduced nontoxic synthetic antioxidants used in the food industry [4]. This decision was important not only because we were the first who introduced antioxidants to animals to protect them from irradiation (although that was a new word in radiobiology), but also because *synthetic* antioxidants were introduced to animals. Previously, we were sure that irrespective of a particular structure of an antioxidant (synthetic or natural), its main characteristic was its ability to react with free radicals. Therefore, we believed that this ability that we had shown in model experiments can persist and manifest itself after introduction of an oxidant into lipids of animal organs. These experiments confirmed, to some extent, the Tarusov's concept about the great role of chain (free-radical) reactions in lipids of exposed animals in the development of radiation-induced damages. (*E.B. Burlakova*)

In 1960, N.M. Emanuel put forward the hypothesis that not only radicals of lipids but also radicals from other biochemical components of cell (DNA, protein, polysaccharides, etc.) that are alien to normal cell and are formed upon exposure may cause multiple damages and death of the cell [5].

It was shown that radicals formed upon exposures of DNA and proteins may, like lipid radicals, enter into exchange reactions with antioxidants; as a result, the free valence passes from biopolymer radical to the antioxidant molecule and forms inactive radical from the antioxidant [InH] [6-8].



In 1961, a supposition was made about the great role of free radicals alien to normal cell in the development of some other diseases and about the feasibility of inhibiting the free-radical reactions by applying synthetic inhibitors to achieve a curing effect [9-11]. This supposition could be made only by physicochemists, first of all, by specialists in kinetics of the Semenov–Emanuel school, who understood the importance of not only (and not so much) of a change in the composition of the reaction components but also of their physicochemical properties, i.e., when the same results may be obtained with different (in composition) components but with the one common physicochemical property – in this case, ability to react with free radicals. Therefore, synthetic compounds of the structure other than that of natural antioxidants may be used instead of (substitute) the latter ones in reactions with free radicals.

In the 1960s, the Emanuel Institute of Biochemical Physics, Russian Academy of Sciences, initiated studies in the new field – chemistry and biology of antioxidants. The scientists of the Institute had to solve an important task – to find out whether the biological activity of antioxidants as inhibitors of radical reactions depends on their properties. For this purpose, nontoxic different-structure antioxidants were synthesized: derivatives of hindered phenols and heterocyclic hydrocarbon hydroxy compounds [12, 13]. The existence of homologous arrays of antioxidant derivatives made it possible to determine the structure–activity dependence and select the most efficient and least toxic compounds.

In *in vivo* experiments, the correlation between the radioprotecting activity and antiradical properties of synthetic antioxidants was determined [14, 15]. Kinetic studies on *natural* antioxidants – vitamins were carried out; their constants as inhibitors of radical processes were determined [16, 17]. In the works by Khrapova et al., the chemiluminescence method adapted to studies on bioantioxidants in lipids was used; with this method, the problems of synergism and antagonism of synthetic and natural antioxidants were studied and the antioxidant system in membrane lipids was characterized as a whole [18].

The above works were concerned mainly with investigating antioxidants in lipid components of cells. However, specially developed photochemiluminescence models were used to assess the antiradical activity of water-soluble natural and synthetic inhibitors; exchange reactions of this type of antioxidants with UV-induced peptide radicals were studied [19-20]. Great attention was given to extending research concerning the role of bioantioxidants in the development of some or other diseases and the feasibility of using antioxidants for prophylactic or curing purposes.

It is necessary to dwell on an important property of antioxidants – the dose–effect dependence of introduced antioxidant. After introduction of antioxidant, the antioxidant activity (AOA) increases, then it returns to normal, and then, after a short-time AOA increasing, it decreases drastically below the normal. Therefore, antioxidants may produce a curing effect by decreasing (at low doses) or increasing (at high doses) the rate of free-radical reactions.

The changes in the antioxidant activity of organs and tissues lipids in the process of carcinogenesis were studied in [21]. The staged mechanism of changes in the antioxidant activity in the process of carcinogenesis caused by different carcinogens: benzopyrene, orthoaminoazotoluene, and γ -irradiation was established. At the initial stage of the carcinogen toxic effect and induction of tumor cells, AOA decreases, then it increases, reaches the normal, and then increases above the normal at the stage of transition from diffusional to localized hyperplasia. The efficiency of synthetic antioxidants depends on their concentration and time of introduction [22]. At the first stage of carcinogenesis, the protective effect is caused by doses that increase AOA; at the late stages, these doses may accelerate the development of carcinogenesis and increase the number of tumors induced. At the late stages, it is necessary to introduce larger antioxidant quantities, which can cause an opposite effect – to decrease AOA [23, 24] and inhibit the process of carcinogenesis.

N.M. Emanuel and O.S. Frankfurt were the first who discovered the anticancer effect of the antioxidant dibutylxytoluene [25].

A great number of works were devoted to studying free-radical processes associated with the tumor growth and the antitumor effects of antioxidants [26-28]. It was found out that tumor growth is associated, as a rule, with an increased level of antioxidants and only high doses of antioxidants produce the antitumor effect. In this case, antioxidants do not increase

the AOA of organs and tissues but, on the contrary, decrease it and act as prooxidants. It should be noted that there is a general trend not only for antioxidants but also for various antitumor agents: their efficiency is the higher, the stronger they decrease AOA [29].

Many specialists at IBCP RAS studied antioxidants with respect to radiation-induced disease. The radioprotective effect of the compounds was in conformity with their AOA [15]. Similar data were obtained not only in experiments in animals but also in model experiments with exposed solutions of DNA, proteins, and lipids [30-32].

A novel field of science was commenced in the 1970s – applications of antioxidants in gerontology. Kinetic studies on model reactions of aging, investigation of age-related changes in antioxidants, theoretical concepts of aging, particular experimental studies of antioxidants as geroprotectors showed that this science field is of both theoretical and practical importance [33-37]. It is very strange that the idea of using antioxidants in gerontology is now put forward as a new one and the authorship is ascribed to people other than those who have been working in this field for 40 years already.

Along with studies on using antioxidants for some particular diseases, extensive studies on the role of antioxidants in normal physiological processes were commenced. Palmina et al., studied the role of antioxidants in cell proliferation and showed that the factors that increase the antioxidant activity accelerate the proliferation; those that decrease it, inhibit [38-40].

Alesenko et al., studied the effect of antioxidants on the genetic apparatus activity [41-43]. The authors showed that bioantioxidants are able to affect the cell lipids composition and change the activity of lipid-dependent enzymes of synthesis and reparation of DNA and affect the activity of chromatin.

The end of 1970s was marked by extensive studies on the role of antioxidants in the normal metabolism of cell. There was drawn the conclusion that AO are universal modifiers of composition, structure, and functional activity of membranes and that many of their effects on cell metabolism may be interpreted from these positions [44, 45]. There was discovered the physicochemical system of regulation of cell metabolism by membranes based on interrelation between membranes lipid peroxidation (LPO), on the one hand, and changes in the composition of membrane lipids and their oxidizability, on the other hand [46, 47].

Proceeding from the parameters of this system, it is possible to use antioxidant to convert a cell, organ, and organism from one metabolic state to another.

In 1970s, antioxidants found wide use in cardiology, oncology, and treatment of neurodegenerative and other classes of diseases [48-50]. Extensive studies on antioxidants were commenced in the field of plant growing and farming as plant growth stimulators and for preventive and curing treatment of cattle and poultry [51-55].

The main conclusions made in the works by Russian scientists in 1970s are as follows:

- (1) Non-toxic inhibitors of radical processes – antioxidants exhibit a wide gamut of biological activity.
- (2) The biological effectiveness of antioxidants correlates with their antioxidantizing properties.
- (3) Depending on dose, antioxidants may either increase (at low doses) the antioxidantizing activity or decrease it .
- (4) The activity of antioxidants for curing any particular disease depends on the time of introduction in the course of medical treatment because the development of the

disease may be accompanied by stages of changing the antioxidizing activity. The compound may be efficient only if it is introduced at a low dose at the stage of reduced AOA or at a high dose at the stage of AOA elevation.

It is natural, and it could not be otherwise, that the pioneering works on antioxidants and free-radical reactions occurring in living systems were attacked furiously by opponents – scientists of various profiles: biologists, medicians, and even some of chemists and physicists. In spite of all arguments, vitalistic tendencies were strong: nobody could even dare to think that synthetic antioxidants may substitute natural ones. “Neither of free radical reactions can develop in a living organism”, the opponents claimed, “because these reactions are not controlled but strict regulation is essential for a living organism”. In addition, according to the concepts prevailing at that time, the membrane structure was such that it excluded the valence transfer from one lipid molecule to another since a lipoprotein model of membrane showed that lipids were separated by protein molecules. The opponents considered the absence of specific enzymes governing these reactions a strong argument against inhibitors of radical reactions and radical processes as such in organisms. The wide-spread opinion was that the antioxidant function, even that of tocopherol, was a *side effect* of its activity and important only for in vitro processes but did not play any role in bioobjects life. This opinion was supported by the fact that the deficiency of tocopherol (E-avitaminosis) can not be cured completely by applying synthetic antioxidants [56, 57]. Finally, it was considered doubtful that works, in which peroxides were detected in lipids isolated from organs and tissues, dealt with true amounts of products of free radical processes in vivo but not with the amounts of products formed during the process of isolation.

All the objections and skepticism have been rejected in due time. Antioxidant enzymes were discovered, the model of membrane was revised. The development of biochemistry and biophysics held the course in the direction of verification of this concept [58, 59].

These several pages of history should be concluded by the acknowledgment that the works carried out by Soviet scientists in the field of free-radical biology were pioneering and many if not all data obtained at that time remain valuable until the present time.

In spite of the fact that antioxidants are much spoken about because of their extensive application for various purposes, we should return to the definition of bioantioxidants.

Bioantioxidants are substances that exhibit the properties of inhibitors in model free-radical reactions of oxidation and retain these properties when introduced into a living organism (cell culture etc.). The absence of even one of these qualities does not permit calling a substance a bioantioxidant (BAO). Although the antioxidizing activity of lipids can be increased by applying substances that are synergists to natural antioxidants or those transformed into antioxidants in the course of metabolism, bioantioxidants, by our definition, should necessarily possess the ability to inhibit an oxidizing free-radical process in model reactions. This property of BAO makes it possible to predict the spectrum of their biological effects and perform a targeted synthesis of compounds.

At present, the following pathways of antioxidants effects on the cell metabolism are considered:

- (1) Interaction of BAO with free radicals of different nature.
- (2) Incorporation of BAO into the membrane structure and changes in the membrane functional activity due to changes in the membrane viscous properties (fluidity).

- (3) Effect of BAO on the activity of membrane proteins – enzymes and receptors.
- (4) Effect of BAO on the cell genetic apparatus including gene expression.
- (5) Effect of BAO on the regulatory systems of cell and, indirectly, on its metabolism as a whole.

Note that the reaction rate constants of the same inhibitors with different radicals differ considerably (by several orders of magnitude) [60, 61] (see Table 1). There are cases when antioxidants that are active for some radicals can not compete in interacting with others and we can not protect cell components from the effects of these radicals because the affinity of radicals to them will be higher than that of inhibitors introduced.

Another obstacle to effective using of antioxidants is their extreme concentration–effect dependence. As noted above, antioxidants applied in high concentrations produce an opposite effect and do not inhibit but accelerate free radical reactions. The phenomenon may be attributed either to a high activity of radicals accumulated from inhibitors or to the prevailing consumption of natural antioxidants as compared with synthetic ones introduced. Many of these effects depend on the initial characteristics of free radical processes and the initial level of antioxidants.

Thus, because of the versatility of antioxidants properties and feasibility of affecting various normal and pathological states, we are obliged to know exactly the nature of radicals responsible for pathological changes, the time of AO introduction, concentration, and elementary constants of inhibitors. A negligence in or an erroneous approach to the antioxidant therapy may lead to negative results.

Table 1. Rate constants of interaction of inhibitors-antioxidants with biologically active radicals

Inhibitors	Radicals (rate constants, 1/m sec			
	OH [•]	R [•] proteins	RO ₂ [•] lipids	O ₂ ^{•-} superoxide anion radical
2-ethyl-6-methyl-3-hydroxypyridine, hydrochloride	3.3 x 10 ¹⁰	1.9 x 10 ⁶	9.0 x 10 ⁵	26-4
N 3.5 ditert-butyl-4-hydroxyphenyl propionic acid (phenozan)	4.4 x 10 ¹⁰	1.2 x 10 ⁶	2..2 x 10 ⁴	10-2
5,7,8-Trimethyltocopherol (α -tocopherol)	8 x 10 ¹⁰		3.4 x 10 ⁶	47 x 10 ⁴ (soluble form)

A study on the mechanism of BAO effects showed that there is a whole system of relations between separate indices of cell metabolism that vary under the action of antioxidants. Investigation of the physicochemical regulatory system maintaining the level of free-radical reactions in lipids, on the one hand, and regulating the metabolism of membrane lipids and the rate of consumption of antioxidants in lipids, on the other hand, has been further developed [46, 47]. The components of this system are antioxidants, free radicals,

peroxidation products, composition and oxidizability of lipids, and the rate of consumption of antioxidants.

It was shown that enhancement of the antioxidant level is associated with reduction of the lipid peroxidation (LPO) rate, reduction of oxidation products concentration, reduction of the rate of lipids exit from membranes and enrichment of membranes with unsaturated lipids, and enhancement of lipids oxidizability. The latter effect results, in turn, in an increase in the rate of consumption of the antioxidant activity and, correspondingly, in returning of the AOA and LPO rate to the normal. An opposite situation is observed with decreasing in the AOA concentration, increasing the LPO rate, etc. Similar systems of regulation were discovered almost for all intracellular and cellular membranes of animals, plants, and microorganisms. Note that changes in the composition and oxidizability degree of lipids are associated with changes in the viscosity of various layers of membranes. The above parameters affect the activity and kinetic characteristics of membrane-bound proteins – enzymes and receptors; changes in the LPO rate may result in changing of not only the structure but also of the functional activity of membranes. In normal membranes, we observe identical relationships between the parameters; the difference concerns the system relaxation time (from several minutes to several days).

Exposure of organism to any damaging factor is associated with changes in this system of regulation. Long-term changes may result from (i) the action of a chronic factor that does not cause breaking bonds in the system of regulation; the system can return to the normal after cessation of the action; (ii) there may occur situations when exposure to a damaging factor results in transition to a new level of regulation; and (iii) there may occur breaking bonds in the system of regulation, which prevents the system to return to the normal. In the latter case, antioxidants may be efficient as a component of complex therapy. Such conclusions were drawn both in experimental studies and in clinical tests.

At present, scientists-pharmacologists must answer the question: whether all pharmacologically active compounds should be multitargeted drugs, i.e., should be aimed at several targets but not at one specific target. The answer to this question is not unambiguous, although the scientists who pose it cite the data that are evidence for the fact that most diseases are associated with changes and defects of various pathways of metabolism and drugs should not be aimed at one critical target but at all affected by the disease.

Meanwhile, an alternative to this approach is complex therapy that uses several compounds aimed each at its specific target; the compounds may be applied at various concentrations (not only at those specified by the compound structure), at various times of application, in various solvents, etc.

In our opinion, both views have the right to exist and different approaches should be taken in each specific cases for the benefit of patients.

As was noted above, breaking bonds in the system of regulation points to impossibility of returning the system to the initial state by applying AO.

Investigation of the regulation system as a whole but not only of separate changes in the system makes it possible to decide when the AO monotherapy is sufficient and when a complex therapy is needed, in which, apart from AO, other biologically active substances aimed at other targets are needed. To some extent, this may be accomplished by synthesis of hybrid molecules.

The term of hybrid antioxidants implies molecules whose structure contains parts responsible for antioxidant properties and fragments of molecules responsible for other specific functions.

In most cases, synthesis of hybrid molecules does not yield a new polyfunctional structure but cross-linked or integrated molecules that produce a high AO effect and are aimed at other targets specific of a certain disease.

Very often, when designing a molecule, it is necessary to retain the specific activity of one of the hybrid components and, at the same time, to reduce side-effects, e.g., toxicity of the compound. One of the promising ways is incorporating nitroxyl radicals in the molecule structure.

Nitroxyl derivatives of biologically active substances are the most numerous and earliest-synthesized hybrid antioxidants. Previously, it was shown that the nitroxyl radical exhibits the AO properties in model reactions of oxidation and in vitro and in vivo experiments. One of the pioneers in organic chemistry who synthesized nitroxyl derivatives of BAS was a Soviet scientist – A.B. Shapiro [62]. Since then, nitroxilation of BAS has been put into practice in pharmacology. Most extensively, antitumor compounds are nitroxylated. Konovalova N.P. [63–68] who had gained a great experience in the field of nitroxyl antitumor compounds made up a list of synthesized and well-studied antitumor agents referred to the class of nitroxyl-containing antibiotics, antimetabolites, and alkylating agents (Table 2).

As is seen from Table 2, nitroxyl derivatives are 5 to 10 times less toxic than the initial compounds.

At present, derivatives of platinum compounds have found wide use in chemotherapy of malignant tumors. It should be noted that, along with their high antitumor effect, these compounds exhibit a high toxicity. Supposedly, their cytotoxic effect and other side-effects (nephro- and ototoxicity, nausea, etc.) are associated with intensification of free-radical processes and formation of active oxygen species [$O_2^{\cdot-}$, OH.] induced in cell by cisplatin. In fact, the antitumor effect is associated, apart from the interaction with the DNA molecule, with enhancement of free-radical reactions. As a rule, reduction of toxicity results in decreasing the antitumor effect. Development of hybrid molecules based on platinum derivatives and nitroxyl radical makes it possible to reduce the toxicity and retain the activity of the agent.

At present, extensive studies are being carried out on the synthesis, structure, and biological activity of mixed-ligand complexes of platinum (II) with aminonitroxyl radicals [69].

The largest group of antitumor compounds includes nitroxyl derivatives of anthracycline antibiotics. One of the major achievements of the chemistry and biochemistry of hybrid antioxidants of this class is the development of emoxypin (ruboxyl) – a nitroxyl derivative of the anthracycline antibiotic – rubomycin.

This compounds have a great advantage of hybrid molecules, namely, in the background of high antitumor effect (higher than that of the parental compound – rubomycin), its toxicity decreased by 40% and cardiotoxicity and depilative properties vanished almost completely. The compound acquired some novel properties that are not characteristic of rubomycin and nitroxyl radical. It is of interest that there appeared no cross-resistance with rubomycin. The development of this compound is the greatest practical achievement in this field of investigation. It has passed the second stage of clinical tests.

Table 2. Nitroxyl derivatives of antitumor agents

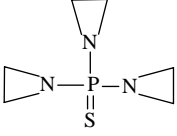
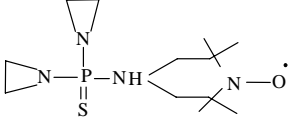
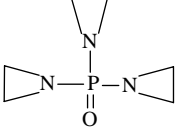
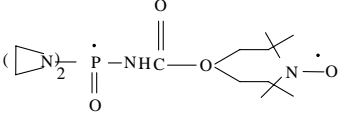
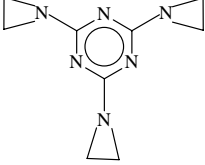
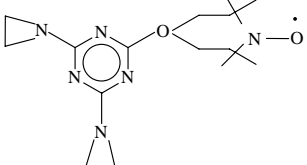
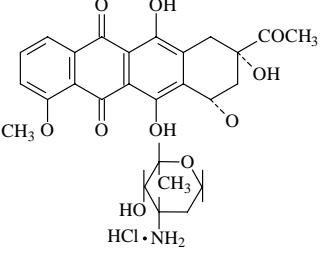
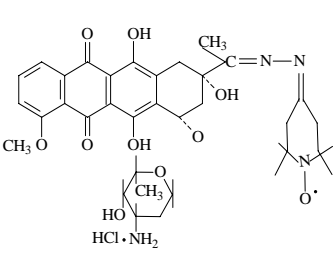
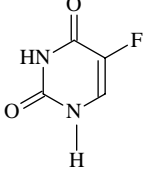
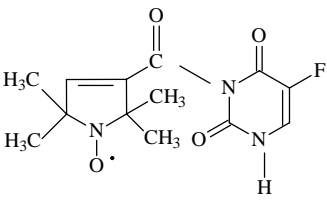
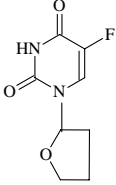
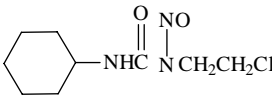
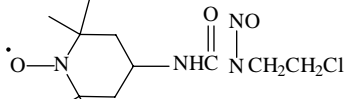
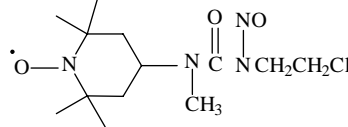
Initial components	LD ₅₀ mg/kg	Nitroxyl derivatives	LD ₅₀ mg/kg
 Thio TEF	18		187
 TEF	15		150
 TEM	1,5		15
 Rubomycin	5,6	 Ruboxyl	50
 5-Fluorouracil	100	 Magnicyl	510
 Fluoroaphur	750		

Table 2. (Continued)

Initial components	LD ₅₀ mg/kg	Nitroxyl derivatives	LD ₅₀ mg/kg
 Cyclohexyl - Nitrosourea	47	 	60 150

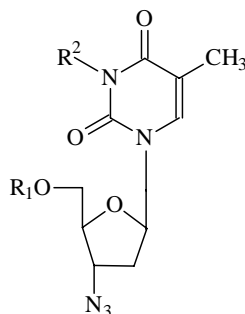
Other promising hybrid compounds are antitumor agents prepared on the basis of mixed-ligand platinum II and platinum IV complexes containing antioxidant fragments of the array of aminonitroxyl radicals. The feasibility of preparing such mixed complexes relies on the fact that cisplatinum ($[\text{NH}_3]_2\text{PtCl}_2$) transforms readily into a $\text{Na}[(\text{NH}_3)\text{PtCl}_3]$ complex, which interacts with primary amines on the background of sodium iodide and transforms into a $(\text{RNH}_2)(\text{NH}_3)\text{PtCl}$ complex. Having been treated with silver nitrate the latter complex exchanges readily halogen anions for the mobile NO_3^- anion; as a result, they can be substituted for other anions – Cl^- and anions of dicarboxylic acids.

The above complexes were characterized in various tumor models; it was shown that the DNA binding rate for these new complexes is comparable with that of cisplatinum but their oxidizing effect is opposite: the initial cisplatinum accelerates oxidation in model radical reaction; the platinum–nitroxyl complexes, on the contrary, inhibit oxidation. From this point of view, it is easy to explain the reduction of the toxicity of the synthesized complexes.

In the recent time, a great interest was aroused for platinum IV compounds. The scientists-organochemists of the Institute of Theoretical Problems of Chemical Physics synthesized complexes of platinum IV with aminonitroxyl radicals. These compounds were tested on the experimental model of P-388 leukemia. In the experiments, the complexes exhibited a strong effect on mice–leukemia-carriers: sometimes to complete recovery; the toxicity reduced two- to four-fold [70].

The most impressive results were obtained for low doses of cisplatinum and complexes of platinum IV with amino nitroxyl radicals applied in combination for treatment of P-388 leukemia. The survival rate for leukemia mice was 100%. As was noted above, nitroxylation of antitumor compounds was successful. There are some other examples of application of hybrid compounds containing nitroxyl radicals in their molecules.

At the Institute of Problems of Chemical Physics, novel biologically active compounds were synthesized – nitroxyl derivatives of azidothymidine of the common formula



where R^1 is the radical containing a nitroxyl group $>N-O$ and $R^2 = R^1$ or H.

These compounds produce the antiviral effect against RNA-containing viruses (human immunodeficiency virus and vesicular stomatitis virus) and the DNA-containing virus – cytomegalovirus [71].

It should be noted that hybrid molecules containing azidothymidine and antioxidant fragments in their structure inhibit the reproduction of cytomegalovirus; other azidothymidine derivatives do not possess this property. Considering that death of immunodeficiency patients is caused by cytomegalovirus-provoked diseases, this property of antioxidant- and azidothymidine-based hybrid molecules should be emphasized particularly.

One of the most promising and important practical areas of the modern chemistry related to phenol bioantioxidants is the synthesis of hybrid compounds that combine the antioxidant activity and the capacity for structural interactions with a biosystem. This type of compounds includes so-called 'buoy' compounds synthesized from quaternized derivatives of dialkylaminoalkylsubstituted 2,4,6-tri-tert-butylphenols and dialkylaminoalkyl ethers of phenoxy acid. For these compounds, a wide spectrum of biological activity was discovered – the antimicrobial, antiviral, analgetic, etc. activities. Also, it was discovered that gradual (step-by-step) redox and solvolytic conversions result in the formation of a cascade of intermediates with different inherent activities – antioxidizing, chelating, capacity for incorporating into the charge transfer chain, etc. In the cascade mechanism of the effect of 2,4,6-tri-tert-butylphenol derivatives, the tendency to the formation of heterocyclic compounds, which make a contribution to the total biological activity, plays a great role.

Another important currently developing research area is the synthesis of hybrids of functional di- and tert-butylphenols and biocompatible macromolecules. In this area, it is possible to achieve the highest values of antioxidizing activity of hybrid compounds of a wide variety of hydrophobic–hydrophilic relationships and particular structural properties in solutions [72].

The presence of the positively-charged nitrogen atom in the hybrid molecule provides for the antioxidant adherence to the surface of a cell membrane and its fixation in a certain place by means of the lipophilic long-chained alkyl fragment R_1 . Such a structure ensures the targeted use of the antioxidant and favors the inhibition of pathological processes in cell, e.g. intensification of LPO and disorders of cell membranes functions.

Hence, a hybrid molecule – an analog of acetylcholine [$CH_3COOCH_2CH_2N^+(CH_3)_3OH$] was constructed. In this molecule, instead of acetic acid, the ester bond is formed by carboxylic acids that contain a 2,6-di-tert-butyl-4-hydroxyphenyl fragment. We called these hybrid antioxidants *ichfans*.

It might be expected that the above structure should give rise to a bioantioxidant with an anticholinesterase activity. Indeed, anticholinesterase compounds are the most efficient up-to-date therapeutic agents applied for the Alzheimer's disease (AD); they make it possible to maintain the level of acetylcholine (responsible for memory and cognitive functions) in the disease-affected sections of brain. On the other hand, the oxidative stress, i.e., promotion of LPO in cell membranes of brain and in cells of peripheral systems and organs plays an important role in the development of AD [73].

The above-described properties and interactions of the AOs with biological systems, e.g., cell membranes, made it possible to suggest using these compounds as drugs for the therapy of the Alzheimer's disease.

In studies performed with the use of various oxidation models, antioxidizing properties of ichfans were determined and assessed quantitatively. It was found out that new hybrid AOs – ichfans – possess the antioxidant activity (revealed in the model of oxidation of homogenate lipids) and anticholinesterase activity that exceed the corresponding indices of the initial substances. The addition of the molecule with alkyl substituents with different lengths of the alifatic chain on the nitrogen atom promotes the AOA and inhibiting properties. With increasing the length of the carbon chain in the alkyl substituent, the capacity of the compounds to inhibit AChE increases. The type of inhibition depends on an alkyl substituent. Although, the inhibiting power of the substances under study for a membrane-bound enzyme is by an order of magnitude lower than that for soluble AChE, the same relationships between the structure and inhibiting activity of the compounds were detected for the membrane-bound and soluble enzyme [81-84].

A strict direct correlation between the anticholinesterase and antioxidative properties of ichfans was detected; the correlation is also of the same character for membrane-bound and soluble AChE.

On the basis of results of *in vitro* experiments, by the criteria of the anticholinesterase and antioxidative properties, the optimum compound was chosen for further *in vivo* studies. That was a hybrid with the radical $R_1 = C_{10}H_{21}$; hereinafter, it will be referred to as ichfan. An additional lengthening of the tail resulted in undesirable perturbing effect on membranes; the effect manifested itself by the erythrocytes increasing sensitivity to hemolysis. In accordance with the data published, the compound with $R_1 = C_{10}H_{21}$ is sufficiently hydrophobic to permeate through the hematoencephalic barrier.

With regard to the AChE and antioxidizing effects and feasibility of permeation through the HEB, ichfan is of considerable interest in view of using it as a drug for treatment of AD.

It should be noted that the oxidative stress as an important factor of AD may be not only a source of free radicals damaging cell structures and macromolecules but also a symptom of a disorder in the operation of the system of homeostasis of lipid peroxidation (LPO) in biological membranes. This system plays an important role in the regulation of cell metabolism; it controls the structure and structure-related functions of various cellular membranes.

An analysis of data [85-97] on changes in the lipid metabolism, composition and structure of the membrane lipid phase, which plays a great role in transmission, processing, and storing the information in cell, showed that the development of AD is associated, along with enhancement of LPO, with enrichment of lipids with unsaturated compounds and increasing the fluidity (decreasing the viscosity) of the lipid phase. In other words, on the background of enhancement of LPO, the lipid bilayer fluidity increases; the effect favors the

increasing of oxidation and, hence, the development of the pathological process. This property of membranes in AD makes it impossible to prevent from the oxidative stress by means of traditional phenol antioxidants, which promote the fluidity increasing and complicate the disease development.

We suggested that addition of a saturated fatty-acid tail (buoy) that incorporates in the antioxidant molecule membrane may make the membrane more rigid and thus contribute to the therapeutic effect of ichfan. As is seen from Table 1, after introduction of the compound to mice, the microviscosity of the membrane near-surface sites studied by the method of EPR spin probes either changes insignificantly or increases; the latter is a desirable effect. It should be emphasized particularly for membranes isolated from a coarse fraction of synaptosomes because AD is associated mostly with damages of nerve fibers.

According to many of the researchers, one of the AD risks is an elevated cholesterol level [98-100]. It should be noted that the cholesterol content in rat brain tissues decreased by 40% within 2 h after introduction of 15 mg/kg of the compound to the animals. The cholesterol content in a cytoplasmic fraction isolated from mice brain decreased almost two-fold within 2.5 h after introduction of 6 mg/kg of ichfan.

Thus, in addition to the ability of ichfan to inhibit the cholinesterase activity, it can inhibit the oxidative stress (LPO) and, in contrast to traditional phenol-type antioxidant, rigidize the structure of the membrane lipid bilayer or at least prevent from increasing its fluidity. The combination of these properties may be beneficial for the therapy of AD through the correction of the AD-damaged system of regulation of lipid peroxidation homeostasis that participates in controlling of cell metabolism. A certain contribution to the therapeutic effect of ichfan may be provided by its lowering effect on the level of cholesterol.

REFERENCES

- [1] Tarusov B.N., *Mechanisms of biological effects of radioactive emissions*, M., Medgiz, 1954, 140 pp. (in Russian).
- [2] Burlakova E.B., Dzantiev B.G., Sergeev G.B., Emanuel N.M., *Izv. vuzov*, 1959, vol. 2, no. 4, p. 533. (in Russian).
- [3] Burlakova E.B., Dzantiev B.G., Sergeev G.B., Emanuel N.M., *Nauchn. dokl. vyssh.shk.*, 1960, vol. 1, p. 145. (in Russian).
- [4] Burlakova E.B., Dzantiev B.G., Sergeev G.B., Emanuel N.M., in Proceedings of Conference "Biochemical and physicochemical principles of biological effects of radiation", M., *Izd. MGU*, 1957, p. 10. (in Russian).
- [5] Emanuel N.M., in Proceedings of the Moscow society of nature researchers, M., *Nauka*, 1963, p. 73. (in Russian).
- [6] Sapezhinskii I.I., Emanuel N.M., *Dokl. AN SSSR*, 1965, vol. 163, no. 4, p. 845. (in Russian)
- [7] Zhizhina G.P., Kruglyakova K.E., Emanuel N.M., *Dokl. AN SSSR*, 1965, vol. 163, no. 4, p. 931. (in Russian).
- [8] Emanuel N.M., Burlakova E.B., Kruglyakova K.E., Sapezhinskii I.I., *Izv. akad. nauk AN SSSR, Ser. biol.*, 1965, no. 2, p. 183. (in Russian).
- [9] Burlakova E., *Moderne Medizin*, 1972, vol. 2, no. 4, p. 215.

- [10] Emanuel N.M., Lipchina L.P., *Dokl. AN SSSR*, 1958, vol. 121, no. /, p. 141. (in Russian).
- [11] Emanuel N.M., Pathways of synthesis and investigation of antitumor drugs, M., *Nauka*, 1962, 22 pp. (in Russian).
- [12] Ershov V.V., Nikiforov G.A., Volodkin A.A., Spatially-hindered phenols, M., *Khimiya*, 1972, 351 pp. (in Russian).
- [13] Smirnov L.D., Sholina S.I., et al., *Izv. AN SSSR, Ser. khim.*, 1963, no. 5, p. 890. (in Russian).
- [14] Burlakova E.B., Alesenko A.V., Molochkina E.M., Palmina N.P., Khrapova N.G., Bioantioxidants for radiation damage and malignant growth, M., *Nauka*, 1975, 214 pp. (in Russian).
- [15] Burlakova E.B., Gaintseva V.D., Slepukhina L.V., Khrapova N.G., Emanuel N.M., *Dokl. AN SSSR*, 1964, vol. 155, p. 1398. (in Russian).
- [16] Burlakova E.B., Khrapova N.G., Yadykin G.I., *Biofizika*, 1971, vol. 16, no. 2, p. 201. (in Russian).
- [17] Aristarkhova S.A., Burlakova E.B., Khrapova N.G., *Izv. akad. nauk, Ser. khim.*, 1971, no. 2, p. 2714. (in Russian).
- [18] Burlakova E.B., Burobina S.A., Khrapova N.G., Yadykin G.I., *Biofizika*, 1971, vol. 16, no. 1, p. 39. (in Russian).
- [19] Sapezhinskii I.I., Biopolymers: Kinetics of radiation-induced and photochemical conversions, M., *Nauka*, 1988, 214 pp. (in Russian).
- [20] Lozovskaya E.L., Sapezhinskii I.I., *Radiation biology. Ecology*, 1993, vol. 33, no. 1(4), p. 601. (in Russian).
- [21] Burlakova E.B., Molochkina E. M., *Biofizika*, 1968, vol. 13, p. 443. (in Russian).
- [22] Burlakova E.B., Burobina S.A., Khrapova N.G., *Dokl. akad. nauk SSSR*, 1971, vol. 200, p. 461. (in Russian).
- [23] Burlakova E.B., Molochkina E. M., *Vopr. onkol.*, 1974, vol. 20, p. 62. (in Russian).
- [24] Burlakova E.B., Palmina N.P., *Vesti AMN SSSR*, 1982, no. 3, p. 74. (in Russian).
- [25] Frankfurt O.S., Lipchina L.P., Bunto T.V., Emanuel N.M., *Bull. experim. biol. med.*, 1967, vol. 8, p. 86. (in Russian).
- [26] Emanuel N.M., Konovalova N.P., Dronova L.M., *Dokl. akad. nauk SSSR*, 1962, vol. 143, no. 3, p. 737. (in Russian).
- [27] Emanuel N.M., Dronova L.M., Konovalova N.P., *Dokl. akad. nauk SSSR*, 1963, vol. 152, no. 2, p. 481. (in Russian).
- [28] Burlakova E.B., Palmina N.P., *Vopr. onkol.*, 1990, no. 10, p. 1155. (in Russian).
- [29] Palmina N.P., Burlakova E.B., *Vesti AMN SSSR*, 1985, no. 1, p. 91. (in Russian).
- [30] Emanuel N.M., Kruglyakova R.E., Nikolaeva N.V., Zakharova N.A., *Dokl. akad. nauk SSSR*, 1964, vol. 157, no. 4, p. 935. (in Russian).
- [31] Sapezhinskii I.I., Silaev Yu.V., Emanuel N.M., *Dokl. akad. nauk SSSR*, 1964, vol. 159, no. 6, p. 1378. (in Russian).
- [32] Sharpatyi V.A., Radiation chemistry of biopolymers, M., *Energoizdat*, 1981, 168 pp. (in Russian).
- [33] Obukhova L.K., *Uspekhi khimii*, 1975, vol. 44, no. 10, p. 1914. (in Russian).
- [34] Emanuel N.M., Obukhova L.K. *Exp. Gerontol.*, 1979, vol. 13, p. 25.
- [35] Obukhova L.K., Nakaidze N.Sh., Serebrjany A.M., Smirnov L.D. Akifiev A.P. *Exp. Gerontol.*, 1979, vol. 14, p. 335.

- [36] Sadovnikova I.P., Obukhiva L.K., Bunto T.V., Smirnov L.D., *Izv. AN SSSR*, 1984, Ser. biol., no. 4, p. 543. (in Russian).
- [37] Emanuel N.M., Obukhova, Bunto T.V., Dyakova V.V., *Izv. AN SSSR, Ser. biol.*, 1997, no. 1, p. 32. (in Russian).
- [38] Burlakova E.B., *Biofizika*, 1967, vol. 12, no. 1, p. 82. (in Russian).
- [39] Burlakova E.B., Palmina N.P., Ruzhinskaya N.L., *Izv. AN SSSR*, 1971, no. 1, p. 134. (in Russian)
- [40] Alesenko A.V., Sokolova I.S., Kukushkina G.V., Burlakova E.B., Gorbacheva L.B., *Dokl. akad. nauk SSSR*, 1989, vol. 254, no. 6, p. 1472. (in Russian).
- [41] Alesenko A.V., Burlakova E.B., *Dokl. akad. nauk SSSR*, 1972, vol. 207, p. 1471. (in Russian).
- [42] Alesenko A.V., Burlakova E.B., Vainson A.A., *Dokl. akad. nauk SSS*, 1972, vol. 202, p. 208. (in Russian).
- [43] Alesenko A. V., Burlakova E. B.//*Bioelectrochemistry*. - 2002. - V. 58. - P. 13.
- [44] Burlakova E.B., Goloshchapov A.N., *Biofizika*, 1975, vol. 10, no. 5, p. 816. (in Russian)
- [45] Burlakova E.B., Dzhalyabova M.I., Molochkina E.M., in "*Structure, biosynthesis and conversions of lipids in animal and human organisms*", 1975, Frunze, Izd. FAN, 1975, p. 70. (in Russian)
- [46] Aristarkhova S.A., Arkhipova G.V., Burlakova E.B., et al., *Dokl. AN SSSR*, 1976, vol. 228, p. 215. (in Russian).
- [47] Burlakova E. B., Dzhalyabova M. I., Molochkina E. M., Khokhlov A. P., *Biophysical and Biochemical Information Transfer in Recognition and Aging*, 1979.- P. 1583.
- [48] Burlakova E.B., *Kardiologiya*, 1980, vol. 20, p. 48.
- [49] Arkhipova G.V., Burlakova E.B., Semiokhina A.F., Fedotova I.B., Krushinskii L.V., *Dokl. AN SSSR*, 1981, vol. 256, no. 3, p. 746. (in Russian).
- [50] Disvetova V.V., Genieva E.I., et al., *Klinich. med.*, 1968, no. 3, p. 126. (in Russian).
- [51] Zoz N.N., Lemanova I.B., Akhmedov S.A., Suleimanov D.S., Serebryanyi A.M., Morozova I.S., Sultanova O.D., *S.-khoz. biol.*, 1985, no. 4, p. 71. (in Russian).
- [52] Lipsits D.D., Kruglyakova K.E., Postnikova M.S., *Dokl. AN SSSR*, 1962, vol. 145, p. 212. (in Russian).
- [53] Sadykov A.S., Kruglyakova K.E., et al., *Chemistry of phyto substances*, Tashkent, FAN, 1968, vol. 3, p. 86. (in Russian).
- [54] Burlakova E.B., Laricheva E.P., *VNIIZh*, 1973, p. 15. (in Russian).
- [55] L.D. Smirnov, Yu.V. Kuznetsov, L.M. Apasheva, K.D. Poltorak, A.L. Grinchenko, K.M. Dyumaev, N.M. Emanuel, *Author's certificate* 1098934, Feb. 23, 1983. (in Russian)
- [56] Krashakov S.A., Burlakova E.B., Khrapova N.G., *Biol. membr.*, 1998, vol. 12, no. 2, p.173. (in Russian).
- [57] Burlakova E.B., Krashakov S.A., Khrapova N.G., Kinetic characteristics of tocopherols as antioxidants, M., *Nauka*, 1988, 247 pp. (in Russian).
- [58] Burlakova E.B., *Uspekhi khimii*, 1975, vol. 44, no. 10, p. 1871. (in Russian).
- [59] Burlakova E.B., Khrapova N.G., *Uspekhi khimii*, 1985, vol. 54, p. 1540. (in Russian).
- [60] Pobedimskii D. G., Burlakova E.B. in Mechanism of Antioxidant Action in Living Organisms, in Atmospheric Oxidation and Antioxidants, *Ed.J. Scott*, v. 3, no.9, p. 223, 1993.

- [61] Burlakova E.B., Khrapova N.G., Shtolko V.N., Emanuel N.M., *Dokl. AN SSSR*, vol. 169, no. 3, p. 688. (in Russian).
- [62] Shapiro A.B., Kropacheva A.A., Suskina V.I., et al., *Mass-spectroscopic study of paramagnetic derivatives of ethylenephosphoramides*, 1971, vol. 4(1), p. 864 (in Russian)
- [63] Konovalova N.P., Nitroxyl radicals as modifiers of biological effects of antitumor compounds, *Khimfizika*, 1991, vol. 10(6), pp. 861-868 (in Russian).
- [64] Emanuel N.M., Konovalova N.P., Povarov L.S., et al., *Author's certificate 977462 SSSR, //BI*, 1980.
- [65] Emanuel N.M., Konovalova N.P., Diatcbkovkaja RF. Potential anticancer agents--nitroxyl derivatives of Rubomycin. *Neoplasma* 1985,v.32, p.285-92.
- [66] Emanuel N.M., Zhdanov R.I., Konovalova N.P., et al., Paramagnetic diethyleneimides of urethan phosphoric acids as antitumor substances, *Voprosy oncol.*, 1980, vol. 36, pp. 54-58. (in Russian).
- [67] Seminara P., Franchi F., Konovalova N. et al. Activity of a nitroxylated analog of daunirubomocin, ruboxyl in B- lymphoproliferative disorders. *Acta Haematol.* 2001, 105: 77-82.
- [68] Emanuel N.M., Rozenberg A.V., Golubev V.A., et al., *Urgent problems of experimental chemotherapy of tumors*, 1987, vol. 5. (in Russian).
- [69] Sen' V.D., Rukina N.A., Tkachev V.V., et al., *Synthesis, structure and biological activity of platinum (II) complexes*, 2000, vol. 9, pp. 1624-1630. (in Russian).
- [70] Sen' V.D., Tkachev V.V., Volkova L.M., et al., Synthesis, structure and antitumor properties of platinum (IV) complexes with aminonitroxide, *Izv AN, Ser. khim.*, 2003, vol. 2, pp. 403-408. (in Russian).
- [71] Sen' V.D., Golubev, V.A., Rukina, N.A., Orlova, T.G., Burlakova, E.B. *Nitroxyl derivatives of 3'-azido-2'3'-dideoxythymidine with antiviral activity*. Patent RU 2103274 C1 1998.
- [72] Behl C. Alzheimer Disease and oxidative stress: implications for novel therapeutic approaches. *J. Biol. Chem.* 1996, 271: 26482-26489.
- [73] Nitsh R., Blusztajns J. K. Pittas A. G. et al. Evidence for a membrane defect in Alzheimer disease brain. *Proc. Natl. Acad. Sci USA* 1992, 89: 1671-1675.
- [74] Zafrilla P., Mulero J., Xandri J.M. et al. Oxidative stress in Alzheimer patients in different stages of the disease. *Curr. Med. Chem.* 2006,13:1075-1083.
- [75] Frank B., Gupta S. A review of antioxidants and Alzheimer's disease. *Ann. Clin. Psychiatry* 2005, 17: 269-286.
- [76] Moreira P.I., Honda K., Liu Q. et al. Oxidative stress: the old enemy in Alzheimer's disease pathophysiology. *Curr. Alzheimer Res.* 2005, 2: 403-408.
- [77] Mariani E., Polidori M.C., Cherubini A. et al. Oxidative stress in brain aging, neurodegenerative and vascular diseases: an overview. *J. Chromatogr. B. Analyt. Technol. Biomed. Life Sci.* 2005, 827: 65-75.
- [78] Moreira P.I., Smith M.A., Zhu X. et al. Oxidative damage and Alzheimer's disease: are antioxidant therapies useful? *Drug News Perspect* 2005, 18:13-19.
- [79] Irizarry M.C. Biomarkers of Alzheimer disease in plasma. *NeuroRx.* 2004,1:226-234.
- [80] Perevozkina M.G., Storozhok N.M., Nikiforov G.A., Correlation between chemical structure and inhibiting properties of sterically-hindered phenols of the ichfan group, *Biomed. khim.*, 2005, vol. 51, pp. 413-423. (in Russian).

-
- [81] Braginskaya F.I., Zorina O.M., Molochkina E.M., et al., Synthetic bioantioxidants as inhibitors of the AChE activity, *Izv. AN SSSR*, 1992, vol. 5, pp. 690-698. (in Russian).
- [82] Braginskaya F. I., Molochkina E. M., Zorina O. M. et al. New synthetic bioantioxidants - acetylcholinesterase (AChE) inhibitors. in: *Alzheimer Disease: From Molecular Biology to Therapy*. R. Becker and E. Giacobini (eds.). Birkhauser-Boston. 1996, 337-342.
- [83] Ozerova I.B., Molochkina E.M., Burlakova E.B. Ichfan – new potential drug for treatment of Alzheimer’s disease. *Advances in Gerontology* 2001, 6: 30.
- [84] Molotchkina E. M., Ozerova I. B., Burlakova E. B. «ICHFAN» - new antioxidant drug for the treatment of Alzheimer’s disease. *Free Rad. Biol. Med.* 2002, 33: 229- 230.
- [85] Buchet R. and Piku S. Alzheimer’s disease: Its origin at the membrane, evidence and questions. *Acta Biochimica Polonica* 2000, 47 : 725–733.
- [86] Prasad M.R., Lovell M.A., Yatin M., Dhillon,H. and Markesbery, W.R. Regional membrane phospholipid alterations in Alzheimer’s disease. *Neurochem. Res.* 1998, 23: 81–88.
- [87] Wells K., Farookui A.A., Liss L. and Horrocks L.A. Neural membrane phospholipids in Alzheimer disease. *Neurochem. Res.* 1995, 20: 1329–1333.
- [88] Soderberg M., Edlund C., Kristensson K. and Dallner G. Fatty acid composition of brain phospholipids in aging and in Alzheimer's disease. *Lipids* 1991 26:421-425.
- [89] Pettegrew J.W., Panchalingam K., Hamilton R.L. et al. Brain membrane phospholipid alterations in Alzheimer's disease. *Neurochem. Res.* 2001, 7:771-782.
- [90] Soderberg M., Edlund C., Alafuzoff I. et al. Lipid composition in different regions of the brain in Alzheimer's disease/senile dementia of Alzheimer's type. *J. Neurochem.* 1992, 5:1646-1653.
- [91] Nitsch R.M., Blusztajn J.K, Pittas A.G. et al. Evidence for a membrane defect in Alzheimer disease brain. *Proc. Natl. Acad. Sci. USA.* 1992, 89: 1671-1675.
- [92] Wells, K., Farookui, A.A., Liss, L. and Horrocks,L.A. Neural membrane phospholipids in Alzheimer disease. *Neurochem. Res.* 1995, 20: 1329–1333.
- [93] Markesbery W.R., Leung P.K., Butterfield D.A. Spin label and biochemical studies of erythrocyte membranes in Alzheimer's disease. *J. Neurol. Sci.* 1980, 45:323-330.
- [94] Zubenko G.S., Kopp U., Seto T et al. Platelet membrane fluidity individuals at risk for Alzheimer's disease: a comparison of results from fluorescence spectroscopy and electron spin resonance spectroscopy. *Psychopharmacology (Berl)* 1999,145:175-180.
- [95] Kozubski W., Swiderek M., Kloszewska I. et al. [Platelet membrane fluidity and receptor exposition in patients with Alzheimer's disease]. *Neurol. Neurochir. Pol.* 1999, 33:1275-1284. (in Polish).
- [96] Muller W.E., Kirsch C., Eckert G.P. Membrane-disordering effects of beta-amyloid peptides. *Biochem. Soc. Trans* 2001, 29:617-623.
- [97] Braginskaya F.I., Zorina O.M., Pal'mina N.P. et al. Some blood biochemistry parameters during the cholinergic treatment of Alzheimer's disease. *Neurosci. Behav. Physiol.* 2001 31: 457-461.
- [98] Simons M., Keller P., De Strooper B et al. Cholesterol depletion inhibits the generation of beta- amyloid in hippocampal neurons. *Proc. Natl. Acad. Sci. USA* 1998, 95: 6460–6464.
- [99] Eckert G.P., Kirsch C., Muller W.E. Brain-membrane cholesterol in Alzheimer's disease. *J. Nutr. Health Aging* 2003,7:18-23.

- [100] Raffai R. L. and Weisgraber K. H. Cholesterol: from heart attacks to Alzheimer's disease. *J. Lipid Res.* 2003, 44: 1423–1430.

Chapter 2

OXIDATIVE RADICAL GENERATION VIA NITROGEN DIOXIDE DIMER CONVERSIONS INDUCED BY AMIDE GROUPS OF MACROMOLECULES

E. Ya. Davydov, I. S. Gaponova, T. V. Pokholok,
G. B. Pariiskii and G. E. Zaikov*

Emanuel Institute of Biochemical Physics,
Russian Academy of Sciences, 4 KosyginSt.,
Moscow, 119991, Russia

ABSTRACT

The features of initiation of free radical reactions in polymers by dimers of nitrogen dioxide are considered. The conversion of planar dimers into nitrosyl nitrate in the presence of amide groups of macromolecules has been revealed. Nitrosyl nitrate initiates radical reactions in oxidative primary process of electron transfer with formation of intermediate radical cations and nitric oxide. As a result of subsequent reactions, nitrogen-containing radicals are produced. The dimer conversion has been exhibited by estimation of the oxyaminoxyl radical yield in characteristic reaction of *p*-benzoquinone with nitrogen dioxide on addition of aromatic polyamide and polyvinylpyrrolidone to reacting system. The isomerisation of planar dimers is efficient in their complexes with amide groups, as confirmed by ab initio calculations.

Keywords: *nitrogen dioxide, nitrosyl nitrate, polyamides, stable radicals, EPR spectra.*

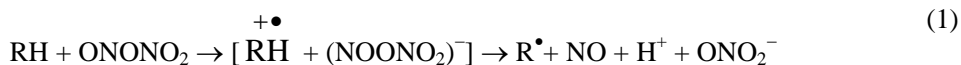
I. INTRODUCTION

Nitrogen dioxide effectively reacts with various low- and high- molecular compounds [1, 2]. Its reactions have a wide application in synthetic chemistry and can be used for chemical

* E-mail: pgb@sky.chph.ras.ru, Fax: (7-095)1374101

modification of polymers specifically for grafting stable nitrogen-containing radicals to macromolecules [3]. However, it should be remembered that NO_2 is a free radical of moderate reactivity: the ONO-H bond strength [4] is $320 \text{ kJ}\cdot\text{mol}^{-1}$. Because of this, NO_2 can initiate free radical reaction by abstracting hydrogen atoms only from the least strong, for example, allyl C-H bonds or by attaching to double C=C bonds [5-8]. Nevertheless, effective formation of stable radicals is observed also in polymers not containing labile hydrogen atoms or double bonds. For example, aromatic polyamidoimides, nylon, polyvinylpyrrolidone (PVP) [3] and aromatic polyamides (AP) [9] exhibit high activity in respect to nitrogen dioxide. These facts allow considering other probable mechanisms of radical initiation. The fact is that major radical products of the nitrogen dioxide interaction with AP and PVP are iminoxyl and acylalkylaminoxyl radicals that are produced from oximes and acylnitroso compounds [3, 9]. The occurrence of these precursors of stable radicals in turn associates with presence of nitric oxide. In this connection, it is necessary to suppose a participation of NO_2 dimeric forms in radical initiation. The main dimers of NO_2 are planar nitrogen tetroxide $\text{O}_2\text{N-NO}_2$ (PD) and nitrosyl nitrate ONONO_2 (NN). Ab initio calculations [8] show that these dimers are formed with the most probability in NO_2 atmosphere; the form of nitrosyl peroxyxynitrite ONOONO is too unstable to be considered as efficient participant of reactions.

As NN has strong oxidative properties [10], the generation of radicals can take place by an electron transfer from donor functional groups with the formation of intermediate radical cations:



The recombination of radicals with nitric oxide gives nitroso compounds that undergo isomerisation into oximes [11] to produce iminoxyl radicals in the reaction with NO_2 :



The nitroso compounds are effective spin traps and a source of stable aminoxyl radicals:



Thus the mechanism involving reactions (1-3) formally could explain an appearance of stable radicals in the polymers not containing specific chemical bonds reacting with NO_2 mono radicals [9]. However, there are certain obstacles connected with energetic properties of NO_2 dimers for realising such mechanism; the energy of syn- and anti forms of NN exceeds that of PD respectively 29.8 and $18.4 \text{ kJ}\cdot\text{mol}^{-1}$ [8]; that is the equilibrium



should be shifted to PD in gas phase. Nevertheless, the nitroso nitrite formation was observed during the interaction of olefins with nitrogen dioxide in liquid phase [8, 12]. This fact is indicative of the participation of NN in these reactions. The shift of equilibrium (4) to NN can

occur in liquid phase reactions, for instance, because of increasing the polarity of medium. In solid polymers with small macroscopic dielectric permeability ($\epsilon = 2-3$), the formation of NN could be promoted by co-ordination of nitrogen dioxide with polar functional groups. However, stable nitrogen-containing radicals were not registered in such polymers with polar ester groups as poly(methyl methacrylate), polycarbonate, acetyl cellulose on exposure to nitrogen dioxide. Based on this fact, one can assume that the effective formation of NN and consequently realisation of ion - radical process (1) are conditioned by specific donor-acceptor interactions of nitrogen dioxide dimers with certain functional groups facilitating the isomerisation of PD into NN.

In the present investigation, the possibility of the PD conversion into NN under the influence of amide groups of PA and PVP with further generation of stable radicals by reactions (1-3) is considered. As the indicator of the dimer conversion, the dependence of yield of typical radicals in the reaction of PD with *p*-benzoquinone (BQ) [13] on the contents of PA and PVP in reacting system was used. The mechanism proposed of dimer conversions has been confirmed by ab initio calculations.

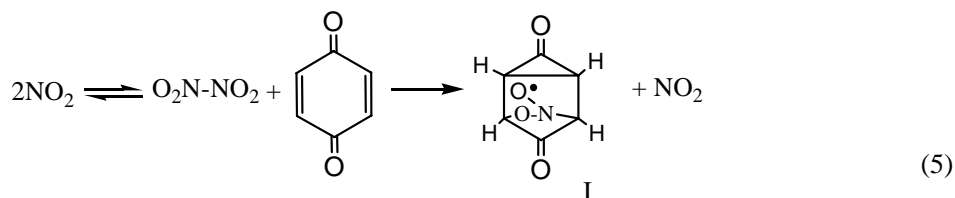
II. EXPERIMENTAL

Nitrogen dioxide was obtained by the thermal decomposition of lead (II) nitrate [14]. Experiments were carried out on BQ "Merck", PVP with $M_n = 3.0 \cdot 10^5$ and PA synthesised by polycondensation of *m*-phenylenediamine and isophthalic acid. Powder-like composites of BQ with AP and PVP containing silica gel "Chemapol" with 100-160 μ diameter of particles were prepared. Samples of BQ+PVP+SiO₂ with constant quantity of BQ (100 mg), SiO₂ (100 mg) and variable quantities of PVP (10-30 mg) were prepared from 10 % combined solutions of BQ and PVP in chloroform containing SiO₂ pre-heated at 400° C. After evaporation of the solvent by stirring at room temperature, samples were dried up carefully by pumping. Similarly composites of BQ (100 mg) +AP (20-100 mg) +SiO₂ (100 mg) were prepared. Samples were placed in quartz tubes for EPR measurements provided with a stopcock and connected to a flask of volume 0.5 l. After pumping to a pressure of $\sim 10^{-3}$ mm Hg, the stopcock was closed, and the flask was filled with NO₂ up to the concentration of 10^{-3} mol·l⁻¹. As soon as NO₂ was drawn into the tube with the sample, EPR spectra were recorded on the spectrometer "EPR-1306". The products of the nitrogen dioxide interaction with *N*-methylpyrrolidone (low-molecular analogue of PVP) "Merck" were analysed in 1:1 mixture with pyridine "Merck" by IR spectroscopy. IR spectra were recorded using a Specord IR-75.

III. RESULTS AND DISCUSSION

III.1 Yields of Nitrogen-Containing Radicals in Composites of BQ with PVP and AP

On exposure of BQ to nitrogen dioxide, the formation of radicals I of oxyaminoxyl type [15] takes place by the following scheme [13]:



The scheme (5) is confirmed by kinetic data according to which the rate of the radical I accumulation is proportional to a square of NO_2 concentration in gas phase [13]. The stationary concentration of radicals I increases with decreasing temperature in the range from 285 K to 300 K, as the equilibrium $2\text{NO}_2 \rightleftharpoons \text{O}_2\text{N-NO}_2$ is shifted to the right with decreasing temperature [2]. The EPR spectrum of radicals I obtained in BQ with SiO_2 at room temperature represents triplet with $a^{\text{N}} = 2.82$ mT and $g = 2.0053$ (Fig 1a). It should be noted that this spectrum does not show an anisotropy that is characteristic for EPR spectra of aminoxyl radicals in the solid phase [16]. This fact is caused by enough high molecular mobility as a result of a destruction of BQ crystal structure in layers between SiO_2 particles due to reactions of the radical I conversion [13]. In addition to I, iminoxyl radicals II occur in composites of BQ with AP on exposure to nitrogen dioxide. Under the same conditions, the sum of radicals II and acylalkylaminoxyl radicals III, along with I, was registered in composites of BQ with PVP. Signals of radicals II and III are masked by an intense signal of radicals I in the EPR spectrum. However one can separate spectra of radicals II and III using the fact that radicals I exist only in an NO_2 atmosphere. In view of rather low thermal stability, radicals I quickly disappear at room temperature within several minutes after pumping out nitrogen dioxide from the samples. Remaining spectra of stable radicals II in AP and the sum of II+III in PVP are shown respectively in Figure 1b and 1c. They represent anisotropic triplets with $A_{\parallel}^{\text{N}} = 4.1$ mT, $g_{\parallel} = 2.0024$ and $A_{\perp}^{\text{N}} = 2.6$ mT, $g_{\perp} = 2.005$ (radical II) [9] and with $A_{\parallel}^{\text{N}} = 1.94$ mT, $g_{\parallel} = 2.003$ (radical III) [3]. Using this procedure, the maximum concentrations of radicals I, II and III were separately determined in composites with the various contents of AP and PVP after exposure to NO_2 within 24 hours. It should be noted that the parameters of spectra of iminoxyl radicals II are identical in AP and PVP, therefore the same designation is accepted for these radicals. Because the formation of radicals of one or another type takes place in separate phases of BQ, AP and PVP, concentrations of radicals in the heterophase composites were determined as a ratio of number of spins calculated by integration of EPR spectra to weight of the given phase.

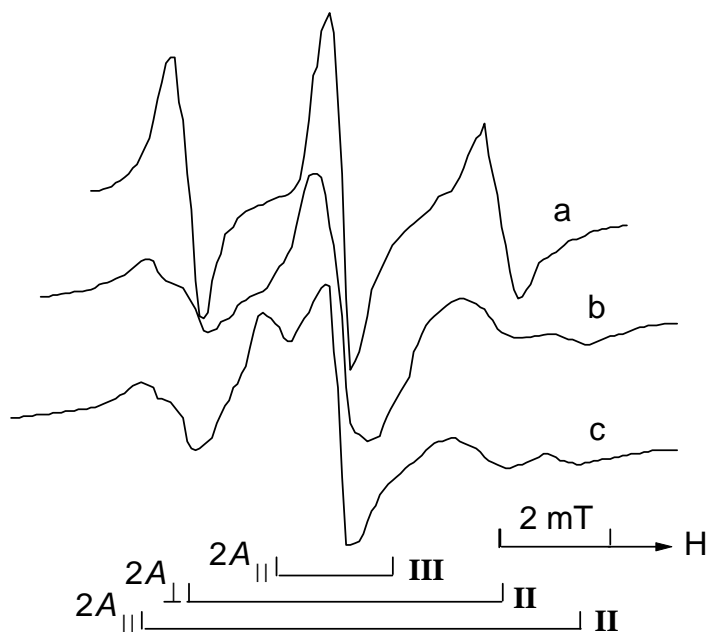
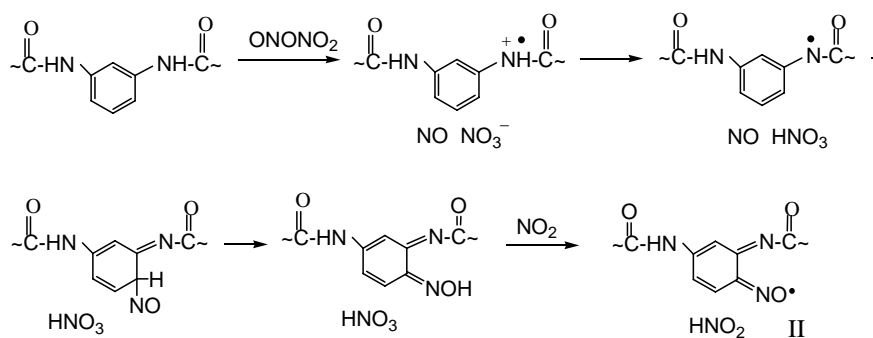


Figure 1. EPR spectra of BQ + SiO₂ after exposure to NO₂ (a); BQ + AP + SiO₂ (b) and BQ + PVP + SiO₂ (c) after preliminary exposure to NO₂ and subsequent pumping-out.

The results obtained are shown in Figure 2a and 2b. As is seen from the figures, the accumulated concentration of radicals I monotonously falls as the relative contents of AP and PVP is increased, while concentrations of radicals II and II + III vary within 10 - 20 % of the average value, that is within the accuracy of integration of EPR spectra. This fact is indicative of obvious dependence of the radical I yield on the contents of polymers with amide groups in composites, suggesting that PD is converted under the influence of amide groups into NN that generates stable radicals II and III in the polymeric phases. It is significant that an appreciable decrease of the yield of radicals I was not observed in control experiments when polymers of other chemical structure, for example, acetyl cellulose were used in composites. Therefore one can conclude that amide groups play special role in the process PD → NN.

Taking into account scheme (1, 2), the radical II formation in AP can be presented as follows:



(6)

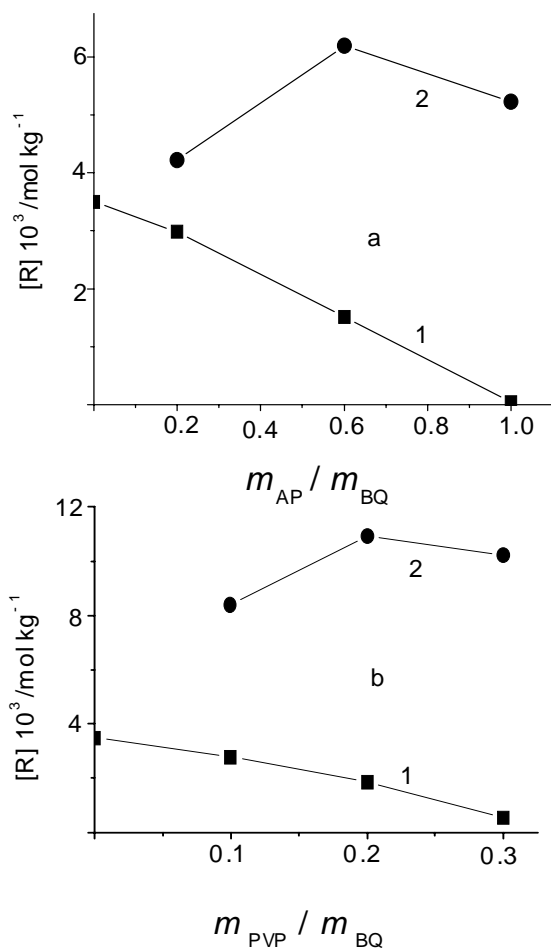
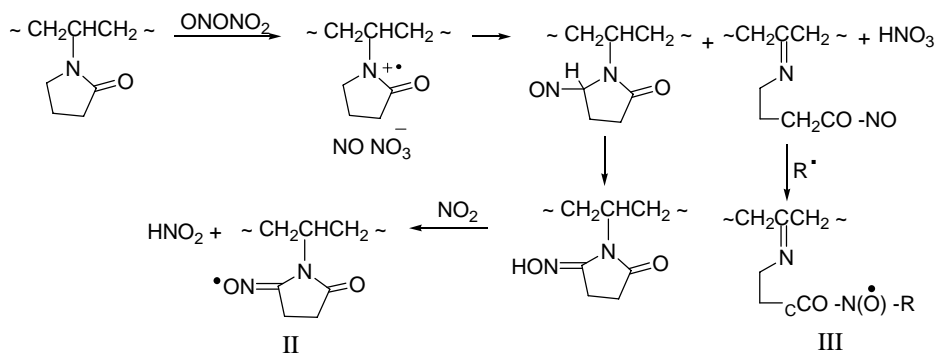


Figure 2. Dependencies of concentrations of radicals I (1), II (2) in BQ + AP + SiO₂ (a) and I (1), II + III (2) in BQ + PVP + SiO₂ (b) after exposure to NO₂ on weight ratio of BQ, AP and PVP.

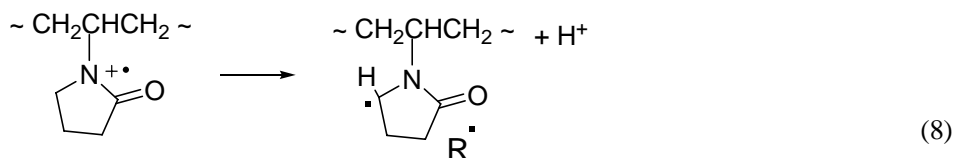
The structure of radicals II is confirmed by quantum-chemical calculations of hyperfine interaction constants [9].

The formation of radicals II and III in PVP can be described by the following reactions:

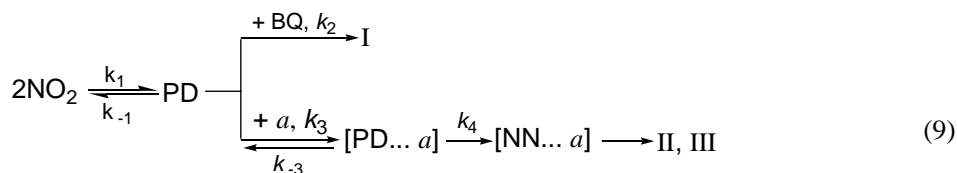


(7)

where R^\bullet appears as a result of the radical cation decomposition:



The decrease of relative yield of radicals I on addition of polymers with amide groups to composites is apparent from the formal kinetic scheme:



where a is an amide group. Taking into consideration stationary state for concentrations of PD, NN, $[\text{PD}\dots a]$, $[\text{NN}\dots a]$ and invariance of BQ contents in composites, the following equations for rates of accumulation of radicals I, II and III can be obtained:

$$\frac{d[\text{I}]}{dt} = \frac{k_1 k_2 [\text{BQ}] (k_{-3} + k_4) [\text{NO}_2]^2}{(k_{-3} + k_4) (k_{-1} + k_2 [\text{BQ}] + k_3 [a]) - k_{-3} k_3 [a]} \quad (10)$$

$$\frac{d[\text{II, III}]}{dt} = \frac{k_1 k_3 k_4 [a] [\text{NO}_2]^2}{(k_{-3} + k_4) (k_{-1} + k_2 [\text{BQ}] + k_3 [a]) - k_{-3} k_3 [a]} \quad (11)$$

where $[\text{NO}_2]$ is the concentration of nitrogen dioxide in gas phase, $[a]$ is the surface concentration of amide groups. These equations can be simplified if concentrations of amide groups in composites are comparatively large, and the conversion of PD into NN occurs enough effectively, that is $k_3 [a] \gg k_{-1} + k_2 [\text{BQ}]$. Then

$$\frac{d[\text{I}]}{dt} = \frac{k_1 k_2 [\text{BQ}] (k_{-3} + k_4) [\text{NO}_2]^2}{k_3 k_4 [a]} \quad (12)$$

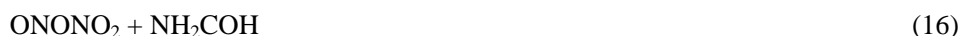
$$\frac{d[\text{II, III}]}{dt} = k_1 [\text{NO}_2]^2 \quad (13)$$

Thus the rate of accumulation of radicals II and III is determined by $[\text{NO}_2]$, and concentrations of these radicals, accumulated on exposure to nitrogen dioxide, not depend appreciably on AP and PVP contents (Figure 2 a, b (curve 2)). In contrast, the yield of radicals I decreases as polyamides are added to composites and $[a]$ is increased. These plots

in character are representative of competitive pathways for PD interactions with BQ and amide groups. Note that the yield of radicals I is not changed in the NO_2 atmosphere in composites of BQ with other polymers, for instance, acetyl cellulose at any ratio of the components.

III. 2. Ab Initio Calculations of Energies for Conversions of Nitrogen Dioxide Dimers

For validating the mechanism proposed of the conversion of PD into NN, the calculations of energy changes in process of nitrogen dioxide interaction with simplest amide (formamide) have been carried out within the framework of density functional theory by the Gaussian 98 program [17]. The B3LYP restricted method for closed and open shell was used. The intention of the calculations is to correlate energy consumptions for $\text{PD} \rightarrow \text{NN}$ with those for other stages of the radical generation process. Energies of the following states according to scheme (9) were calculated:



The geometry optimization of all structures was performed applying the basis set 6-31G (d, p). The given process includes intermediate molecular complexes of PD and NN with formamide (17, 18). The changes of minimum energies are shown in Figure 3 a. One can see that the formation of PD from NO_2 is energetically advantageous process [8], whereas NN is generated from NO_2 in an endothermic reaction. The complexation of PD with formamide is accompanied by release of energy: $\Delta E = 28 \text{ kJ}\cdot\text{mol}^{-1}$. However, PD in complex (17) is not capable to react with formamide and can only leave the reacting cage. At the same time, PD in the complex can be converted approximately with the same energy consumption into NN (18), which further reacts by the electron transfer reactions (19, 20) giving radicals, nitric oxide, nitric acid and significant release of energy ($44\text{-}57 \text{ kJ}\cdot\text{mol}^{-1}$). Such sequence of transformations seems to be more efficient in comparison with a direct interaction of NN and formamide in state (15), as the energy of dimers in complexes (17) and (18) is lower than that of initial state (14). Thus the results of calculations are not contrary to the mechanism proposed on the basis of experimental plots of Figure 2.

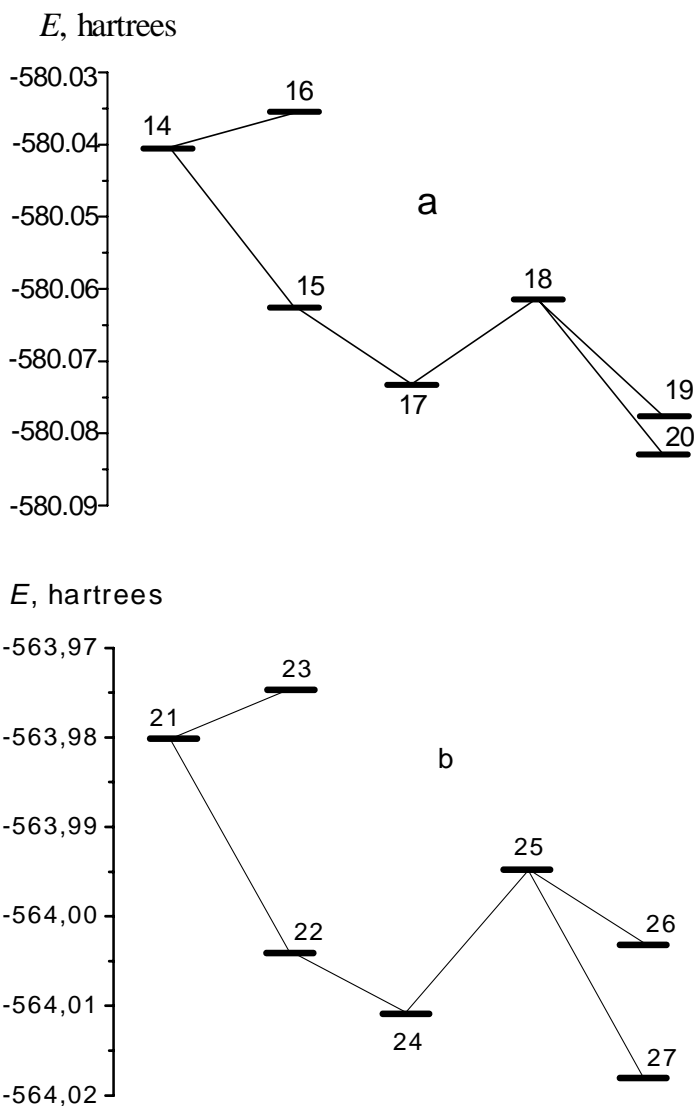


Figure 3. Changes of minimum energies calculated for reactions of NO₂ with formamide (a) and acetaldehyde (b).

The specific role of amide groups of macromolecules in the process of PD into NN conversion is also apparent from similar calculations performed for interaction of the dimers with different functional groups, for instance, carbonyls. The results of calculations for the following reaction stages of the nitrogen dioxide interaction with acetaldehyde

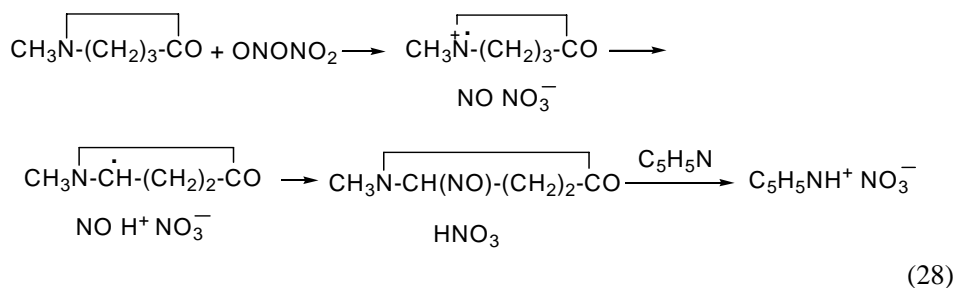




are represented in Figure 3 b. There are principal distinctions associated with capability for isomerisation of PD into NN in complexes (17) and (24). As indicated by Figure 3 b, this process for complex (24) necessitates additional expenditure of $\sim 24 \text{ kJ}\cdot\text{mol}^{-1}$ as compared with the energy for transforming (24) into (22) with an exit of PD from reacting cages. Thus the coordination of PD with polar carbonyl groups can make difficulties for conversion of PD into NN.

III. 3. Detection of Intermediate Radical Cations in Reactions of NN

The registration of radical cations by EPR could serve as a direct experimental evidence of the initiation of radical processes by scheme (1). However in view of high reactivity and fast decomposition [18], these intermediates are difficult to detect by this method. Nevertheless, the formation of radical cations can be discovered indirectly in their decomposition accompanied by proton elimination. For detection of protons, we used pyridine, which is known to be capable of accepting protons to yield pyridinium cations. These products can be easily identified from their typical IR spectrum. Note that pyridine does not react directly with NO_2 [19] and can serve only as a trap of protons formed in ion-radical reactions (1). Figure 4 shows IR spectra of mixtures 1:1 of pyridine and *N*-methylpyrrolidone (low-molecular analogue of PVP) before and after exposure to nitrogen dioxide. After 30 min exposure, two intense bands were observed in the spectrum (2) at 2400-2600 and 2200 cm^{-1} corresponding to the NH^+ stretching vibrations of pyridinium cations [20]. The scheme of reactions proceeding in this system includes the consecutive stages:



It appears that nitrogen dioxide can exhibit a noticeable activity for radical generation by an ion-radical mechanism discussed above selectively, namely, in the polymers containing functional groups which assist $\text{PD} \rightarrow \text{NN}$ conversions.

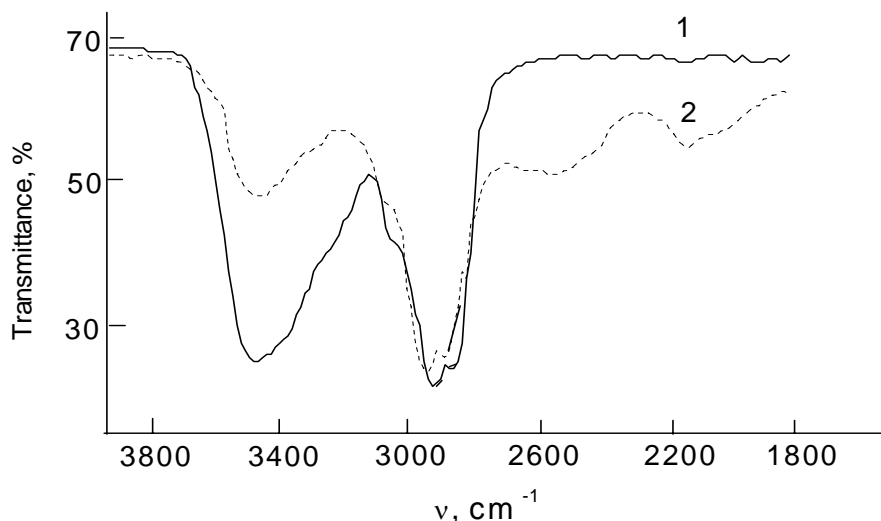


Figure 4. IR spectra of 1:1 *N*-methylpyrrolidone and pyridine mixture (1) and after exposure the mixture to NO_2 (2).

CONCLUSIONS

Amide groups are capable to induce isomerisation of planar dimers of NO_2 into nitrosyl nitrate having pronounced oxidative properties. Nitrosyl nitrate initiates a number of consecutive radical reactions with formation of nitrosation products and stable nitrogen-containing radicals. Most likely, the conversion is realised due to specific interactions of the dimers with amide groups of macromolecules. These interactions can provoke high activity of nitrogen dioxide in reactions even with such stable polymers as aromatic polyamides.

REFERENCES

- [1] Titov A. I. The free radical mechanism of nitration. *Tetrahedron* 1963; 19: 557-70.
- [2] Jellinek H. H. G. *Aspects of Degradation and Stabilization of Polymers*. New York: Elsevier; 1978.
- [3] Pariiskii G. B., Gaponova I. S., Davydov E. Ya. Reactions of nitrogen oxides with polymers. *Russian Chem. Rev.* 2000; 69 (11): 985-99.
- [4] Calvert J., Pitts J. *Photochemistry*. New York: Wiley; 1966.
- [5] Pokholok T. V., Pariiskii G. B. Formation of spin-labeled macromolecules in reactions of elastomers with nitrogen dioxide. *Polymer Science, Ser A* 1997; 39 (7): 765-71.
- [6] Giamalva D. H., Kenion G. B., Church D. F., Pryor W. A. Rates and mechanisms of reaction of nitrogen dioxide with alkenes in solution. *J. Am. Chem. Soc.* 1987; (109): 7059-63.
- [7] Park J. S. B., Walton J. C. Reactions of nitric oxide and nitrogen dioxide with functionalised alkenes and dienes. *J. Chem. Soc., Perkin Trans. 2* 1997; 2579-83.

-
- [8] Golding P., Powell J. L., Ridd J. H. Reactions of nitrogen dioxide with hexenes. The mechanistic and structures factors controlling the product composition. *J. Chem. Soc., Perkin Trans. 2* 1996; 813-19.
- [9] Pokholok T. V., Gaponova I. S., Davydov E. Ya., Pariiskii G. B. Mechanism of stable radical generation in aromatic polyamides on exposure to nitrogen dioxide. *Polym. Degrad. Stab.* 2006; 91 (10): 2423-28.
- [10] White E. H. The chemistry of the *N*-nitrosoamides. I. Methodes of preparations. *J. Am. Chem. Soc.* 1955; 77 (22): 6008-10.
- [11] Feuer H, editor. *The chemistry of the nitro and nitroso groups*. New York: Wiley; 1969.
- [12] Shoenbrunn E. F, Gardner J. H. Oxidation of isobutylene with dinitrogen tetroxide. *J. Am. Chem. Soc.* 1960; 82 (9): 4905-8.
- [13] Davydov E. Ya., Gaponova I. S., Pariiskii G. B. Generation of nitroxyl radicals in reactions of nitrogen dioxide with *p*-benzoquinones. *J. Chem. Soc. Perkin Trans 2* 2002; 1359-63.
- [14] Pauling L. *General Chemistry*. San Francisco: Freeman; 1958.
- [15] Gabr I., Symons M. C. R. Reactions of conjugated dienes with nitrogen monoxide end dioxide. *J. Chem. Soc., Faraday Trans.* 1996; 92 (10): 1767-72.
- [16] Royer R, Keinath S, editors. *Molecular motion in polymers by ESR*. Michigan: MMI press; 1979.
- [17] Frisch M. J, Trucks G. W., Schlegel H. B., Scuseria G. E., Robb M. A., Cheeseman J. R., et al. *Gaussian 98*. Pittsburgh PA: Gaussian Inc.; 1998.
- [18] Greatorox D., Kemp T. J. Electron spin resonance studies of photo-oxidation by metal ions in rigid mediaat low temperatures. Part 3. Ce(IV) photo-oxidations of aldehydes, ketones, esters and amides. *J. Chem. Soc., Faraday Trans.* 1972; 68 (1): 121-29.
- [19] Suzuki H., Iwaya M., Mori T. *C*-Nitration of pyridine by the kyadai-nitration modified by the Bakke procedure. A simple route to 3-nitropyridine and mechanistic aspect of its formation. *Tetrahedron Lett.* 1997; 38 (32): 5647-50.
- [20] Bellamy L. J. *The infra-red spectra of complex molecules*. London: Methuen; 1957.

Chapter 3

ADDITION OF OZONE TO MULTIPLE BONDS: COMPETITION OF THE REACTION PATHWAYS

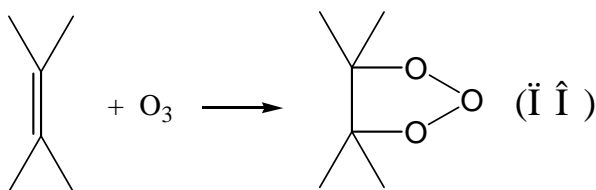
B. E. Krisyuk* and A. A. Popov**

*Institute of Problems of Chemical Physics,
Russian Academy of Sciences, Chernogolovka,
Moscow District, Russia

**Emanuel Institute of Biochemical Physics,
Russian Academy of Sciences, Moscow, Russia

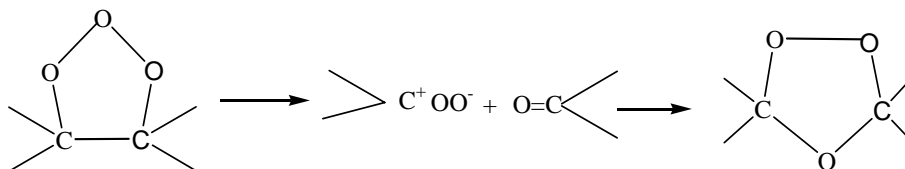
1. INTRODUCTION

Interaction of ozone with a double bond is one of the most specific reactions of unsaturated compounds. This reaction is widely used in quantitative and qualitative analyses, synthesis, and chemical technology [1–3]. It is one of the best-studied reactions, which is described in hundreds of works and dozens of reviews and monographs published in the past 40 years [1–6]. The mechanism of this reaction was studied both theoretically and experimentally during the past 50-60 years; until recently, it has been considered as an unambiguously established one. Many authors consider it as a classic example of simultaneous (coordinated) 1.3-addition with the formation of five-membered cyclic primary ozonide in the first event (the Kriege mechanism [7]):



* Boris Eduardovich Krisyuk, Dr.Sc.(Chem.), *Leading Researcher* Areas of scientific interests: theoretical chemistry, kinetics; e-mail: bkris@mail.ru

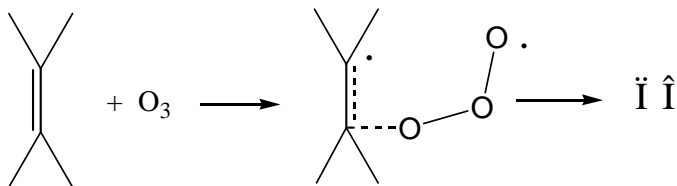
At moderate temperatures, PO is unstable and decomposes readily into a bipolar ion and a carbonyl compound (aldehyde or ketone), which, in turn, recombine and form normal ozonide:



This reaction scheme was supported by numerous direct and indirect experimental data. At low temperatures, primary ozonide was obtained [8]; under the action of ozone on asymmetrical olefins, cross ozonides are formed [9]. This scheme and arguments for it were analyzed in detail in [1, 2].

Some other schemes of the process were suggested, but they were rejected for various reasons. At present, the problem under discussion is whether the reaction proceeds as coordinated addition or by two stages through the intermediate biradical state. Most often, it is assumed that the former mechanism prevails for solutions; the latter one, for the gas phase [4–6, 10, 11]. However, at present, the mechanism of coordinated addition is considered prevailing for the gas phase too [12–14].

The reaction mechanism, according to which ozone reacts with a double bond like a peroxide radical and forms intermediate biradical, was suggested in [15] for the reaction with acetylene in an effort of elucidating the difference in its Arrhenius parameters and parameters for the reaction of ozone with ethylene:



Later, the reaction with acetylene was studied by more advanced methods of quantum chemistry and this reaction mechanism was rejected [16]. However, this mechanism may account for the formation of such products as oxides and aldehydes as a result of decomposition of molozonide. In favor for this mechanism, other arguments may be suggested; an analysis of them was made in [17].

2. MODERN CONCEPTS ON THE REACTION MECHANISM

At present, there is an opinion that the first stage of the reaction proceed by another pathway. First of all, the reaction for ethylene and acetylene proceeds through formation of an intermediate weakly-bound complex, which was determined experimentally and theoretically [12–14, 16, 18]. Similar complexes were determined by methods of quantum chemistry for ozone with cis- and trans-butene-2 [19]. In [20], by approximation of the restricted Hartree–

Fock method (RHF), the shape of the potential plane of the reaction of ozone with ethylene was calculated; it was shown that the reaction proceeding through asymmetric states in the region of transient state is not energy-advantageous with the basic singlet state of the reagents. In the coordinated addition, the potential plane of the reaction between the initial reagents and PO has two extrema: the minimum refers to the formation of a π -complex with an asymmetrical structure and equal C...O (R_{CO}) distances of the order of 2.6–3.5 Å and the maximum refers to the symmetrical transient state with R_{CO} of the order of 2 Å [12–14, 16–20]. The energy diagram of the reaction of ozone with multiple bonds is shown in Figure 1. Thus, results of the recent studies are in favor of the mechanism of coordinated addition with the formation of an intermediate complex of ozone with a multiple bond.

However, the calculations were performed in terms of the restricted Hartree–Fock method (i.e., with a strictly-defined zero spin) in the one-determinant approximation. This approach may account for a loss of solutions for cases of complex systems where the spin squared deviates from zero although all reagents are in the singlet state. Hence, this solution may have the physical meaning [21], as is the case with ozone. In the literature, these cases are considered as unstable Hartree–Fock's solutions. In [22], calculations were performed with allowance for this condition in terms of the unrestricted Hartree–Fock (UHF) method; the calculations showed that the reaction may proceed by non-coordinated addition but with the induction of higher-spin states ($S^2 = 0.7–1.2$).

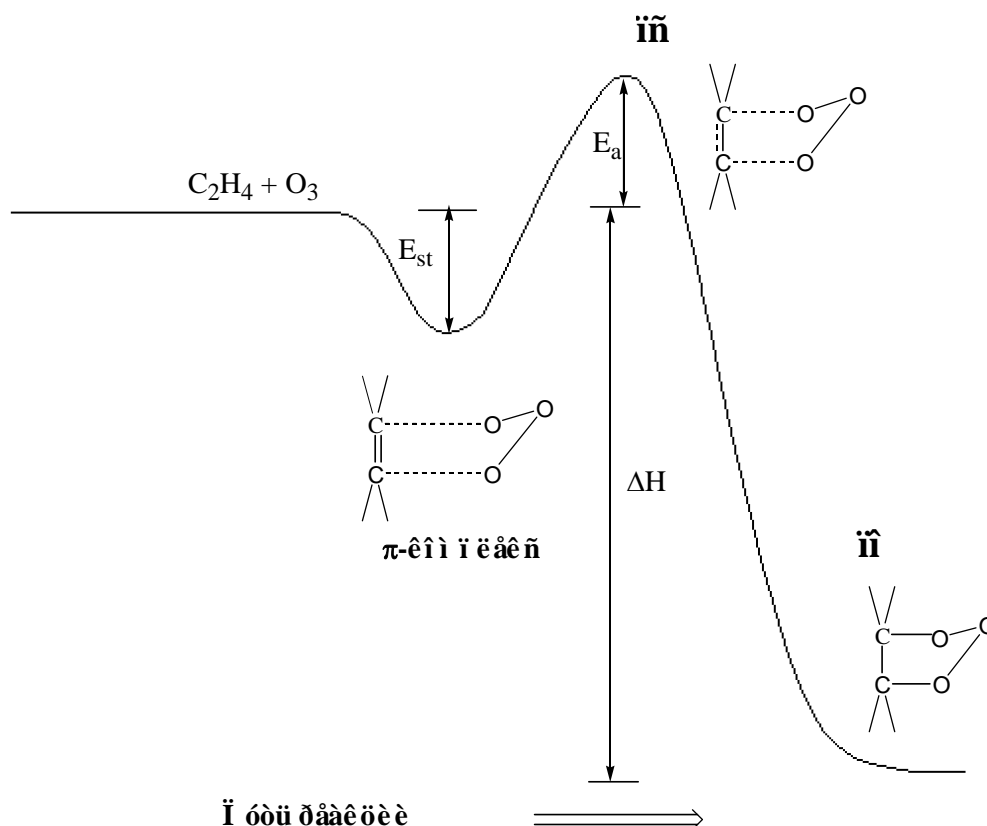
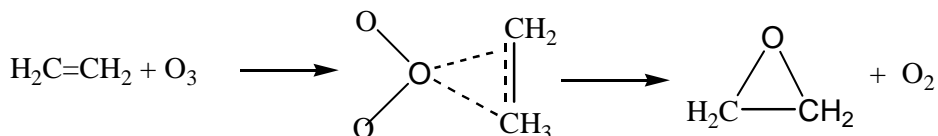


Figure 1. Energy diagram of addition of ozone to ethylene.

In [23], another reaction pathway was analyzed: where ozone attacks ethylene with its central atom:



The authors [23] applied the method of density functional (exchange-correlation functional B3LYP) and calculated the profiles of the potential energy for the interaction of ozone with ethylene. It was shown that, according to the scheme of ozonolysis of ethylene, the reaction pathway through the direct epoxidation of the double C=C bond requires high energy of activation and is improbable, both for thermochemical and photochemical reactions of ozonolysis.

In spite of the progress in investigating the mechanism of the reaction of ozone with multiple bonds, another pathway of the reaction mentioned in [16], in which ozone is the donor of atomic oxygen, has not been studied yet.

In many reactions, ozone behaves as a radical¹. For example, the reaction of ozone with saturated hydrocarbons proceeds with detachment of a H atom [25, 26]. This fact was supported by the following data [27]:

- 1) Ozonolysis of alkanes and polymers results in formation of free radicals.
- 2) Ozone initiates chain oxidation of hydrocarbons both in the liquid and gaseous phases.
- 3) The isotope effect correlates with the strength of C-H and C-D bonds.

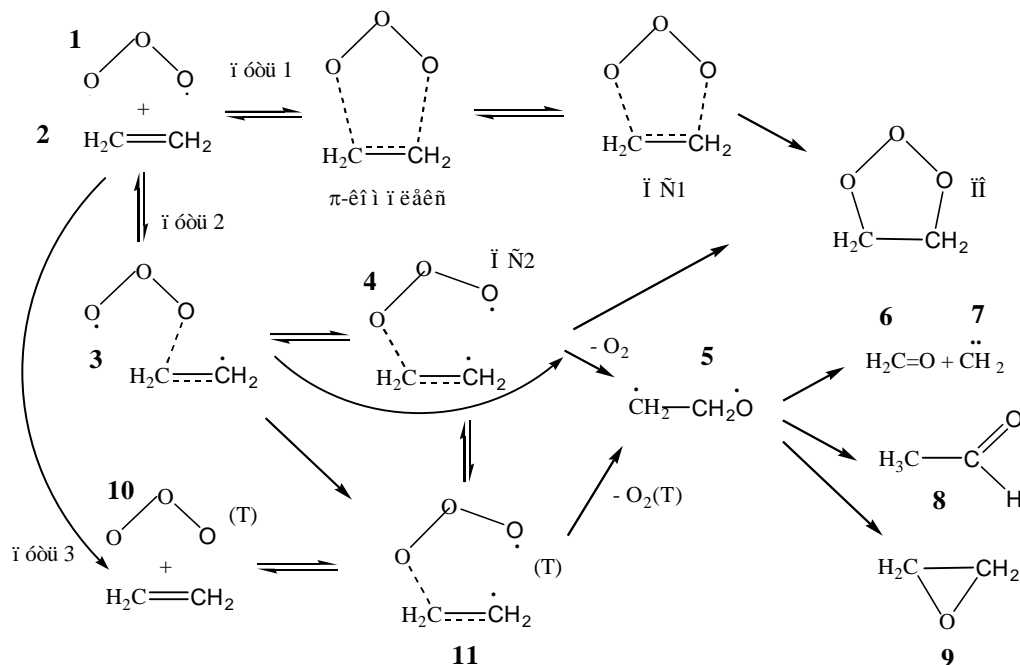
Consequently, ozone is a H atom acceptor similar to methyl radical or halogen atoms. This is evidence for the biradical nature of ozone and, hence, for a principal feasibility of the reaction proceeding through an intermediate biradical state by analogy with peroxide radical reactions. It may be expected that ozone as biradical may change to the triplet state readily; the mechanism of the reaction through triplet states has not been elucidated yet.

Thus, to sum up the above data and suppositions, the scheme of the first stage of the interaction of ozone with ethylene may be represented as follows:

Here, pathway 1 (reaction 1) is the coordinated addition of ozone (1) to ethylene (2), which proceeds through the formation of a weakly-bound complex that transforms into primary ethylene ozonide (PO) or 1.2.3-trioxolene upon passing through the symmetrical transient state (TS1). Pathway 2 (reaction 2, the DeMore mechanism [15]) involves the collision during spontaneous orientation of the reagents (3) and the rotational transition to the biradical transient state (TS2) (4) followed by the formation of the same PO. Proceeding from the above-said, we supplement this pathway with the reaction of detachment of molecular oxygen and the formation of intermediate biradical (5); the latter may either decompose with the formation of formaldehyde (6) and carbene (7) or transform into acetaldehyde (8) or epoxide (9). Finally, pathway 3 involves the transition of ozone into the triplet state (10). This pathway is similar to reaction 2. Here, the same biradical (5) is formed; it transforms into the

¹ The basic state of ozone is a superposition of zwitterion and biradical; the share of the latter reaches 100% [24].

products (6–8). The aim of this work is to compare different pathways of the reaction using data of the nonempirical quantum calculations.



3. CALCULATION METHODS

The calculations were performed at the IPCP Computer Center on a CLI 16-processor cluster that incorporates four 4-processor units of 64-digit Intel Itanium 2 1.5 GHz processors with the cash 4 MB, 20 GB, HDD SCSI 3 x 146 GB 10,000 rpm. In the quantum calculations, we used a GAUSSIAN-03 program [28], *ab initio* HF and MP2 methods involving the restricted and unrestricted Hartree–Fock (RHF and UHF, respectively) methods, and the density functional B3LYP method involving the restricted and unrestricted Cone–Scham methods (DFT analogs of RHF and UHF). In all cases, we applied a 6-31G set of basic functions. The parameters of states corresponding to the potential plane minima were determined by complete optimization of all variables; the transient states were determined from the complex and ozonide geometries. The zero fluctuation frequencies were calculated at the extreme points of the potential plane. The calculations for the initial and transient states were performed by the MCSCF method. The thermodynamic parameters of the reaction were determined from results of the quantum calculations using the MOLTRAN program developed by S.K. Ignatov [29].

The shape of the potential plane in proximity to the transient state was determined by points. In this case, calculations were performed at given pairs of R_{CO} distances with other coordinates being optimized. The values of R_{CO} were varied from 1.8 to 3.1 Å for each pair of atoms (R_1, R_2); thus, a two-dimensional data file was obtained: the full energy as a function of two distances $U(R_1, R_2)$. Then, this data file was described by a plane passing through the

calculated points. To plot a graph, we passed a section through the plane obtained at a constant energy – the isoline.

4. OZONE+ETHYLENE REACTION

4.1. Initial Substances

The ethylene molecule is stable with highly occupied orbitals. The triplet state is high and, as may be expected, the UHF calculations performed show the same result: the energy does not vary and remains in the singlet state with a zero spin. The total energy U and the reacting bond length R_{CC} calculated by different methods are listed in Table 1.

For ozone, the situation is different. Here, solution of the one-determinant problem yields two states: one with a zero S^2 and another with $S^2 = 0.4-1.2$ depending on the calculation technique. Therefore, the UHF calculations yield different results. The UHF and UB3LYP calculations show a lower energy of the molecule and stability of solutions. In this case, the states geometry is other than that determined by RHF and the spin squared is about 1 (UHF) or 0.4 (UB3LYP) (Table 2). After the annihilation procedure, S^2 are 0.10 and 0.004, respectively. The MP2 method does not yield such solutions for ozone. The reason may be a known specificity of the MP2 method: it yields a too high energy of states with open shells.

The ozone triplet state is higher than the singlet one stabilized at 80 kJ/mol (UB3LYP); its geometry differs from that of the singlet state. The valence angle increases to 130° . Here, $S^2 = 2$; as might be expected, after the annihilation procedure, S^2 remains unchanged.

The above results show that application of the one-determinant approximation to ozone in the *ab initio* methods results in significant errors and an abnormal spin squared. The DFT approximation is more efficient. The validity of the results may be verified in terms of the multi-determinant approximation.

Table 1. State parameters of ethylene

Method	Basis	R_{CC} , A	U , Hartree
HF	6-31G**	1,3165	-78,0388415
	6-31+G**	1,3208	-78,0430662
	6-311G**	1,3165	-78,0547235
	6-311+G**	1,3185	-78,0560772
B3LYP	6-31G**	1,3301	-78,5938076
	6-31+G**	1,3341	-78,5996455
	6-311G**	1,3269	-78,6139783
	6-311+G**	1,3288	-78,6155126
MP2	6-31G**	1,3352	-78,3172813
	6-31+G**	1,3392	-78,3231984
	6-311G**	1,3373	-78,3442916
	6-311+G**	1,3392	-78,3463029

Table 2. State parameters of ozone

Method	Basis	$R_{OO, A}$	α	S^2	U , Hartree
HF	6-31G**	1,204	119,0	0	-224,2614365
	6-31+G**	1,204	119,2	0	-224,2688212
	6-311G**	1,194	119,2	0	-224,3226419
	6-311+G**	1,194	119,4	0	-224,3296045
UHF	6-31G**	1,295	111,6	0,955	-224,3375691
	6-31+G**	1,293	111,8	0,956	-224,343609
	6-311G**	1,284	112,0	0,951	-224,3984805
	6-311+G**	1,284	112,2	0,953	-224,4052178
CAS triplet	6-311G**	1,284	112,0	0	-224,4708544
	6-311G**	1,241	131,2	2,064	-224,3093288
B3LYP	6-31G**	1,264	117,9	0	-225,4064536
	6-31+G**	1,263	118,1	0	-225,419503
	6-311G**	1,258	118,2	0	-225,4707934
	6-311+G**	1,256	118,4	0	-225,48056
UB3LYP triplet	6-31G**	1,287	115,9	0,415	-225,4095947
	6-31+G**	1,285	116,3	0,394	-225,4222195
	6-311G**	1,281	116,3	0,408	-225,4738096
	6-311+G**	1,279	116,6	0,395	-225,483326
	6-311G**	1,297	129,6	2,012	-225,4377512
MP2/UMP2	6-31G**	1,300	116,3	0	-224,8695447
	6-31+G**	1,301	116,5	0	-224,8861916
	6-311G**	1,282	116,8	0	-224,978195
	6-311+G**	1,282	117,1	0	-224,9916749
CAS triplet	6-311G**	1,282	116,8	0	-224,9386337
	6-311G**	1,274	129,3	2,076	-224,9042515

The results of MCSCF/6-311G** calculations for ozone (CAS(x,y) for “x” electrons and “y” MO) are shown below:

Method	Energy, a.u.
RHF	-224,3226373
CAS(2,2)	-224,3297811
CAS(4,4)	-224,4323912
CAS(6,6)	-224,470855
CAS(8,8)	-224,5277802
MP2	-224,9612847

The MCSCF calculations showed that two MO in ozone are single-occupied, i.e., it is more advantageous for electrons to occupy spatially separated orbitals. This means that ozone in the basic state is singlet biradical. Hence, deviation of S^2 from zero is a result of solution of a two-statement problem in the one-determinant approximation; the solution is real and not a calculational artefact. Consequently, the UB3LYP results are reliable and we will analyze data obtained by this method.

4.2. Complex

The convergence of reagents until induction of a transient state results in the formation of a weakly bound π -complex. According to the above-cited works, the complex structure is symmetrical with $R_1 = R_2 \sim 2.5\div 3.6$ Å depending on the calculation method. The complex structure is shown in Figure 2. However, an analysis of the complex showed that solutions relative to the RHF \leftrightarrow UHF transition are unstable both for the complex and initial ozone. The change-over to UB3LYP in the DFT calculations showed a lower total energy of the system and stabilization of solutions. The decrease in the energy of the symmetrical complex without optimization of its geometry is ~ 5 kJ/mol at the B3LYP level (Table 3).

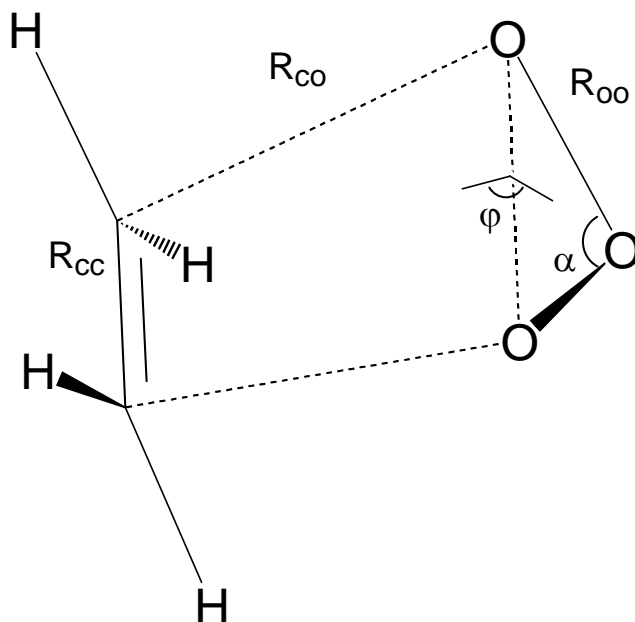


Figure 2. Structure of π -complex and transient state in the coordinated (TS1) addition of ozone to ethylene.

Table 3. Parameters of ozone+ethylene complex

Method	Basis	$R_1=R_2$, Å	R_{OO} , Å	R_{CC} , Å	α	S^2	U , Hartree
B3LYP	6-31G**	2,625	1,275	1,344	116	0	-304,00553
	6-31+G**	2,705	1,274	1,345	116,4	0	-304,022243
	6-311G**	2,66	1,267	1,339	116,6	0	-304,089716
	6-311+G**	2,75	1,265	1,339	116,9	0	-304,099168
UB3LYP	6-31G**	2,846	1,286	1,337	115,7	0,313	-304,006715
	6-31+G**	3,03	1,284	1,338	116	0,326	-304,023487
	6-311G**	2,874	1,279	1,333	116,1	0,313	-304,090941
	6-311+G**	3,041	1,278	1,333	116,4	0,332	-304,100568

4.3. Transient State

To verify whether the solutions for TS are unique or not and to determine the type of TS, we studied the pattern of the potential energy plane (PEP) of the ozone–ethylene reaction. The shape of this plane in the TS phase was determined by the HF [20], UHF, and UB3LYP methods [30] as a dependence of the energy U on two variables R_1 and R_2 (R_{CO} values for each pair of carbon and oxygen atoms).

In [20], the RHF calculations showed that the PEP has one saddling point in the TS region; this point corresponds to symmetrical TS with $R_1 = R_2 = 2.165$ Å. The TS structure is similar to that of the π -complex; schematically, it is shown in Figure 2 (TS1). Consequently, for the intreraction of ozone with ethylene considered in the one-determinant approximation (where $S^2 = 0$), the reaction pathway through the formation of symmetrical TS is more energy-advantageous.

Table 4 shows the energies and geometries of symmetrical transient states. Similar results were reported in [12–14, 20, 22].

The calculations with open shells showed a drastically different PEP pattern. Here, the reaction pathway is different (through the asymmetrical TS with coordinates about 1.9 and 3.1); according to the UB3LYP data, PEP has two saddles. Here, the reaction pathway from the complex to ozonide is feasible both through symmetrical and asymmetrical TS (Figure 3).

Figure 4 shows the TS geometry determined by methods applicable to cases with open shells. This state is asymmetrical and of the biradical nature; this is evidence for the reaction proceeding by the mechanism described in [15]. This state may be referred to as TS2; its parameters are listed in Table 5.

Table 4. TS1 parameters

Method	Basis	$R_1 = R_2$	R_{OO}	R_{CC}	E_{act} , kJ/mol
HF	6-31G**	2,164	1,239	1,362	59,06
	6-31+G**	2,164	1,239	1,365	66,61
	6-311G**	2,149	1,232	1,365	63,31
	6-311+G**	2,153	1,232	1,366	68,69
CAS	6-311G**	2,149	1,232	1,365	269,85
B3LYP	6-31G**	2,348	1,288	1,359	-13,05
	6-31+G**	2,339	1,291	1,364	-6,56
	6-311G**	2,274	1,288	1,363	-10,43
	6-311+G**	2,276	1,289	1,366	-4,66
UB3LYP	6-31G**	2,348	1,288	1,359	-4,81
	6-31+G**	2,339	1,291	1,364	0,57
	6-311G**	2,274	1,288	1,363	-2,51
	6-311+G**	2,276	1,289	1,366	2,61
MP2(UMP2)	6-31G**	1,986	1,329	1,392	15,14
	6-31+G**	1,987	1,334	1,396	13,76
	6-311G**	1,965	1,311	1,397	27,29
	6-311+G**	1,973	1,313	1,399	24,88

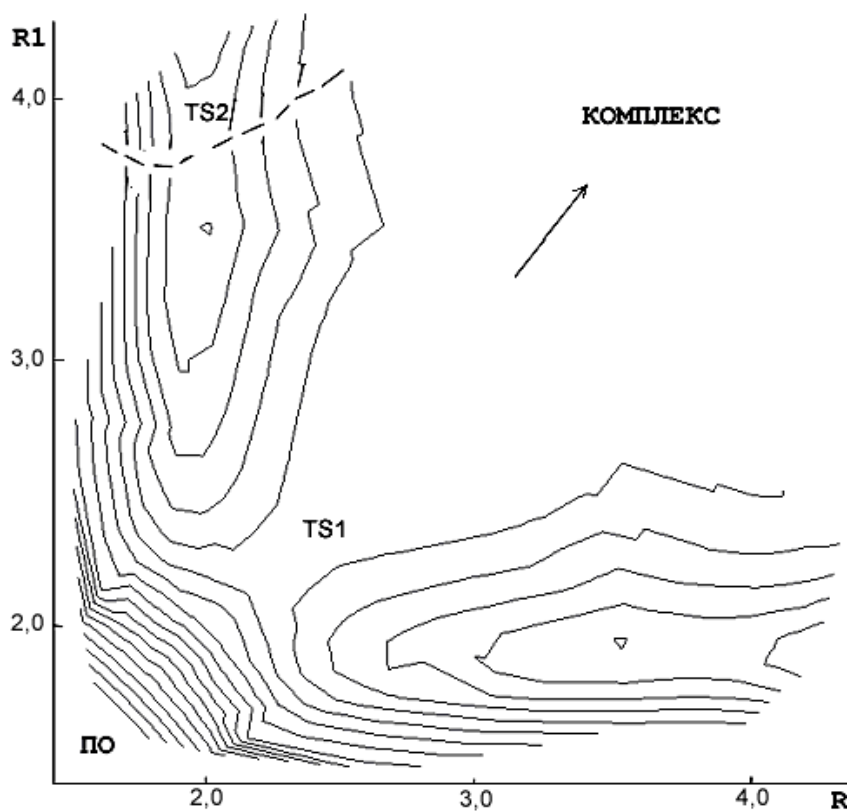


Figure 3. Plane of potential energy in the region of TS in the interaction of ozone with ethylene; UB3LYP calculations.

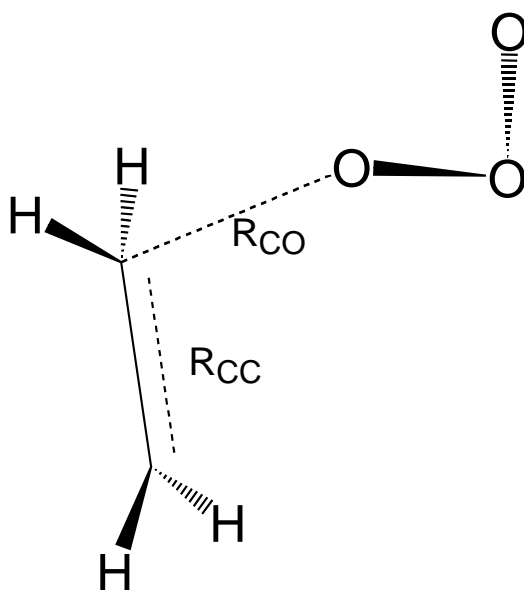


Figure 4. Transient state ($TS2$) in the non-coordinated addition of ozone to ethylene.

Table 5. TS2 Parameters

Method	Basis	R_1	R_2	R_{Oo1}	R_{Oo2}	R_{CC}	S^2	α	E_a , kJ/mol
UHF	6-31G**	1,888	3,125	1,350	1,28	1,398	1,221	110,7	67,62
	6-31+G**	1,893	3,177	1,348	1,279	1,399	1,217	111	73,13
	6-311G**	1,881	3,123	1,339	1,27	1,398	1,212	111,2	72,58
	6-311+G**	1,885	3,181	1,338	1,27	1,398	1,216	111,3	76,08
	triplet 6-311G**	1,913	3,922	1,350	1,28	1,394	2,26	109,7	35,96 ²
UMP2	6-31G**	2,019	3,051	1,369	1,287	1,342	1,207	112,1	207,18
	6-31+G**	2,024	3,150	1,370	1,286	1,344	1,202	112,5	212,57
	6-311G**	1,995	3,035	1,355	1,266	1,347	1,198	112,7	208,72
	6-311+G**	2,002	3,122	1,355	1,266	1,347	1,197	113	212,45
	triplet 6-311G**	2,061	3,802	1,400	1,284	1,336	2,22	110,1	237,51 ¹
UB3LYP	6-31G**	1,947	3,911	1,374	1,29	1,376	0,718	113,9	15,75
	6-31+G**	1,944	3,945	1,377	1,29	1,381	0,726	113,9	20,49
	6-311G**	1,926	3,902	1,379	1,282	1,377	0,740	114	19,74
	6-311+G**	1,926	3,902	1,379	1,282	1,377	0,740	114	23,49
	triplet 6-311G**	1,926	3,902	1,379	1,282	1,377	2,02	114	52,22 ¹

The calculations on the frequency of oscillations showed that both TS1 and TS2 have the same imaginary frequency and are true transient states. Note that the TS2 geometry determined at all calculation levels is approximately the same but its energy determined by MP2 and B3LYP is a little higher (according to the HF data, lower) than that of TS1 (Tables 4, 5). As is seen from Tables 4 and 5, TS1 is a true singlet state ($S^2 = 0$) but TS2 has a higher spin squared ($S^2 = 0.7 \div 1.2$). After annihilating procedure, S^2 becomes nearly zero (0.005–0.03), like that for ozone. Figure 5 shows the energy profile of the this reaction pathway and changes in S^2 associated with it. It is evident that S^2 increases gradually and reaches 1 at a distance of C...O about 1.55 Å; here, it intercrosses with the triplet plane.

The reaction on the triplet plane is similar in many respects to that through TS but here it is limited by the singlet–triplet transition. For the initial ozone, this transition requires considerable energy (about 80 kJ/mol) and it hardly probable for a thermal reaction. When the reaction proceeds in the light, the transition is feasible upon absorption of a quantum of visible light [1]. As the reaction proceeds, the basic and triplet states levels converge but the planes intercross after TS2 (Figure 5). According to the UB3LYP data, the reaction on the triplet plane proceeds without a barrier (Figure 5) by detachment of triplet oxygen and formation of the same products as in the reaction with TS2 but without PO. It is the pathway, where ozone is a donor of molecular oxygen.

To verify the fact that the data obtained for TS2 are not an artefact, we performed the MCSCF calculations for both TS. In the calculations, we used two to eight MO. The calculation results showed that the change-over to MCSCF results in a decrease in the total energy of reagents (ozone) and TS. (Tables 4 and 5 show the results obtained for six MO; the results for other variants are similar).

² Relative to singlet ozone.

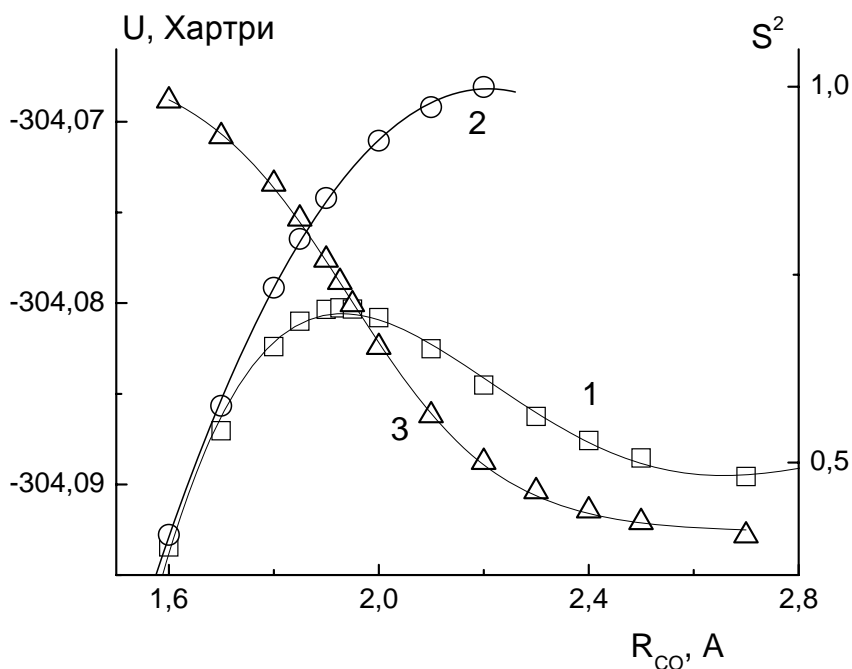


Figure 5. Change in the energy of the ethylene+ozone system by the pathway of non-coordinated addition (1) in the singlet and (2) triplet states and (3) change in the S^2 value in the former case; UB3LYP calculations.

Both for ozone and TS2, only two MO are single-occupied, which is evidence for the biradical nature of this TS. The anomalous value of S^2 obtained in the calculations performed in the one-determinant approximation is associated with this effect. For TS1, the MCSCF calculations showed that all MO are occupied by electron pairs; for this pathway, the one-determinant approximation is adequate. The MCSCF calculations showed that the energies of both TS are similar and both pathways may take place in parallel. Note that only the UB3LYP method describes adequately both TS.

The above data show that three pathways exist for the reaction of ozone with ethylene: coordinated and non-coordinated addition in the singlet state and a reaction in the triplet state. The latter pathway is hardly possible for the thermal reaction; the former two pathways exist in competition. To assess the efficiency of each pathway, we calculated the corresponding reaction rate constants. For this purpose, a MOLTRAN program and results of the quantum chemical calculations were used to calculate the enthalpies (ΔH^\ddagger) and entropies (ΔS^\ddagger) of activation of the two reaction pathways. From the data obtained, the corresponding rate constants k were calculated in terms of the standard transient state theory:

$$k = \frac{k_B T}{h} \cdot \frac{RT}{P_0} \cdot e^{-\frac{\Delta G^\ddagger}{RT}}$$

where P_0 is the standard pressure and h is the Planck's constant. The results obtained are listed in Table 6.

Table 6. Thermodynamic parameters of TS1 and TS2 (ΔH^\ddagger and ΔG^\ddagger in $\text{kJ}\cdot\text{mol}^{-1}$, ΔS^\ddagger in $\text{J mol}^{-1}\text{deg}^{-1}$) and corresponding values of rate constants k ($\text{l}^{-1}\text{s}^{-1}$). UB3LYP calculations

Reaction	Basis	ΔH^\ddagger	ΔS^\ddagger	ΔG^\ddagger	k
(1)	6-31G**	5,60	-166,65	50,48	$2,15\cdot 10^5$
	6-31+G**	5,63	-166,71	55,90	$2,41\cdot 10^4$
	6-311G**	5,85	-170,24	54,09	$5,01\cdot 10^4$
	6-311+G**	5,72	-157,88	55,39	$2,96\cdot 10^4$
(2)	6-31G**	1,61	-149,58	61,95	$2,10\cdot 10^3$
	6-31+G**	1,53	-153,43	67,76	$2,01\cdot 10^2$
	6-311G**	1,62	-155,04	67,58	$2,16\cdot 10^2$
	6-311+G**	1,68	-135,66	65,62	$4,78\cdot 10^2$

As is seen from Table 6, the reaction rate constants for both pathways are comparable and differ by 1 ÷ 2 order. This is evidence for simultaneous occurrence and competition of two pathways. The experimental reaction rate constant for 293 K is $1.77\cdot 10^{-18} \text{ cm}^3/\text{s}\cdot\text{molec}$ [31] or $1.07\cdot 10^3 \text{ l/s}\cdot\text{mol}$, i.e., approximately an average for these two pathways. On the whole, the assessment results point to the fact that the reaction for ethylene proceeds by 99% the mechanism of coordinated addition, which is consistent with the conclusions of the above-cited works.

5. OZONE + TETRAFLUOROETHYLENE REACTION

We studied the reaction of ozone with tetrafluoroethyne (TFE) by taking the suggested approaches. The reaction was analyzed in detail in [32], where it was shown that this reaction proceeds like that with ethylene. Here, the formation of a weakly bound complex also precedes TS. In this reaction, the PPE structure in the TS region was similar to that for ethylene; in the region of the complex, it is almost flat. The plane has two saddles (two transient states) – TS1 and TS2. As is the case with ethylene, TS1 is symmetrical ($R_1 = R_2 = 2.3 \text{ \AA}$); it corresponds to the reaction proceeding by the Kriege mechanism. The asymmetrical TS2 ($R_1 = 2.0, R_2 = 4.0 \text{ \AA}$) corresponds to the reaction proceeding by the DeMore mechanism.

Table 7 shows the electron contribution to the energy of activation determined from a GAUSSIAN-03 and the Gibbs energy of transient state calculated with the aid of a MOLTRAN program from the zero oscillation frequencies. Also, Table 7 shows the rate constant we determined for the symmetrical and asymmetrical reaction pathways and the experimental value borrowed from [33]. The latter value was obtained by the method of cryokinetic calorimetry (direct measurements on the rate constants of the reaction of TFE with pure ozone were performed at 90–150 K). The measurements showed that the rate constant may be described as follows:

$$k \approx 2\cdot 10^{-13} \cdot e^{1-10000/RT} \text{ cm}^3/\text{s}$$

A comparison of the calculated rate constants for two reaction pathways showed that the reaction (2) constant determined for 150 K agrees better with the experiment; k for the reaction (1) is considerably lower.

Table 7. Energies of activation of the reaction E_a (UB3LYP calculations), Gibbs energy of TS induction ΔG^\ddagger (kJ/mol), reaction rate constants k at 150K ($l^*(\text{mol}\cdot\text{s})^{-1}$) for the reaction of ozone with TFE

Basis	E_a	ΔG^\ddagger	k
Reaction 1			
6-31G**	5,9	58,08	$2,24\cdot 10^{-7}$
6-31+G**	19,59	72,25	$2,59\cdot 10^{-12}$
6-311G**	14,12	66,89	$1,90\cdot 10^{-10}$
6-311+G**	21,95	74,79	$3,37\cdot 10^{-13}$
cc-pvdz+	18,98	69,80	$1,84\cdot 10^{-11}$
Reaction 2			
6-31G**	4,99	45,92	$3,84\cdot 10^{-3}$
6-31+G**	14,19	56,90	$5,75\cdot 10^{-7}$
6-311G**	9,07	51,83	$3,34\cdot 10^{-5}$
6-311+G**	20,32	58,92	$1,14\cdot 10^{-7}$
cc-pvdz+	15,99	56,93	$5,64\cdot 10^{-7}$
Experiment[31]			$3,28\cdot 10^{-7}$


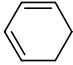
It should be noted that the k values showed in Table 7 do not include possible rotation of the ozone fragment in TS2 (see the text above). Using a MOLTRAN program, we evaluated the contribution of this rotation to the TS entropy. With allowance for the rotation, ΔG^\ddagger changes to 1.3 kJ/mol, which results in 2- to 3-fold increasing the calculated values of k for the reaction with TS2 ; for the reaction with TS1, k does not vary. Hence, the asymmetrical reaction pathway is more advantageous.

The above data show that the reaction pathway (2) is more advantageous for the reaction of ozone with TFE. According to these data, the share of the reaction proceeding by the MeMore mechanism is not less than 99%.

6. COMPETITION OF TWO PATHWAYS FOR REACTIONS OF OTHER COMPOUNDS

In [17], two approaches were taken to assess the role of each reaction pathway: quantum-chemical calculations and parabolic simulation of the reaction of addition (semiempirical method of intercrossing parabolas, MIP) [34-36]. Using these approaches in combination, the authors could evaluate independently the reaction rate constants for each pathway and compare their contributions to the total ozonation of olefins of different structures. The comparison results are listed in Table 8. We note a good agreement between the calculated and experimental constants values.

Table 8. Comparison of pathways 1 and 2 rate constants ($l\text{ mol}^{-1}\text{ s}^{-1}$, 300 K) calculated for reactions of olefins with ozone (liquid phase)

Olefin	$k(1)$ / share	$k(2)$	$k(1) + k(2)$	k_{exp}
$\text{CH}_2=\text{CH}_2$	1.17×10^5 / 100%	55.8	1.17×10^5	4.72×10^4
$\text{CH}_2=\text{CHMe}$	1.83×10^5 / 100%	17.8	1.83×10^5	1.40×10^4
$\text{CH}_2=\text{CHEt}$	1.83×10^5 / 100%	25.1	1.83×10^5	1.49×10^5
$\text{CH}_2=\text{CMe}_2$	6.45×10^5 / 100%	64.4	6.45×10^5	1.50×10^5
<i>E</i> - $\text{MeCH}=\text{CHMe}$	2.85×10^5 / 100%	32.1	2.85×10^5	
<i>Z</i> - $\text{MeCH}=\text{CHMe}$	2.85×10^5 / 100%	96.7	2.85×10^5	1.89×10^5
$\text{MeCH}=\text{CMe}_2$	9.78×10^5 / 100%	1.67×10^2	9.78×10^5	5.80×10^5
$\text{Me}_2\text{CH}=\text{CMe}_2$	3.11×10^6 / 100%	2.11×10^3	3.11×10^6	1.58×10^7
	2.85×10^5 / 100%	5.43×10^3	2.86×10^5	8.90×10^5
$\text{CH}_2=\text{CHPh}$	3.99×10^3 / 32%	8.52×10^3	1.25×10^4	3.48×10^5
$\text{CH}_2=\text{CMePh}$	2.14×10^4 / 72%	8.14×10^3	2.95×10^4	
<i>E</i> - $\text{MeCH}=\text{CHPh}$	6.53×10^3 / 50%	6.50×10^3	1.30×10^4	
$\text{CH}_2=\text{CPh}_2$	1.55×10^3 / 2.7%	5.54×10^4	5.69×10^4	
<i>E</i> - $\text{PhCH}=\text{CHPh}$	2.65×10^2 / 0.02%	1.12×10^6	1.12×10^5	1.85×10^5
<i>Z</i> - $\text{PhCH}=\text{CHPh}$	2.65×10^2 / 0.00%	2.47×10^8	2.47×10^8	
$\text{CH}_2=\text{CHCH}=\text{CH}_2$	3.14×10^3 / 10%	2.80×10^4	3.11×10^4	8.01×10^4
<i>E</i> - $\text{CH}_2=\text{CHCH}=\text{CHMe}$	5.20×10^3 / 17%	2.60×10^4	3.12×10^4	
$\text{CH}_2=\text{CMeCMe}=\text{CH}_2$	1.27×10^4 / 4.9%	2.46×10^5	2.59×10^5	3.25×10^5
	1.77×10^4 / 0.8%	2.18×10^6	2.20×10^6	

As is seen from Table 8, from the point of view of the reactions (1) and (2) competition, unsaturated hydrocarbons may be divided into three groups.

- 1) *Olefins*. Here, the reaction of asymmetrical addition of ozone prevails. The reaction (2) share is less than 0.1%. The reaction (2) enthalpy for these olefins is $-10 \div +6\text{ kJ/mol}^{-1}$; thus, the reaction of asymmetrical addition prevails. The conclusion agrees with the data of quantum-chemical calculations for ethylene and conclusions of many works on the reactions with olefins [1-3].
- 2) *Styrenes and dienes*. The formation of π -bonds neighboring with the reacting site results evidently in increasing the classic potential barrier of the thermally neutral reaction; on the other hand, it makes the reaction (2) more exothermal (the enthalpy of such reactions vary over the range $-35 \div -64\text{ kJ/mol}^{-1}$). Hence, the reaction (2) makes a great contribution and, in cases of ozonation styrenes and dienes, it sometimes prevails.
- 3) *Diphenylethylenes*. In reactions of ozone with diphenylethylenes, the reaction (2) prevails. The enthalpies of these reactions are low enough (they vary over the range $-55 \div -84\text{ kJ/mol}^{-1}$).

CONCLUSION

Thus, the results presented show that the first stage of addition of ozone to multiple bonds may proceed by two different pathways on the singlet plane. The reaction on the triplet plane of potential energy is also probable. The ratio of the rates of the reactions (1) and (2) may vary over a wide range. The reaction (1) share in the overall ozonation is 100% for olefins. For TFE and diphenylethylenes the reaction (2) prevails. For styrenes and dienes, the reaction rates are comparable.

REFERENCES

- [1] Razumovskii S.D., Zaikov G.E. Ozone and its reactions with organic compounds. M., Nauka, 1974. (In Russian).
- [2] Razumovskii S.D., Zaikov G.E. // *Uspekhi khimii*, 1980, vol 49, no., pp. 2344 – 2376. (In Russian).
- [3] Lunin V.V., Popovich M.P., Tkachenko S.N. *Physical chemistry of ozone*, M., 1998. (In Russian).
- [4] Bailey P.S. in: *Ozonation in Organic Chemistry*. vol. 1, 2. New York: Academic Press, 1968.
- [5] Kuczkowski R.L. // *Acc. Chem. Res.* 1983. V. 16. N 1. P.42.
- [6] Bunnelle W.H. // *Chem. Rev.* 1991. V. 91. N . P.335.
- [7] Criegee R. // *Angew. Chem.* 1975. V. 87. P. 765.
- [8] Razumovskii S.D., Berezova L.V., *Izv. akad. nauk. AN SSSR, Ser.*, 1968, p. 207.
- [9] Murray R.W., Yossefueh R.D., Storey P.R. // *J. Amer. Chem. Soc.* 1967. V. 89. P. 2429.
- [10] Cremer D. // *J. Amer. Chem. Soc.* 1981. V. 103. № . P. 3627.
- [11] Ollzmann M., Kraka E., Cremer D., Gutbrod R., Andersson S.J. // *Phys. Chem.* 1998. V. 101. N . P. 9421.
- [12] McKee M.L., Rohlfing C.M. // *J. Amer. Chem. Soc.* 1989. V. 111. № 7. P. 2497 – 2500.
- [13] Gillies J.Z., Gillies C.W., Suenram R.D., Lovas F.J., Stahl W. // *J. Amer. Chem. Soc.* 1989. V. 111. № 8. P. 3073.
- [14] Gillies C.W., Gillies J.Z., Suenram R.D., Lovas F.J., Kraka E., Cremer D. // *J. Amer. Chem. Soc.* 1991. V. 113. № 7. P. 2412 – 2421.
- [15] DeMore W.B. // *Int. J. Chem. Kinetics.* 1969. V. 1. № 1. P. 209.
- [16] Cremer D., Kraka E., Crehuet R., Anglada J., Grafenstain J. // *Chem. Phys. Lett.* 2001. V. 347. P. 268 – 276.
- [17] Denisov E.T., Krisyuk B.E., *Khim. fizika*, 2007, vol. 26. (In Russian) (In press).
- [18] Gillies J.Z., Gillies C.W., Lovas F.J. ... // *J. Amer. Chem. Soc.* 1991. V. 113. № 17. P.6408-6415.
- [19] Krisyuk B.E., *Zhurnal fiz. khimii*, 2004, vol. 78, no. 4, p. 1 – 5. (In Russian).
- [20] Krisyuk B.E., Maiorov A.I., Popov A.a., *Khim. fizika*, 2003, vol. 22, no. 9, pp. 3-9. (In Russian).
- [21] Zhidomirov G.M., Bagaturyants A.A., Abronin I.A., *Applied quantum chemistry*, M., *Khimiya*, 1979. 295 pp. (In Russian).
- [22] Krisyuk B.E., *Khim. fizika*, 2006, vol. 25, no. 6, p. 13. (In Russian).

- [23] *Epoxidation*.
- [24] Floriano W.B., Blazskowski S.R., Nascimento M.A.C. // *J. Molec. Struct.(Theochem.)*. 1995. V. 335. P. 51.
- [25] Krisyuk B.E., Polianchik E.V., *Khim. fizika*, 1990, vol. 9, vol. 1, p. 127. (In Russian).
- [26] Timerghazin Q.K., Khursan S.L., Shereshovetz V.V. // *J. Molec. Struct.(Theochem.)*. 1999. V. 489. P. 87.
- [27] Denisov E.T., Denisova T.G. // *Russ. Chem.Bull.* 2002. .V 71. № 5. P. 417.
- [28] Frisch M. J., Trucks G. W., Schlegel H. B., Scuseria G. E., Robb M. A., Cheeseman J. R., Montgomery J. A., Jr., Vreven T., Kudin K. N., Burant J. C., Millam J. M., Iyengar S. S., Tomasi J., Barone V., Mennucci B., Cossi M., Scalmani G., Rega N., Petersson G. A., Nakatsuji H., Hada M., Ehara M., Toyota K., Fukuda R., Hasegawa J., Ishida M., Nakajima T., Honda Y., Kitao O., Nakai H., Klene M., Li X., Knox J. E., Hratchian H. P., Cross J. B., Adamo C., Jaramillo J., Gomperts R., Stratmann R. E., Yazyev O., Austin A. J., Cammi R., Pomelli C., Ochterski J. W., Ayala P. Y., Morokuma K., Voth G. A., Salvador P., Dannenberg J. J., Zakrzewski V. G., Dapprich S., Daniels A. D., Strain M. C., Farkas O., Malick D. K., Rabuck A. D., Raghavachari K., Foresman J. B., Ortiz J. V., Cui Q., Baboul A. G., Clifford S., Cioslowski J., Stefanov B. B., Liu G., Liashenko A., Piskorz P., Komaromi I., Martin R. L., Fox D. J., Keith T., Al-Laham M. A., Peng C. Y., Nanayakkara A., Challacombe M., Gill P. M. W., Johnson B., Chen W., Wong M. W., Gonzalez C., and Pople J. A., *Gaussian 03, Revision C.02*, Gaussian, Inc., Wallingford CT, 2004.
- [29] Ignatov S.K. Moltran v.2.5, Nizhny Novgorod, 2004, <http://ichem.unn.runnet.ru/tcg/Moltran.htm>.
- [30] Krisyuk B. e., Maiorov A.I., Popov A.A., *Khim. fizika*, (In press) (In Russian).
- [31] Razumovskii S.D., *Khim. fizika*, 2000, vol. 19, no. 7, pp .58-62. (In Russian).
- [32] Krisyuk B. e., Maiorov A.I., Popov A.A., *Khim. fizika*, (In press) (In Russian).
- [33] Kiryukhin D.P., Barkalov I.M., Ismoilov I.L., *Khim. fizika*, 2003, vol. 22, no. 2, p.123. (In Russian).
- [34] Denisov E.T., Afanas`ev I.B. *Oxidation and Antioxidant in Organic Chemistry and Biology*. Taylor and Francis: Boca Raton, 2005. P. 101.
- [35] Denisov E.T., *Uspekhi khimii*, 2000, vol. 69, no. 2, p. 166. (In Russian).
- [36] Denisov E. T., *Models for Abstraction and Addition Reactions of Free Radicals in General Aspects of the Chemistry of Radicals*, Z. B. Alfassi, (Ed.), John Wiley and Sons Ltd.: London, 1999, P. 79-137.

Chapter 4

PECULIARITIES OF ELECTRON MAGNETIC RESONANCE SPECTRA OF THE LINEAR AGGREGATES OF FERROMAGNETIC NANOPARTICLES

O. N. Sorokina and A. L. Kovarski*

Emanuel Institute of Biochemical Physics, Russian Academy of Sciences
Kosygin str. 4, Moscow, Russia 119334

ABSTRACT

The peculiarities of electron magnetic resonance (EMR) spectra of magnetic nanoparticles of Fe_3O_4 and their linear aggregates in liquid and solid matrices have been studied. Concentration, temperature and angular dependences of EMR spectra of these systems have been viewed. EMR spectra of aggregates demonstrate an additional peak which position depends on aggregate orientation in magnetic field (MF) of spectrometer. Qualitative and quantitative analysis of EMR spectra has been carried out with phenomenological equation taking into account demagnetizing fields. Values of magnetization of linear aggregates were calculated.

Keywords: *Electron Magnetic Resonance, Ferrofluids, Magnetite, Nanoparticles, Linear aggregates.*

INTRODUCTION

A great interest attracted to the magnetic nanoparticles results from their unusual magnetic properties and a wide variety of the technical application in different areas of science and industry, namely material science [1], biology [2], medicine [3], computer science [4] and etc. Quite a lot of theoretical and experimental works have been done during

* Contact author: O.N. Sorokina, Kosygin Str. 4, Moscow, Russia, 119991. Tel: (495) 939-73-66; Fax: (495) 1374101 ; E-mail: alsiona@gmail.com

the last decade in the area of magnetic nanoparticle study by different approaches [5]. As it has been shown the electron magnetic resonance (EMR) is one of the most powerful techniques for the investigation of nanoparticles possessing the magnetic moments. The fundamental interest connects with the investigation of superparamagnetic systems. Nanoparticles in such systems have very high rotational mobility and turn with its magnetic moment under the external MF. In this case the anisotropy factors and dipole-dipole interactions have to be averaged by rapid motion. Superparamagnetism is typical for the diluted solutions of non-interacting nanoparticles in inviscid media. There are several theoretical approaches for the explanation and simulation of EMR spectra [6 – 8] but no one of them can give the accurate spectra fitting.

It should be emphasized that in concentrated suspensions we cannot neglect dipole-dipole interaction even in inviscid media where nanoparticles rotate with a high velocity. The external MF leads to the formation of the linear aggregates from nanoparticles due to dipole interaction [9]. In present work the strong effect of aggregate formation on the shape of ESR line has been investigated. Special features of such spectra may give valuable information.

This work is deal with the development of new approaches for the investigation of magnetically ordered composites containing magnetic nanoparticles by EMR. The concentration, temperature and angular dependences of EMR spectra of these systems have been viewed. We have studied peculiarities of EMR spectra of linear aggregates and made an attempt to calculate some characteristics of the examined systems such as saturation magnetization of aggregates in liquid and solid matrices.

EXPERIMENTAL TECHNIQUE

Ferrimagnetic nanoparticles of magnetite (Fe_3O_4) in diamagnetic matrices have been studied. Nanoparticles have been obtained by alkaline precipitation of the mixture of Fe(II) and Fe(III) salts in a water medium [10]. Concentration of nanoparticles was 50 mg/ml (1 vol.%). The particles were stabilized by phosphate-citrate buffer (pH = 4.0) (method of electrostatic stabilization). Nanoparticle sizes have been determined by photon correlation spectrometry. Measurements were carried out at real time correlator (Photocor-SP). The viscosity of ferrofluids was 1.01 cP, and average diffusion coefficient of nanoparticles was $2.5 \cdot 10^{-7} \text{ cm}^2/\text{s}$. The size distribution of nanoparticles was found to be log-normal with mean diameter of nanoparticles 17 nm and standard deviation 11 nm.

The experimental samples of the magnetic films were prepared using mentioned above hydrosol of magnetite and water-soluble polyvinylpyrrolidone (PVP). Nanoparticles from ferrofluid have been embedded into solid diamagnetic PVP matrix. Ferrofilms of PVP have been dried in air for several hours with and without external MF of 1500 G intensity.

The EMR studies were performed in the range of MFs from 1000 to 5500 G using X-band EPR spectrometer Bruker EMX-8/2. The commercial gas-flow cryostat was used to achieve temperature in the range of $-100^\circ - 90^\circ \text{ C}$. Ferrofluid spectra in a quartz flat cell and PVP films in a quartz tubes. Microwave frequency power did not exceed 0.1 mW.

RESULTS AND DISCUSSION

The EMR spectra of the ferrofluid demonstrate a broad line with peak-to-peak width depending on concentration and temperature (Figure 1). The increasing of line width with concentration increasing and temperature decreasing occurs due to dipole-dipole interaction and local MF influence. In diluted suspension at room temperature where dipole-dipole interaction can be neglected the peak-to-peak width is equal to 680 G. It is typical for resonance of microparticles with a broad size distribution of the particles [11 – 13]. Center of this line at room temperature locates in the MF near 3400 G (g-factor = 2.25). With temperature decreasing the center shifts to lower MFs.

As it can be seen from Figure 1 the additional peak appears on the low fields of the ferrofluid spectra (2000 – 2500 G) with concentration increasing and temperature decreasing. This peak is considered to be a result of the linear aggregates formation. It is known that under external MF action, in particular under the MF of EMR spectrometer, magnetic nanoparticles collect into long chains (linear aggregates) due to dipole-dipole interaction. These chains orientate along the flux of MF.

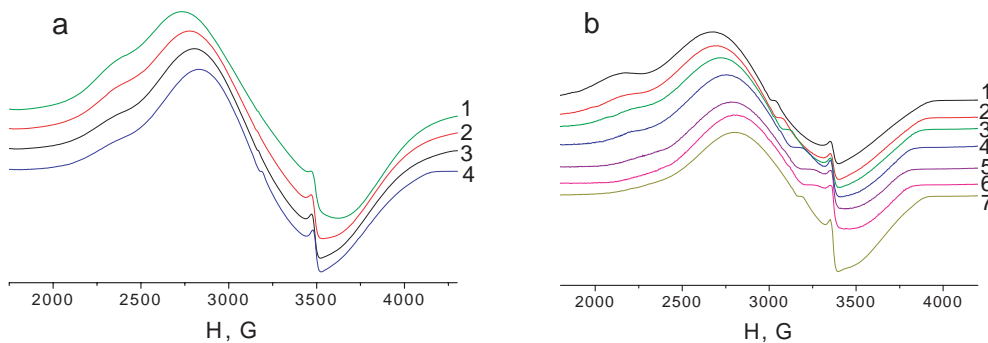


Figure 1. EMR spectra of ferrofluid depending on concentration of nanoparticles (a) at 25° C: 1a – 1, 2a – 0.5; 3a – 0.25; 4a – 0.125 vol.%; and temperature (b) at $C_{NP} = 0.125$ vol. %: 1b – 5°; 2b – 15°; 3b – 25°; 4b – 35°; 5b – 45°; 6b – 55°; 7b – 85° C.

It should be taken into account that only part of the particles collect into chain structure and others remain separated. Both types of particles are in thermal equilibrium. Using EMR spectra it is possible to calculate the fraction of particles, which belong to aggregate by spectra separation procedure. The fraction of magnetite involved in aggregates increases with concentration (Figure2).

The obtained spectra can be explained in the limits of the phenomenological resonance equations for highly anisotropic ferromagnets [14]. Such features are characteristic for uniaxial anisotropy, which rises from the deviation of nanoparticles shape from spherical. The resonance frequency ω of spherical nanoparticles according to the theory of ferromagnetic resonance is determined by the following equation:

$$\omega / \gamma = H_e \quad (1)$$

where ω is the resonant frequency, γ is the magnetogiric ratio, H_e is the external MF.

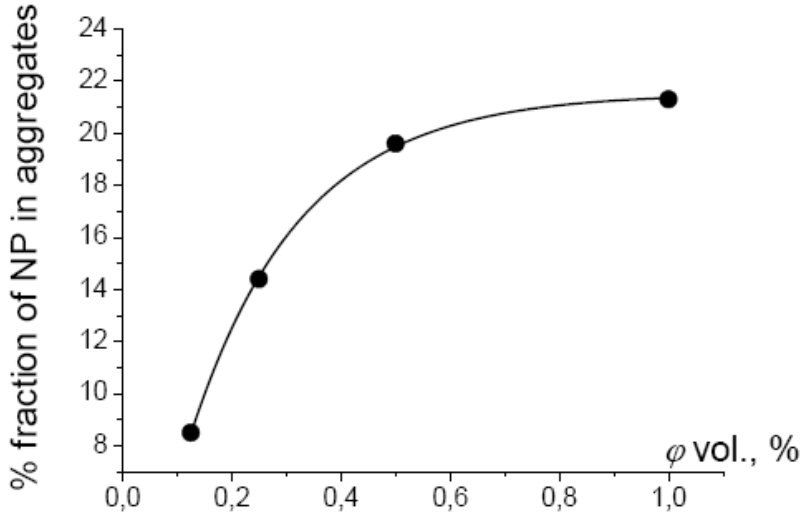


Figure 2. The plot of aggregated particles versus the total concentration of nanoparticles.

In the case when the shape deviates from spherical the demagnetizing factors N have to be taken into account. This factor is a result of internal MFs inherent due to demagnetizing action of poles in cylindrical and ellipsoidal samples. Demagnetizing field (H_{dem}) can be considered to be proportional to sample's magnetization with a high accuracy ($H_{\text{dem}} = NM_0$). Thus the equation for the long cylinder looks the following way (for the longitudinal orientation of the magnetization):

$$\omega/\gamma = H_e + 2\pi M_0 \quad (2)$$

where M_0 is the magnetization.

It also should be noted that with temperature and concentration decreasing the low field component of spectra shifts to the lower MFs and the distance between central and additional line increases. It can be considered to be an exchange interaction between particles forming the magnetic chains and single nanoparticles. As it is well known from the theory of proton exchange interaction [15] the magnetic moments precessing at different frequencies can switch places and then the resonant frequencies are averaged. Therefore two peaks of spectrum move to each other to one average resonant frequency. The same situation is observed in EMR spectra of nanoparticles in hydrosol.

Nanoparticles in inviscid media possess a high mobility and their aggregates reorientate very fast when the direction of MF changes. That's why we can't study the angular dependence of EMR spectra of linear aggregates in hydrosols. For making this investigation possible we have prepared the rigid films made of PVP. MF of the magnet has been directed such the way to form aggregates aligned along the sample plane.

The EMR spectra of polymer films prepared without external field demonstrate quite broad lines (Figure 3). Center of these lines is strongly dependent on the sample orientation in MF of spectrometer. This results from the anisotropy of demagnetizing fields, which determine resonance conditions for the thin magnetic film:

$$(\omega / \gamma)^2 = H_e (H_e + 4\pi M_0) \text{ (for the tangent orientation of magnetization)} \quad (3)$$

$$\omega / \gamma = H_e - 4\pi M_0 \text{ (for the normal orientation of magnetization)} \quad (4)$$

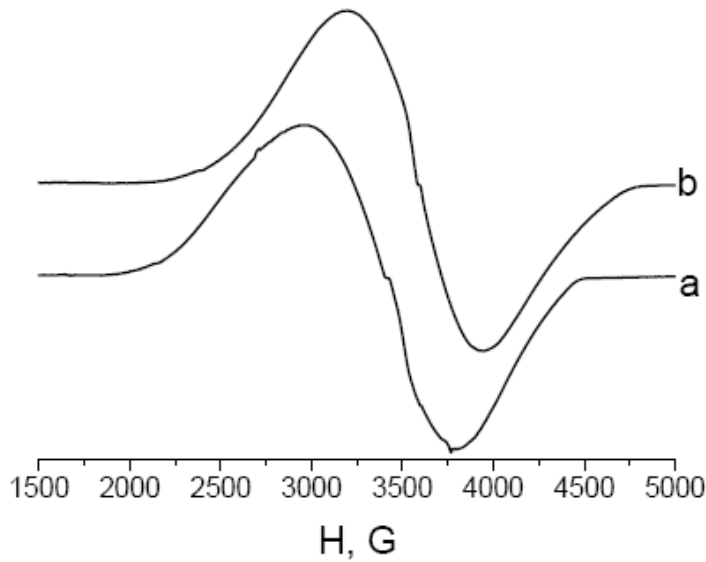


Figure 3. EMR spectra of PVP film prepared without external magnetic field with parallel (a) and perpendicular orientation in the magnetic field of spectrometer.

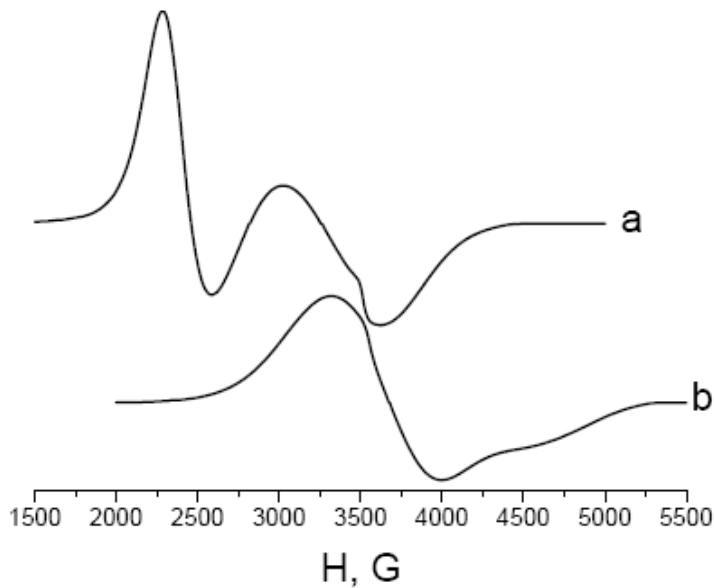


Figure 4. EMR spectra of PVP films framed in magnetic fields with parallel (a) and perpendicular (b) orientation of the sample in the external magnetic field of spectrometer.

The EMR spectra of magnetite nanoparticles in polymer films formed in MFs (Figure 4) are differ from spectra of the films obtained without field and ferrofluid spectra. Firstly, EMR spectra of the films formed in MF demonstrate a great splitting between the high field and low field lines, which is significantly higher then in ferrofluid. These effects are concerned with the less mobility of nanoparticles and their aggregates in the vitrified films of PVP than in liquid medium. Thus in ferrofluid the rotation of the particle and its magnetic moment occur simultaneously while in vitrified matrix changes in MF orientation do not accompanied by particle reorientation.

Secondly, in both cases of the films specific angular dependence of the resonance field is observed especially for the films obtained in external MF. As one can see (Figure 4) the additional peak of EMR spectra of magnetic films form under MF action shifts toward lower field if the measuring field is parallel to the sample plane and towards higher if the field is perpendicular. The orientation dependence of the shape of EMR line and its resonant position results from the predomination of uniaxial type of magnetic anisotropy due to the formation of motionless anisotropic linear structures.

The qualitative and quantitative analysis of obtained spectra has been carried out using the phenomenological equations for the resonance conditions of long cylinder. The influence of demagnetizing factors tends to the following equations: for the longitudinal orientation of the magnetization it's eq. 2 and for the transversal it is:

$$(\omega/\gamma)^2 = H_e(H_e - 2\pi M_0) \quad (5).$$

The longitudinal orientation of magnetization corresponds to parallel orientation of the sample in MF of spectrometer and transversal orientation to the perpendicular. The line shift arises from variation of aggregate axis orientation in MF upon angle $\pi/2$ depends on the magnetization. Values of M, obtained using eqs. 2 and 5 are shown in the table.

Table 1. Magnetization values M for linear aggregates of magnetite nanoparticles at different orientations in MF of spectrometer at 298 K (PVP is a matrix)

Orientation of linear aggregate axis in MF	Central line position in MF, G	Magnetization, G
Parallel	2300	180
perpendicular	4025	150

EMR spectra of ferrofilm are also depends on temperature. The EMR lines broaden with temperature decreasing and shift. The direction of line displacement is defined by sample orientation in MF. It shifts to lower MFs in the case of parallel orientation and to higher when orientation is perpendicular. It can be explained by the fact that magnetization value rises with temperature decreasing and effect of demagnetizing fields become stronger. Spectra of perpendicular orientated sample become more symmetric with temperature decreasing.

CONCLUSIONS

The obtained results show, that EMR spectra of linear aggregates of magnetic particles are differ from randomly distributed nanoparticles spectra in both solid and liquid diamagnetic matrices. They demonstrate additional peak, which position depends on aggregate orientation in MF of spectrometer. Thus, EMR spectroscopy can be used for identification of linear structures in various systems. Using EMR spectra the fraction of particles collect in aggregates can be calculated and the plot of their fraction can be obtained in dependence on total particle concentration and temperature. The mean value of saturation magnetization of aggregates can be calculated by phenomenological equations for magnetic resonance in approximation of long cylinder.

These experimental results should help to find the most convenient theoretical approaches for spectra simulation and getting more characteristic parameters of anisotropic magnetic nanostructures in composite materials and biological objects.

REFERENCES

- [1] N. Guskos, J. Typek, T. Bodziony, Z. Roslaniec, U. Narkiewicz, M. Kwiatkowska, M. Maryniak // *Rev. Adv. Mater. Sci.* 12 (2006) 133-138.
- [2] B.P. Weiss, S.S. Kim, J.L. Kirschvink, R.E. Kopp, M. Sankaran, A. Kobayashi, A. Komeili // *Earth and planetary Sci. Letters* 224 (2004) 73-89.
- [3] A.A. Kuznetsov // The first symposium "Application of biomagnetic carries in medicine" Moscow (2002) 3-4.
- [4] B.K. Middleton// *J.Magn.Magn.Mater.*, 193 (1999) 24.
- [5] S.P. Gubin, Yu.A. Koksharov, G.B. Khomutov, G.Yu. Yurkov // *Uspehi Himii* 74 (2005) 539.
- [6] R.S. de Biasi, C. Devezas // *J.Appl. phys.* 49 (1978) 2466-2469.
- [7] Yu.L. Raikher, V.I. Stepanov, *Sov. Phys.-JETP* 75 (1992) 764.
- [8] R. Berger, J.-C. Bissey, J. Kliava, H. Daubric, C. Estournes. // *J. Magn. Magn. Mater.* 535 (2001) 535.
- [9] A.L. Kovarski, O.N. Sorokina // *J. Magn. Magn. Mat.* (accepted for publication).
- [10] S.Taketomi, S. Tikadzumi, *Nikkan Kogio Simbuhsya*, (Fudziosi, Tokio 1988).
- [11] J. M. Patel, S. P. Vaidya, and R. V. Mehta, *J. Magn. Magn. Mater.* 65, 273 (1987).
- [12] M. M. Ibrahim, G. Edwards, M. S. Seehra, B. Ganguly, and G. P. Huffman, *J. Appl. Phys.* 75, 5873 (1994).
- [13] N. Noginova, F. Chen, T. Weaver, E.P. Geannelis, A.B. Bourlinos, V.A. *Atsarkin* (2006) internet resource.
- [14] S.V. Vonsovskii, *Ferromagnetic Resonance* (Pergamon, Oxford, 1966).
- [15] Carrington, A.D. McLachlan *Introduction to Magnetic Resonance with Application to Chemistry and Chemical Physics* (HarperandRow, N-Y, 1967).

Chapter 5

THEORETICAL INVESTIGATION OF STRUCTURE OF BORON CARBONITRIDE NANOTUBES

***P. B. Sorokin**, *P. H. Pardo*[#] and *L. A. Chernozatonskii*[★]**

*Emanuel Institute of Biochemical Physics of Russian Academy of Sciences,
119991 Moscow, Russia

[#]University of Barcelona, Barcelona, Spain

The discoverer of single-walled carbon nanotubes were for Iijima [1] in 1991. Since this moment a lot of different kinds of nanotubes are discovered. A great variety of incarbon nanotubes composed of different elements, for example, chalcogenides: MoS₂ [2], WS₂ [3], oxides: BeO [4], SiO₂ [5], TiO₂ [6], nitrides: BN [7-9], GaN [10] has been synthesized experimentally or predicted theoretically.

These novel microstructures have extraordinary combination of physical and chemical properties [11-13], for this reason they become an important scheme of actually science work. One example of such nanomaterials is boron carbonitride (BNC) with graphite-like structure. Based on theoretical calculations, the existence of nanotube structures of BN was predicted in 1994, which was soon verified by the first synthesis of BN nanotubes in 1995.

The BNC nanotubes can have a metallic behavior if they do not have a band gap or a semi conductor behavior if there are band gaps. The importance of this phenomenon is that the electric properties of BCN compounds can be controlled by varying the atomic composition and atomic arrangement of the compounds. In addition, their mechanical properties could be similar to these of diamond and cubic BN, providing new super-hard materials [14].

Stephan was the first to attempted direct synthesis of the B and N multi walled carbon nanotubes (BCN-MWNTs) in 1994 [15-17]. Since then, considerable progress has been made in the synthesis of BCN-MWNTs by different means of arc-discharge [16-18], laser ablation [18-20], prylolysis methods [18,21], and chemical vapor deposition [18,20-24]. Aligned BNC nanotubes have been successfully fabricated by bias assisted hot filament chemical vapor deposition [27,28]. Up to now, the only existing BCN-SWNTs synthesis was achieved via an

* PBSorokin@gmail.com

alternative post growth treatment route, by substitution reaction of the presynthesized pristine C-SWNTs with B_3O_2 and N_2 at high temperature [29-31]. The BCN-SWNTs' growth by HF-CVD was achieved over the powdery MgO-supported Fe-Mo bimetallic catalyst by using CH_4 , B_2H_6 , and ethylenediamine vapor as the reactant gases [32-34]. In addition, B-C-N nanotubes were synthesized by a substitution reaction using multiwalled carbon nanotubes as a template [35], B_2O_3 powder was placed in a crucible covered with carbon nanotubes [36].

However, analysis on the microstructure, especially nanoscale distributions of the compositional elements, of the BNC nanotubes grown in experiment is far from being well understood. In this work, we calculated the electronic band structure and physical properties of BCN nanotubes of different diameters chiralities and arrangements of B-C-N atoms.

COMPUTATIONAL METHOD

All the calculations were performed with the Siesta code [37]. This program package makes it possible to perform ab initio calculations based on the pseudopotential method in the framework of the general gradient approximation formalism in parameterization of Perdew, Burke and Ernzerhof [38]. In our calculations, we used non-local norm-conserving pseudopotential of Troullier-Martins [39] in Kleinman-Bylander form [40], DZP basis and cutoff energy of 100 Ry. We used 8 and 16 Monkhorst-Pack k-points mesh [41] in periodical tube direction for geometry optimization for long zigzag tubes and short armchair tubes respectively. For electronic structure calculation, we used 32 and 64 k-points meshes for zigzag and armchair BCN-NTs, respectively.

Before the beginning of calculation we performed testing of our parameters on already studied BC_2N flatten structure [42]. We compared results from the changing of following parameters: quantity of k-points, the electronic temperature, the points of mesh-cutoff, the basis type and the basis size to found the best results for a BNC nanotube and the dependence of the results with each parameter. Results of our test calculations showed us that we could predict with good accuracy geometrical, energetical and electronic structures of $B_xC_yN_z$ compounds.

RESULTS AND DISCUSSION

It is possible to generate BNC nanotubes starting with a carbon nanotube and replace some carbon atoms by boron and nitrogen. Then the properties and the stability of the nanotubes obtained depend of the number carbon atoms changed and the bonds obtained, for example the bond B-B or N-N are not favorable.

Since flatten $B_xC_yN_z$ are hexagonal structures, BCN nanotubes (BCN-NT) must have hexagonal lattice like carbon or boron nitride nanotubes [43]. So BCN-NT are conveniently described in terms of two integral indices (n,m) specifying a two-dimensional developed hexagonal lattice: $C_h = na_1 + ma_2$, where the length of the chiral vector C_h is equal to the circumference of the cylindrical layer consisting of atoms. BCN-NT can be divided into three classes: (i) armchair nanotubes with $n=m$, (ii) zigzag nanotubes with $n \neq 0$ and $m = 0$, and (iii) chiral nanotubes with $n \neq m$.

From geometrical point of view, we obtain that BCN nanotubes have “selective chirality” – they can have only $(3n, 3m)$ type. So we studied two kind of BNC nanotubes the armchair $(3,3)$ nanotubes and the zigzag $(6,0)$ nanotubes, to compare the results for each kind and for all nanotubes.

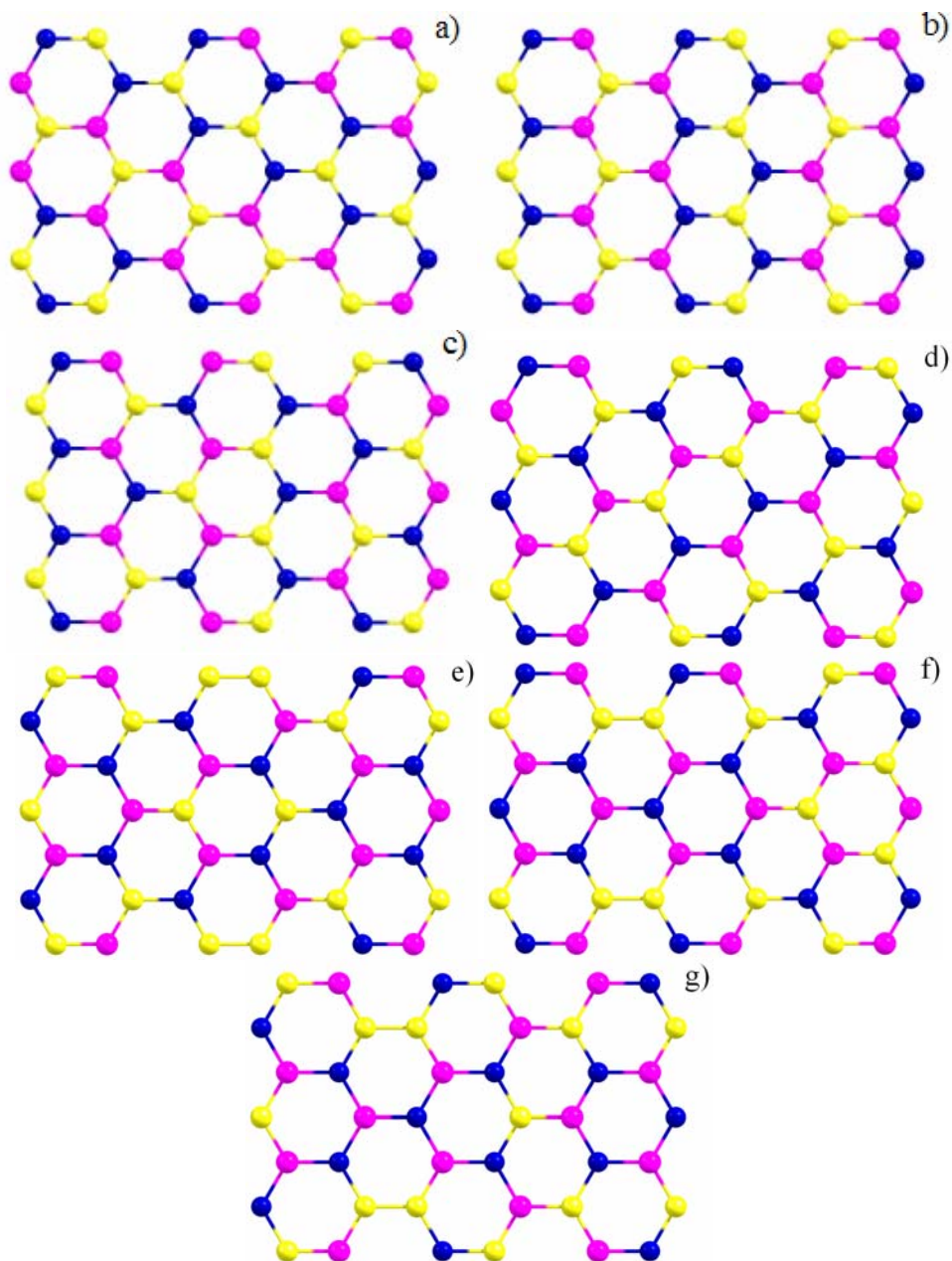


Figure 1. Different type of arrangement of B-C-N atoms in layered structures a) “type-1” b) “type-2” etc. Yellow (white) atoms – carbon, red (gray) atoms – boron, blue (dark) atoms – nitrogen.

We described 7 different arrangements of B-C-N atoms in nanotubes (Fig 1). Moreover it is possible to change B and N atoms by places (invert the tube) so we described 14 various BCN-NT. Example of typical BCN-NT is shown in the Figure 2.

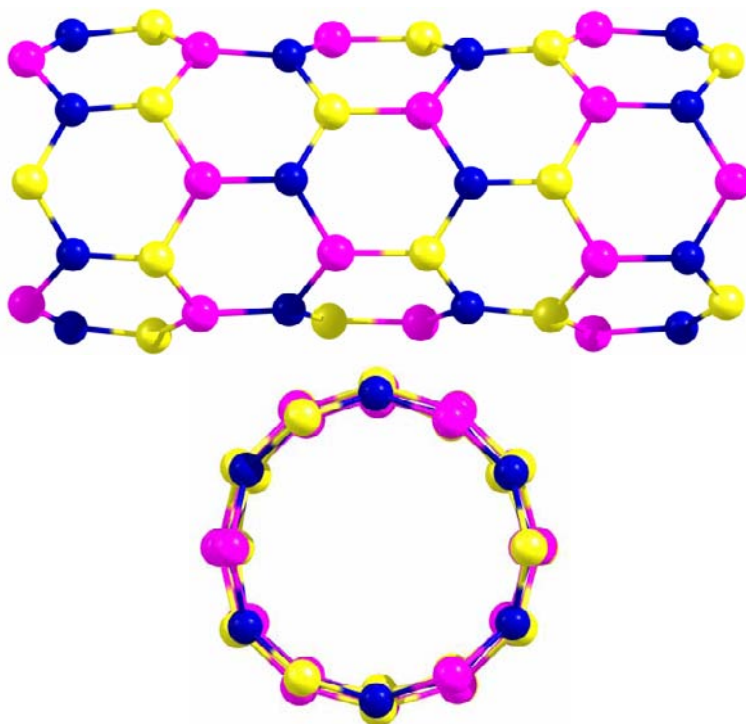


Figure 2. Structure of BCN-NT (6,0) “type-3”.

We studied the cohesive energy of the BCN-NT and found that zigzag nanotubes are more stable than armchair nanotubes. Moreover, we found that tubes of “type-5” and “type-6” have lowest energy so they should be synthesized by methods described above.

Table 1. Cohesive energy of different BCN-NTs

Group	Armchair	Energy (eV/atom)	Zigzag	Energy (eV/atom)
1	(3,3)	-10.28879	(6,0)	-10.3330
	(3,3) inverted	-10.28882	(6,0) inverted	-10.3332
2	(3,3)	-10.229	(6,0)	X
	(3,3) inverted	X	(6,0) inverted	-10.3727
3	(3,3)	-10.230	(6,0)	-10.3606
	(3,3) inverted	-10.238	(6,0) inverted	-10.373
4	(3,3)	-10.24318	(6,0)	X
	(3,3) inverted	-10.24310	(6,0) inverted	-10.374
5	(3,3)	-10.3507	(6,0)	-10.492
	(3,3) inverted	-10.3518	(6,0) inverted	-10.487
6	(3,3)	-10.3524	(6,0)	-10.455
	(3,3) inverted	-10.3517	(6,0) inverted	X
7	(3,3)	-10.3311	(6,0)	X
	(3,3) inverted	-10.3313	(6,0) inverted	X

We obtained the electronic structure and found as semiconductor as metal BCN-NT behavior (see the *Ошибка! Источник ссылки не найден.*). As for example in the Figure 3 we shown the semiconductor and metal density of states (DOS) for some NT. Furthermore, it is clear from *Ошибка! Источник ссылки не найден.* and *Ошибка! Источник ссылки не найден.* that most stable BCN-NT is semiconductor.

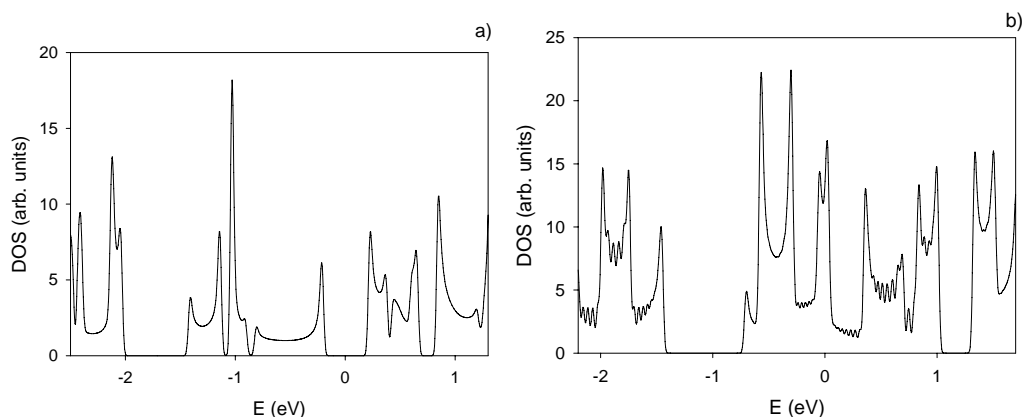


Figure 3. DOS for a) semiconductor BCN-NT (3,3) “type-6” and b) metal BCN-NT (6,0) “type-3”. The Fermi level energy is taken as zero.

Table 2. Band gap of different BCN-NTs

Group	Armchair	Band gap (eV)	Zigzag	Band gap (eV)
1	(3,3)	0.281	(6,0)	0.156
	(3,3) inverted	0.288	(6,0) inverted	0.184
2	(3,3)	0.521	(6,0)	X
	(3,3) inverted	X	(6,0) inverted	Metal
3	(3,3)	0.809	(6,0)	Metal
	(3,3) inverted	0.669	(6,0) inverted	Metal
4	(3,3)	0.308	(6,0)	X
	(3,3) inverted	0.308	(6,0) inverted	Metal
5	(3,3)	0.737	(6,0)	0.769
	(3,3) inverted	X	(6,0) inverted	0.657
6	(3,3)	0.444	(6,0)	0.160
	(3,3) inverted	0.629	(6,0) inverted	X
7	(3,3)	0.140	(6,0)	X
	(3,3) inverted	X	(6,0) inverted	X

We theoretically described the structures of single-walled BCN nanotubes. It was shown that these nanotubes are thermodynamically stable. From geometrical point of view we obtained that BCN nanotubes have “selective chirality” – they can have only (3n, 3m) type. So we studied two kind of BNC nanotubes with different arrangements of atoms the armchair (3,3) nanotubes and the zigzag (6,0) nanotubes. We obtained cohesive energy for some BNC-NTs and found that zigzag tubes are more stable than corresponding armchair tubes. We

found that BCN-NT can have as semiconductor as metal behavior and most stable tubes are semiconductors with band gap ~ 1 eV.

REFERENCES

- [1] S. Iijima, *Nature* (London), 354, 56 (1991).
- [2] R. R. Chianelli, E. Prestridge, T. Pecorano and J. P. DeNeufville, *Science*, 203, 1105 (1979).
- [3] R. Tenne, M. Homyonfer and Y. Feldman, *Chem. Mater.*, 10, 3225 (1998).
- [4] P.B. Sorokin, A.S. Fedorov, L.A. Chernozatonskii, *Physics of the Solid State*, 48, 2, 373 (2006).
- [5] L.A. Chernozatonskii, P.B. Sorokin, A.S. Fedorov, *Physics of the Solid State*, 48, 10, 2021 (2006).
- [6] T. Kasuga, M. Hiramatsu, A. Hason, T. Sekino and K. Niihara, *Langmuir*, 14, 3160 (1998).
- [7] J. L. Corkill and M. L. Cohen, *Phys. Rev. B*, 49, 5081 (1994).
- [8] Y. Miyamoto, A. Rubio, S. G. Louie and M. L. Cohen, *Phys. Rev. B*, 50, 18360 (1994).
- [9] Z. W. -Sieh, K. Cherrey, N. G. Chopra, X. Blasé, Y. Miyamoto, A. Rubio, M. L. Cohen, S. G. Louie, A. Zettl and P. Gronsky, *Phys. Rev. B*, 51, 11229 (1994).
- [10] F. L. Deepak, A. Govindaraj and C. N. R. Rao, *J. Nanosci, Nanotechno*, 1, 303 (2001).
- [11] E. G. Wang, *Adv. Mater.*, 11, 1129 (1999).
- [12] E. G. Wang, *Prog. Mater. Sci.*, 41, 241 (1997).
- [13] E. G. Wang, Y. Chen, and L. P. Guo, *Phys. Scr.*, T46, 108 (1997).
- [14] Universidade Estadual de Feira de Santana, Brazil, *Eur. Phys. Journal B*, 44, 203 (2005).
- [15] Ste´phan, O.; Ajayan, P. M.; Colliex, C.; Redlich, Ph.; Lambert, J. M.; Bernier, P.; Lefin, *P. Science*, 266, 1683 (1994).
- [16] Wengsieh, Z.; Cherrey, K.; Chopra, N. G.; Blase, X.; Miyamoto, Y.; Rubio, A.; Cohen, M. L.; Louie, S. G.; Zettl, A.; Gronsky, A., *Phys. Rev. B*, 51, 11229 (1995).
- [17] Redlich, P.; Loeffler, J.; Ajayan, P. M.; Bill, J.; Aldinger, F.; Ru´hle, *M. Chem. Phys. Lett.*, 260, 465 (1996).
- [18] C. Journet, P. Bernier, *Appl. Phys. A*, 67, 1 (1998).
- [19] T. Guo, P. Nikolaev, A.G. Rinzler, D. Tomanek, D.T. Colbert, R.E. Smalley, *J. Phys. Chem.*, 99, 10694 (1995).
- [20] T. Guo, P. Nikolaev, A. Thess, D.T. Colbert, R.E. Smalley, *Chem. Phys. Lett.* 243, 49 (1995).
- [21] J. Bill, R. Riedel and G. Passing, *Z. Anorg. Atlg. Chem.*, 610, 83,(1992).
- [22] R. Badzian, S. Appenheimer, T. Niemyski and E. Olkusnik, *American Nuclear Society*, 747 (1972).
- [23] J. Loeffler, F. Steinbach, J. Bill, J. Mayer and F. Aldinger, *Z. Metallkd*, 87, 170 (1996).
- [24] R.B. Kaner, J. Kouvertakis, C.E. Warble, M.L. Sattler and N. Bartlett, *Mater. Res. Bull.* 22, 399 (1987).
- [25] Terrones, M.; Grobert, N.; Terrones, *N. Carbon*, 40, 1665 (2002).

-
- [26] Ma, R.; Golberg, D.; Bando, Y.; Sasaki, T. *Philos. Trans. R. Soc. London A*, 362, 216 (2004).
- [27] Yu J, Ahn J, Yoon S F, Zhang Q, Rusli, Gan B, Chew K, Yu M B, Bai X D and Wang E G, *Appl. Phys. Lett.*, 77, 1949 (2000).
- [28] Zhi CY, Bai X D and Wang E G, *Appl. Phys. Lett.*, 80, 3590 (2002).
- [29] Golberg D., Bando Y., Han W., Kurashima K., Sato T., *Chem. Phys. Lett.*, 308, 337 (1999).
- [30] Golberg D., Bando Y., Bourgeois L., Sato T., *Carbon*, 38, 2017 (2000).
- [31] Tomoaki Yoshioka, Hidekatsu Suzuura, and Tsuneya Ando, *Journal of the Physical Society of Japan*, Vol. 72, No. 10, 2656 (2003).
- [32] Yu J., Wang, E. G., *Appl. Phys. Lett.*, 74, 2984 (1999).
- [33] Bai, X. D., Guo, J. D., Yu, J., Wang, E. G., Yuan, J., Zhou, W., *Appl. Phys. Lett.*, 76, 2624 (2000).
- [34] Zhi, X. Y.; Guo, J. D.; Bai, X. D.; Wang, E. G., *J. Appl. Phys.*, 91, 5325 (2002).
- [35] W. Q. Han et al., *Appl. Phys. Lett.*, 73, 3085 (1998).
- [36] B. C. W. Chang, Wei-Qiang and Han and A. Zettl., *J. Vac. Sci. Technol. B*, 23 (2005).
- [37] J.M. Soler, E. Artacho, J.D. Gale, A. Garcia, J. Junquera, P. Ordejón, D. Sanchez-Portal., *J. Phys. Cond. Matter*, 14, 11, 2745 (2002).
- [38] J.P. Perdew, K. Burke, M. Ernzerhof., *Phys. Rev. Lett.* 77, 18, 3865 (1996).
- [39] N. Troullier, J.L. Martins., *Phys. Rev. B*, 43, 3, 1993 (1991).
- [40] L. Kleinman, D.M. Bylander., *Phys. Rev. Lett.*, 48, 20, 1425 (1982).
- [41] H.J. Monkhorst, J.D. Pack., *Phys. Rev. B*, 13, 12, 5188 (1976).
- [42] A.Y. Liu, R.M. Wentzcovitch, M.L. Cohen., *Phys. Rev. B.*, 39, 1760 (1989).
- [43] M. S. Dresselhaus, G. Dresselhaus, and P. C. Eklund, *Science of Fullerenes and Carbon Nanotubes* (Academic, London, 1995).

Chapter 6

**EFFECT OF STERIC FACTOR ON THE TRIPLET STATE
QUENCHING OF *MESO*-SUBSTITUTED
THIACARBOCYANINE DYES IN COMPLEXES
WITH DNA**

*Pavel G. Pronkin**, *Alexander S. Tatikolov* and
Vladimir A. Kuzmin

Emanuel Institute of Biochemical Physics,
Russian Academy of Sciences, Kosygin str. 4,
Moscow, 119991 Russia

ABSTRACT

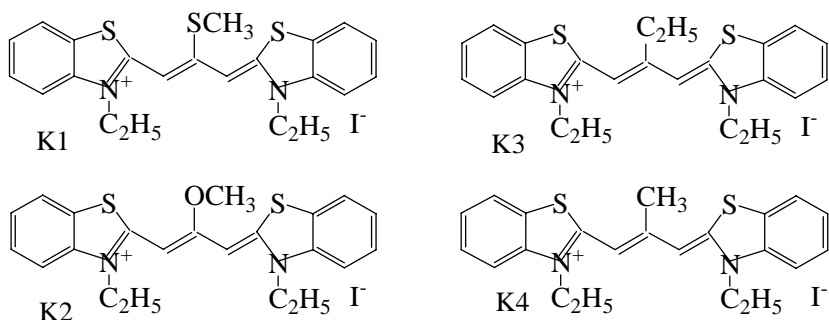
The effects of DNA were studied on photochemical properties of a number of meso-substituted thiacyanine dyes (3,3'-diethyl-9-thiomethylthiacyanine iodide (K1), 3,3'-diethyl-9-methoxythiacyanine iodide (K2), 3,3'-9-triethylthiacyanine iodide (K3), 3,3'-diethyl-9-methylthiacyanine iodide (K4)). Interaction of the dyes with DNA leads to the formation of stable noncovalent complexes. Complexation with DNA leads to an increase in the triplet state quantum yields of the selected dyes. The rate constants for quenching of the triplet state by a stable nitroxyl radical, iodide ion, and oxygen were determined in solutions and in complexes with DNA. The quenching of the triplet state of cyanine dyes by chemically different quenchers provides valuable information on the structure of the dye–DNA complex and the localization of dye molecules in the biopolymer matrix. Using nitroxyl radical and iodide ion as quenchers, we have shown that cyanine dyes form with DNA two types of complexes: superficial (in the minor groove of DNA) and intercalation complexes.

Keywords: *DNA, meso-substituted thiacyanine dyes, triplet state quantum yield, stable nitroxyl radical, iodide ion, oxygen.*

* E-mail: pronkinp@mail.ru

INTRODUCTION

Noncovalent interaction of dyes and related compounds with various biomacromolecules attracts considerable attention due to the possibility of proceeding of a variety of photochemical processes in vivo [1]. It makes possible to use dyes both in biomedical studies as DNA labels and in clinical practice [2]. Complex formation of cyanine dyes with double-helical DNA is of great interest due to unique photophysical and photochemical properties of these dyes, which change dramatically in the presence of DNA [1, 3, 4]. There are two main types of dye–DNA bonding: complexes of dyes intercalated between DNA base pairs and complexes in which dye molecules are located in the minor groove of the double helix of the biopolymer (superficial bonding) [5].



This work is deal with the obtaining information on the properties of dye molecules bound to a biopolymer (for example, on the type of the complex formed) from a study of the quenching of dye excited states by various quenchers. Interaction with biomacromolecules leads to a number of cases to partial shielding of ligands, which results in hindered access of quencher molecules to the excited state of the dye in complexes with DNA and a decrease in the rate constant of triplet state quenching.

To reveal the mode of dye–DNA binding, we studied quenching of the triplet states of thiocarbocyanine dyes K1 – K4 in solutions and in complexes with DNA (aqueous phosphate buffer, pH 7) by the stable nitroxyl radical 4-hydroxy-2,2,6,6-tetramethylpiperidine-1-oxyl (4-hydroxy-TEMPO), iodide ion, and oxygen. To study the properties of the triplet states of the dyes, we used flash photolysis technique.

MATERIAL AND METHODS

The absorption spectra of the dyes were measured with a Shimadzu UV-3101 PC spectrophotometer (Japan) in a cell with a 1-cm optical path length. The fluorescence and fluorescence excitation spectra were studied with the use of a Shimadzu RF-5301 PC spectrofluorimeter. To study the triplet state of the dyes, apparatuses of flash photolysis with xenon lamp excitation (with an energy of 50 J and a pulse length at half maximum of $\tau_{1/2} = 7 \mu\text{s}$) [6] was used. To detect the triplet state of the dyes, the solutions were deoxygenated using a vacuum unit or purged with argon for experiments on the laser flash photolysis apparatus. A

manometric unit was used for the air pressure measurement in a working cell in experiments on triplet state quenching by oxygen.

In this work, we used the dyes provided by the Research Center NIKHIMFOTOPROEKT and commercial chicken DNA (Reanal, Hungary) [7]. DNA concentrations were determined using the extinction coefficient of a base pair of $13200 \text{ l mol}^{-1} \text{ cm}^{-1}$ at a wavelength of 250 nm [8]. An aqueous phosphate buffer solution (pH 7, at a concentration of 20 mmol l^{-1}), isopropanol, methanol, isopropanol, hexanol and dimethyl sulfoxide (reagent grade) were used as solvents.

The viscosity of solutions was measured with an Ostwald viscometer. All experiments were conducted at room temperature ($20 \pm 3^\circ\text{C}$).

RESULTS AND DISCUSSION

Properties of the Triplet State of Cyanines

The triplet states of dyes K1–K4 and of their complexes with DNA were studied by the flash photolysis technique. Upon the direct photolysis of deoxygenated solutions of dyes K1, K3 and K4 in phosphate buffer and isopropanol, no triplet–triplet absorption signals were observed.

The lack of the triplet–triplet absorption of carbocyanine dyes is due to low values of the intersystem crossing rate constants as compared with the rate constants of competing processes [5, 9]. The dye-DNA interactions lead to an increase in the quantum yield of the triplet state of the dye molecules, since the complexation impedes the processes of photoisomerization and vibrational relaxation (nonradiative deactivation), thus permitting the detection of T–T absorption spectra of the bound dyes upon direct photoexcitation. In the presence of DNA in the solutions, the triplet lifetimes of the dyes comprise hundreds of microseconds [10].

In the case of K2, the direct flash photoexcitation of their DNA-free deoxygenated solutions in isopropanol and phosphate buffer led to an appearance of T–T absorption signals. Figure 1 shows the differential triplet spectrum of K2 in phosphate buffer pH 7 (curve 1). The decay kinetics of the triplet state of K2 follows the first order law at a rate constant (k_1) of 2.5×10^3 and $7.5 \times 10^3 \text{ s}^{-1}$ in water (phosphate buffer) and isopropanol, respectively.

The signal of T–T absorption observed for K2 in liquid solutions in the absence of DNA may be explained by the strong steric effect of its meso-substituent distorting the planar structure of the dye.

A comprehensive analysis of the spectral and kinetic data on T–T absorption has shown that the triplet state decay kinetics for thiocarbocyanine dyes in the presence of DNA are not single-exponential and can be presented as a sum of two exponents:

$$[{}^3\text{Dye}^*] = A_1 \exp(-k_1 t) + A_2 \exp(-k_2 t), \quad (1)$$

where A_1 and A_2 are the amplitudes of the exponential components of the kinetic dependence observed experimentally.

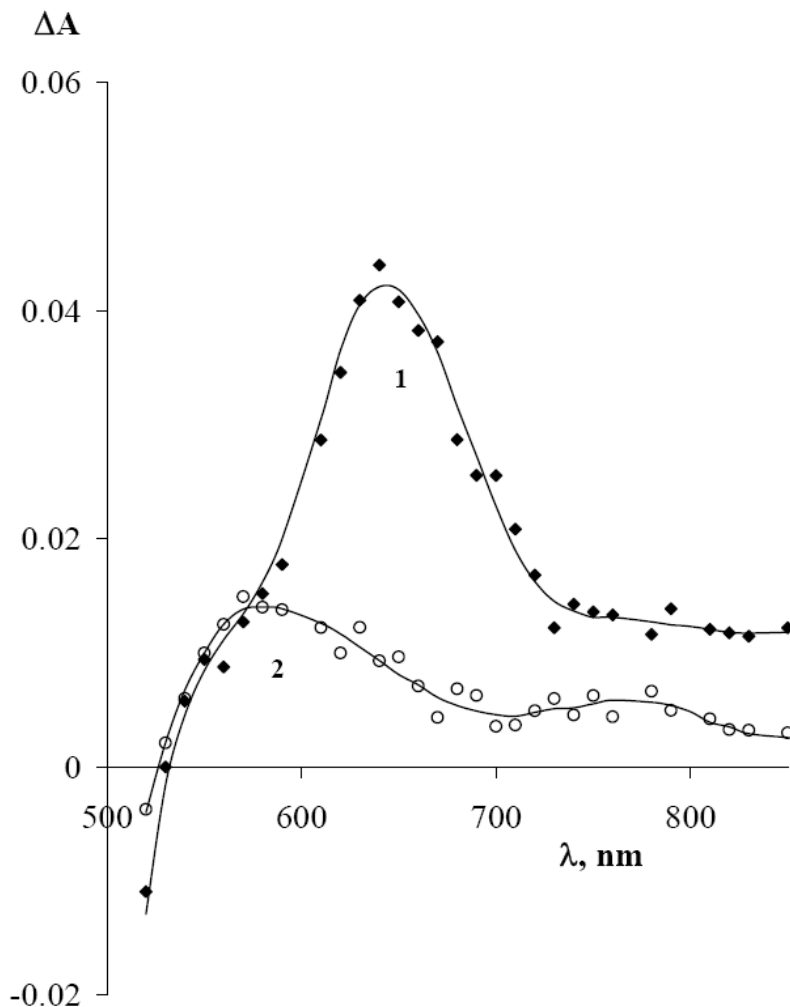


Figure 1. Differential T-T absorption spectra of dye K2 ($c_{K2} = 1.6 \times 10^{-6} \text{ mol l}^{-1}$) in phosphate buffer (1) in the absence of DNA and (2) at the DNA concentration of $2.5 \times 10^{-4} \text{ mol l}^{-1}$ obtained upon direct photoexcitation (at 60 μs after a flash).

Table 1 presents the results of kinetic calculations with the use of the two-exponential kinetic model within the context of the nonlinear optimization algorithm. The differential absorption spectra of two K2 triplet components (Figure 2) attributed to different types of dye-DNA complexes were obtained from the kinetic analysis of the experimental data. The two-exponential character of the triplet state decay kinetics for thiocarbocyanine dyes bound to the biopolymer may be explained by the formation of two different types of complexes (superficial binding and intercalation) [11, 12]. In dye-DNA complexes of these two types the triplet states of bound dye molecules should possess different spectral and kinetic characteristics, which are reflected in the two-exponential character of the triplet state decay kinetics.

The possibility of intercalation of thiocarbocyanines K1-K3 and K4 is revealed by the results of viscosity measurements of DNA solutions in the presence of these dyes.

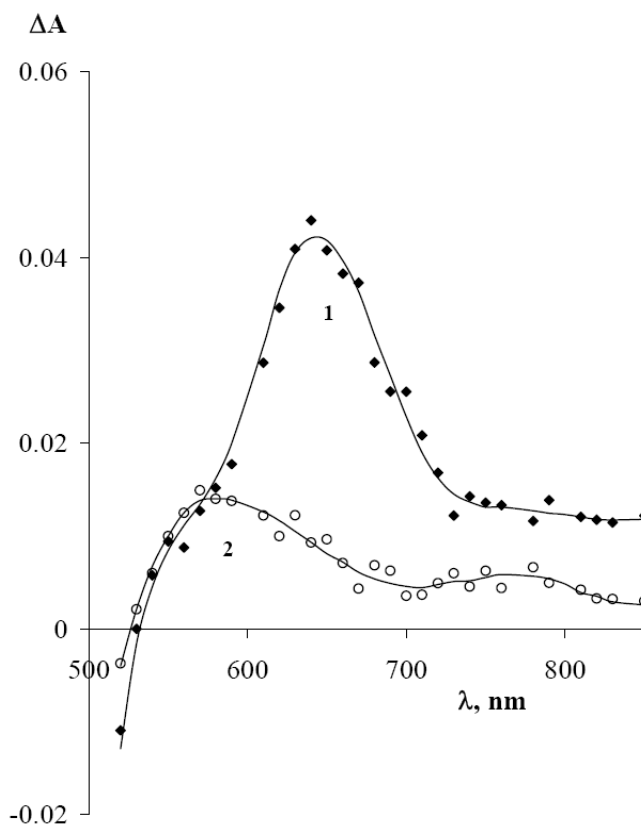


Figure 2. Differential T-T absorption spectra of two triplet components of dye K2 ($c_{K2} = 1.6 \times 10^{-6} \text{ mol l}^{-1}$) in the presence of DNA: (1) the long-lived component and (2) the short-lived component.

Table 1. Decay rate constants (k_1 and k_2) and rate constants for quenching of the triplet state of dyes K1–K3 and K4 by the nitroxyl radical in isopropanol solutions (k_q) and of the long-lived component of the triplet state in the presence of DNA ($k_q(\text{DNA})$) in aqueous buffer solution ($c_{\text{DNA}} = 2.5 \times 10^{-4} \text{ mol l}^{-1}$)

Dye	Substituent	k_1	k_2	k_q	$k_q(\text{DNA})$
		s^{-1}		$\text{l mol}^{-1} \text{s}^{-1}$	
K1	SCH ₃	7.70×10^3	2.52×10^3	$1,5 \times 10^7$	1.6×10^5
K2	OCH ₃	1.08×10^4	1.92×10^3	$7.34 \times 10^7 / 1.4 \times 10^{8(a)}$	3.3×10^6
K3	C ₂ H ₅	8.97×10^3	2.05×10^3	—	5.3×10^6
K4	CH ₃	9.35×10^3	1.98×10^3	3×10^6	3.6×10^6

For example, the relative increase in the viscosity of a DNA solution with K4 ($c_{\text{DNA}} = 5 \times 10^{-5} \text{ mol l}^{-1}$) reached 5.7% at the dye/DNA concentration ratio of 0.5 (an increase in the viscosity was also observed for other meso-substituted thiacyanines). The increase in the DNA solution viscosity is explained in this case by the fact that some “unwinding” of coils of the DNA double helix occurs upon dye intercalation, which leads to elongation of the biomolecule [12]. The possibility of formation of intercalation complexes K4-DNA were also made by Biver et al. [13].

Quenching of the Triplet State of K4 by Iodide Ion

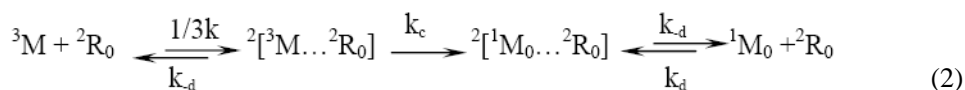
The results of quenching experiments of the K4 triplet state by iodide ion confirm the given above explanation of the two-exponential character of the triplet state decay kinetics of the cyanine dyes observed in the presence of the DNA by the formation of two different types of complexes.

Iodide ion is known to be an efficient quencher of excited states of dyes [14]. In this case, the external heavy atom effect and, possibly, the mechanism of electron transfer from iodide ion to dye contribute to quenching of the dye triplet state. Due to the anionic nature of DNA and electrostatic repulsion, iodide ion is incapable of interacting with dye molecules bound in the complex, and can quench only free triplet molecules being in the solution. Quenching of the triplet state of dye K4 by iodide ion was studied in solution (isopropanol) and in complexes with DNA ($c_{\text{DNA}} = 2.5 \times 10^{-4} \text{ mol l}^{-1}$) by the flash photolysis method. Since T–T absorption signals were not detected upon direct photolysis at the absorption band of K4, the triplet levels of the dye in isopropanol were populated by energy transfer, in which 1,2-benzanthracene was used as a triplet energy donor ($E_T = 16500 \text{ cm}^{-1}$ [15]). The value of k_q for K4 was found to be about $1 \times 10^6 \text{ l mol}^{-1} \text{ s}^{-1}$. In phosphate buffer solution in the presence of DNA ($c_{\text{DNA}} = 2.5 \times 10^{-4} \text{ mol l}^{-1}$), we did not observe noticeable quenching of the K4 triplet state by iodide ($k_q < 10^5 \text{ l mol}^{-1} \text{ s}^{-1}$) in spite of high quencher concentrations (up to $4.6 \times 10^{-2} \text{ mol l}^{-1}$).

This points to the absence in the system triplet dye–DNA of free dye in the triplet state (otherwise, its quenching by iodide would observe in the presence of DNA). The two-exponential character of the decay kinetics of the K4 triplet state in the presence of DNA is due to the presence of two types of dye binding to the biopolymer: on the surface of a DNA molecule (probably, in the minor groove) and by dye intercalation between DNA base pairs.

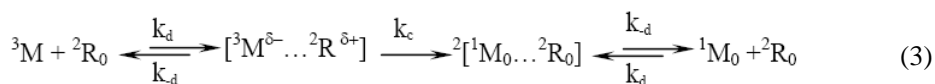
Quenching of the Triplet State of Carbocyanine Dyes by Nitroxyl Radical

Apart from iodide ion, radicals are efficient quenchers of excited states of molecules [16]; the processes of quenching of excited states of various molecules by radicals were studied earlier in detail [17 - 19]. It was shown that the triplet states of usual cyanine dyes are mainly quenched by the mechanism of acceleration of the intersystem crossing to the ground state (T– S_0). In this case, the quenching process is described by the following scheme:



from which the quenching rate constant $k_q = 1/3 k_d k_c / (k_d + k_c)$. Here k_d is the diffusion rate constant for formation of the encounter complex, k_{-d} is the rate constant for its dissociation, k_c is the rate constant for deactivation of the encounter complex, and $1/3$ is the spin statistical factor.

The charge transfer mechanism contributes to the triplet quenching process for some cyanine dyes [18], whose scheme is presented below:



Unlike quenching by the mechanism of acceleration of intersystem crossing, the dependence of the quenching rate constant on the solvent polarity is characteristic of the quenching process by the charge transfer mechanism: the quenching rate constant increases with growing polarity [19].

The processes of triplet state quenching of dyes K1–K3 and K4 by nitroxyl radical in liquid solutions and in complexes with DNA ($c_{DNA} = 2.5 \times 10^{-4} \text{ mol l}^{-1}$) were studied by the flash photolysis method.

The treatment of triplet state decay kinetics of the dyes obtained in the presence of DNA with the use of the two-exponential model shows that, within the chosen range of nitroxyl radical concentrations ($c_R = 0\text{--}6 \times 10^{-4} \text{ mol l}^{-1}$; in some experiments, c_R reached $2 \times 10^{-3} \text{ mol l}^{-1}$), only one of the kinetic triplet components is quenched, namely, the long-lived component. The addition of the radical to the dye–DNA system does not lead to a noticeable increase in the decay kinetics of the short-lived components of the carbocyanine triplet states.

For dyes K1–K4 bound to DNA, linear dependences of the decay rate constants for the long-lived triplet components (k_T) on the radical concentration were observed. From their slopes, the values of k_q for the long-lived component of the triplet state of the dyes were obtained (Table 1).

In the presence of DNA in phosphate buffer solution ($c_{DNA} = 2.5 \times 10^{-4} \text{ mol l}^{-1}$), the dyes with alkyl meso-substituents (K3 and K4) exhibit relatively low and close k_q values for long-lived components of the decay kinetics of their triplet states (Table 1).

To reveal the contributions of mechanisms (2) and (3) to the process of triplet state quenching of selected dyes and the effect of meso-substituent on the values of triplet state rate constants, we determined k_q for dyes K1, K2, and K4 in solutions in the absence of DNA.

The K1 and K4 triplet states were produced in isopropanol by triplet–triplet energy transfer from 1,2-benzanthracene. As the result, we obtained estimated values of k_q for the triplet states of K1 and K4 in isopropanol, which were 1.5×10^7 and $3 \times 10^6 \text{ l mol}^{-1} \text{ s}^{-1}$, respectively. For K4, the k_q value is typical for quenching by the mechanism of acceleration of intersystem crossing to the ground state (2) [17]. The higher value of the constant for K1 permits assumption of contribution of the charge transfer mechanism (3) to quenching of its triplet state.

For dye K2 with methoxy group as the meso-substituent, the relatively high quantum yield to the triplet state permitted experiments with direct photoexcitation of the dye. We studied quenching of the triplet state of dye K2 by the radical in aqueous medium (phosphate buffer, pH 7, 20 mmol l⁻¹) and in organic solvents: alcohols (methanol, isopropanol, hexanol) and dimethyl sulfoxide. Table 2 presents the rate constants for quenching of the K2 triplet state by the radical ($c_R = 0-7 \times 10^{-5} \text{ mol l}^{-1}$).

Table 2. Rate constants for quenching of the triplet state of dye K2 by the nitroxyl radical (k_q) in organic solvents (ϵ is the dielectric permittivity and η the viscosity of a solvent)

Solvent	ϵ (25°C)	η , cP (25°C)	$k_q(R)$, l mol ⁻¹ s ⁻¹
Hexanol	12.0	4.14	3.59×10^7
Isopropanol	18.3	2.10	7.34×10^7
Methanol	32.6	0.545	1.18×10^8
Dimethyl sulfoxide	49.0	1.980	2.20×10^8

The relatively high k_q values for K2 and the observed dependence of k_q on the dielectric permittivity (polarity) of the solvent (Table 2) show that in polar solutions, the charge transfer mechanism (3) becomes crucial in the quenching process. This is probably explained by the redox properties of the dye favorable for the charge transfer mechanism. Correlation of k_q with the solvent viscosity is not observed, which indicates the absence of contribution of diffusion of reactants to the quenching process (the quenching occurs in the kinetic regime).

A comparison of the experimental data on quenching of triplet states of dyes in solutions in the absence and in the presence of DNA permits estimation of the steric complexation effect on the quenching process and conclusions about the structure of the dye–DNA complexes formed. In the case of dye K4, we may conclude that complexation with the biopolymer has relatively weak effect on the k_q value. This is probably due to the fact that the quenching process for K4 occurs in the kinetic regime ($k_c \ll k_{-d}$, see reaction (2)), and diffusion of the quencher to dye molecules bound to DNA exerts no substantial effect on k_q (another assumed reason for this phenomenon could be partial decomposition of the dye(T)–DNA complex and the presence of free triplet dye molecules in the solution; however, the experiments on quenching of the K4 triplet state by iodide ion considered above reject this possibility).

For dye K2, the k_q value decreases by ~40 times on passing from an aqueous solution to a complex with DNA. Similarly, k_q obtained upon quenching of the triplet state of dye K1 bound to DNA is much lower than the values of the constants typical for the mechanism of acceleration of the intersystem crossing to the ground state ($\sim 1 \times 10^6 \text{ l mol}^{-1} \text{ s}^{-1}$). The possible reason for these phenomena is bulky substituents in the polymethine chain (OCH₃ and SCH₃), which create additional spatial hindrances to quencher molecules upon complexation with DNA. Hence, diffusion of the quencher to the triplet molecules is strongly impeded (k_d and k_{-d}).

k_d decrease, and k_{-d} becomes much smaller than k_c), and the quenching turns to the diffusion regime with a low rate constant ($k_q = 1/3 k_d$).

The long-lived components of the triplet state observed in the presence of DNA apparently correspond to dye molecules bound on the surface of the double helix of the biopolymer (probably, in the minor groove). In this case, molecules of the radical quencher undergo some steric hindrances due to the complexation, which can be manifested as a decrease in the k_q values with respect to those observed for free dyes in solutions (for example, for K2). However, the steric hindrances in this case appear to be not so strong as to completely eliminate the quenching.

The absence of quenching by nitroxyl radical of the short-lived triplet component observed for carbocyanines K1–K4 in the presence of DNA suggests that this component corresponds to the complex of intercalation of dye molecules between base pairs of the biopolymer, since in this case the access of the radical quencher to molecules of the bound dye is strongly impeded. Spatial hindrances upon intercalation completely block the access of the radical to dye molecules bound in such a manner.

Quenching of the Triplet States of K1–K4 by Oxygen

Quenching of the triplet states of dyes K1–K4 in complexes with DNA by oxygen showed that, due to steric hindrances appeared upon complexation, the quenching rate constants were much lower than the values expected for the diffusion-controlled reactions ($k_q(\text{O}_2) \sim 2 \times 10^8 \text{ l mol}^{-1} \text{ s}^{-1}$). For oxygen, however, the steric hindrances are insufficient for elimination of quenching of intercalated dye molecules. Here the triplet states of the dye–DNA complexes of both types (superficial and with intercalation) are quenched with roughly the same efficiency. The difference in the behavior of oxygen and the radical (which does not quench the triplet states of intercalation complexes) may be explained by small size of the oxygen molecule, which permits oxygen to diffuse even to intercalated dye molecules. On the other hand, the quenching center N–O in the radical structure is strongly shielded by four methyl groups, which decreases the quenching efficiency and does not permit quenching of intercalated triplet dye molecules.

In summary, the triplet decay kinetics of K1–K4 in the presence of DNA are biexponential; the two observed components are attributed to two different complexes between the dye and DNA. Using nitroxyl radical and iodide ion as quenchers, we have shown that cyanine dyes form with DNA two types of complexes: formed by binding of the dye in the groove of a DNA molecule and by intercalation of the dye between base pairs.

This work was supported by the Russian Foundation for Basic Research, project no. 05-03-32775, and the Program of Basic Research of the Russian Academy of Sciences (2006) “Development of Methods of Preparation of Chemical Compounds and Creation of New Materials” (the Subprogram “Organic and Hybrid Nanostructured Materials for Photonics”).

REFERENCES

- [1] A.N. Glazer, and H.S. Rye, *Nature* 359 (1992), 859.
- [2] E.S. Voropay, M.P. Samtsov, A.P. Ludovsky, and A.N. Sevchenko, *Proc. SPIE-Int. Soc. Opt. Eng.* 4749 (2004), 221.
- [3] E. Delaey, F. van Laar, D. De Vos, A. Kamuhabwa, P. Jacobs, and P. de Witte, *Photochem. Photobiol. B.* 55 (2000), 27.
- [4] S.C. Benson, Z. Zeng, A.N. Glazer, *Anal. Biochem.* 231 (1995), 247.
- [5] A.A. Ishchenko, *Usp. Khim.* 60 (1991), 1708.
- [6] Yu.E. Borisevich, A.S. Tatikolov, and V.A. Kuz'min, *Khim. Vys. Energ.* 5 (1978), 474.
- [7] G. Kelly, and T. Kurucsev, *Biopolymers* 15 (1976), 1481.
- [8] B.C. Baguley, and E.-M. Falkenhang, *Nucleic Acids Res.* 5 (1978), 161.
- [9] C. Rullière, *Chem. Phys. Lett.* 43 (1976), 303.
- [10] M.Yu. Anikovskii, A.S. Tatikolov, P.G. Pronkin, P.P. Levin, V.I. Sklyarenko, and V.A. Kuz'min, *High Energy Chem.* 37 (2003), 398.
- [11] D. Sah, J.B. Chaires, *Bioorg. Med. Chem.* 3 (1995), 723.
- [12] K.C. Hannah, R.R. Gil, B.A. Armitage, *Biochemistry* 44 (2005), 15925.
- [13] T. Biver, A. De Biasi, F. Secco, M. Venturini, S. Yarmoluk, *Biophys. J.* 89 (2005), 374.
- [14] V.V. Brukhanov, G.A. Ketsle, L.V. Levshin, L.K. Sokolova, *Zh. Prikl. Spectrosk.* 36 (1982), 607.
- [15] S.P. McGlynn, T. Azumi, M. Kinoshita, *Molecular Spectroscopy of the Triplet State*, Prentice-Hall, Inc., Englewood Cliffs, New Jersey, 1969.
- [16] O.L.J. Gijzeman, F. Kaufman, G. Porter, *J. Chem. Soc. Faraday Trans. II* 69 (1973), 727.
- [17] V.A. Kuzmin, A.S. Tatikolov, *Chem. Phys. Lett.* 53 (1978), 606.
- [18] V.A. Kuzmin, A.S. Tatikolov, Yu.E. Borisevich, *Chem. Phys. Lett.* 53 (1978), 52.
- [19] V.A. Kuzmin, A.S. Tatikolov, Yu.E. Borisevich, *Doklady Akad. Nauk SSSR* 229 (1976), 1159.

Chapter 7

HEME OXYGENASE ACTIVITY IN RAT LIVER DEPENDING ON ACTION OF CoCl_2 , ANIT AND TWEEN

F. Greulich¹ and A. V. Alessenko²

¹Friedrich – Schiller University of Jena

²Institute of Biochemical Physics

ABSTRACT

Heme oxygenase (HO) is the rate – limiting enzyme in heme degradation. But its role is more important than this. Especially the inducible form HO-1 plays a key role in preventing oxidative damage. Ottenbein et al. 2003 called HO-1 a "therapeutic funnel" for substances and factors seeming to be cell protective. So, especially HO-1 is a target of pharmaceuticals and diseases research. For examining different disease states (Alzheimers disease, asthma, reperfusion/ischemia – induced injury, arteriosclerosis...) or effects of distinct substances under both toxic and therapeutic conditions it is very important to have an assay determining HO activity. In this report the starting development of a working method for detection of HO activity is described. Basing on the method developed by Tenhunen et al. (1968) we used modified assays described by Ryter et al. (1998), Srisook et al. (2004) and modifications made by our self. Besides normal rats (controls) we used also CoCl_2 , Tween-80 and ANIT treated rats for testing the assay conditions. At the end, we could prove the induction of HO enzyme activity by CoCl_2 and ANIT described previous by Maines et al. (1974) and Agarwall et al. (1989). Furthermore we could show that Tween-80 also induces HO activity.

INTRODUCTION

Heme oxygenase (HO) is a microsomal enzyme catalysing the breakdown of b-type heme to equimolar amounts of biliverdin IXa, ferrous iron and carbon monoxide (CO) by cleaving the -meso carbon bridge. All of these products are biological active. Ferrous iron facilitates free radical formation but induces also ferritin an antioxidant iron sequestering protein. CO

like NO seems to be a signal transducer and promotes vasodilatation. Furthermore CO has anti-apoptotic and anti-inflammatory properties by using the MKK2/p38 MAPK pathway and is a key product of HO preventing several disease (arteriosclerosis, lung disease (asthma...), reperfusion/ischemia-induced injury). Biliverdin is converted immediately to bilirubin by the cytosolic enzyme biliverdin reductase (BR). Bilirubin is an important antioxidant. It prevents TNF- α -mediated apoptosis for example by inhibiting sphingomyelinase. This is the reason why this enzyme is in "our" interest of studies. There are different isoforms of HO described in literature. The HO-1 is a 32 kDa inducible enzyme little expressed under normal conditions. Especially cellular stress mediated by heme, heavy metals, UVA radiation, glutathione depletion, hypoxia, hyperoxia and many others increases its gene expression. So it seems to be responsible for protection against oxidative stress and plays a key role in ageing and disease. On the other hand, HO-2 (36 kDa) is constitutively synthesised and plays a role the normal process of heme degradation. Under normal conditions HO-2 is highly expressed in several tissues like spleen, liver and brain. HO-3 a third isoform of HO is not well studied, yet. Its gene consists of no introns and is high homolog to HO-2. So HO-3 seems to be a retransposed HO-2 gene.

In our experiments we concentrate on detection of HO activity independent on the isoform. As mentioned above only HO-1 is inducible. So inducers of HO activity used in this experiment seem to enhance HO-1 activity. First we used CoCl_2 witch is known to increase the HO activity around 10 times 24 h after treatment of rats (Maines et al. 1974, Hoshi et al. 1989). Possible mechanisms are suggested by Kaliman et al. (2000). On one hand, some metal ions like Co^{2+} incorporate to protoporphyrin IX (catalyzed by ferrochetalase) substituting for iron and generating Co-PP which induces HO by forming a complex with hemopexin. The binding of this complex to hemopoxin receptor induces NF- κ B transfer from cytosol to nucleus and therefore activates c-Jun N-terminal kinase (JNK) which phosphorylates the c-Jun protein of the AP-1 complex. The HO-1 promotor includes binding sides for both NF- κ B and AP-1. On the other hand, the released iron enhances ROS formation and also leads to HO induction.

In a second experiment we used α -naphthylisothiocyanate (ANIT) for inducing HO activity. ANIT treated rats were evaluated as a model for lipoprotein metabolism in cholestatic diseases. Further, it causes bile stasis, hyperbilirubinemia, bile duct hyperblasia and biliary cirrhosis. The mechanism of ANIT action is not clear, yet. But Agarwal et al. (1989) have shown that ANIT inhibits the microsomal and mitochondrial Ca^{2+} uptake by decreasing Ca^{2+} ATPase activity and increases concentration of free and conjugated bilirubin. ANIT also induces inflammation by raising the permeability of liver tight junctions (Kan et al. 1986).

Tween-80 usually used as detergent is also tested because of its usage as solvent for ANIT.

METHODS AND MATERIALS

For these experiments Wistar rats (male) treated with 60 mg/kg CoCl_2 , 120 mg/kg α -naphthylisothiocyanate (ANIT) diluted in Tween-80 (1 drop in 3.5 ml dH_2O), Tween-80 (1

drop in 3.5 ml dH₂O) and untreated rats were used. The injection of each substance is performed subcutane 40 h before killing them.

Isolation of Rat Liver Microsomes

Rats were anesthetized with butanol (C₄H₁₀O), killed by cutting through the heart and the liver is perforated with cold 0.25 M sucrose solution. After preparation of the liver, it is stored in cold 0.25 M sucrose. Afterwards it is weighted and a 33.3 % homogenise with 0.25 M sucrose solution is performed using a cold French press and Douncer. After centrifugation at 12,000 rpm for 30 minutes at 4 °C the post-mitochondrial supernatant is transferred to new centrifugation tubes and centrifuged 1 hour at 31,000 rpm (Beckmann centrifuge) and 4 °C. The post - microsomal supernatant is then separated from the pellet (microsomes). The microsomes are resuspended in 4 ml Tris – KCl buffer (20 mM Tris(hydroxymethyl)aminomethan (Merck), 125 mM KCl (Radelkis) pH= 7,4) and destroyed with a douncer.

Heme Oxygenase Assay

The assay consists of:

- 0.2 ml post-michrosomal supernatant diluted 1:1 containing biliverdin reductase
 - 0.1, 0.2 or 0.4 ml microsomal solution containing heme oxygenase (with constant hemin amount of 0.2 ml)
 - 0.1, 0.2 or 0.5 ml 0.5 mM hemin (Fluka) (solubilised in 1 drop 1 M NaOH and 0.375 mM BSA) → with constant amount of microsomes (0.1 ml)
 - 0.1 ml 12,5 mM Glucose 6-phosphate (Sigma)
 - 9 1 166.66 U/ml Glucose 6-phosphate dehydrogenase
 - 0.1 ml 8.7 mM NADP⁺ or NADPH + H⁺ (Sigma)
 - ad. 1.5 ml with Tris-KCl buffer
- => Assay composition (1,5 ml)
- 0.033, 0.066, 0.166 mM hemin
 - 0.025, 0.05, 0.125 mM BSA
 - 0.83 mM glucose 6-phosphate (G6P)
 - 1.5 U glucose 6-phosphate dehydrogenase (G6P-DH)
 - 0.58 mM NADP⁺ or NADPH + H⁺ → 0.8 mM
 - 12.00, 10.66, 6.66 mM Tris (0.1 ml microsomes) or 10.66, 9.33, 6.66 mM Tris (0.2 ml hemin)
 - 75.00, 66.66, 41.66 mM KCl (0.1 ml microsomes) or 66.66, 58.33, 41.66 mM KCl (0.2 ml hemin)

After mixing all components by vortexing the assay is incubated for 1.5 h at 37 °C (water bath or drying board). The concentration of formatted bilirubin can be determined by measuring the difference in absorbance between 468 nm and 530 nm in a difference spectrum

to control. As blank a control solution containing the same concentrations of hemin, BSA, microsomes and microsomal supernatant as the probes is used.

Calculation of heme oxygenase activity was performed by using Lambert – Beer's law with $\epsilon = 40 \text{ mM}^{-1} \cdot \text{cm}^{-1}$.

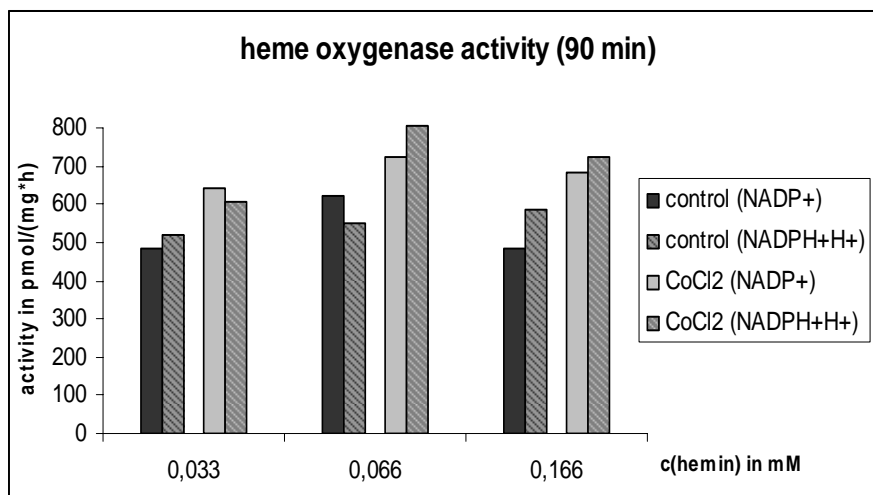
Protein Determination After Lowry (1951)

The microsomal solution is diluted 1:50 in 0.1 % SDS. 0.4 ml of this solution is transferred to a new tube and 2 ml of a solution containing 0.4 % (w/v) NaOH, 2% (w/v) Na_2CO_3 , 0.002 % (w/v) Sodiumcitrate and 0.01 % (w/v) $\text{Cu}_2\text{SO}_4 \cdot 5\text{H}_2\text{O}$ is added. After addition of 0.2 ml 50 % (v/v) Folin and Ciocateu's phenol reagent and vortexing the tubes were incubated for 30 min at RT. The absorbance of the built protein complex is measured at 750 nm (blank 0.1 % SDS) and the protein concentration is determined with the help of a BSA standard curve.

RESULTS

At first, we measure the HO activity of one control and one CoCl_2 treated rat in dependency on different hemin concentrations. The results are displayed in table/graph 1. As you see the highest HO activity is reached with 0.066 mM hemin in the assay. Furthermore, only little difference between usage of NADP^+ and $\text{NADPH}+\text{H}^+$ could be seen. In case of CoCl_2 treatment this difference raises with increased HO activity. Because of the addition of G6P-DH reducing NADP^+ by oxidizing G6P there is no necessary to add $\text{NADPH}+\text{H}^+$ to the assay, but in case of higher HO activity G6P-DH seems to become the limiting enzyme so that the addition of $\text{NADPH}+\text{H}^+$ accelerates the HO reaction (only in case of CoCl_2 treatment). In correspondence to other authors (Maines et al. (1974), Hoshi et al. (1989)) we could show that CoCl_2 increases the HO activity in 17 – 42 %.

treatment	c(hemin) in mM		A(468 nm)	A(530 nm)	\Delta A	c(Bilirubin) in μM	c(Protein) in mg/ml	Activity in pmol/(h*mg (Prot))
no	0,033	NADP^+	0,051	0,037	0,014	0,350	7,241	483,36
		$\text{NADPH}+\text{H}^+$	0,016	0,001	0,015	0,375	7,241	517,88
	0,066	NADP^+	0,032	0,014	0,018	0,450	7,241	621,46
		$\text{NADPH}+\text{H}^+$	0,006	-0,010	0,016	0,400	7,241	552,41
	0,166	NADP^+	-0,006	-0,020	0,014	0,350	7,241	483,36
		$\text{NADPH}+\text{H}^+$	0,002	-0,015	0,017	0,425	7,241	586,94
CoCl_2	0,033	NADP^+	0,044	0,028	0,016	0,400	6,207	644,43
		$\text{NADPH}+\text{H}^+$	0,004	-0,011	0,015	0,375	6,207	604,16
	0,066	NADP^+	0,007	-0,011	0,018	0,450	6,207	724,99
		$\text{NADPH}+\text{H}^+$	-0,008	-0,028	0,020	0,500	6,207	805,54
	0,166	NADP^+	0,002	-0,015	0,017	0,425	6,207	684,71
		$\text{NADPH}+\text{H}^+$	-0,003	-0,021	0,018	0,450	6,207	724,99



Table/Graph 1. CoCl₂ treatment.

A CoCl₂ treated rat (~ 40 h) has been killed and a microsomal solution is isolated as described above. The HO activity in dependency of different hemin concentration is measured and the results are visible in this table and graph.

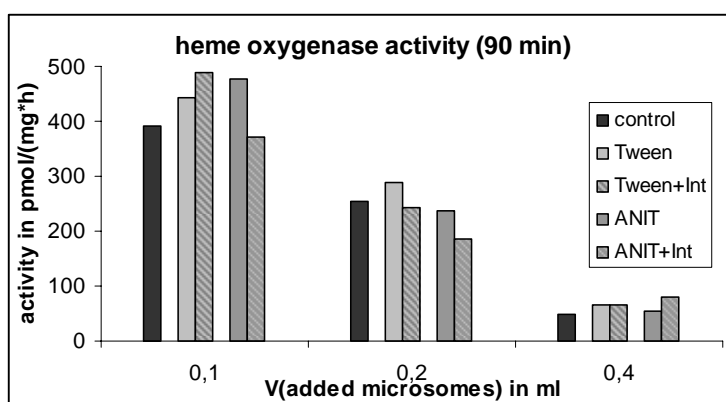
You can see that CoCl₂ acts as an inducer of HO activity either by increasing the enzyme activity or by raising the amount of HO relative to the whole microsomal protein amount.

In another experiment, we studied the dependency of the HO assay from the volume of added microsomal solution and the effect of ANIT and Tween-80.

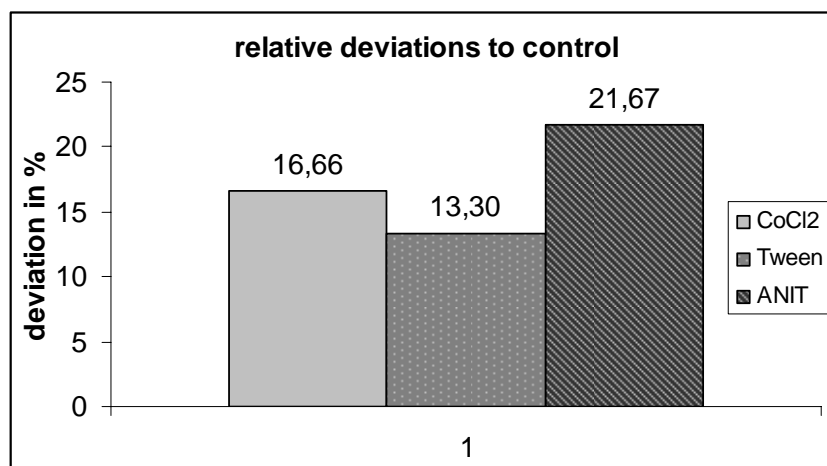
Rats are treated with 120 mg/kg ANIT and Tween-80 in the same amount as used for diluting ANIT. After approximately 40 h the rats were killed and microsomes isolated as described above. Here you can see the results of the heme oxygenase activity measurement by using 0.2 ml hemin solution and different amounts of microsomal solution. The highest activity is measured with 0.1 ml added microsomes and decreases 5 to 9-fold at 0.4 ml added microsomes. So 0.2 ml hemin solution is too little for an increased (more than 0.1 ml) microsomal volume. So HO is rate-limited.

As you can see in Table/Graph 2, both ANIT and Tween-80 induce HO activity. But the assay does not work perfect at this moment. The HO activity enhancement of only 22 % for ANIT is less than described in literature (Kaliman et al. (1989)). The cause seems to be the same as mentioned above for CoCl₂. In this experiment, we could further show that Tween-80 without ANIT also increases the HO activity. The mechanism is not clear. In opposite to ANIT, Tween-80 must activate HO by a non-cytotoxic mechanism because of its application in food processing.

treatment	V(microsomal solution) in ml	A(468 nm)	A(530 nm)	ΔA	c(fBilirubin) in μM	c(Protein) in mg/ml	Activity in pmol/(h*mg(Prot))
No	0,1	0,040	0,030	0,010	0,250	6,389	586,95
	0,2	0,009	-0,004	0,013	0,325	12,778	381,52
	0,4	0,004	-0,001	0,005	0,125	25,556	73,37
Tween-80	0,1	0,005	-0,005	0,010	0,250	5,639	665,01
	0,2	0,008	-0,005	0,013	0,325	11,278	432,26
	0,4	0,006	0,000	0,006	0,150	22,556	99,75
ANIT + Tween	0,1	-0,001	-0,010	0,009	0,225	4,726	714,13
	0,2	0,008	-0,001	0,009	0,225	9,452	357,07
	0,4	0,003	-0,001	0,004	0,100	18,904	79,35
Tween + Int	0,1	0,000	-0,011	0,011	0,275	5,639	731,51
	0,2	0,010	-0,001	0,011	0,275	11,278	365,76
	0,4	0,005	-0,001	0,006	0,150	22,556	99,75
ANIT + Int	0,1	0,001	-0,006	0,007	0,175	4,726	555,44
	0,2	0,001	-0,006	0,007	0,175	9,452	277,72
	0,4	0,001	-0,005	0,006	0,150	18,904	119,02



Table/Graph 2. Heme oxygenase activity dependency on volume of added microsomes dependency on volume of added microsomes.



Graph 3. relative deviations of HO activity from control by treatment with CoCl₂, ANIT and Tween-80.

In this picture the differences in HO activity between CoCl₂, Tween-80 and ANIT treated rats is shown. As you can see, all of them induce the HO activity but much lower than described in literature.

DISCUSSION

At first, we could prove that CoCl₂ induces HO activity. Whether CoCl₂ increases the enzyme activity or the enzyme amount relative to the whole microsomal protein concentration is not yet clear by this experiment. So we can not say that the higher HO activity is a result of inducing HO-1 gene expression and therefore of raised HO protein concentration or enhanced HO activity by CoCl₂ acting as an enzyme activator. Because of studies from Maines et al. (1975) observing raised liver weight and total microsomal protein after CoCl₂ treatment of rats, an induction of HO-1 by increasing the available enzyme amount seems to be probable. Furthermore, the increase of HO activity compared with control rats is very low referring to literature. This could be an effect of a too long incubation. So we missed the top of the HO activity induction by CoCl₂. Gonzales et al. (2005) have shown that the highest bilirubin formation is reached around 12 h after injection of CoCl₂ and decreases up to 36 h after treatment, when enzymatic activity was similar to control values. On the other side, it is not clear if the increase of HO activity is an effect of deviations produced by the method. For example change pH conditions after solubilisation of heme with one drop of 1 M NaOH.

Also α -naphthylisothiocyanate (ANIT) enhances the measured HO activity. ANIT is a drug causing bile stasis, hyperbilirubinemia acutely, bile duct hyperplasia and biliary cirrhosis (Leonard et al. (1981), Ushida et al. (2002)). Therefore its HO activity enhancing potential is well known.

The induction of HO activity by Tween-80 was not known, yet. Because of the application of Tween-80 in food processing, a mechanism of HO induction by damaging cells seems to be improper. For sure results, this experiment should be repeated. If it is possible, measurements of HO activity after treatment with ANIT (without Tween-80) and CoCl₂ + Tween-80 should be done.

During the next weeks, this assay should be modified further especially concerning the ratio of hemin concentration and used volume of microsomal fraction. Because of the pH dependency of biliverdin reductase (XXX) the pH should be checked at every step. The optimal pH for using NADPH as cofactor is 8.7 (Maines et al. 1988).

REFERENCES

- [1] Agarwal, Arvind K.; Zinermon, Wanda D.: Effect of Alpha-naphthyl Isothiocyanate and CCl₄ Interaction on Hepatocellular Calcium Transport.: *Bull. Environ. Contam. Toxicol.*, No. 42: 464-470; 1989.
- [2] Baranano, David R.; Rao, Mahil; Ferris, Christopher D.; u.a.: Biliverdin reductase: A major physiologic cytoprotectant.: *PNAS*, No. 25: 16093-16098; 2002.
- [3] Baranano, David E.; Snyder, Solomon H.: Neural roles for heme oxygenase: Contrasts to nitric oxide synthase.: *PNAS*, No. 20: 10996-11002; 2001.

-
- [4] Bell, Ellis J.; Maines, Mahin D.: Kinetic properties and regulation of biliverdin reductase.: *Biochem. and Biophys.*, No. 1: 1-9; 1988.
- [5] Dulak, Jozef; Jozkowicz, Alicija: Carbon monoxide - a new gaseous modulator of gene expression. In: *Acta Biochimica Polonica*, No. 1: 31-47; 2003.
- [6] Gonzales, Soledad; Polizio, Ariel H.; Erario, Maria A. et al.: Gluthamin is highly effective in preventing in vivo cobalt – induced oxidative stress in rat liver.: *World J Gastroenterol*, No. 11 (23): 3533-3538; 2005.
- [7] Kaliman, P.A.; Nikitchenko; I.V.; Sokol, O.A.; et al.: Regulation of Heme Oxygenase Activity in Rat Liver during Oxidative Stress Induced by Cobalt Chloride and Mercury Chloride.: *Biochemistry (Moscow)*, No. 1: 77-82; 2001.
- [8] Kan, Kwok S.; Coleman, Roger: 1-Naphthylisothiocyanate-induced permeability of hepatic tight junctions to proteins.: *Biochem. J.*, No. 236: 323-328; 1986.
- [9] Lowry, OH; Rosbrough, NJ; Farr, AL et al.: Protein measurements with the Folin phenol reagent.: *J. Biol. Chem.* 193: 265-275; 1951.
- [10] Maines, Mahin D.; Kappas, Attallah: Cobalt induction of hepatic heme oxygenase; with evidence that cytochrome P-450 is not essential for this enzyme activity.: *PNAS*, 71 (11): 4293-4297; 1974.
- [11] Maines, Mahin D.: Heme oxygenase: function, multiplicity, regulatory mechanisms, and clinical applications.: *FASEB J.*, No. 2: 2557-2568; 1989.
- [12] Morse, Danielle; Choi, Augustine M.: Heme Oxygenase-1. The "emerging molecule" has arrived: *Am. J. Respir. Cell Mol. Biol.*, No. 27: 8-16; 2002.
- [13] Otterbein, Leo E.; Soares, Miguel P.; Yamashita, Kenichiro; u.a.: Heme oxygenase-1: unleashing the protective properties of heme.: *TRENDS in Immunology*, No. 8: 449-455; 2003.
- [14] Ryter, Stefan W.; Kvam, Egil; Richman, Larry et al.: A chromatographic assay for heme oxygenase activity in cultured human cells: application to artificial heme oxygenase overexpression.; *Free Radical Biol. Med.*: 24(6), 959-971, 1998.
- [15] Ryter, Stefan W.; Ottenbein, Leo E.; Morse Danielle; et al.: Heme oxygenase/carbon monoxide signaling pathways: Regulation and functional significance.: *Mol Cell Biochem*, No. 234/235: 249-263; 2002.
- [16] Srisook, Klaokwan; Cha YN: Biphasic induction of heme oxygenase-1 expression in macrophages stimulated with lipopolysaccharide.: *Biochem Pharmacol*, No. 68: 1709-1720; 2004.
- [17] Tenhunen, Raimo; Marver, Harvey S.; Schmid, Rudi: Microsomal Heme Oxygenase. Characterisation of an enzyme.: *J. Biolog. Chem.*, No. 244: 6388 – 6394; 1969.
- [18] Tenhunen, Raimo; Marver, Harvey S.; Schmid, Rudi: THE ENZYMIC CONVERSION OF HEME TO BILIRUBIN BY MICROSOMAL HEME OXYGENASE.: *PNAS*, No. 61: 748-755; 1968.
- [19] Tosaik, Arpad; Das, Dipak K.: The role of heme oxygenase signaling in various disorders.: *Mol Cell Biochem*, No. 232: 149-157; 2002.

Chapter 8

GENETIC CONSTRUCT ENCODING THE BIOSYNTHESIS OF N-HIS₆-E-PHFLUORIN_S-OPH IN *E. COLI* CELLS

I. Lyagin¹, D. Gudkov², V. Verkhusha³ and E. Efremenko^{1,2*}

¹Institute for Biochemical Physics, RAN, Kosygin str. 4, Moscow, 117334, Russia

²Chemical Enzymology Department, Chemistry Faculty, The M.V. Lomonosov Moscow State University, Lenin's Hills 1/11, Moscow, 119992, Russia

³Department of Anatomy and Structural Biology, Albert Einstein College of Medicine, 1300 Morris Park Avenue, Bronx, New York, 10461, USA

INTRODUCTION

A high interest to the enzymatic or microbial detoxification of organophosphorous compounds (OPC) being derivatives of orthophosphoric and alkylphosphonic acids (Efremenko and Sergeeva, 2001) exists, since pesticides, widely used in agriculture, and neurotoxic chemical warfare agents (Vx, sarin, soman), that should be destructed according to the Chemical Weapons Convention, belong to the discussed group of OPC.

Organophosphorus hydrolase (OPH, EC 3.1.8.1) catalyses the hydrolysis of a rather broad spectrum of OP neurotoxins and can be used for "Green solution" of the problem (Singh and Walker, 2006). The elaboration of new genetic constructs encoding OPH linked to different fusion partners should enable improved protein folding and increase in the yield of active form of enzyme. The unique features of several green fluorescent protein (GFP) variants (Gurskaya *et al.*, 2006; Peña *et al.*, 2006), such as dependence of visible fluorescence intensity or change of fluorescence wavelengths on pH of the environment, are very attractive for the elaboration of OPH fused with these proteins. This approach should considerably simplify the control of pH-conditions favorable for decontamination by OPC making it visualized.

* E-mail: efremenko@enzyme.chem.msu.ru

The introduction of hexahistidine tag (His₆-tag) to the N-terminus of chimeric protein significantly simplify the protein purification procedure, enabling isolation of target protein directly from crude cell extract (Efremenko *et al.*, 2006). There were two main tasks in this work was: i) to obtain the genetic construct encoding synthesis of fusion protein N-His₆-X-OPH, where X = superecliptic-pH-sensitive fluorine; ii) to reveal conditions (host-strain, temperature and inductor concentration) favorable for construct expression in *E.coli* cells.

MATERIALS AND METHODS

The following chemicals used in the work were purchased from Sigma (St. Louis, MO, USA): *O,O*-diethyl-*O*-(4-nitrophenyl)-phosphate (Paraoxon); imidazole; Coomassie brilliant blue (R-250); isopropyl- β -D-thiogalactoside (IPTG); chicken egg albumin (protein standard for Bradford assay); lysozyme; cobalt chloride hexahydrate. Tryptone and yeast extract were bought from Difco (Detroit, MI, USA). Middle range molecular weight protein markers for electrophoresis and restrictase *Bam*HI, *Sal*I and *Sma*I were purchased from Fermentas (Vilnius, Lithuania). The polyacrylamide cryogel modified by iminodiacetic acid as metal-chelating ligand (IDA-cryoPAAG) was provided by Protista Biotechnology AB (Lund, Sweden). All other chemicals were of analytical grade and purchased from Reachim (Moscow, Russia).

Plasmid pTES-His₆-OPH was restricted in the *Bam*HI and *Sal*I sites (Efremenko *et al.*, 2005). The *Bam*HI/*Sal*I fragment (4275 bp) was isolated by electrophoresis in 0.8% agarose gel. The gene of e-pHluorin_s was cloned from plasmid pGEX-4T2-e-pHluorin_s (Schuster *et al.*, 2005). The following PCR primers were used:

FOR-pH: AGGAGAGGATCCAGTAAAGGAGAAGAAGACTTTT (33)

REV-pH: AGGAGTCCCAGGGCCTCCTCTACCTTTGTATAGTTCATCCATGC (45)

FOR-op: AGGAGTCCCAGGGGGTGGCGGAAGAATCGGCACAGGCGATCGGAT (45)

REV-op: TCGAAAGTCGACACATCGACAATCGTTTCGCAC (33)

The PCR of pGEX-4T2-e-pHluorin_s with primers FOR-pH and REV-pH was carried out to introduce restriction sites *Bam*HI and *Sma*I to the N- and C-terminus, respectively. Additionally, 12 bp nucleotide sequence encoding synthesis of 4 amino acid (GGRG, the first part of spacer) was inserted to the C-terminus of e-pHluorin_s gene. After PCR the 754 bp fragments were isolated and treated by restrictases *Bam*HI and *Sma*I. The final sequence (738 bp) was isolated using 1.3% agarose gel.

The PCR of pTES-His₆-OPH with primers FOR-op and REV-op was realized to insert the restriction site *Sma*I and the 12 bp nucleotide sequence encoding synthesis of 4 amino acid (GGGR, the second part of spacer) to the N-terminus of OPH. The PCR fragments (278 bp) were isolated and restricted by *Sma*I and *Sal*I. The final sequence (260 bp) was isolated using 1.3% agarose gel.

The vector assembling was carried out by combination of ligation of three obtained fragments with T4-ligase (4 h, 12°C). The scheme of pTES-His₆-e-pHluorin_s-OPH shown in Figure 1.

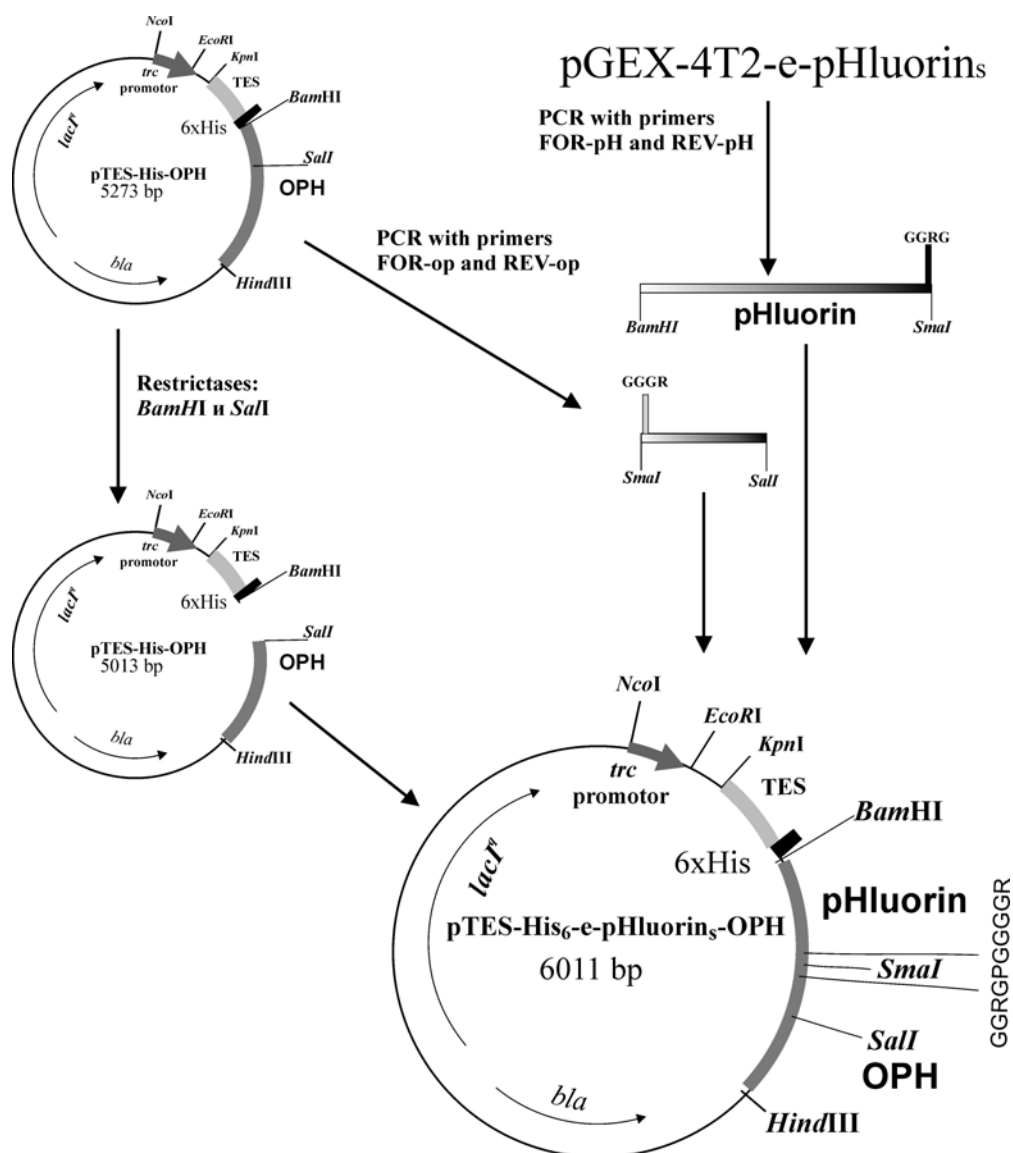


Figure 1. Scheme of constructed pTES-His₆-e-pHluorin₅-OPH.

The *E. coli* JM1 cells were transformed by pTES-His₆-e-pHluorin₅-OPH and two clones (No.6 and No.16) were used to isolate the constructed plasmids for its further use in transformation of following *E. coli* strains: DH5 α , BL21 and W3110.

The overnight cultures of all *E. coli* strains grown at 30°C in Luria-Bertani (LB) medium containing 100 $\mu\text{g mL}^{-1}$ ampicillin and 1 mM CoCl₂ was inoculated to the same medium with 0.1, 0.5 or 1 mM IPTG as inducer of N-His₆-e-pHluorin₅-OPH biosynthesis. The cells were cultivated for 20 h in thermostatically controlled shaker Adolf Kuhner AG (Basel, Switzerland) with constant agitation (37°C, 180 rpm) and harvested using centrifuge Beckman J2-21 (Fullerton, CA, USA) at 8,000 \times g for 20 min.

Isolation and purification of N-His₆-e-pHluorin₅-OPH was undertaken as previously described (Efremenko *et al.*, 2006). Cell biomass (5 g) was suspended in 50 mM K-phosphate

buffer (pH 7.5, 25 mL) containing 0.3 M NaCl and 1 g L⁻¹ lysozyme. The cell debris was removed by centrifugation (30 min, 15,000×g). Supernatant was loaded at a flow rate 5 mL min⁻¹ onto 100-mL column filled with Co²⁺-IDA-cryoPAAG equilibrated with 50 mM K-phosphate buffer (pH 7.5) containing 0.3 M NaCl. The system was washed at the same flow rate with 50 mM K-phosphate buffer (pH 7.5) containing 0.3 M NaCl and 10 mM imidazole until OD₂₈₀ became less than 0.01.

Enzymatic activity was determined spectrophotometrically using Agilent 8453 UV-visible spectroscopy system equipped with a thermostatted cell (Agilent Technology, Germany). The accumulation of *p*-nitrophenolate anion as product of Paraoxon hydrolysis was monitored at 25°C and 405 nm. The amount of enzyme hydrolyzing one μmole of substrate for 1 min at 25°C and pH 10.5 (100 mM Na-carbonate buffer) was considered as one unit of enzymatic activity.

RESULTS AND DISCUSSION

Obtaining of Genetic Construct

In this work pTES-His₆-OPH was used as a base plasmid since it was previously successfully used for biosynthesis of N-His₆-OPH (Votchitseva *et al.*, 2006). The plasmid contained: a) the sequence encoding His₆-tag; b) an element containing the T5-phage promotor and *lac* operon; c) the synthetic ribosome-binding domain developed for optimal recognition and binding of m-RNA; d) the translation stop-codons in all reading frames; e) the terminator of transcription from λ-phage; f) the replication region and gene sequence of β-lactamase. The successful biosynthesis of N-His₆-e-pHluorin_s-OPH was obtained using developed plasmid pTES-His₆-e-pHluorin_s-OPH. The green fluorescence of *E.coli* cells transformed by constructed plasmid was confirmed using a fluorescent microscope “Biomed YX-1” (Russia) (Figure 2).

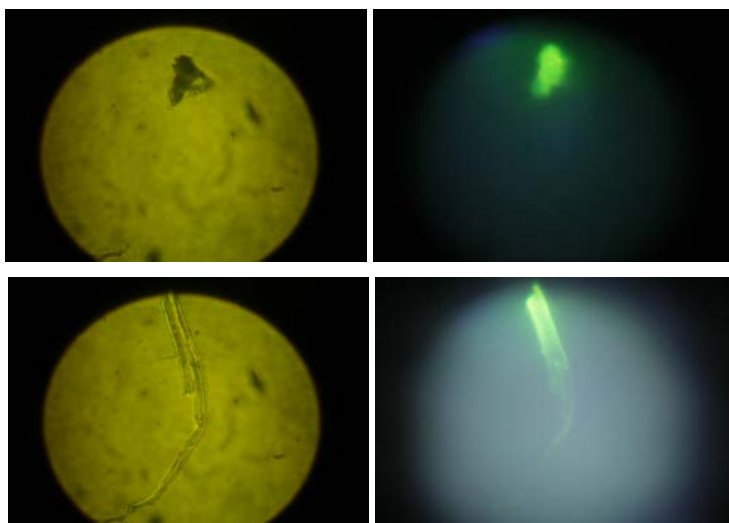


Figure 2. Continued on next page.

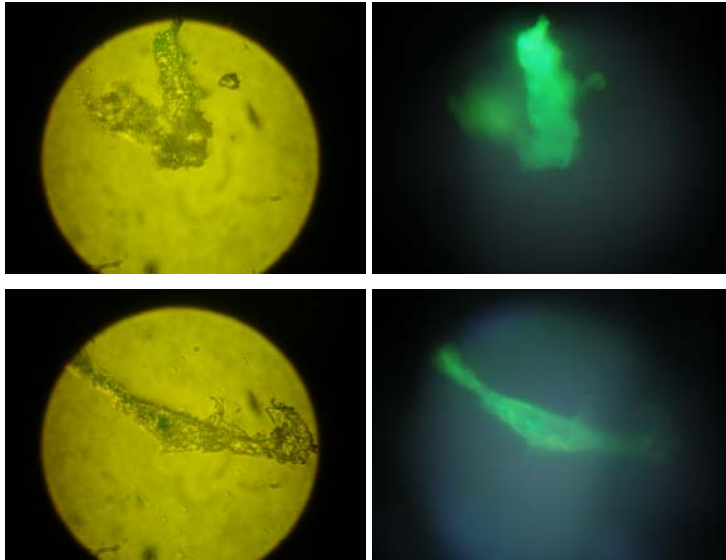


Figure 2. The images of *E. coli* JM1 (1), DH5 α (2), BL21 (3) and W3110 (4) cells transformed by pTES-His₆-e-pHluorin_s-OPH obtained with optical microscope “Biomed YX-1” in visible (a) and UV-light (b).

Gene Expression

Investigation of expression of vectors, isolated from two clones of *E. coli* JM1 and transformed to *E. coli* DH5 α cells, did not show any difference between results (Figure 3). Analysis of electrophoretic data obtained after study of samples taken from different cell cultivation periods showed accumulation of N-His₆-e-pHluorin_s-OPH with molecular mass 72 kDa (Figure 4). The most appropriate conditions for biosynthesis of target protein were following: cultivation time after induction – 5 h, IPTG concentration – 1 mM.

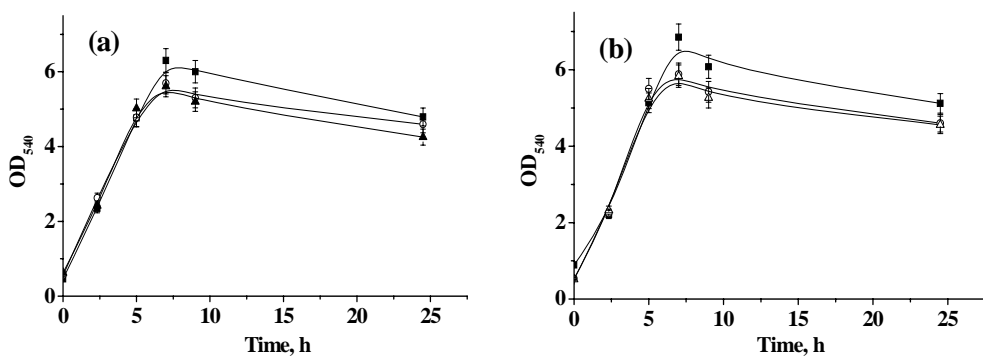


Figure 3. Growth kinetics of *E. coli* DH5 α cells, transformed by pTES-His₆-e-pHluorin_s-OPH isolated from clone No.6 (a) and clone No.16 (b) in the presence of various IPTG concentrations: ■ – 0.1 mM, ○ – 0.5 mM, ▲ – 1 mM.

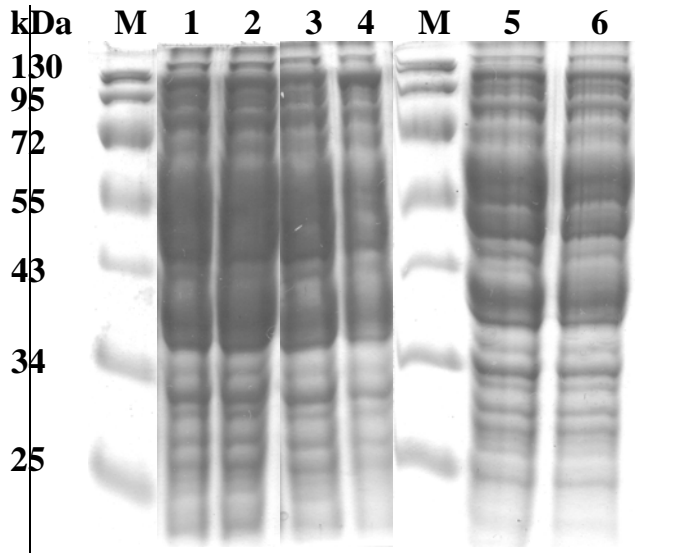


Figure 4. The electrophoretic analysis of *E.coli* DH5 α cells transformed by pTES-His₆-e-pHlourin_s-OPH isolated from clone No. 6 (lanes 1, 3, 5) and No. 16 (lanes 2, 4, 6) in the presence of various IPTG concentrations (0.1 mM – lanes 1-2; 0.5 mM – lanes 3-4; 1 mM – lanes 5-6). M – molecular weight markers.

The plasmids isolated from clones No.6 and No.16 were used to transform *E.coli* BL21 and W3110 strains. The cell cultivation conditions were similar to those applied for *E.coli* DH5 α cells. The accumulation of protein with molecular mass 72 kDa was demonstrated (Figure 5, 6).

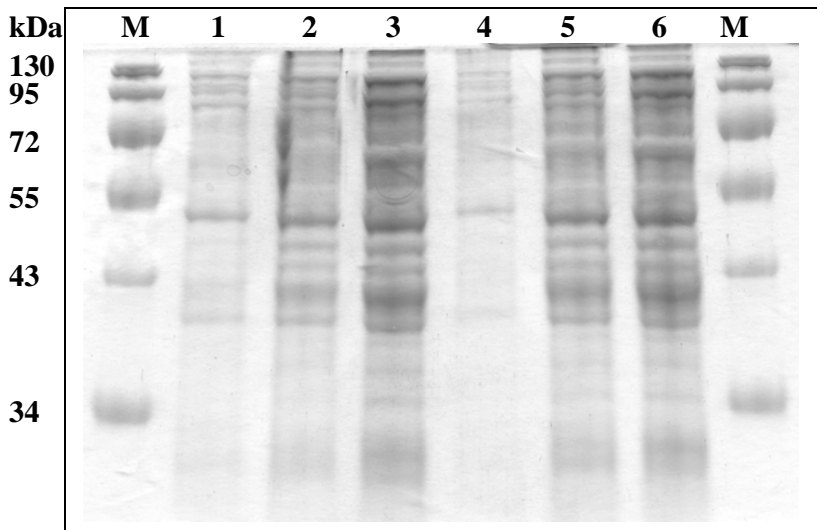


Figure 5. The electrophoretic analysis of *E.coli* BL21 cells transformed by pTES-His₆-e-pHlourin_s-OPH isolated from clone No. 6 (lanes 1-3) and No. 16 (lanes 4-6) and sampled: before induction (lanes 1 and 5) and 2 h (lanes 2 and 5) and 4 h (lanes 3 and 6) after induction. M – molecular weight markers.

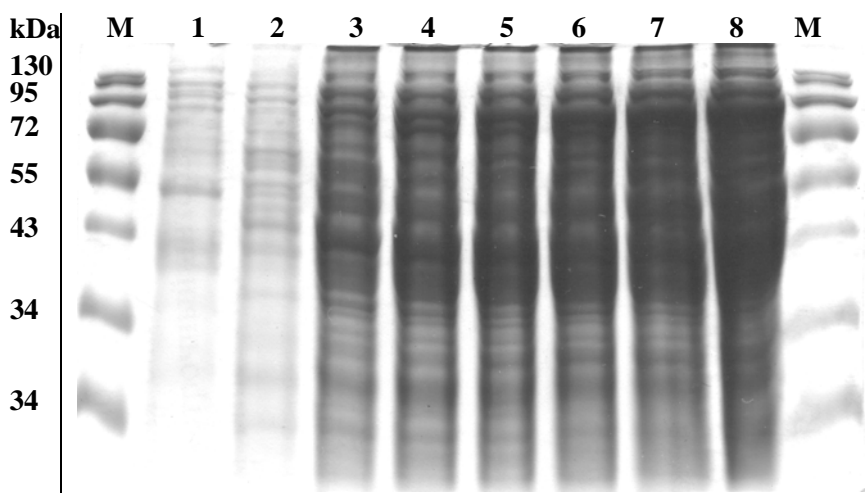


Figure 6. The electrophoretic analysis of *E. coli* W3110 cells transformed by pTES-His₆-e-pHluorin₅-OPH isolated from clone No. 16 and sampled: before induction (lane 1) and 1 h (lane 2) and 2 h (lane 3) and 4 h (lane 5), 5 h (lane 6), 6 h (lane 7) and 7h after induction (lane 8). M – molecular weight markers.

Purified N-His₆-e-pHluorin₅-OPH

The N-His₆-e-pHluorin₅-OPH purified by metal-chelating chromatography was characterized in terms of its homogeneity and relative catalytic activity in reaction of Paraoxon hydrolysis. It was shown by SDS-PAAG electrophoresis that the homogeneity of purified proteins were 95% (Figure 7). The specific activity of N-His₆-e-pHluorin₅-OPH in reaction of Paraoxon hydrolysis was $90 \pm 3 \text{ U (mg protein)}^{-1}$.

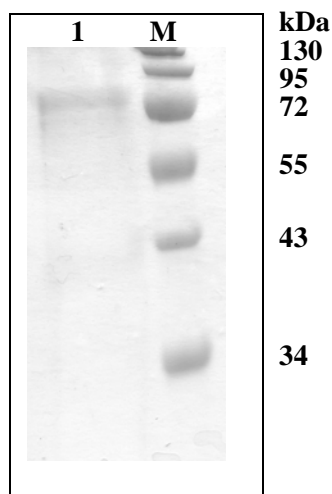


Figure 7. The electrophoretic analysis of purified N-His₆-e-pHluorin₅-OPH (lane 1). M – molecular weight markers.

CONCLUSION

Thus, new protein N-His₆-e-pHluorin_s-OPH was obtained owing to the application of construct p-His₆-e-pHluorin_s-OPH developed in the work. This protein, possessing both OPH-activity and pH-sensitive green fluorescence properties, can be used for monitoring of hydrolytic processes with pH changes.

ACKNOWLEDGEMENT

This research was financially supported by NATO Linkage Grant No. CBP.NR.NRCLG.981752.

REFERENCE

- Efremenko, E.N., and Sergeeva, V.S. (2001) Organophosphate hydrolase – an enzyme catalyzing degradation of phosphorous-containing toxins and pesticides, *Russian Chem. Bul. (Int. Ed.)* 50: 1826-1832.
- Efremenko, E.N., Votchitseva, Yu.V., Aliev, T.K., and Varfolomeyev, S.D. (2005) Recombinant plasmid DNA pTES-His-OPH encoding synthesis of polypeptide with properties of organophosphate hydrolase, and strain *E.coli* – producer of polypeptide with properties of organophosphate hydrolase. *Patent RU 2255975*.
- Efremenko, E., Votchitseva, Yu., Plieva, F., Galaev, I., and Mattiasson, B. (2006) Purification of His₆-organophosphate hydrolase using monolithic supermacroporous polyacrylamide cryogels developed for immobilized metal affinity chromatography, *Appl. Microbiol. Biot.* 70(5): 558-563.
- Gurskaya, N.G., Verkhusha, V.V., Shcheglov, A.S., Staroverov, D.B., Chepurnykh, T.V., Fradkov, A.F., Lukyanov, S., and Lukyanov, K.A. (2006) Engineering of a monomeric green-to-red photoactivatable fluorescent protein induced by blue light. *Nat. Biotechnol.* 24: 461 – 465.
- Peña, P.V., Davrazou, F., Shi, X., Walter, K.L., Verkhusha, V.V., Gozani, O., Zhao, R., and Kutateladze, T.G. (2006) Molecular mechanism of histone H3K4me3 recognition by plant homeodomain of ING2. *Nature* 442: 100-103.
- Schuster, S., Enzelberger, M., Trauthwein, H., Schmid, R.D., and Urlacher, V.B. (2005) pHluorin-based in vivo assay for hydrolase screening. *Anal. Chem.* 77: 2727-2732.
- Singh, B.K., and Walker, A. (2006) Microbial degradation of organophosphorus compounds, *FEMS Microbiol. Rev.* 30: 428-471.
- Votchitseva, Yu.A., Efremenko, E.N., Aliev, T.K., and Varfolomeyev, S.D. (2006) Properties of hexahistidine-tagged organophosphate hydrolase. *Biochemistry (Moscow)* 71(2): 167-172.

Chapter 9

MICROWAVE HEAT TREATMENT OF TEXTILES AND A REVIEW ON MATHEMATICAL MODEL OF DRYING

*A. K. Haghi**

The University of Guilan, P.O.Box 3756, Rasht, Iran

ABSTRACT

Microwave heating techniques have been widely used in textile chemistry. This paper presents a state-of-the-art review of microwave technologies and industrial applications. The characteristics of microwave interactions with textile materials are outlined together with microwave fundamentals in the heat-setting process. Further more, the limitations in current understanding are included as a guide for potential users and for future research and development activities.

1. INTRODUCTION

Radiation is a form of electromagnetic energy transmission and takes place between all matter providing that it is at a temperature above absolute zero. Infra-red radiation form just part of the overall electromagnetic spectrum. Radiation is energy emitted by the electrons vibrating in the molecules at the surface of a body. The amount of energy that can be transferred depends on the absolute temperature of the body and the radiant properties of the surface.

Electromagnetic radiation is a form of energy that propagates through a vacuum in the absence of any moving material. We observe electromagnetic radiation as light and use it as radio waves, X-rays, etc. Here, we are mostly interested in a form of electromagnetic radiation called microwaves that can be used to heat and dry textile materials.

The word *microwave* is not new to every walk of life as there are more than 60 million microwave ovens in the households all over the world. On account of its great success in processing food, people believe that the microwave technology can also be wisely employed

* Haghi@Guilan.ac.ir

to process materials. Microwave characteristics that are not available in conventional processing of materials consists of : penetrating radiation, controllable electric field distribution, rapid heating, selective heating materials and self-limiting reactions. Single or in combination, these characteristics lead to benefits and opportunities that are not available in conventional processing methods.

Since world war II , there have been major developments in the use of microwaves for heating applications. After this time it was realized that microwaves had the potential to provide rapid, energy-efficient heating of materials. This main applications of microwave heating today include food processing, wood drying, plastic and rubber treating as well as curing and preheating of ceramics. Broadly speaking, microwave radiation is the term associated with any electromagnetic radiation in the microwave frequency range of 300 MHz-300 Ghz. Domestic and industrial microwave ovens generally operate at a frequency of 2.45 Ghz corresponding to a wavelength of 12.2 cm. However, not all materials can be heated rapidly by microwaves. Materials may be classified into three groups, *i.e.* conductors insulators and absorbers. Materials that absorb microwave radiation are called dielectrics, thus, microwave heating is also referred to as dielectric heating. Dielectrics have two important properties:

- They have very few charge carriers. When an external electric field is applied there is very little change carried through the material matrix.
- The molecules or atoms comprising the dielectric exhibit a dipole movement distance. An example of this is the stereochemistry of covalent bonds in a water molecule, giving the water molecule a dipole movement. Water is the typical case of non-symmetric molecule. Dipoles may be a natural feature of the dielectric or they may be induced. Distortion of the electron cloud around non-polar molecules or atoms through the presence of an external electric field can induce a temporary dipole movement. This movement generates friction inside the dielectric and the energy is dissipated subsequently as heat[1].

The interaction of dielectric materials with electromagnetic radiation in the microwave range results in energy absorbance. The ability of a material to absorb energy while in a microwave cavity is related to the loss tangent of the material.

This depends on the relaxation times of the molecules in the material, which, in turn, depends on the nature of the functional groups and the volume of the molecule. Generally, the dielectric properties of a material are related to temperature, moisture content, density and material geometry.

An important characteristic of microwave heating is the phenomenon of “hot spot” formation, whereby regions of very high temperature form due to non-uniform heating. This thermal instability arises because of the non-linear dependence of the electromagnetic and thermal properties of material on temperature. The formation of standing waves within the microwave cavity results in some regions being exposed to higher energy than others. This result in an increased rate of heating in these higher energy areas due to the non-linear dependence. Cavity design is an important factor in the control, or the utilization of this “hot spots” phenomenon.

Microwave energy is extremely efficient in the selective heating of materials as no energy is wasted in “bulk heating” the sample. This is a clear advantage that microwave

heating has over conventional methods. Microwave heating processes are currently undergoing investigation for application in a number of fields where the advantages of microwave energy may lead to significant savings in energy consumption, process time and environmental remediation.

Compared with conventional heating techniques, microwave heating has the following additional advantages:

- higher heating rates;
- no direct contact between the heating source and the heated material;
- selective heating may be achieved;
- greater control of the heating or drying process;
- reduced equipment size and waste.

The benefit of microwave technology has been realized over the past decade with the growing acceptance of microwave ovens in the home. This, together with the gloomy outlook of a worldwide energy crisis, has paved the way for extensive research into new and innovative heating and drying processes. The use of microwave drying cannot only greatly enhance the drying rates of textile materials, but it may also enhance the final product quality.

While cost present a major barrier to wider use of microwave in textile industry, an equally important barrier is the lack of understanding of how microwaves interact with materials during heating and drying. The design of suitable process equipment is further confounded by the constraint that geometry places on the prediction of field patterns and hence heating rates within the materials. Effects such as resonance within the material can occur as well as large variations in field patterns at the textile material surface.

The phenomenon of drying has been investigated at considerable length and treated in various texts. However in general, there is only a very small section of this literature devoted to microwave to microwave drying of textile materials.

One of the main features which distinguishes microwave drying from conventional drying processes is that because liquids such as water absorb the bulk of the electromagnetic energy at microwave frequencies, the energy is transmitted directly to the wet material. The process does not rely on conduction of heat from the surface of the textile material and thus increased heat transfer occurs, speeding up the drying process. This has the advantage of eliminating case hardening of textile material which is usually associated with convective hot air drying operations. Another feature is the large increase in the dielectric loss factor with moisture content. This can be used with great effect to produce a moisture leveling phenomenon during the drying process since the electromagnetic energy will selectively or preferentially dry the wettest regions of the solid [2].

Meanwhile, infrared heating on textile lines has been in use for many years on dyeing lines to set the dyes prior to the tenter oven and to predry a host of fabric finishes or topical coatings on fabrics. The renewed interest in infrared predrying is due in large part to the need for ever-increasing line speeds and the availability of improved infrared hardware. Infrared predrying of the dyed or finished fabric rapidly preheats and predries wetted fabrics far faster than the typical convection tenter dryer. Typically an air dryer requires 20-25% of its length just to preheat the wetted fabric to a temperature where water is freely evaporated. The infrared preheater/predryer section takes over this function in a fraction of the length required

in the convection dryer. For dyed fabrics, infrared predryers are typically vertical in configuration, and are generally mounted on the line prior to the tenter frame. The systems consist of arrays of electric infrared emitters positioned on both sides of the fabric. The emitters are typically controlled from the fabric temperature. The evaporative load on the predryer dictates how much energy is required and how many vertical sections the predryer must be. With today's more efficient and higher powered emitters most predryers are one or two passes. In applications where two-sided heating is not required, such as latex backcoatings, an infrared predryer can be enclosed around pin and clip tenter frames immediately prior to the tenter oven. As a result, line speeds are increased as the added energy accelerates the heating or drying process that has previously taken place only inside the oven. Heatsetting operations can benefit from preheating as well.

It should be noted that controlling shade variations and shade shifts in dyed fabrics has typically been problematic for manufacturing engineers. Without predrying, the likelihood of shade variation from one side of the fabric to the other increases. Dyestuffs tend to migrate to the heated side of the fabric as it passes through the oven. The migration is due partly to gravity, and partly to fluid dynamics. Dyed fabrics come onto the tenter frame at usually 50% to 80% wet pickup. Optimum product quality requires that wet pickup be reduced to the 30% to 60% range with equal water removal from both sides of the fabric. The predried fabric is then presented to the horizontal tenter oven with the dyes "locked in" to position. Additional quality benefits can be realized on topical finishes or coatings. Rapid heating with infrared immediately after coating applications tends to keep the coating from deeply wicking into the fabric. For example, the infrared predrying of foamed on fluorochemical finishes for stain resistance tend to keep the coating more towards the surface of the fabric where they do the most good [3].

2. BACKGROUND

This section reviews the basic principles of physics pertaining to microwave heating.

Energy: energy is the capacitance to do work, and work is defined as the product of a force acting over a distance, that is,

$$E = W = (F)(x) \tag{1}$$

where E = energy, W = the equivalent work, F = force that performs the work, x = distance a mass is moved by the force.

- *Atomic particles* : all matter are composed of atoms. Atoms, in turn, consist of a nuclei surrounded by orbiting electrons. The nucleus consists of positively charged protons and unchanged neutrons. The surrounding electrons are negatively charged. In neutral atoms, the number of protons in the nucleus equals the number of electrons, resulting in a 0 net charge.
- *Electrostatic forces* : if some electrons are removed from a piece of material, the protons will outnumber the electrons and the material will take on a positive charge.

Similarly, if some electrons are added to a piece of material, the material will take a negative charge. If two positively charged objects are brought near to each other, they will each feel a force pushing them apart. Similarly, if two negatively charged objects are brought together, they will each experience a force pushing them apart. On the other hand, if a negatively charged object is brought near a positively charged object, each will experience a force pulling them together.

Columb's law: if two charges of magnitude q_1 and q_2 are separated by a distance r each will feel a force magnitude ;

$$F = k \frac{q_1 q_2}{r^2} \quad (2)$$

It is clear from Equation (2) that the force is proportional to the magnitude of each charge and inversely proportional to the square of the distance between them. If, for example, we double the charge on either object, the force will double. On the other hand, if we double the distance between them, the force will be reduced to 1/4 of its previous value.

Electric fields: Electrostatic force is defined as "force at a distance" (Equation 1). If we have a charge Q , and a test charge q is placed a distance R away from it, Q will push on q across that distance. The magnitude of push will depend on the magnitudes of Q , q , and r as given in Equation (2).

Another way to look at this is to say that Q creates a field in the space that surrounds it. At any point in that space , the field will have a strength E that depends on Q and r . If a test charge is placed at some point in the space, the field at that point will push on it with a force depends on the field strength E at that point and on q . To make these two explanations mathematically equivalent, we separate Equation (2) into two parts; thus

$$F = k \frac{Qq}{r^2} \left(k \frac{Q}{r^2} \right) (q) \quad (3)$$

The second part is simply the charge of the second particle. The first part we call E , the field strength at distance r away from Q :

$$E = \left(k \frac{Q}{r^2} \right) \quad (4)$$

Now the force on q can be defined in terms of the field strength times the magnitude of q :

$$F = E.q \quad (5)$$

A microwave oven consists of three major parts:

The magnetron is the device that generates the microwaves.

Wave guides direct these waves to the oven cavity.

The oven cavity holds the material to be heated so that microwaves can impinge on them.

Magnetron: It generates microwaves and consists of the following parts:

- a) Central cathode. The cathode is a metal cylinder at the center of the magnetron that is coated with an electron-emitting material. In operation, the cathode is heated to a temperature high enough to cause electrons to boil off the coating.
- b) Outer anode. There is a metal ring called an anode around the magnetron that is maintained at a large positive potential (voltage) relative to the cathode. This sets up an electrostatic field between the cathode and anode that accelerates the electrons toward the anode.

Magnetic field: a strong magnetic field is placed next to the anode and cathode in such an orientation that it produces a magnetic field at right angles to the electrostatic field. This field has the effect of bending the path of the electrons so that, instead of rushing to the anode, they begin to circle in the space between the cathode and anode in a high-energy swarm.

Resonant cavities: they have been built into the anode. Random noise in the electron swarm causes occasional electrons to strike these cavities are such that most radiation frequencies die out. Microwave frequencies, on the other hand, bounce around the cavities and tend to grow, thus getting their energy from the magnetron, passes through the wave guides, and enters the cavity.

However, not all materials can be heated rapidly by microwaves. Materials are reflected from the surface and therefore do not heat metals. Metals in general have high conductivity and are classed as conductors. Conductors are often used as conduits (waveguide) for microwaves. Materials which are transparent to microwaves are classed as insulators. Insulators are often used in microwave ovens to support the material to be heated. Materials which are excellent absorbers of microwave energy are easily used and are classed as dielectric.

Microwaves from part of a continuous electromagnetic spectrum that extends from low frequency alternating currents to cosmic rays shown in Table 1.

Table 1. The electromagnetic spectrum

Region	Frequencies (Hz)	Wavelength
Audio frequencies	$30-30 \times 10^3$	10mm-10km
Radio frequencies	$30 \times 10^3 - 30 \times 10^{11}$	10km-1m
Infrared	$30 \times 10^{11} - 4 \times 10^{14}$	1m-730nm
Visible	$4 \times 10^{14} - 7.5 \times 10^{14}$	730nm-0.3nm
Ultraviolet	$7.5 \times 10^{14} - 1 \times 10^{18}$	400nm-0.3nm
X-rays	$>1 \times 10^{17}$	< 3nm
Gamma rays	$>1 \times 10^{20}$	< 3nm
Cosmic rays	$>1 \times 10^{20}$	< 3nm

In this continuum, the radio-frequency range is divided into bands as depicted in Table 2. Radio-frequency (r.f.) energy has several possible benefits in textile processing.

Table 2. Frequency bands

Band	Designation	Frequency limits
4	Very low frequency (VLF)	3-30 kHz
5	Low frequency (LF)	30-300 kHz
6	Medium frequency (MF)	300 kHz- 3MHz
7	High frequency (HF)	3-300 MHz
8	Very high frequency (VHF)	30-300 MHz
9	Ultra high frequency (UHF)	300-3 GHz
10	Super high frequency (SHF)	3-30 GHz
11	Extremely high frequency (EHF)	30-300 GHz

Substitution of conventional heating methods by radio-frequency techniques may result in quicker and more uniform heating, more compact processing machinery requiring less space, and less material in-process at a particular time. Radio-frequency energy has been used for many years to heat bulk materials such as spools of yarn. Bands 9, 10, and 11 constitute the microwave range that is limited on the frequency side by HF and on the high frequency side by the infrared. These microwaves propagate through empty space through empty space at the velocity of light. The frequency ranges from 300 MHz to 300 GHz.

Pertinent electromagnetic parameters governing the microwave heating:

The loss tangent can be derived from material’s complex permittivity. The real component of the permittivity is called the dielectric constant whilst the imaginary component is referred to as the loss factor. The ratio of the loss factor to the dielectric constant is the loss tangent. The complex dielectric constant is given by:

$$\epsilon = \epsilon' - j\epsilon'' \tag{6}$$

where ϵ is the complex permittivity, ϵ' is the real part of dielectric constant; ϵ'' is the loss factor, and $\epsilon'/\epsilon'' = \tan \delta$ is the loss tangent.

Knowledge of a material’s dielectric properties enables the prediction of its ability to absorb energy when exposed to microwave radiation. The average power absorbed by a given volume of material when heated dielectrically is given by the equation:

$$P_{av} = \omega \epsilon_0 \epsilon_{eff}'' E_{rms}^2 V \tag{7}$$

where P_{av} is the average power absorbed (W); ω is the angular frequency of the generator (rad/s); ϵ_0 is the permittivity of free space; ϵ_{eff}'' is the effective loss factor; E is the electric field strength (V/m); and V is the volume (m^3).

The effective loss factor ϵ_{eff}'' includes the effects of conductivity in addition to the losses due to polarization. It provides an adequate measure of total loss, since the mechanisms contributing to losses are usually difficult to isolate in most circumstances.

Another important factor in dielectric heating is the depth of penetration of the radiation because an even field distribution in a material is essential for the uniform heating. The properties that most strongly influence the penetration depth are the dielectric properties of the material. These may vary with the free space wavelength and frequency of the propagating wave. For low loss dielectrics such as plastics ($\epsilon'' \ll 1$) the penetration depth is given approximately by :

$$D_p = \frac{\lambda_0 \sqrt{\epsilon'}}{2\pi\epsilon_{eff}''} \quad (8)$$

where D_p is the penetration depth; λ_0 is the free space wavelength; ϵ' is the dielectric constant; and ϵ_{eff}'' is the effective loss factor.

The penetration depth increases linearly with respect to the wavelength, and also increases as the loss factor decreases. Despite this, however, penetration is not influenced significantly when increasing frequencies are used because the loss factor also drops away maintaining a reasonable balance in the above equation.

As the material is heated, its moisture content decreases leading to a decrease in the loss factor. It can be seen from equation (8) that the decrease in loss factor causes in the penetration depth of radiation.

Microwaves cause molecular motion by migration of ionic species and/or rotation of dipolar species. Microwave heating a material depends to a great extent on its "dissipation" factor, which is the ratio of dielectric loss or "loss" factor to dielectric constant of the material. The dielectric constant is a measure of the ability of the material to retard microwave energy as it passes through; the loss factor is a measure of the ability of the material to dissipate the energy. In other words "loss" factor represents the amount of input microwave energy that is lost in the material by being dissipated as heat. Therefore, a material with high "loss" factor is easily heated by microwave energy. In fact, ionic conduction and dipolar rotation are the two important mechanisms of the microwave energy loss (i.e., energy dissipation in the material). Non-homogeneous material (in terms of dielectric property) may not heat uniformly, that is, some parts of the materials heat faster than others. This phenomenon is often referred to as thermal runaway.

Continuous temperature measurement during microwave irradiation is a major problem. Luxtron fluoroptic or accufiber can be employed to measure temperature up to 400°C but are too fragile for most industrial applications. An optical pyrometer and thermocouple can be employed to measure higher temperatures. Optical pyrometers, such as thermovision infrared camera, only records surface temperature, which is invariably much lower than the interior sample temperature. When a thermocouple (metallic probe) is employed for temperature measurements, arcing between the sample and the thermocouple can occur leading to temperature measurements, arcing between the sample and thermocouple can occur leading to

failure in thermocouple performance. A recent development is the ultrasonic temperature probe, which covers temperature up to 1500 °C.

In summery, microwave heating is unique and offers a number of advantages over conventional heating such as:

- non-contact heating;
- energy transfer, not heat transfer;
- rapid heating;
- material selective heating;
- volumetric heating;
- quick start-up and stopping;
- heating starts from interior of the material body;
- higher level of safety and automation.

Some glossaries of microwave heating system are shown in Table 3[4].

Table 3. Some glossaries of microwave heating system

Applicator or cavity	A closed space where a material is exposed to microwaves for heating
Choke	Barriers placed at entrance and exit of the applicator to prevent leakage of microwaves.
Circulator	A three port ferrite device allowing transmission of energy in one direction but directing reflected energy into water load (dummy load) connected at the third port.
Coupling	The transfer of energy from one portion of a circuit to another.
Dielectric	It is a measure of a sample's ability to retard microwave energy as it passes through.
Dielectric loss or loss factor	It is a measure of a sample's ability to dissipate microwave energy.
Hertz (Hz)	1 Hz = 1 cycle/s.
Magnetron	An electronic tube for generating microwaves.
Single mode applicator	Dimension of applicator or cavity is comparable with the wave length of microwave.
Multimode applicator	An applicator dimension is large in relation to the wave leghth of incident microwaves.

3. BASIC CONCEPTS OF MICROWAVE HEATING

As it was mentioned earlier, microwaves are electromagnetic waves having a frequency ranging from 300 MHz and 0.3 THz. Most of the existing apparatuses, however, operate between 400 MHz and 60 GHz, using well defined frequencies, allocated for industrial, Scientific and Medical (ISM) applications. Among them, the 2.45 GHz is widely used for

heating applications, since it is allowed word-wide and it presents some advantages in terms of costs and penetration depth.

It was also mentioned earlier, that quantitative information regarding the microwave-material interaction can be deduced by measuring the dielectric properties of the material, in particular of the real and imaginary part of the relative complex permittivity, $\varepsilon = \varepsilon' - j\varepsilon''_{eff}$, where the term ε''_{eff} includes conduction losses, as well as dielectric losses. The relative permeability is not a constant and strictly depends on frequency and temperature. A different and more practical way to express the degree of interaction between microwaves and materials is given by two parameters; the power penetration depth (D_p) and the power density dissipated in the material (P), as defined earlier in a simplified version as follows:

$$D_p = (\lambda_0 \sqrt{\varepsilon'}) / 2\pi\varepsilon'' \quad P = 2\pi f \varepsilon_0 \varepsilon''_{eff} E_{rms}^2 \quad (9)$$

where $\varepsilon = \varepsilon' - j\varepsilon''_{eff}$ is the complex permittivity of the material under treatment, λ_0 is the wavelength of the radiation, f is its frequency, $\varepsilon_0 = 8.854 \cdot 10^{-12}$ F/m is the permittivity of empty space and E_{rms} is the electric field strength inside the material itself. It should be noted that P, D_p and can only give quantitative and often misleading information, especially when it is critical to determine the temperature profiles inside the material. Others are the variables involved, however from this two parameters can be deduced most of the peculiarities which make the microwave heating a unique process[5].

First of all, it can be noticed the existence of temperature profile inversion with respect to conventional heating techniques. The air in proximity of the materials during the heat treatment, in fact, is not a good microwave absorber so that it can be considered that the atmosphere surrounding the material is essentially at low temperature.

Viceversa, the material under treatment, interacting in a stronger way with the electromagnetic field, heats up and reaches higher temperature. The result is that, in most cases, the surface temperature of the sample is lower than inside the material itself. This effect is more pronounced for poor heat conducting materials.

Since the given formulation for D_p and P show a strong dependence upon the real and imaginary part of the material permittivity, for multiphase systems having components with quite different permittivities, it is expected a strong selectivity of the microwave heating process. Power, in fact, is transferred preferentially to lossy materials (high ε''_{eff}) so that it can be possible to rise the temperature of just a single phase or component, or to spatially limit the heat treatment to the material, without involving the surrounding environment. This peculiarities can be particularly useful when treating composite materials.

The rapid variations of the permittivity as a function of temperature is responsible for a not always desirable phenomenon, the thermal runaway, that is to say the rapid and uncontrollable overheating of parts of the material under processing. Considering a low thermal conductivity material, whose permittivity increases as the temperature rises, in particular ε'' increasing the temperature growing, it will be subject to gradient of temperature, being colder in the regions where heat is rapidly dissipated or the field strength is lower, and

hotter in the remaining zones. These zones, presenting higher values of ϵ'' , and thus of P, will start absorbing microwaves more than the cold ones, further rising their temperature and consequently the local value of ϵ'' , strengthening the phenomenon.

Finally, dielectric heating is penetrating, depending on the operating wavelength, and permits to directly heat treat the surface and the core of the body, without waiting for the heat to reach the core of the sample by means of conduction, particularly time-taking for low thermal conductivity materials, like most polymers are. In these materials, the penetration depth is high, of the order of some tens of centimeters, thus facilitating the processing of large bodies, too[6].

4. HEAT AND MASS TRANSFER CLASSICAL EQUATIONS

The conservation of mass and energy for a textile material give the following equations:

$$\frac{\partial X}{\partial t} = D_n \nabla^2 X \quad (9)$$

$$C_{pn} \rho_n \frac{\partial T}{\partial t} = \nabla (K_n \nabla T) + Q(r, z, t) \quad (10)$$

where $n = 1$ and 2 refers to the inner and outer layer of material, and D is diffusivity (m^2/s); X the moisture content (kg/kg dry basis); k the thermal conductivity ($W/m K$); ρ the density (kg/m^3); C_p the heat capacity ($J/kg K$); and Q is the microwave source term (W/m^3).

The empirical model for calculating moisture diffusivity as a function of moisture and temperature;

$$D = \frac{1}{1+X} D_0 \exp \left[-\frac{E_0}{R} \left(\frac{1}{T} - \frac{1}{T_r} \right) \right] + \frac{1}{1+X} D_i \exp \left[-\frac{E_i}{R} \left(\frac{1}{T} - \frac{1}{T_r} \right) \right] \quad (11)$$

where D (m^2/s) is the moisture diffusivity; X the moisture content (kg/kg dry basis); T ($^{\circ}C$) the material temperature; T_r a reference temperature, and $R=0.0083143$ $kJ/mol K$ is the ideal gas constant; D_0 (m^2/s) the diffusivity at moisture $X=0$ and temperature $T = T_r$; D_i (m^2/s) the diffusivity at moisture $X=\infty$ and temperature $T = T_r$; E_0 (kJ/mol) the activation energy of diffusion in dry material at $X=0$ and E_i (kJ/mol) is the activation energy of diffusion in wet material at $X=\infty$. The proposed model may uses the estimated parameters in Table 4.

Table 4. Numerical values for wool (based on data from various authors)

Diffusion coefficient of water vapor - 1st stage :

$$(1.04 + 68.20W_c - 1342.59W_c^2)10^{-14}, t < 540s$$

Diffusion coefficient of water vapor - 2nd stage :

$$1.6164\{1 - \exp[-18.163\exp(-28.0W_c)]\}10^{-14}, t \geq 540s$$

Diffusion coefficient in the air : $2.5e^{-5}$

Volumetric heat capacity of fiber : $373.3 + 4661.0W_c + 4.221T$

Thermal conductivity of fiber :

$$(38.49 - 0.720W_c + 0.113W_c^2 - 0.002W_c^3)10^{-3}$$

Heat of sorption: $1602.5\exp(-11.72W_c) + 2522.0$

Porosity of fiber : 0.92

Density of fiber ; $1300 \text{ kg}/\text{m}^3$

Radius of fiber ; $1.03 e^{-5} \text{ m}$

Mass transfer coefficient : 0.137 m/s

Heat transfer coefficient : $99.4 \text{ W}/\text{m}^2 \text{ K}$

- Initial conditions: At time $t=0$: $T = T_0(r, z)$, $X = X_0(r, z)$

- Boundary conditions: $\frac{\partial X}{\partial t} \Big|_{(r=0, H/2=0, t)} = 0$, $\frac{\partial T}{\partial t} \Big|_{(r=0, H/2=0, t)} = 0$

Figure 1 shows that there is an increase in drying rate because of the microwave power density.

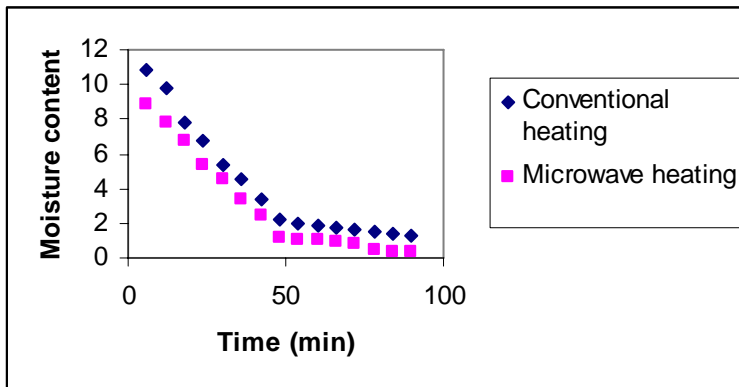


Figure 1. Comparison of conventional and microwave on average moisture content.

This can be attributed to the effect of microwave on moisture by rapidly increasing the moisture migration to the surface and increased evaporation. A comparison of these drying curves demonstrates improvement in drying times, under microwave heating. Nevertheless the results show significant improvement in average drying times over the conventional heating method.

5. HEAT AND MASS TRANSFER EXPONENTIAL MODEL

It has been recognized that microwaves could perform a useful function in textile drying in the leveling out of moisture profiles across a wet sample. This is not surprising because water is more reactive than any other material to dielectric heating so that water removal is accelerated. An exponential model presented here.[7] can be used to describe the drying curves.

$$X = (a - X_{eq}).\exp(-b.t^d) + X_{eq} \quad (12)$$

and its derivative form:

$$(-dX / dt) = b.d.t^{(d-1)}.X \quad (13)$$

Parameters a , b , d can be determined by regression by the least square method. The quantities b and d vary with the experimental conditions and they are drying coefficients. X is the moisture content of the drying material, dX/dt is the drying rate and t is the drying time. Parameter (a) represents the initial moisture content. The incident power strongly influenced the drying kinetics of a textile sample, reducing the drying time by raising the microwave heating power.

6. COMBINED MICROWAVE AND CONVECTIVE DRYING OF CARPET

It should be noted that because of the higher temperature and pressure gradients generated during combined microwave and convective drying, greater care must be taken not to damage the textile material to be dried, whilst still taking advantage of the increased drying rates provided by the microwave environment. To fully understand the heat and mass transfer phenomenon occurring within the material during combined microwave and convective drying, it is required to analyse the moisture, temperature and pressure distributions generated throughout the process.

It was shown by Ilic and Turner [8] that a theory based on a continuum approach led to the following equations of motion governing the drying of a slab of material:

Total mass:

$$\frac{\partial}{\partial t}(\phi S_g \rho_g + \phi S_w \rho_w) + \nabla \cdot (\chi_g \rho_g V_g + \chi_w \rho_w V_w) = 0 \quad (14)$$

Total liquid:

$$\frac{\partial}{\partial t}(\phi S_g \rho_{gv} + \phi S_w \rho_w) + \nabla \cdot (\chi_g \rho_{gv} V_{gv} + \chi_w \rho_w V_w) = 0 \quad (15)$$

Here, S is the volume saturation, ϕ is the porosity, ρ [kg m^{-3}] is the density of the fibers χ is the surface porosity, ϕ is the porosity.

Total enthalpy:

$$\begin{aligned} & \frac{\partial}{\partial t} \left(\phi S_g \rho_{gv} h_{gv} + \phi S_g \rho_{ga} h_{ga} + \phi S_g \rho_{ga} h_{ga} + \phi S_w \rho_w h_w + (1 - \phi) \rho_s h_s - \phi \rho_w \int_0^{S_w} \Delta h_w(S) dS \right) \\ & + \nabla \cdot (\chi_g \rho_{gv} V_{gv} h_{gv} + \chi_g \rho_{ga} V_{ga} h_{ga} + \chi_w \rho_w V_w h_w) \\ & = \nabla \cdot ((K_g X_g + K_w \chi_w + K_s (1 - \chi)) \nabla T) + \phi \end{aligned} \quad (16)$$

where ϕ is the internal microwave power dissipated per unit volume, K [m^2] is permeability, and h [J kg^{-1}] is the averaged enthalpy. In equation (16) the effects of viscous dissipation and compressional work have been omitted.

The equations (14, 15 and 16) are augmented with the usual thermodynamic relations and the following relations:

Flux expressions are given as follows:

Gas flux :

$$\chi_g \rho_g V_g = - \frac{K K_g (S_w) \rho_g}{\mu_g(T)} [\nabla P_g - \rho_g g] \quad (16a)$$

Here, g [ms^{-2}] is the gravitational constant and K_g is the relative permeability of gas.

Liquid flux :

$$\chi_w \rho_w V_w = - \frac{K K_w (S_w) \rho_w}{\mu_w(T)} [\nabla (P_g - P_c(S_w, T)) - \rho_w g] \quad (16b)$$

where, K_w is the relative permeability of water, and $\mu [Hm^{-1}]$ is the permeability of free spaces.

Vapour flux :

$$\chi_g \rho_{gv} V_{gv} = \chi_g \rho_{gv} V_g - \frac{\chi_g \rho_g D(T, P_g) M_a M_v}{M^2} \nabla \left(\frac{P_{qv}}{P_g} \right) \quad (16c)$$

Here, $V [ms^{-1}]$ is the averages velocity and $M [kgmol^{-1}]$ is the molar mass.

Air flux :

$$\chi_g \rho_{ga} V_{ga} = \chi_g \rho_g V_g - \chi_g \rho_g V_{gv} \quad (16d)$$

Relative humidity (Kelvin effect):

$$\psi(S_w, T) = \frac{P_{gv}}{P_{gvs}(T)} = \exp \left(\frac{2\sigma(T) M_v}{r(S_w) \rho_w RT} \right) \quad (17)$$

here ψ is the relative humidity and $P_{gvs}(T)$ is the saturated vapour pressure given by the Clausius-Clapeyron equation.

Differential heat of sorption :

$$\Delta h_w = R_v T^2 \frac{\partial(\ln \psi)}{\partial T} \quad (18)$$

Enthalpy-Temperature relations :

$$h_{ga} = C_{pa} (T - T_R) \quad (19)$$

$$h_{gv} = h_{vap}^0 + C_{pv} (T - T_R) \quad (20)$$

$$h_w = C_{pw} (T - T_R) \quad (21)$$

$$h_s = C_{ps} (T - T_R) \quad (22)$$

The expressions for K_g , K_w are those given by Turner and Ilic [8], and μ_g , μ_w have had functional fits according to the data by Holman [9]. The diffusivity $D(T, P_g)$ given by Quintard and Puiggali [10] and the latent heat of evaporation given by,

$$h_{vap}(T) = h_{gv} - h_w \quad (23)$$

After some mathematical manipulations [11-14], the one-dimensional system of three non-linear coupled partial differential equations which model the drying process in a thermal equilibrium environment are given by [15-20]:

$$a_{s1} \frac{\partial S_w}{\partial t} + a_{s2} \frac{\partial T}{\partial t} = \frac{\partial}{\partial z} \left[K_{s1} \frac{\partial S_w}{\partial z} + K_{T1} \frac{\partial T}{\partial z} + K_{P1} \frac{\partial P_g}{\partial z} + K_{gr1} \right] \quad (24)$$

$$a_{T1} \frac{\partial S_w}{\partial t} + a_{T2} \frac{\partial T}{\partial t} = \frac{\partial}{\partial z} \left(K_e \frac{\partial T}{\partial z} \right) - \phi \rho_w h_{vap} \frac{\partial}{\partial z} \left[K_s \frac{\partial S_w}{\partial z} + K_T \frac{\partial T}{\partial z} + K_P \frac{\partial P_g}{\partial z} + K_{gr} \right] + \left[\phi \rho_w C_{pw} \left(K_{s2} \frac{\partial S_w}{\partial z} + K_{T2} \frac{\partial T}{\partial z} + K_{P2} \frac{\partial P_g}{\partial z} + K_{gr2} \right) \right] \frac{\partial T}{\partial z} + \Phi(S_w, T) \quad (25)$$

$$a_{P1} \frac{\partial S_w}{\partial t} + a_{P2} \frac{\partial T}{\partial t} + a_{P3} \frac{\partial P_g}{\partial t} = \frac{\partial}{\partial z} \left[K_s \frac{\partial S_w}{\partial z} + K_T \frac{\partial T}{\partial z} + K_{P3} \frac{\partial P_g}{\partial z} + K_{gr3} \right] \quad (26)$$

The capacity coefficients a_{s1} , a_{T1} , a_{P1} and the kinetic coefficients K_{s1} , K_{T1} , K_{P1} , K_{gr1} all depend on the independent variables : Saturation S_w , Temperature T and total pressure P_g . The boundary conditions are written in one dimension as [21-22]:

At $z=0$ (Drying surface) :

$$K_{s1} \frac{\partial S_w}{\partial z} + K_{T1} \frac{\partial T}{\partial z} + K_{P1} \frac{\partial P_g}{\partial z} + K_{gr1} = \frac{K_m M_v}{R \phi \rho_w} \left(\frac{P_{gV}}{T} - \frac{P_{gV0}}{T_0} \right) \quad (27a)$$

$$K_e \frac{\partial T}{\partial z} - \phi \rho_w h_{vap} \left(K_s \frac{\partial S_w}{\partial z} + K_T \frac{\partial T}{\partial z} + K_P \frac{\partial P_g}{\partial z} + K_{gr} \right) = Q(T - T_0) \quad (27b)$$

$$P_g = P_o \quad (27c)$$

At $z=L$ (Impermeable surface):

$$K_{s1} \frac{\partial S_w}{\partial z} + K_{T1} \frac{\partial T}{\partial z} + K_{P1} \frac{\partial P_g}{\partial z} + K_{gr1} = 0 \quad (28a)$$

$$K_e \frac{\partial T}{\partial Z} - \phi \rho_w h_{vap} \left(K_S \frac{\partial S_w}{\partial Z} + K_T \frac{\partial T}{\partial Z} + K_P \frac{\partial P_g}{\partial Z} + K_{gr} \right) = 0 \quad (28b)$$

$$(K_{S1} - K_S) \frac{\partial S_w}{\partial Z} + (K_{T1} - K_T) \frac{\partial T}{\partial Z} + (K_{P1} - K_{P3}) \frac{\partial P_g}{\partial Z} + (K_{gr1} - K_{gr3}) = 0 \quad (28c)$$

Initially:

$$T(z,0) = T_1 \quad (29a)$$

$$P_g(z,0) = P_0 \quad (29b)$$

$$\frac{\partial P_c}{\partial Z} = -\rho_w g \quad (29c)$$

Figures 2 show a comparison of convective drying with or without microwaves [23]. Whilst for convective drying there are definite constant rate and falling rate periods, when microwaves are added the form of the curves changes [24-25].

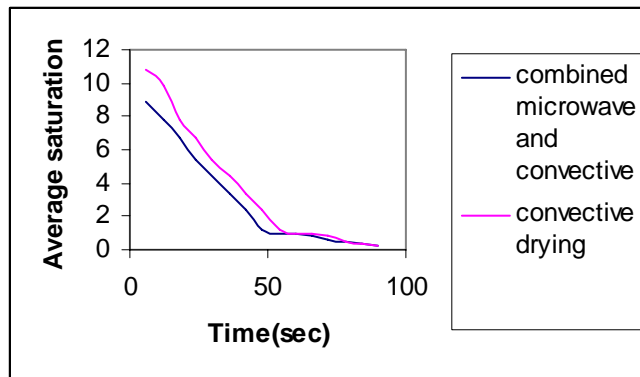


Figure 2 Average saturation profiles in time for drying with or without microwaves.

CONCLUSION

From the earlier discussions, it will be clear that there are a lot of factors that have to be considered before employing microwave irradiation for textile materials. Blind applications of microwave energy in textile chemistry will usually lead to disappointment. On the other hand, wise application of this technology will have greater benefits that has been anticipated. In general, the savings achieved through application of microwave techniques in textile chemistry will be other than energy as the saving in this respect would not be enormous. The benefits will be in time saving, increased process yield, environmental compatibility, space savings and unique characteristics of the textile products.

REFERENCES

- [1] D.A.Jones, T.P. Lelyveld, S.D. Mavrofidis, S.V. Kingman, and N. J. Miles, Microwave heating application in environmental engineering, *Resources, Conservation and Recycling*, 34, 75-90, 2002.
- [2] I.W. Turner and P.G. Jolly, Combined microwave and conventional drying of a porous material, *Drying technology*, 9(5), 1209-1269, 1991.
- [3] T.V. Denend, *Infrared predrying yields significant benefits*, American Dyestuff Reporter, 45-51, December 1998.
- [4] K. E. Haque, Microwave energy for mineral treatment processes, *Int. J. Miner. Process*, 57 , 1-24, 1999.
- [5] A.C. Metaxas and R.J. Meredith, *Industrial microwave heating*, Peter Peregrinus Ltd, London 1993, pp. 7-24.
- [6] P. Veronesi, C. Leonelli, G. Pellacani and A. Boccaccini, Unique microstructure of glass-metal composites obtained by microwave assisted heat-treatment, *J. Thermal Anal. Cal.*, 72, 1141-1149, 2003.
- [7] D. Skansi, Z. Bajza an A. Arapovic, Experimental evaluation of the microwave drying of leather, *J. of the society of Leather Thechnologies and chemists*, 79, 171-177.
- [8] Ilic, M. and Turner, I.W.: Convective drying of a consolidated slab of wet porous material, *Int.J.Heat Mass Transfer*, , 32 (12),(1989).
- [9] Holman, J. P., 1989, *Heat Transfer*, McGraw-Hill Book Company.
- [10] Quintard M., and Puiggali J.R., 1986, Numerical modeling of transport processes during the drying of granular porous medium, *J. Heat and Technology*, 4, 2.
- [11] Haghi,A.K. and Rondot,D. , may 1994. Determination des Coefficients de Transfert de Chaleur lors du Sechage de Textiles par Thermographie Infrarouge et Microscopie Thermique a Balayage , *Poster presentation,SFT*,2(11), 34-40, Paris, (In French).
- [12] Haghi,A.K. and Rondot,D., may 1994. Determination des Coefficient de Transfert de Chaleur lors du Sechage, *2nd DAS Int. Conf. Proc.*,Vol.2, 189-196, Romania, (In French).
- [13] Haghi,A.K., and Rondot, D., may 1996. Determination of Heat Transfer Coefficients During the Process of Through Drying of Wet Textile Materials with an Optico-Mechanical Scanning pyrometer and I.R thermograph, *3rd DAS Int. Conf. Proc.*,Vol. 3, 25-32, Romania.
- [14] Haghi,A.K. and Rondot, D., may 1998. Controle de Materiaux par Thermographie Infrarouge : Modelisation et Experiences, *4rth DAS Int. Conf. Proc.*,Vol. 1, 65-76, Romania, (In French).
- [15] Haghi,A.K. and Rondot, D., may 2000.A Thermal Imaging Technique for Measuring Transient Temperature Field, *5th DAS Int. Conf. Proc.*, 80-87, Romania.
- [16] Haghi,A.K., 2001. Experimental Investigations on Drying of Porous Media Using Infrared Radiation, *Acta Polytechnica*, 41, 55-57.
- [17] Haghi,A.K., 2000. *Some Aspects of Microwave Drying*, The Annals of Stefan Cel Mare University, 8(14), 60-65, Romania.
- [18] Haghi,A.K., 2001, A Mathematical Model of the Drying Process, *Acta Polytechnica*, 41, 20-24.

- [19] Haghi, A.K., 2001. Simultaneous Moisture and Heat Transfer in Porous System, *J. of computational and applied mechanics* 2, 195-204.
- [20] Haghi, A.K., 2003, Thermal Analysis of Drying Process, *J. Thermal Anal. And Cal.*, 74, 827-382.
- [21] Haghi, A.K., 2003, The Diffusion of Heat and Moisture Through Textiles, *Int. J. of Applied Mechanics and Engineering*, 8(2), 233-243.
- [22] Haghi, A.K., 2003, Experimental Evaluation of the Microwave Drying of Natural Silk, *J. of Theoretical and Applied Mechanics*, 33, 83-95.
- [23] Haghi, A.K., 2003, Heat and Mass Transport through Moist Porous Materials, The 14th International Symp. *On Transport Phenomena*, 6-9 July, 209-215.
- [24] Haghi, A.K., 2004, Heat and Mass Transfer of Leather in the Drying Process, *Iran. J. Chem and Chem. Eng*, 23 (1), 25-34.
- [25] Haghi, A.K., 2004, Relations for Water- Vapor Transport Through Fibers, *J. Computational and Applied Mechanics*, 5(2), 263-274.

*Chapter 10***ELECTROSPUN NANOFIBERS:
A FIBER DIGEST FOR BEGINNERS***A. K. Haghi* and M. Akbari*

University OF Guilan

P.O.BOX: 3756

Rasht, Iran

ABSTRACT

Electrospinning is a process by which a polymer solution is charged to high voltage to produce submicron scaled fibers. At a voltage sufficient to overcome surface tension forces, fine jets of polymer solution shoot out toward a grounded collector. The jet is stretched and elongates before it reaches the target, dries and is collected as an interconnected web of small fibers with typical diameter of several hundreds of nanometers. Recent achievements and developments as a condensed review are reported in this paper. Theory as well as experiments is examined with a view to extracting the fundamental elements that should allow the readers to build their own perspective of the subject.

NOMENCLATURE R = radius of the jet R' = slope of the jet surface Q = constant volume flow rate I = constant total current in the jet σ = surface charge density v = velocity E = z component of the electric field

* E-mail: Haghi@guilan.ac.ir

K = conductivity of the liquid

γ = surface tension

E_t = tangential components of the electric field at the surface

E_n = normal components of the electric field at the surface

g = gravity

τ_{zz} = axial viscous normal stress

P = pressure

t_n^e = normal traction on the surface of the jet due to electricity

t_t^e = tangential traction on the surface of the jet due to electricity.

ε = dielectric constants of the jet

$\bar{\varepsilon}$ = dielectric constants of the ambient air

η = viscosity

1. INTRODUCTION

An emerging technology of manufacturing of thin natural fibers is based on the principle of electrospinning process. In conventional fiber spinning, the mechanical force is applied to the end of a jet. Whereas in the electrospinning process the electric body force act on element of charged fluid. Electrospinning has emerged as a specialized processing technique for the formation of sub-micron fibers (typically between 100 nm and 1 μ m in diameter), with high specific surface areas. Due to their high specific surface area, high porosity, and small pore size, the unique fibers have been suggested for wide range of applications.

Electrospinning of natural fibers offers unique capabilities for producing novel natural nanofibers and fabrics with controllable pore structure. Current research effort has focused in understanding the electrospinning of natural fibers in which the influence of different governing parameters are discussed.

Electrospinning [1–10] is an economical and simple method used in the preparation of polymer fibers. The fibers prepared via this method typically have diameters much smaller than is possible to attain using standard mechanical fiber-spinning technologies [11]. Electrospinning of polymer solutions has gain much attention in the last few years as a cheap and straightforward method to produce nanofibers [12-16]. Electrospinning differs from the traditional wet/dry fiber spinning in a number of ways, of which the most striking differences are the origin of the pulling force and the final fiber diameters. The mechanical pulling forces in the traditional industrial fiber spinning processes lead to fibers in the micrometer range and are contrasted in electrospinning by electrical pulling forces that enable the production of nanofibers [14]. Depending on the solution properties, the throughput of single-jet electrospinning systems ranges around 10 ml/min. This low fluid throughput may limit the industrial use of electrospinning. A stable cone-jet mode followed by the onset of the characteristic bending instability, which eventually leads to great reduction in the jet diameter, necessitate the low flow rate [6,17] When the diameters of polymer fiber materials are shrunk from micrometers (e.g. 10–100 μ m) to submicrons or nanometers, there appear

several amazing characteristics such as very large surface area to volume ratio (this ratio for a nanofiber can be as large as 103 times of that of a microfiber), flexibility in surface functionalities, and superior mechanical performance (e.g. stiffness and tensile strength) compared with any other known form of the material. These outstanding properties make the polymer nanofibers to be optimal candidates for many important applications[18]. These include filter media [19-21], composite materials [18, 22], biomedical applications (tissue engineering scaffolds [23-27], bandages [28], drug release systems [29-30]), protective clothing for the military [31-34], optoelectronic devices and semi-conductive materials [35-38], biosensor/chemosensor [39-42].

1.1. Electrospinning Set Up

A schematic diagram to interpret electrospinning of polymer nanofibers is shown in Figure 1. There are basically three components to fulfill the process: a high voltage supplier, a capillary tube with a pipette or needle of small diameter, and a metal collecting screen. In the electrospinning process a high voltage is used to create an electrically charged jet of polymer solution or melt out of the pipette. Before reaching the collecting screen, the solution jet evaporates or solidifies, and is collected as an interconnected web of small fibers [43-45]. One electrode is placed into the spinning solution/melt or needle and the other attached to the collector. In most cases, the collector is simply grounded. The electric field is subjected to the end of the capillary tube that contains the solution fluid held by its surface tension. This induces a charge on the surface of the liquid. Mutual charge repulsion and the contraction of the surface charges to the counter electrode cause a force directly opposite to the surface tension [46]. As the intensity of the electric field is increased, the hemispherical surface of the fluid at the tip of the capillary tube elongates to form a conical shape known as the Taylor cone [47].

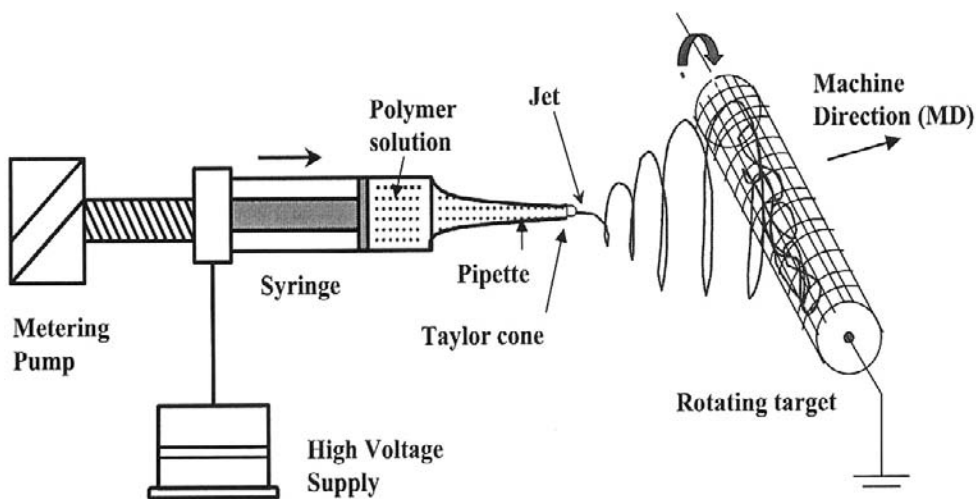


Figure 1-a..Schematic of electrospinning set up.

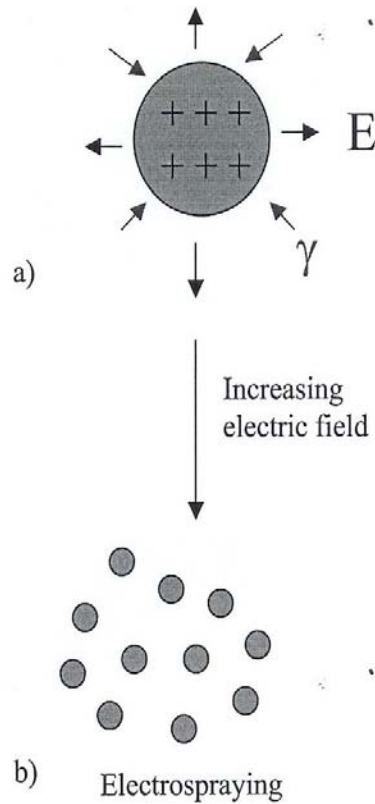


Figure 1-b. Phenomena of the electrospinning : when the electrostatic repulsive forces Overcome the surface tension of the liquid, the droplet (a) disintegrates into Smaller droplets (b).

Further increasing the electric field, a critical value is attained with which the repulsive electrostatic force overcomes the surface tension and the charged jet of the fluid is ejected from the tip of the Taylor cone [18, 48]. The jet exhibits bending instabilities due to repulsive forces between the charges carried with the jet. The jet extends through spiraling loops, as the loops increase in diameter the jet grows longer and thinner until it solidifies or collects on the target [49].

This technique makes use of an electrical field that is applied across a polymer solution and a collector plate, to force a polymer solution jet out from a small hole. As the solution jet travels, the solvent evaporates and leaves behind a charged polymer fiber, which is elongated by an electrical force and attracted to the collecting plate with an opposing or zero polarity. To understand the fundamental principle underlying the process of electrospinning , consider a spherically charged droplet of a low molecular weight conducting liquid that is held in vacuum. As shown in figure 1-b , the droplet is under the influence of two forces , viz.

1) the disintegrative electrostatic repulsive force. 2) the surface tension that strives to hold the droplet within a spherical shape.

At equilibrium , the tow forces completely balance each other, as is depicted by : $\frac{1}{8\pi\epsilon_0} =$

$8\pi\sigma_s R$ where Q is the electrostatic charge on the surface of the droplet , R is the radius of the droplet , ϵ_0 is the dielectric permeability of vaccum and σ_s is the surface tension coefficient

2. EFFECT OF SYSTEMATIC PARAMETERS ON ELECTROSPUN NANOFIBERS

It has been found that morphology such as fiber diameter and its uniformity of the electrospun polymer fibers are dependent on many processing parameters [50]. These parameters can be divided into three groups: a) solution properties, b) processing conditions, c) ambient conditions. Each of the parameters has been found to affect the morphology of the electrospun fibers.

2.1. Solution Properties

Solution parameters such as viscosity of solution, polymer concentration, molecular weight of polymer, electrical conductivity, elasticity and surface tension, those are which attribute to polymer and its solution characteristics has important effect on morphology [18].

2.1.1. Viscosity

The viscosity range of a different polymer solution which is spinnable is different. One of the most significant parameters influencing the fiber diameter is the solution viscosity. A higher viscosity results in a large fiber diameter. Figure 2 shows the representative images of beads and beaded fibers for solutions with a range of viscosity. Beads and beaded fibers are less likely to be formed for the more viscous solutions. The diameter of the beads become bigger and the average distance between beads on the fibers longer as the viscosity increases. Meanwhile, the shape of the beads gradually changes from spherical to spindle-like [51].

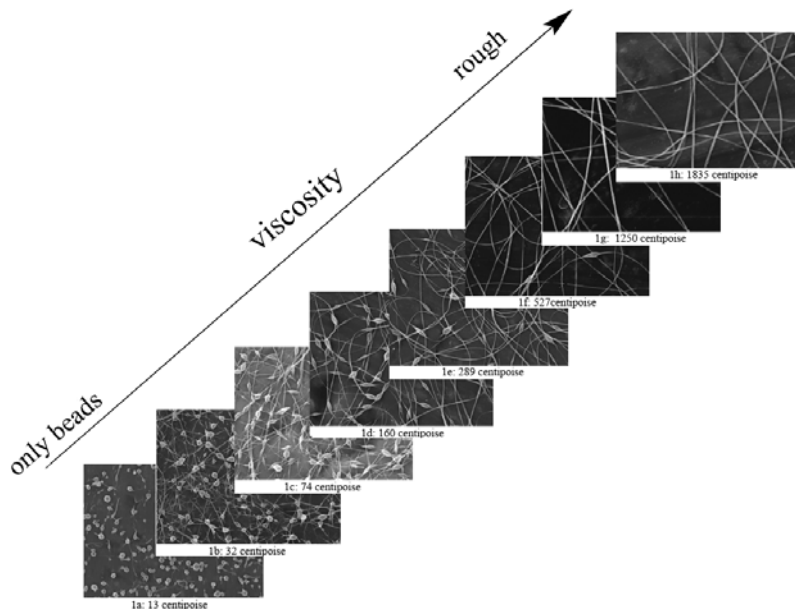


Figure 2. The morphology of beaded fibers versus solution viscosity [51].

2.1.2. Solution Concentration

As the solution concentration increase, a mixture of beads and fibers is obtained [52]. Higher solution concentration may result in fewer beads. The shape of the beads changed from spherical to spindle-like when the solution concentration varied from low to high levels [18,53]. The fiber distribution became gradually broader with increasing concentration, which is in consistency with the results obtained by Ryu et al. and Kidoaki et al. [54]. The fiber diameter increased with increasing solution concentration because the higher viscosity resisted the extension of the jet [50,55]. However, it is impossible to electrospin if the solution concentration or the corresponding viscosity is too high due to the difficulty in liquid jet formation [56-58].

2.1.3. Molecular Weight

Molecular weight also has a significant effect on the rheological and electrical properties such as viscosity, surface tension, conductivity and dielectric strength. It has been reported that too low molecular weight polymer tend to form beads rather than fibers and high molecular weight polymers give fibers with larger average diameter [59].

2.1.4. Surface Tension

The surface tension seems more likely to be a function of solvent compositions, but is negligibly dependent on the solution concentration. Different solvents may contribute different surface tensions. However, not necessarily a lower surface tension of a solvent will always be more suitable for electrospinning. Generally, surface tension determines the upper and lower boundaries of electrospinning window if all other variables are held constant. The formation of droplets, bead and fibers can be driven by the surface tension of solution and lower surface tension of the spinning solution helps electrospinning to occur at lower electric field [57].

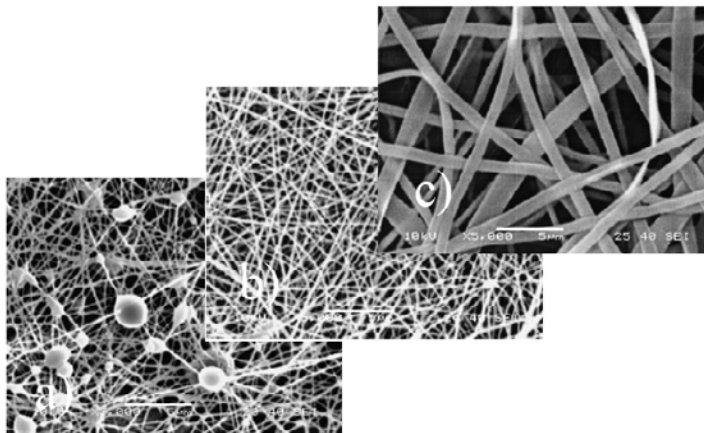


Figure 3. Photographs showing the typical structure in the electrospun polymer for various molecular weights. The samples were obtained at the center of the deposition area. (a) 9000–10,000 g/mol; (b) 13,000–23,000 g/mol; and (c) 31,000–50,000 g/mol (solution concentration: 25 wt.%) [58].

2.1.5. Number of Entanglements

The above variables aren't independent of each other. Solution viscosity is a function of both concentration and polymer molecular weight. Also these two parameters affect on number of entanglements [52].

2.1.6. Solution Conductivity

Jun et al.[56] have shown that increasing solution conductivity by addition of a salt can significantly aid fiber formation (Figure 4). Addition of a salt, it has positive effect on the electrospinning number ($Vq/\gamma R^2$). Specifically, the electrical energy (Vq) increases. On the other hand, the change in the surface free energy due to change in surface tension is not expected significant. As the charges carried by the jet increased, higher elongation forces were imposed to the jet under the electrical field, resulting in smaller bead and thinner fiber diameters.

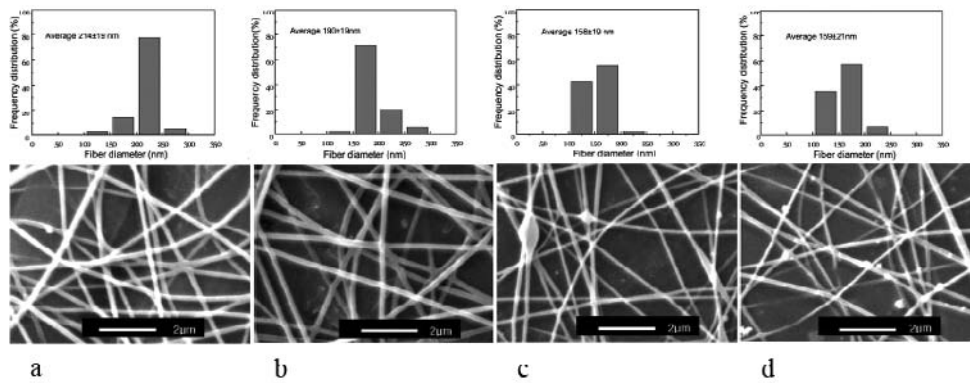


Figure 4. Effect of NaCl amount in the PVA solution on fiber morphology (DH = 98%, voltage = 5kV, tip–target distance = 10cm; flow rate = 0.2 ml/h). NaCl amount based on H₂O: (a) 0.05%; (b) 0.10%; (c) 0.15%; (d) 0.2%. Original magnification 10k [55].

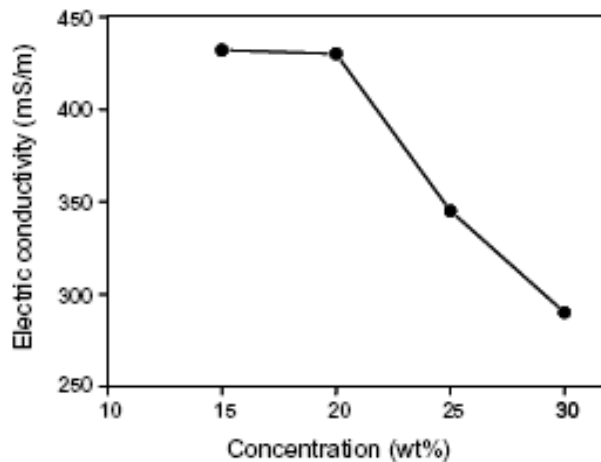


Figure 5. Electric conductivity as a function of polymer solution concentration [60].

2.1.7. Solution Conductivity

A comparison of the diameter of the electrospun fibers with the electrical conductivity of the solutions was shown in Figure 6. There was a significant drop in the diameter of the electrospun polymer fibers when the electrical conductivity of the solution increased. Beads were also observed due to low conductivity of the solution, which results in insufficient elongation of a jet by electrical force to produce uniform fiber.

Electrospun polymer nanofibers with the smallest fiber diameter were obtained with the highest electrical conductivity. This interprets that the drop in the size of the fibers was due to the increased electrical conductivity [50].

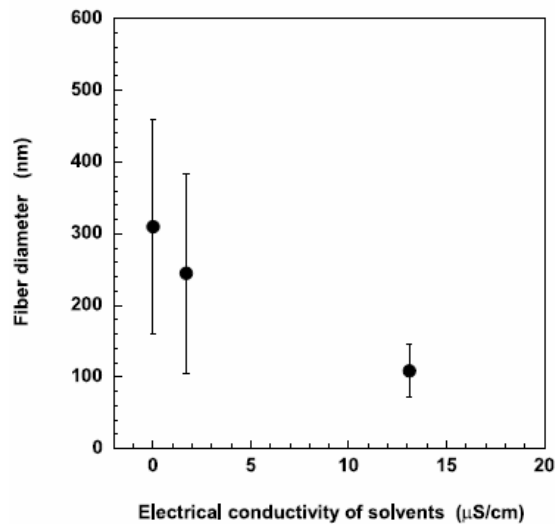


Figure 6. Solution conductivity effects on the diameter of the electrospun P(LLA-CL) (70/30 wt%) fibers[50].

2.1.8. Effect of Salt Addition

Figure 7 shows the SEM images of PAA nanofibers fabricated by electrospinning into solutions with different ionic strengths. Magnified PAA nanofibers are shown also. At the concentration of 1 M NaCl, no PAA nanofibers were synthesized. Bead structures were observed from all prepared PAA nanofibers. With increasing the concentration of NaCl, the relative viscosity slightly decreased. Variations in viscosity may be caused by the chain conformation change of PAA in solution upon adding NaCl. With increasing the ionic strength of the solution, the chain conformation of PAA changes from the extended linear conformation to the coil conformation because PAA is a polyelectrolyte. Although relative viscosity decreases slightly with increasing the amount of NaCl [61].

The effect of NaCl addition on the morphology of electrospun PVA fibers was shown in Figure 8. Even a little sodium chloride added in the solution made its conductivity increase sharply. Net charge density carried by the jet in the electrospinning process can be affected by the conductivity of the solution PVA fiber diameters were gradually decreased from $214 \pm 19\text{nm}$ to $159 \pm 21\text{nm}$ with increasing content of NaCl from 0.05% to 0.2%, for the higher net charge density increased the electrical force exerted on the jet and led to decreased fiber

diameter. When 0.2% NaCl was added in PVA solution, many small particles, perhaps sodium chloride crystals were observed on the SEM micrograph [Figure 8].

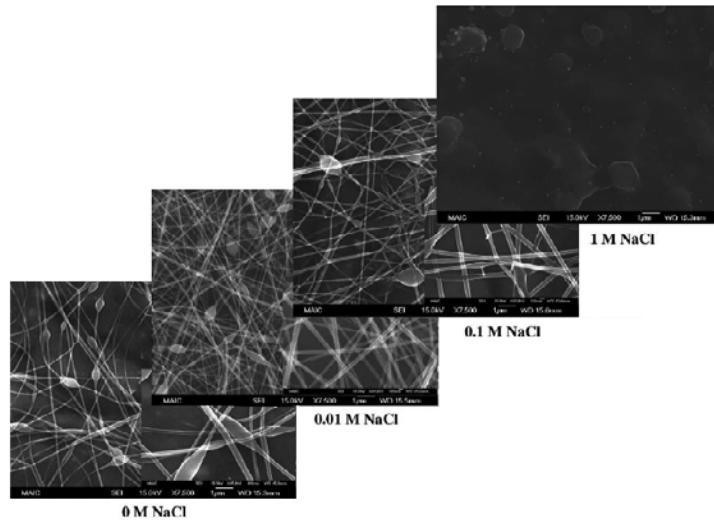


Figure 7. The SEM images of PAA nanofibers with different concentrations of NaCl [61].

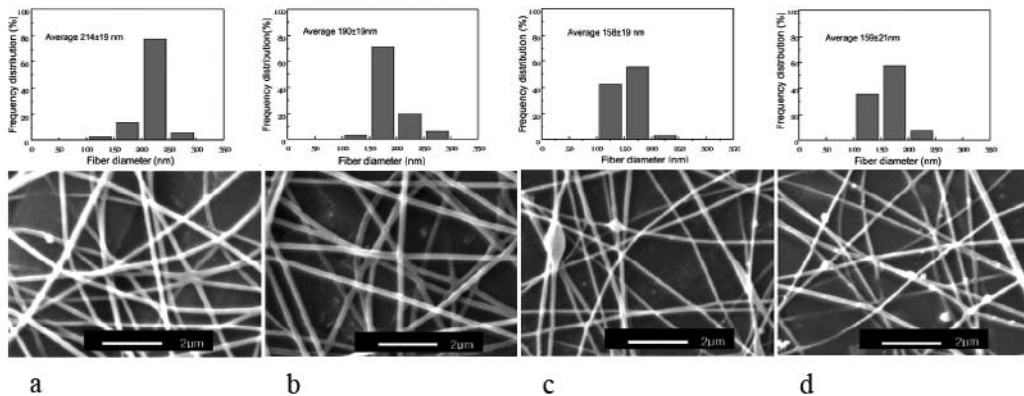


Figure 8. Effect of NaCl amount in the PVA solution on fiber morphology (DH = 98%, voltage = 5kV, tip–target distance = 10cm; flow rate = 0.2 ml/h). NaCl amount based on H₂O: (a) 0.05%; (b) 0.10%; (c) 0.15%; (d) 0.2%. Original magnification 10k.[56].

2.1.9. Solvent

The effects of solvents and their properties on electro-spinnability of the as-prepared polystyrene (PS) solutions and the morphological appearance of the as-spun PS fibers were investigated qualitatively by means of a scanning electron microscope (SEM) in [62]. The eighteen solvents used were benzene, t-butylacetate, carbon tetrachloride, chlorobenzene, chloroform, cyclohexane, decahydronaphthalene (decalin), 1, 2-dichloroethane, dimethylformamide (DMF), 1,4-dioxane, ethylacetate, ethylbenzene, hexane, methylethylketone (MEK), nitrobenzene, tetrahydrofuran (THF), 1,2, 3,4-

tetrahydronaphthalene (tetralin), and toluene. DMF was the best solvent to dissolve PS pellets within six hours, while others were found to dissolve PS pellets within one to three days, with the exception of hexane which was not able to dissolve PS pellets after seven days. Only the PS solutions in 1,2-dichloroethane, DMF, ethylacetate, MEK, and THF could produce fibers with high enough productivity, while the PS solutions in benzene, cyclohexane, decalin, ethylbenzene, nitrobenzene, and tetralin were not spinnable [62].

2.2. Processing Condition

2.2.1. Applied Voltage

In the case of electrospinning, the electric current due to the ionic conduction of charge in the polymer solution is usually assumed small enough to be negligible. The only mechanism of charge transport is the flow of polymer from the tip to the target. Thus, an increase in the electrospinning current generally reflects an increase in the mass flow rate from the capillary tip to the grounded target when all other variables (conductivity, dielectric constant, and flow rate of solution to the capillary tip) are held constant [16].

With the increase of the electrical potential the resulting nanofibers became rougher. It was already reported that a diameter of electrospun fibers was not significantly affected by an applied voltage. This voltage effects was particularly diminished when the polymer concentration was low. According to past works, higher voltage was reported to induce not only larger diameter but also smaller diameter. Applied voltage may affect some factors such as mass of polymer fed out from a tip of needle, elongation level of a jet by an electrical force, morphology of a jet (a single or multiple jets), etc. A balance among these factors may determine a final diameter of electrospun fibers. It is also noted that beaded fibers have been found to be electrospun with too high level of applied voltage. Although voltage effects show different tendencies, the voltage did not show a significant role in controlling the fiber morphology [59].

A series of experiments were carried out when the applied voltage was varied from 5 to 13kV and the tip to target distance was held at 15cm. Results were shown in [Figure 9](#). There was a slightly increase in average fiber diameter with increasing applied electric field. A considerable amount of thin fibers with diameters below 150nm were found when the applied voltage is above 10kV. A narrow distribution of fiber diameters was observed at a lower voltage of 5kV, while broad distribution in the fiber diameter was obtained at higher applied voltages of 10–13kV. Increasing the applied voltage, i.e., increasing the electric field strength will increase the electrostatic repulsive force on the fluid jet which favors the thinner fiber formation. On the other hand, the solution will be removed from the capillary tip more quickly as jet is ejected from Taylor cone. This results in the increase of the fiber diameter. Corona discharge was observed at voltages above 13kV, making electrospinning impossible [56]. Also an increase in voltage from 9.2 kV to 25 kV did not induce a significant change in the mean diameter of the fibers [54]. The diameter of electrospun PAN fibers did not change significantly over the range of applied voltage for the various solution concentrations in the experimental region [56].

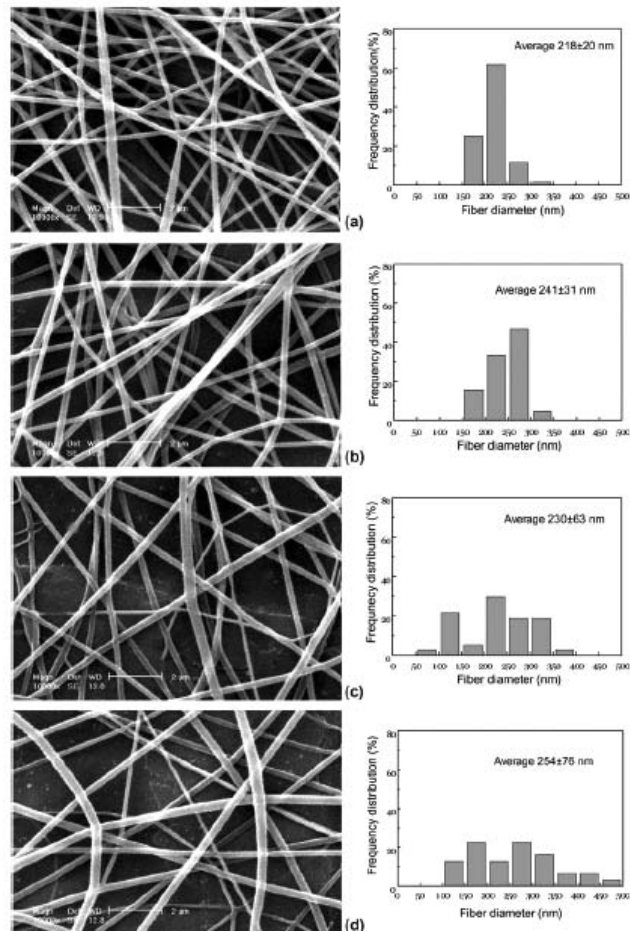


Figure 9. Effect of voltage on morphology and fiber diameter distribution from a 7.4% PVA/water solution (DH = 98%, tip–target distance = 15cm, flow rate = 0.2 ml/h). Voltage: (a) 5kV; (b) 8kV; (c) 10kV; (d) 13kV. Original magnification 10kx [56].

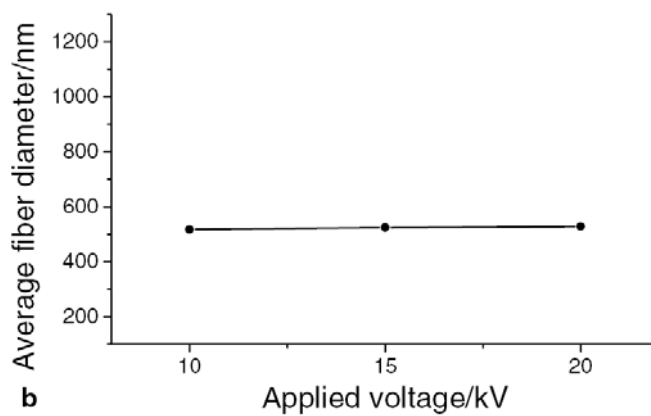


Figure 10. Main effect plots of applied voltage (b) on average fiber diameter [55].

SEM micrographs of nanofibers electrospun at different electrospinning voltage from a constant polymer concentration of 5wt% are shown in Figure 11a. A fiber diameter tended to decrease with increasing electrospinning voltage, although the influence was not as great as that of polymer concentration. Figure 11b shows fiber diameter as a function of electrospinning voltage. The increase of the electrospinning voltage causes increase of the electrostatic stress on the jet, which may be analogous to increase of the draw rate in conventional fiber spinning [64].

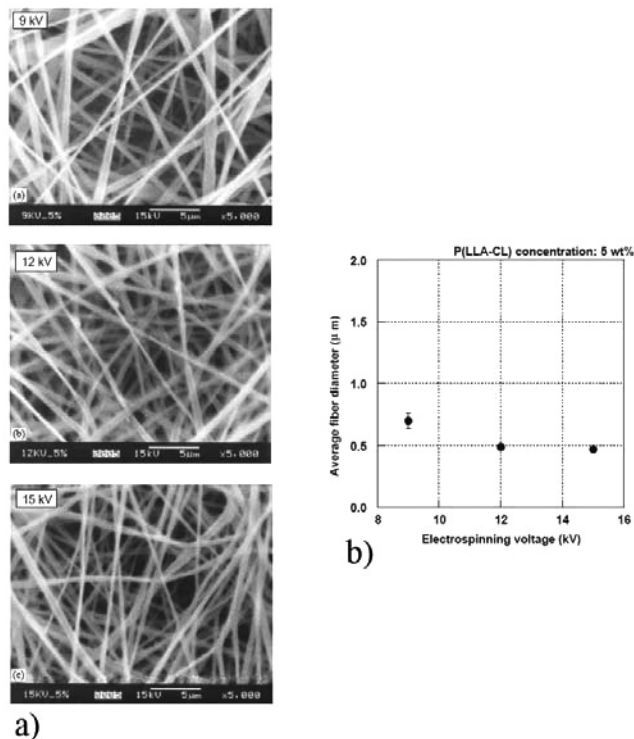


Figure 11 a). SEM micrographs of P(LLA-CL) fibers electrospun from a polymer concentration of 5wt% at different applied voltage: (a) 9 kV; (b) 12 kV and (c) 15 kV. b) Relation between fiber diameter and applied voltage in the electrospinning with 5wt% P(LLA-CL) solution [64].

2.2.2. Feed Rate

The morphological structure can be slightly changed by changing the solution flow rate as shown in Figure 12. At the flow rate of 0.3 ml/h, a few of big beads were observed on the fibers. The flow rate could affect electrospinning process. When the flow rate exceeded a critical value, the delivery rate of the solution jet to the capillary tip exceeded the rate at which the solution was removed from the tip by the electric forces. This shift in the mass-balance resulted in sustained but unstable jet and fibers with big beads were formed [56].

Figure 13 shows that the diameter of the electrospun HM-PLLA fibers was not significantly changed with varied volume feed rate. The influence due to the volume feed rate also diminished when the polymer concentration is low.

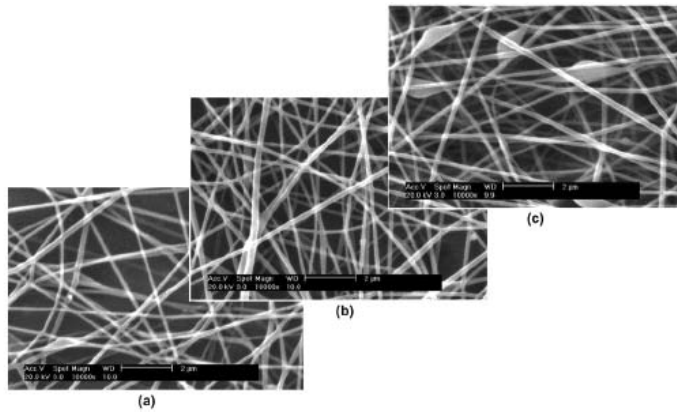


Figure 12. Effect of flow rate of 7% PVA water solution on fiber morphology (DH = 98%, voltage = 8kV, tip–target distance = 15cm). Flow rate: (a) 0.1 ml/h; (b) 0.2 ml/h; (c) 0.3 ml/h. Original magnification 10k.[56].

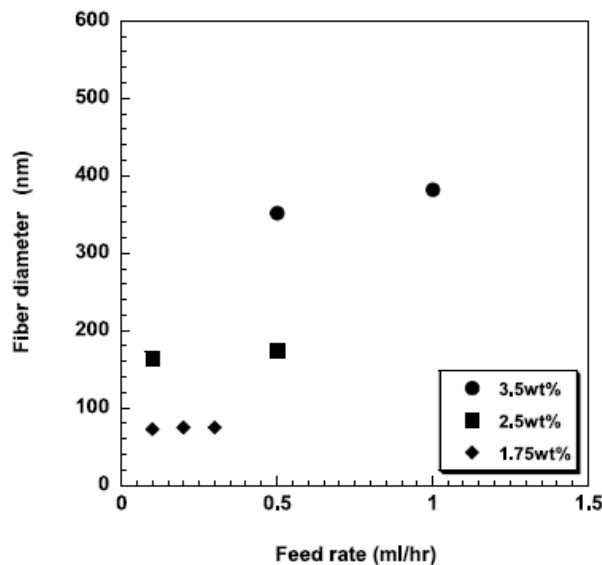


Figure 13. Volume feed rate effects on the diameter of the PLLA (Mw: 300 K) fibers electrospun from solutions with different polymer concentration [50].

The solution's electrical conductivity, were found as dominant parameters to control the morphology of electrospun polymer fibers [9]. In the case of low-molecular-weight liquid, when a high electrical force is applied, formation of droplets can occur. A theory proposed by Rayleigh explained this phenomenon. As evaporation of a droplet takes place, the droplet decreases in size. Therefore the charge density of its surface is increased. This increase in charge density due to Coulomb repulsion overcomes the surface tension of the droplet and causes the droplet to split into smaller droplets. However, in the case of a polymer solution (high molecular weight liquid) the emerging jet does not break up into droplets, but is stabilized and forms a string of beads connected by a fiber. As the concentration is increased, a string of connected beads is seen, and with further increase there is reduced bead formation

until only smooth fibers are formed. And sometimes spindle-like beads can form due to the extension causing by the electrostatic stress. The changing of fiber morphology can probably be attributed to a competition between surface tension and viscosity. As concentration was increased, the viscosity of the polymer solution increased. The surface tension attempted to reduce surface area per unit mass, thereby caused the formation of beads/spheres. Viscoelastic forces resisted the formation of beads and allowed for the formation of smooth fibers. Therefore formation of beads at lower polymer solution concentration (low viscosity) occurred where surface tension had a greater influence than the viscoelastic force. However, bead formation was reduced and finally eliminated at higher polymer solution concentration, where viscoelastic forces had a greater influence in comparison with surface tension. But when the concentration was too high, high viscosity and rapid evaporation of solvent made the extension of jet more difficult, thicker and ununiform fibers were formed [55].

2.2.3. Distance of Needle Tip to Collector

Tip–target distance had no significant effect on the electrospun fiber morphology of fully hydrolyzed PVA, as shown in Figure 14. The micrographs were undistinguishable for electrospinning at 8–15cm of tip–target distance. It was assumed that solution jets were elongated and solidified quickly after they flowed out of the needle tip because of the high conductivity of fully hydrolyzed PVA used [56].

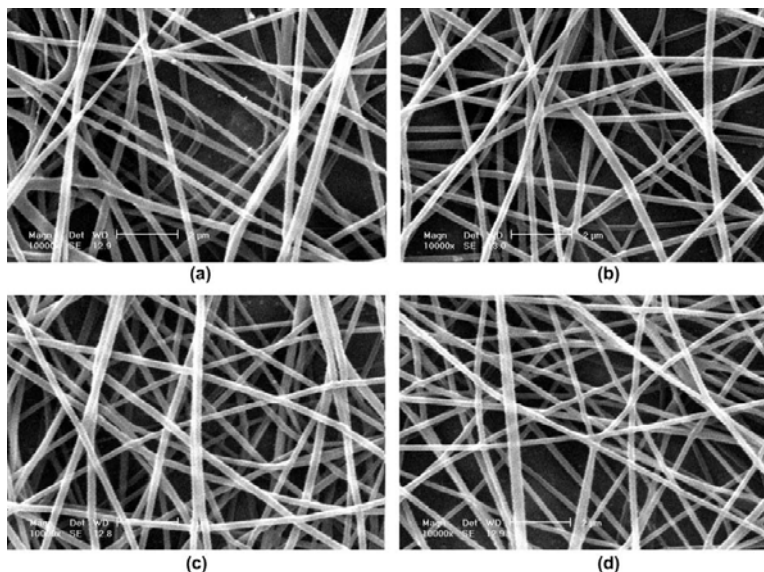


Figure 14. Effect of tip–target distance on fiber morphology from a 7.4% PVA/water solution (DH = 98%, voltage = 5kV, flow rate = 0.2 ml/h). Tip–target distance: (a) 8cm; (b) 10cm; (c) 12cm; (d) 15cm. Original magnification 10k [56].

Based on the processing parameter studies, all the parameters effects on the morphology of the electrospun nanofibers were summarized in a processing map (Figure 15). Suitable level of processing parameters must be optimized to electrospin polymers into nanofibers with desired morphology and the parameters levels are dependent on properties of polymers and solvents used in each of electrospinning process. Understanding of the concept how each of processing parameter affect the morphology of the electrospun nanofibers is essential. All

the parameters have been divided into two groups; i.e. one with parameters which affect the mass of polymer fed out from a tip of needle, and the other with parameters which affect an electrical force during electrospinning. Polymer concentration, applied voltage and volume feed rate were considered to affect the mass of polymer. Polymer concentration and feed rate directly reflect to the mass of polymer. Increased polymer concentration and feed rate tend to bring more mass of polymer into the polymer jet. It is noteworthy that the minimum polymer concentration to electrospin uniform fibers was determined by the molecular weight of polymer. High molecular weight of polymer provides enough level of solution viscosity to produce a uniform jet during electrospinning even when polymer concentration is relatively low. Applied voltage reflects to force to pull a solution out from the needle hence higher applied voltage causes more solution coming out. On the other hand, it was considered that solution electrical conductivity and applied voltage affect a charge density thus an electrical force, which acts to elongate a jet during electrospinning. Hence, higher solution electrical conductivity and applied voltage increase the jet elongation. Therefore, it is summarized that electrospun fibers with smaller diameter can be produced with lower polymer concentration, feed rate and applied voltage when the effects of mass of polymer dominates to determine the final diameter of electrospun fibers, while smaller diameter of fibers can be electrospun with higher solution electrical conductivity and applied voltage when the effects of the jet elongation is dominant.

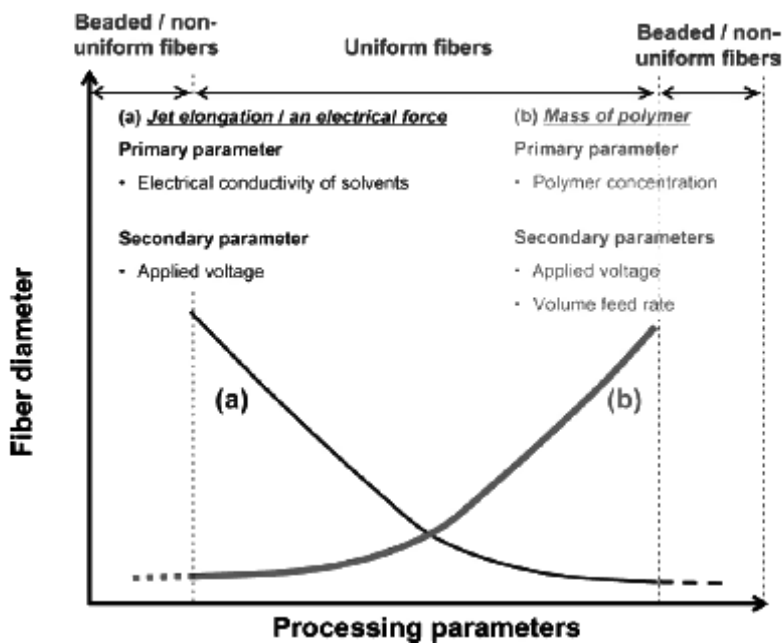


Figure 15. Processing map obtained based on the systematic parameter study: (a) jet elongation/an electrical force (affected by electrical conductivity of solvents, applied voltage), (b) mass of polymer (affected by polymer concentration, applied voltage, volume feed rate) [50].

For both cases, non-uniformed/ beaded fibers were found if the parameters were either too high or too low. In fact, applied voltage affects both the polymer mass and the jet elongation, however, the effects is not as dominant as the other parameters for controlling the morphology of electrospun fibers. It must be noted that polymer concentration, molecular

weight and solution electrical conductivity play a primal role in determining the morphology of electrospun fibers. Polymer fibers with smaller diameter can be electrospun with higher electrical conductivity of solution and lower polymer concentration which can be further decreased by higher molecular weight of polymer [50].

3. THEORY AND MODELING

Though easily realizable in the laboratory, electrospinning is a complex phenomenon to analyze because of the coupling between the electric field and the deformation of the fluid, the latter in turn determined by the rheology of the material. Typically, electrospinning has two stages. In the first, the polymer jet issues from a nozzle and thins steadily and smoothly downstream. In the second stage, the thin thread becomes unstable to a non-axisymmetric instability and spirals violently in large loops. The enormously increased contour length produces a very large stretch ratio and a nanoscale diameter.[9] For the steady stretching in stage one, Spivak and Dzenis[65] published a simple model that assumes the electric field to be uniform and constant, unaffected by the charges carried by the jet. (Reneker et al. modeled the viscoelasticity of the jet by a linear Maxwell equation [9]. Hohman *et al.*[67,68] developed a slender-body theory for electrospinning that couples jet stretching, charge transport, and the electric field. The model encounters difficulties, however, with the boundary condition at the nozzle.

For stage two, the bending instability has been carefully documented by two groups (Reneker *et al.*[69,70] Shin *et al.*[71]); each has proposed a theory for the instability. Reneker *et al.* modeled the polymer jet by a linear Maxwell equation. Like-charge repulsion generates a bending force that destabilizes the jet. Hohman *et al.*[67] built an electrohydrodynamic instability theory, and predicted that under favorable conditions, a nonaxisymmetric instability prevails over the familiar Rayleigh instability and a varicose instability due to electric charges. In theoretical work to date, the rheology of the polymer jet has been represented by a Newtonian viscosity [67,68] a power-law viscosity [66] and the linear Maxwell equation.[9,69,71].

The jet is governed by four steady-state equations representing the conservation of mass and electric charges, the linear momentum balance, and Coulomb's law for the E field [9]. Mass conservation requires that

$$\pi R^2 v = Q \quad (1)$$

where Q is a constant volume flow rate. Charge conservation may be expressed by

$$\pi R^2 KE + 2 \pi R v \sigma = I \quad (2)$$

where E is the z component of the electric field, K is the conductivity of the liquid, and I is the constant total current in the jet. The momentum equation is formulated by considering the forces on a short segment of the jet (Figure 16):

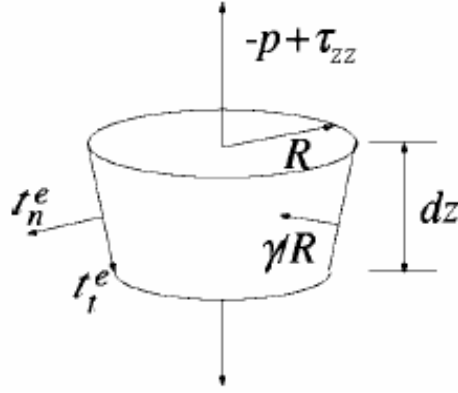


Figure 16. Momentum balance on a short section of the jet [9].

$$\frac{d}{dz}(\pi R^2 \rho v^2) = \pi R^2 \rho g + \frac{d}{dz}[\pi R(-P + \tau_{zz})] + \frac{\gamma}{R} \cdot 2\pi R R' + 2\pi R(t_t^e - t_n^e R'), \quad (3)$$

where τ_{zz} is the axial viscous normal stress, p is the pressure, γ is the surface tension, and t_t^e and t_n^e are the tangential and normal tractions on the surface of the jet due to electricity. The prime indicates derivative with respect to z , and R' is the slope of the jet surface. The ambient pressure has been set to zero. The electrostatic tractions are determined by the surface charge density and the electric field:

$$t_n^e = \left\| \frac{\varepsilon}{2} (E_n^2 - E_t^2) \right\| \approx \frac{\sigma^2}{2\varepsilon} - \frac{\varepsilon' - \varepsilon}{2} E^2, \quad (4)$$

$$t_t^e = \sigma E_t \approx \sigma E \quad (5)$$

where ε and $\bar{\varepsilon}$ are the dielectric constants of the jet and the ambient air, respectively, E_n and E_t are the normal and tangential components of the electric field at the surface, and $\|*\|$ indicates the jump of a quantity across the surface of the jet. We have used the jump conditions for E_n and E_t : $\| \varepsilon E_n \| = \bar{\varepsilon} \bar{E} - \varepsilon E_n = \sigma$, $\| E_t \| = \bar{E}_t - E_t = 0$, and assumed that $\varepsilon E_n \ll \bar{\varepsilon} \bar{E}$ (see Ganan-Calvo [13]) and $E_t \approx E$. The overbar indicates quantities in the surrounding air. The pressure $p(z)$ is determined by the radial momentum balance, and applying the normal force balance at the jet surface leads to

$$-p + \tau_{rr} = t_n^e - \frac{\gamma}{R} \quad (6)$$

Inserting Eqs. (4)-(6) into Eq. (3) yields:

$$\rho v v' = \rho g + \frac{3}{R^2} \frac{d}{dz} (\eta R^2 v') + \frac{\gamma R'}{R^2} + \frac{\sigma \sigma'}{\varepsilon} + (\varepsilon - \bar{\varepsilon}) E E' + \frac{2\sigma E}{R} \quad (7)$$

4. NATURAL FIBERS

The fibers in modern textile manufacture can be classified into two groups (a) natural (b) man-made fibers. A vast classification of fibers illustrated in figure 17. Natural fibers are those are provided by nature in a ready made fibrous form. Natural fibers can be subdivided into three main classes, according to the nature of their source.

- 1) vegetable fibers
- 2) animal fibers
- 3) mineral fibers

Vegetable fibers include the most important of all textile fibers cotton – together with flax, hemp, jute and other fibers which have produced by plants. They are base on cellulose, the material used by nature as a structural material in the plant world. Animal fibers include wool and other hair-like fibers, and fibers such as silk, produced as filaments by cocoon-spinning creatures. These animal fibers are based on proteins, the complex substances from which much of the animal body is made [72].

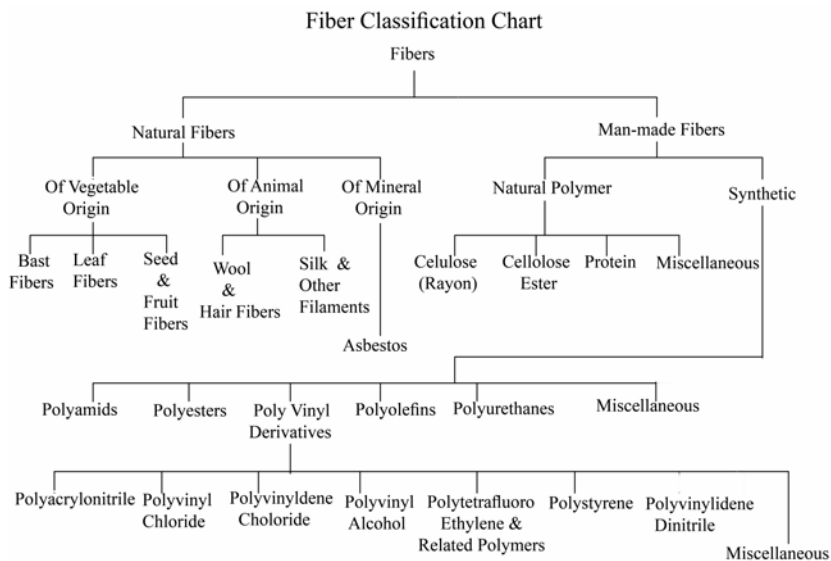


Figure 17. A vast classification chart for fibers[72].

5. EL ECREOSPINNING OF SILK FIBERS

5.1. Introduction

The silk fiber protein is synthesized by the silk gland cells and stored in the lumen of silk gland .Subsequently; it is converted into silk fibers. Each strand of silk fiber is a double structure with 2 fibroin filaments covered by sericin (Figure 18).

In the fibroin, alanine and glycine together account for 70 % of the total composition, whereas in the sericin they make up about 15%. The chief component of sericin is another amino acid, serine (30% of the total).

- Silk is the only natural fibre which exists as a continuous filament. Each *Bombyx mori* cocoon can yield up to 1600 meters of filament. These can be easily joined together using the adhesive qualities of sericin to form a theoretically endless filament.
- The silk fiber's triangular cross-section gives it excellent light reflection capability.
- The silk fiber is smooth, unlike those of wool, cotton and others. This is one of the reasons why silk fabrics are so lustrous and soft.
- Silk can absorb up to 30 % of its weight in moisture without creating a damp feeling. When moisture is absorbed it generates 'wetting-heat' which helps to explain why silk is comfortable to wear next to the skin.
- Silk has a tenacity of approximately 4.8 grams per denier, slightly less than that of nylon.
- Silk has poor resistance to ultraviolet light and for this reason is only recommended for those curtains that are lined or not exposed to direct sunlight [73].

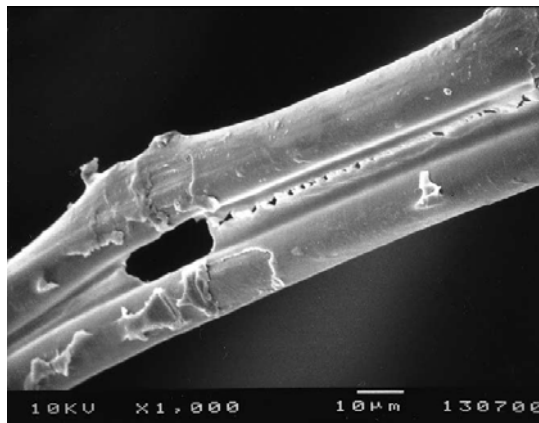


Figure 18. Silk micrograph (ITF) [73].

5.2. Crystal Structure of Silk (Fibroin) in Various Stages of Electrospinning

The physiological properties of SF matrices strongly depend on its molecular conformation and surface texture. SF exhibits at least three crystalline forms: silk I, silk II, and alpha-helix. All three conformations can be formed from the appropriate preparation conditions and each is interchangeable under certain conditions. Crystallization of SF involved the conformational transition that can be easily induced by simple physical (thermal), mechanical or chemical treatments. The most common method to convert the distorted conformation (random coil or silk I) of SF into the more stable β -sheet (silk II) conformation is to treat the SF film with an organic solvent. It is well known that organic

solvents, particularly methanol, are highly effective in the crystallizing SF from a distorted conformation to α -sheet.

Infrared spectroscopy (IR) has been often applied to study the molecular conformation of silk fibroin fibers or films. The sensitive absorption bands on the IR spectrum are located in the spectral regions of $\sim 1625\text{ cm}^{-1}$ (amide I), $\sim 1528\text{ cm}^{-1}$ (amide II), $\sim 1230\text{ cm}^{-1}$ (amide III), and $\sim 700\text{ cm}^{-1}$ (amide V). To characterize the structure of SF matrices, the ATR-IR spectra in the amide I and II regions is examined. The IR spectra of SF matrices are shown in Figure 19(a)–(c). The as-spun SF-N matrix was characterized by absorption bands at 1651 cm^{-1} (amide I) and 1528 cm^{-1} (amide II), attributed to the random coil conformation, as shown in Figure 19a. The methanol-treated SF-N matrix showed strong β -sheet absorptions at 1622 and 1514 cm^{-1} within a methanol-treating time of 10 min, indicating that the random coil conformation of the SF nanofibers rapidly converted into β -sheet structure (Figure 19b) [75]. On the contrary, both the as-prepared SF-F and SF-M matrices showed strong β -sheet absorptions at 1622 and 1514 cm^{-1} without methanol treatment, as shown in Figure 19c and d. The raw SF had highly ordered intermolecular hydrogen bonds (β -sheet), and the SF film took a mainly β -sheet conformation, when cast from the formic acid solution.

Solid-state ^{13}C NMR has been shown to be a more effective analytical tool for demonstrating the formation of β -sheets in polypeptides and proteins, because the isotropic ^{13}C NMR chemical shifts of carbon atoms in proteins are sensitive to the β -sheet's secondary structure. It is well established that SF conformations are dependent upon the species of silkworms and conditions of the sample preparation. In particular, it has been reported that fibroin from *Bombyx mori* adopts two dimorphic structures, silk I and silk II. The silk II form is identified by the ^{13}C chemical shifts of glycine (Gly), serine (Ser), and alanine (Ala) that are indicative of β -sheets, while the silk I form produces chemical shifts that are associated with a loose helix or distorted β -turn. However, when compared with silk II, the less stable silk I shows a relatively unresolved structure, and the conformation of the soluble form of SF rapidly undergoes a transition to the insoluble silk II conformation.

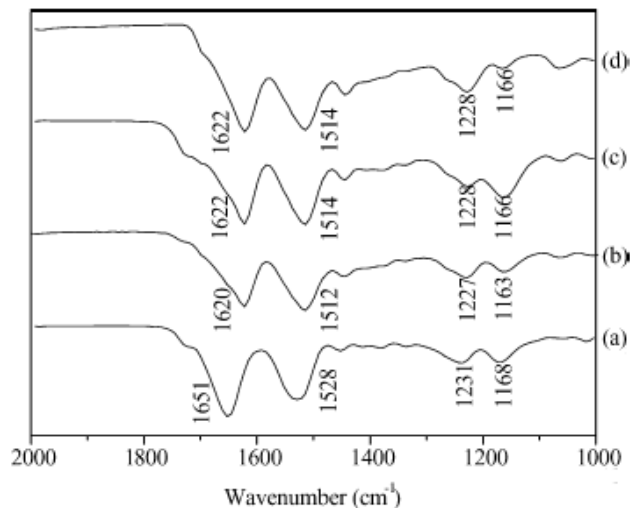


Figure 19. ATR-IR spectra of the as-prepared and methanol-treated SF matrices: (a) as-spun SF-N; (b) methanol-treated SF-N; (c) as-cast SF-F; (d) SF-M [75].

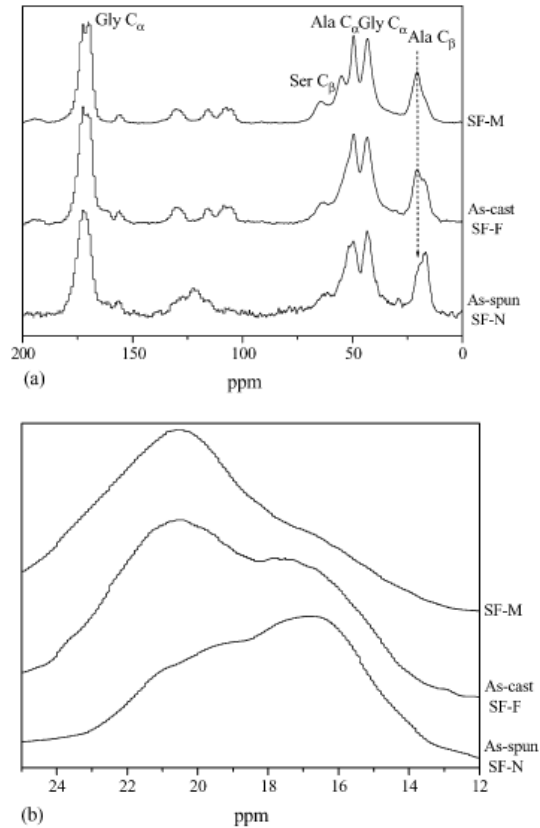


Figure 20. ^{13}C CP/MAS NMR spectra (a) and the expanded ^{13}C NMR spectra of the methyl alanine region (b) of SF matrices. The dotted arrow indicates the chemical shift of alanine in the β -sheet conformation[75].

In ^{13}C CP/MAS NMR structural analyses of *B. mori* silk fibroins, the two crystalline forms of silk fibroins, silk I and silk II (β -sheet), have been distinguished by the conformation-dependent ^{13}C chemical shifts of the respective amino acid residues. Figure 20 shows ^{13}C CP/MAS NMR spectra (a) and the expanded ^{13}C NMR spectra of the methyl alanine region (b) of SF matrices. The dotted arrow indicates the chemical shift of alanine in the β -sheet conformation. solid-state ^{13}C NMR spectra of the as-prepared SF-N and SF-F matrices, together with that of the SF-M. Assignments were made according to the literature. The chemical shifts of the Ala residue in Figure 20a were 17.6 ppm for Ala C_β , 49.9 ppm for Ala C_α , and 173.5 ppm for Ala $\text{C}=\text{O}$ carbon. The observed ^{13}C NMR chemical shifts of the peaks suggest that the Ala residue of the SF-N matrix takes a mainly non β -sheet conformation (random coil and silk I). The vertical dashed line and arrow in Figure 20 show the chemical shift of Ala in the β -sheet conformation. A shoulder was detected at ~20.4 ppm and assigned to Ala C_β in a β -sheet conformation, indicating that as-spun SF-N take some β -sheet conformations. The β -sheet structure of as-spun SF nanofibers could be formed partially by the elongational forces during the electrospinning process. However, the characteristic resonances of SF-F matrix, especially the Ala C_β at 20.4 ppm and Ala C_α at 48.9 ppm in are similar with that of the SF-M matrix [75]. Shimizu has reported that there are two types of

crystal formation during solidification of liquid fibroin (by losing water) inside the silk gland. One of them corresponds to the crystal form of fibrous fibroin. The fibroin molecular chain which constitutes the spatial crystal form is considered to be the intermediate form during the course of shifting the molecular chain of liquid silk to the fibrous fibroin molecule chain, that is, β -chain. It is therefore named as α -type of fibroin. The condition for the appearance of a type thereafter include solidification when there is no stress from liquid silk and the temperature being less than 40°C. It becomes β type when the temperature is above 50°C. Both α and β types of none stretched are insoluble in water and α type is softer than β type [76].

β Structure of Silk

β structure is the structure where the polypeptide chain is elongated. The structure can be the type where all the molecular chain run in the same direction and form a parallel pleated sheet or the type where the molecular chain run in the alternate direction and form anti parallel chain pleated sheet. In the case of β -structure, there are three important features, namely the period that is repeating period of the polypeptide chain, the spacing of the molecular chain in the sheet and the distance between the sheets [76].

5.3. Spinning Dope Preparation for Electrospinning

5.3.1. Degumming

The natural gum, sericin is normally left on the silk during reeling, throwing and weaving. It acts as a size which protects the fiber from mechanical injury. The gum is removed from finished yarns or fabrics, usually by boiling whit soap and water [73]. The fibers were heated in an aqueous Na_2CO_3 (0.02 M) or 0.5 % (w/w) NaHCO_3 and rinsed with water to extract sericin.[77, 75].

5.3.2. Dissolving of Fibroin

The extracted fibers (degummed silk) were then dissolved in 50% CaCl_2 [77] (100°C, then cooled) or in 9.3 M LiBr solution at 60°C yielding a solution. The solution pours into regenerated cellulose dialysis tubing to carry out dialysis against 1000 ml deionized water (for 48 h at 23 °C). Another way reported by Min et al. [76,75] degummed silk (SF) is dissolved in ternary $\text{CaCl}_2/\text{CH}_3\text{CH}_2\text{OH}/\text{H}_2\text{O}$ (1:2:8 in molar ratio) at 70°C for 6 h and then dialyzed with cellulose tubular membrane. After these stages the regenerated silk fibroin sponge is obtained by lyophilization. The silk sponge solution is electrospun in formic acid (98-100%).

5.4. Electrospinning of Silk Fibroin

Electrospinning generally produces non-woven matrices with randomly arranged, ultrathin fibers that have nanometerscale diameters. Figure 21 shows a SEM micrograph (magnification 500×) of the woven SF microfiber and as-spun SF nanofiber matrix. From the image analysis, the SF nanofibers have an average diameter of 80 nm and their diameters

ranged from 30 to 120 nm, while the diameter of the SF microfiber was 11 nm. The average diameter of SF nanofibers corresponds to about two orders of magnitude smaller than a SF microfiber [75].

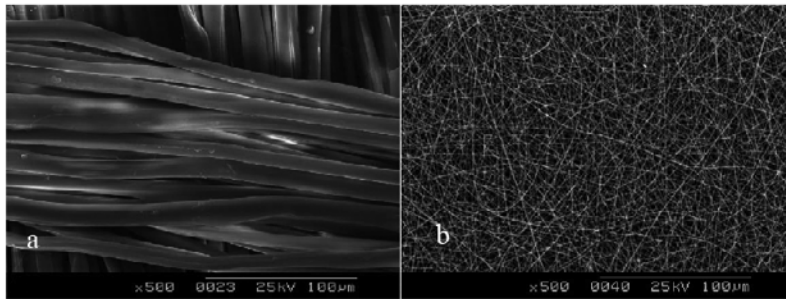


Figure 21. SEM image of woven SF microfibers and nonwoven SF nanofibers [75].

5.4.1. Effect of Silk Polymer Concentration on Fiber Diameter

Silk concentration plays a major role in fiber diameter. No fibers were formed at less than 5% silk concentration for any electric field and spinning distances. Figures. 22 and 23 show the morphology of fibers obtained at the electric fields of 3 and 4 kV/cm, respectively, at silk/formic acid concentrations of 5, 8, 10, 12, 15, and 19.5% with a constant tip-to-collection plate distance of 7 cm.

	magnification			Fiber diameter (nm)
	1000 x	5000 x	35000 x	
5%	No fiber			
8%	No fiber			
10%				AV:57.1 STDV:22.69 Max:125.8 Min:18.5
12%				AV:56.0 STDV:21.36 Max:149.0 Min:20.0
15%				AV:65.1 STDV:27.11 Max:167.1 Min:14.8
19.5 %				AV:368.8 STDV:179.29 Max:1277.4 Min:110.9

Figure 22. The morphology of fibers at electric field of 3 kV/cm at concentrations from 5 to 19.5% with a constant spinning distance of 7 cm. The figure also shows the average, standard deviation, maximum and minimum values of the fiber diameter [77].

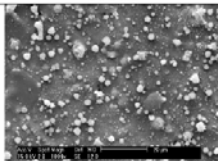
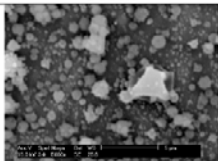
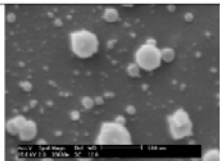
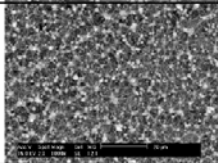
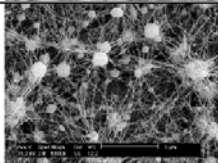
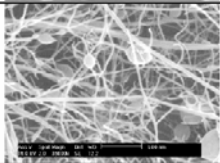
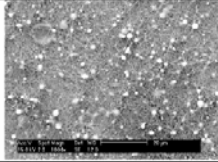
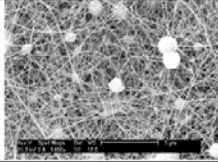
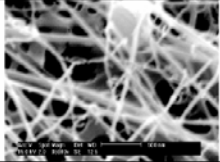
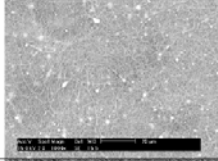
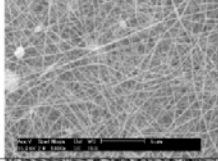
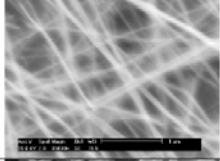
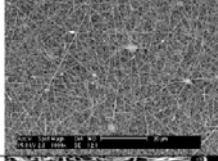
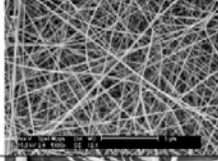
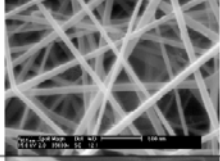
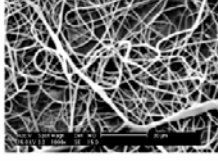
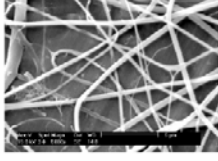
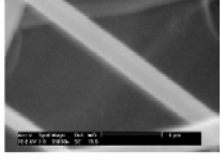
	magnification			Fiber diameter (nm)
	1000x	5000x	35000x	
5%				
8%				AV:26.3 STDV:12.58 Max:79.1 Min:11.9
10%				AV:40.5 STDV:14.23 Max:91.0 Min:15.38
12%				AV:41 STDV:17.0 Max:118.6 Min:15.5
15%				AV:71.0 STDV:29.29 Max:188.0 Min:19
19.5 %				AV:379.3 STDV:201.36 Max:1472.9 Min:109.66

Figure 23. The morphology of fibers at electric field of 4 kV/cm at concentrations from 5 to 19.5% with a constant spinning distance of 7 cm [77].

At 8% concentration less than 30 nm diameter fibers were formed with beads (drops of polymer over the woven mesh) and they were not uniform and were branched off (Figure 23). At 10% concentration with 5 cm spinning distance and 2, 3 and 4 kV/cm electric fields, drops were formed instead of fibers. Continuous fibers were obtained above 12% regardless of electric field and distance (Figures 22 and 23). At 19.5%, the average fiber diameter was much larger than that of fibers spun at lower concentrations. In the short distance as well as low concentration (10%), the solution reaches the collection plate before the solvent fully evaporates. This explains the formation of droplets and beads at the low concentration and distance. Fewer beads were observed in electrospun fibers at higher concentration.

Increase in the regenerated silk concentration in the formic acid increases the solution viscosity. At low concentrations beads are form instead of fibers and at high concentrations the formation of continuous fibers are prohibited because of inability to maintain the flow of the solution at the tip of the needle resulting in the formation of larger fibers. Continuous

nanofibers were obtained above 12% regardless of electric field and distance and at higher concentration of 19.5% the average fiber diameter was larger than at lower concentrations [77].

The SEM micrographs of nanofibers electrospun from the SF solutions with different concentrations or viscosities ranged from 3% to 15% by weight were shown in Figure 24. At the concentration below 9% by weight, beads or beaded fibers were generated by electrospinning. The continuous nanofibers can be obtained at the concentration above 12% by weight, and this concentration appears to correspond to the onset of significant chain entanglements in the viscosity data shown in Figure 24. Therefore, it can be concluded that extensive chain entanglements are necessary to produce the continuous fibers by electrospinning [75].

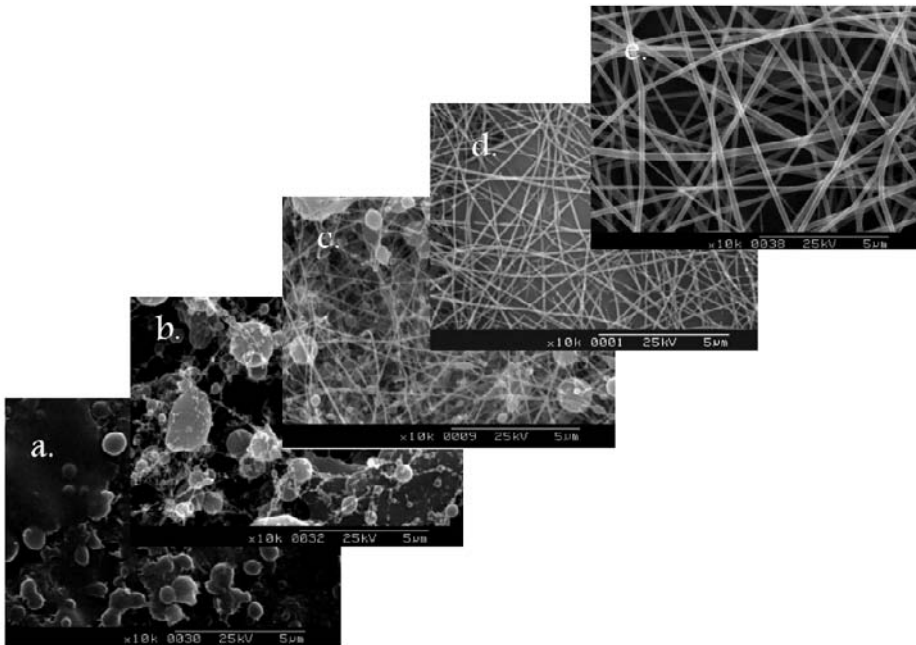


Figure 24. SEM micrographs of electrospun SF nanofibers with concentration of (a) 3%, (b) 6%, (c) 9%, (d) 12%, or (e) 15% by weight [75].

5.4.2. Effect of Voltage and Spinning Distance on Morphology and Diameter

Figure 25 shows the relationship between mean fiber diameter and electric field with concentration of 15% at spinning distances of 5, 7 and 10 cm. The mean fiber diameter obtained at 2 kV/cm is larger than other electric fields. The effect of two factors, concentration and electric field on fiber diameter was investigated by two-way analysis of variance. The interaction effect between two factors is also obtained from this analysis [77].

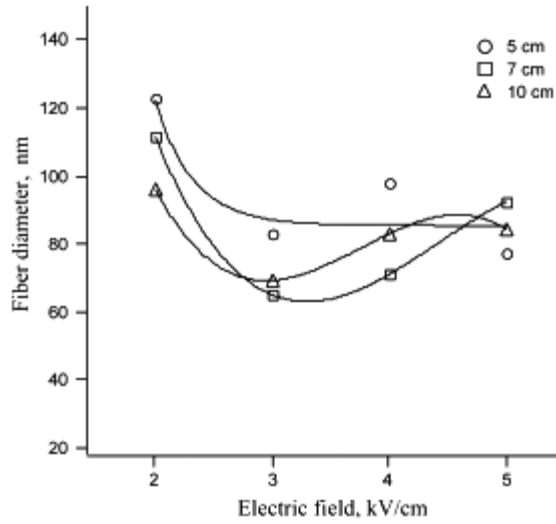


Figure 25. The relationship between mean fiber diameter and electric field with concentration of 15% at spinning distances of 5, 7 and 10 cm. (Please refer to text for explanation) [77].

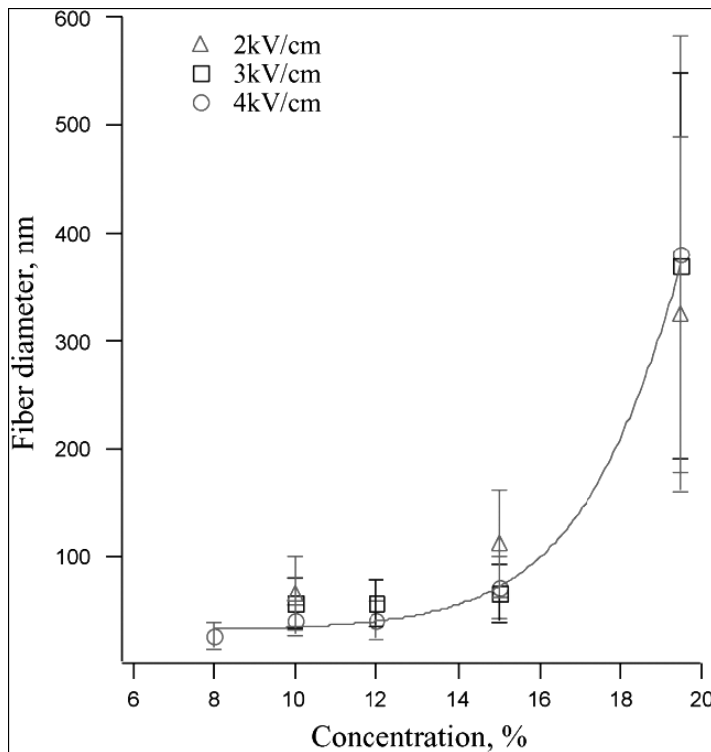


Figure 26. The relationship between the fiber diameter and the concentration at three electric fields (2, 3, 4 kV/cm)[77].

Figure 26 shows that the concentration apparently has more effect on the fiber diameter than electricfield. The multiple regression analysis was carried out to evaluate the contribution of concentration and electric field on the fiber diameter [77].

Sukigara et al.[78] used RSM analysis (Response Surface Methodology) to the experimental results to develop a processing window which will produce nanoscale regenerated silk fibers by electrospinning process. RSM is used in situations where several variables influence a feature (called the response) of the system. The steps in the procedure are described briefly as follows.

- 1) Identification of variables $\zeta_1; \zeta_2; \zeta_3 \dots$ for response η ;
- 2) Calculation of corresponding coded variables $x_1; x_2; x_3 \dots$ by using the following equation.

$$x_i = \frac{\zeta_i - [\zeta_{A_i} + \zeta_{B_i}]/2}{[\zeta_{A_i} - \zeta_{B_i}]/2} \quad (1)$$

where ζ_{A_i} and ζ_{B_i} refer to the high and low levels of the variables ζ_i ; respectively.

- 3) Determination of the empirical model by multiple regression analysis to generate theoretical responses (\hat{y}): The second-order model is widely used in RSM. The general equation for response h of the second-order model is given by:

$$\eta = \beta_o + \sum_{i=1}^k \beta_i x_i + \sum_{i=1}^k \beta_{ii} x_i^2 + \sum_{i < j=2}^k \sum_{i < j=2}^k \beta_{ij} x_i x_j \quad (2)$$

where k is the number of factors, x_i are the coded variables and β are coefficients.

- 4) Calculation of the Coefficients B to Fit the Experimental Data as Close as Possible

The relationship between the response and the variables is visualized by a response surface or contour plot to see the relative influence of the parameters, to find an optimum parameter combination, and to predict experimental results for other parameter. for two variables , When $k = 2$; the empirical model from the general Eq. (2) becomes

$$y = \beta_o x_1 + \beta_1 x_1 + \beta_2 x_2 + \beta_{11} x_1^2 + \beta_{22} x_2^2 + \beta_{12} x_1 x_2 + \varepsilon, \quad (3)$$

RSM procedure to optimize the process parameters for the electrospinning silk is shown in Figure 27.

Sukigara et al. [78] designed a factorial experiment by using two factors (electric field and concentration). For a quadratic model, experiments must be performed for at least three levels of each factor. These levels are best chosen equally spaced. The two factors (silk concentration and electric field) and three levels resulted in nine possible combinations of factor settings. A schematic of the experimental design is shown in Figure 28(A) and (B).

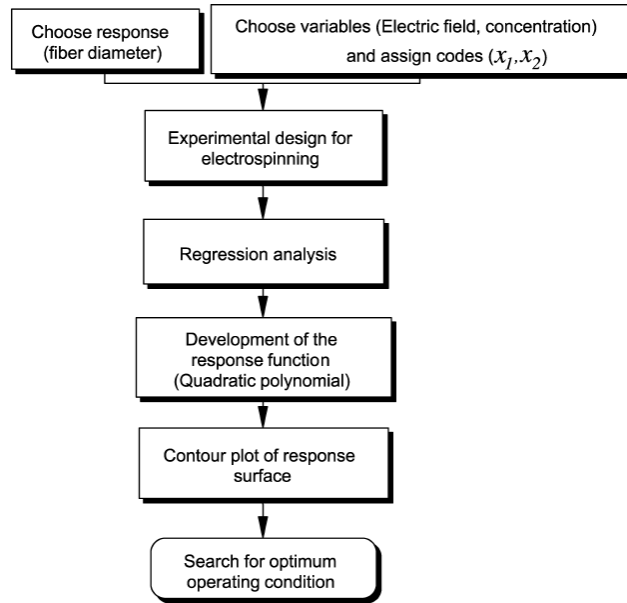


Figure 27. RSM procedure to optimize the electrospinning condition of regenerated silk [78].

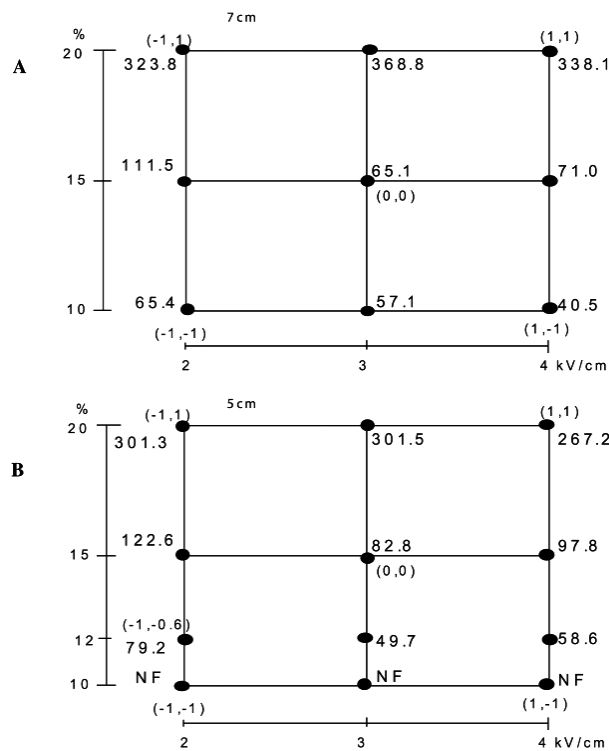


Figure 28. Experimental design (A) spinning distance 7 cm and (B) spinning distance 5 cm. The values at the coordinate points show the mean fiber diameter (nm) of 100 measurements and coded values are shown in the brackets (electric field and concentration). NF: no fiber formation [78].

5.5. Characterization

The conformational changes of the secondary structure of silk fibroin, which occur during the electrospinning process, were analyzed by Raman spectroscopy. The spectra for pristine, degummed and electrospun fibers are shown in Figure 29(A). Pristine and degummed silk fibroins display characteristic conformational bands in the range 1650–1667 and 1241–1279 cm^{-1} which correspond to amide I and complex amide III, respectively. In this study, the amide I (random coil) pristine band was observed at 1665 cm^{-1} and the amide III (β -sheet) pristine band at 1231 cm^{-1} . These well-defined bands were chosen because they give a clear indication of changes in the secondary structures from random to β -sheet. The degummed silk also shows absorption bands at these wavelengths. No significant spectral changes were observed indicating that the fibroin conformation is unchanged during the degumming process. The Raman spectra of the electrospun fiber are essentially the same as that of the pristine and degummed fibers although minor bands and some differences in peak intensities appear. This shows that the electrospinning process preserves the natural conformation of the fibroin. Figure 29(B) shows the amide I (1665 cm^{-1} , random) to amide III (1228 cm^{-1} , β -sheet) ratio of the electrospun fiber is less than that of the pristine fiber. This means that the electrospun fiber has a higher β -sheet content than the pristine fiber.

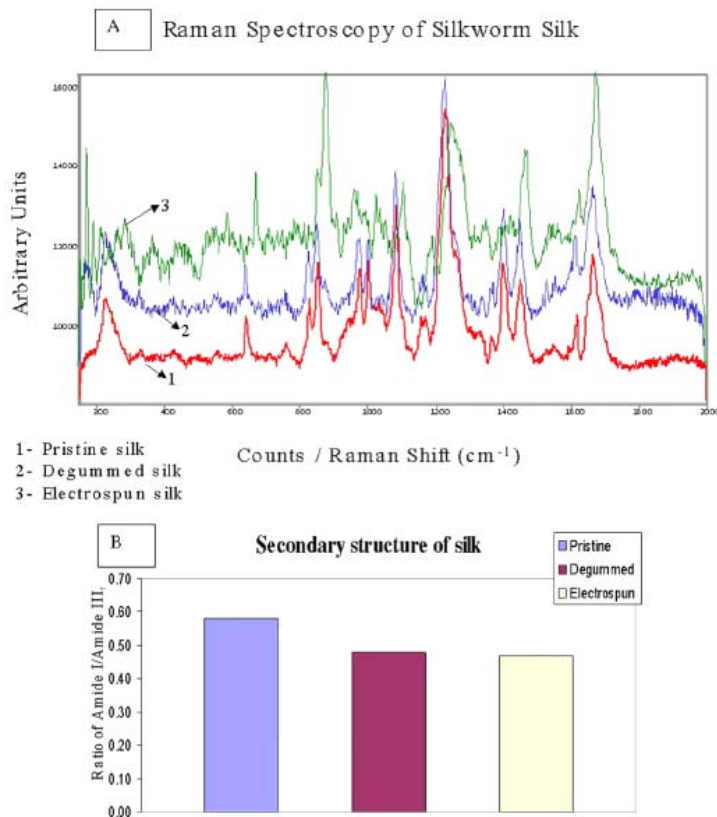


Figure 29. (A) Raman spectroscopy of pristine, degummed and electrospun nonwoven silk mat. (B) Secondary structural compositions of silk fibroin showing the fraction of Amide I to Amide III conformations [79].

6. ELECTROSPINNING OF CELLULOSE AND CELLULOSE ACETATE

Cellulose is the most abundant naturally occurring polysaccharide formed out of glucose-based repeat units, connected by 1,4-beta-glucosidic linkages. Cellulose and its derivatives are widely used as tough versatile materials. Cellulose nitrate, cellulose acetate (CA) and cellulose xanthate (rayon) can be easily molded or drawn into fibers for textile applications, for designing composite materials (safety glass), as thermoplastics etc [80].

6.1. Electrospinning of CTA Solution

CTA was dissolved in MC or solvent mixtures of MC/EtOH (90 / 10, 85 / 15, and 80 / 20, v/v). The needle (ID=0.495 mm) was connected to the high voltage supply (Chungpa EMT, CPS-40K03), which can generate positive DC voltages up to 40 kV. The distance between the needle tip and the collecting target was 10 cm. Positive voltage applied to polymer solutions were 15 kV. CA solutions were delivered via a syringe (20 mL) with a mass flow rate of 1mL/h. The optimum concentration of CTA solution for fiber formation was 5 wt.%. All electrospinnings were carried out at room temperature [81].

Figure 30 shows SEM photographs of ultrafine CTA fibers electrospun from a 5 wt.% CTA solution in MC. CTA fibers showed a mixed pattern of flat ribbons and round shapes [Figure 30(a)]. These flat ribbons were wrinkled or twisted in an irregular way. At a higher magnification ($\times 20,000$), it was found that ultrafine CTA fibers had isolated circular shape pores with a narrow size distribution in the range of 50–100 nm [Figure 30(b)]. The porous structure was induced by phase separation resulting from the rapid evaporation of MC during the electrospinning process. The polymer-rich phase formed the fiber matrix and solvent-rich phase gave rise to the pores. Figure 30(c) shows a SEM image for the fractured cross-section of the porous CTA fiber. Isolated pores were also observed inside the fiber, which were larger than those in the fiber surface. In liquid–liquid demixing of polymer solution, the resulting polymer morphology is dependent on the phase separation mechanism. The structure formed by the spinodal decomposition (SD) mechanism shows interconnected pores, whereas nucleation and growth (NG) mechanism mainly results in isolated spherical pores [81].

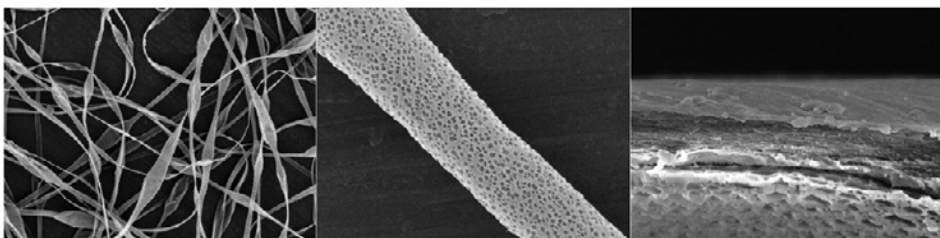


Figure 30. SEM images of electrospun CTA fibers: (a) magnification $\times 1000$, (b) magnification $\times 20,000$, and (c) fractured cross-section of porous CTA fibers [81].

Figure 31 shows SEM photographs of ultrafine CTA fibers electrospun from different ratios of MC/ EtOH (90 / 10, 85 / 15, and 80/20 v/v). All ultrafine CTA fibers were

electrospun with the same electrospinning condition for a CTA solution in MC. It was found that the addition of EtOH changed not only the pore structure but also the fiber diameter. In the case of MC/EtOH (90 / 10), the resulting CTA fibers had interconnected pores in the range of 200–500 nm, indicating phase separation proceeded according to SD mechanism. However, non-porous corrugated fibers were obtained from the other mixed solvents [Figure 31(b) and (c)] [81].

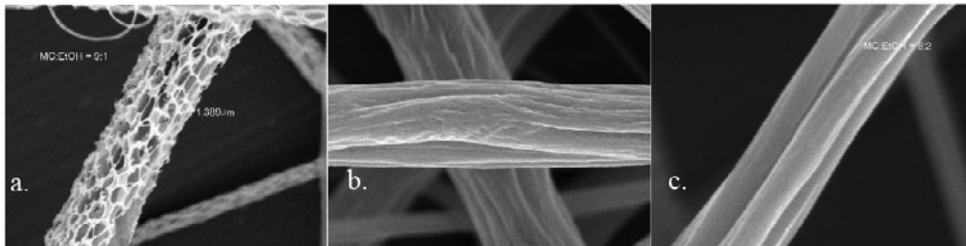


Figure 31. SEM images of ultrafine CTA fibers electrospun using different volume ratios of MC/EtOH: (a) 90/ 10, (b) 85/ 15, and (c) 80/ 20 [81].

7. CONCLUDING REMARKS

Nanotechnology has become in recent years a topic of great interest to scientists and engineers, and is now established as prioritized research area in many countries. The reduction of the size to the nano-meter range brings an array of new possibilities in terms of material properties, in particular with respect to achievable surface to volume ratios. Electrospinning of natural fibers is a novel process for producing superfine fibers by forcing a solution through a spinnerette with an electric field. A comprehensive review on this technique has been made in this paper. Based on this review, many challenges exist in the electrospinning process of natural fibers, and a number of fundamental questions remain open. The electrospinning technique provides an inexpensive and easy way to produce natural nanofibers on low basis weight, small fiber diameter and pore size. It is hoped that this chapter will pave the way toward a better understanding of the application of electrospinning of natural fibers.

Nevertheless, Among the biodegradable and biocompatible polymers, SF was extensively studied as one of the candidate materials for biomedical applications, because it has several distinctive biological properties including good biocompatibility, biodegradability, and minimal inflammatory reaction. One of the promising applications of SF in biomedical engineering is as scaffolding materials for tissue engineering. It was reported that SF matrices could be useful for the culture of fibroblasts and osteoblasts as well as stem cells, and could enhance the adhesion, growth, and differentiation of the cells in a manner similar to that of collagen matrices. nonwoven matrices of electrospun nanofibers could be prepared from a regenerated SF solution, and that the matrices were effective in the cell attachment and spreading of normal human keratinocytes and fibroblasts [82].

REFERENCES

- [1] YQ. Wan, Q. Guo, N. Pan. 2004. Thermo-electro-hydrodynamic model for electrospinning process. *Int. J. Nonlinear Sci. Num. Simul.*,5.pp5–8.
- [2] JH. He, YQ. Wan, JY. Yu. 2004. Allometric scaling and instability in electrospinning. *Int. J. Nonlinear Sci. Num. Simul.*,5(3).pp.243–52.
- [3] JH.He, YQ. Wan, JY. Yu . 2004.Application of vibration technology to polymer electrospinning. *Int. J. Nonlinear Sci. Num Simul.*,5(3).pp.253–61.
- [4] JH He, YQ Wan. 2004. Allometric scaling for voltage and current in electrospinning. *Polymer*,45(19).pp-6731–4.
- [5] X-H .Qin, YQ ,Wan, JH .He . 2004. Effect of LiCl on electrospinning of PAN polymer solution: theoretical analysis and experimental verification. *Polymer*,45(18).pp.6409–13.
- [6] SA. Theron, E. Zussmana, AL. Yarin. 2004. Experimental investigation of the governing parameters in the electrospinning of polymer solutions. *Polymer*,45.pp.2017–30.
- [7] MM .Demir, I .Yilgor, E. Yilgor, B Erman. 2002. Electrospinning of polyurethane fibers. *Polymer*,43.pp.3303–9.
- [8] AM. Ganan-Calvo. 1999. The surface charge in electrospaying: its nature and its universal scaling laws. *J. Aerosol. Sci.*;30(7):863–72.
- [9] JJ. Feng. 2003. Stretching of a straight electrically charged viscoelastic jet. *J. Non-Newtonian Fluid Mech.*, 116.pp.55–70.
- [10] YM .Shin, MM. Hohman, MP. Brenner, GC. Rutledge. 2001. Experimental characterization of electrospinning: the electrically forced jet and instabilities. *Polymer*, 42.pp.9955–67.
- [11] J. He, Y. Wan, J-Y.Yu. 2005. Scaling law in electrospinning: relationship between electric current and solution flow rate. *Polymer*, 46.PP. 2799–2801.
- [12] PK. Baumgarten. 1971. Electrostatic spinning of acrylic microfibers. *J. Colloid Interface Sci.*,36.pp.71–79.
- [13] J .Doshi, DH. Reneker. 1995. Electrospinning process and applications of electrospun fibers. *J. Electrostat.*,35.pp.151–60.
- [14] DH. Reneker, AL. Yarin, H. Fong, S. Koombhongse. 2000. Bending instability of electrical charged liquid jets of polymer solutions in electrospinning. *J. Appl. Phys.*,87.pp.4531– 4547.
- [15] M. Bognitzki, W. Czando, T. Frese, A. Schaper, M Hellwig, M. Steinhart, A. Greiner, JH. Wendorff. 2001 Nanostructured fibers via electrospinning. *Adv. Mater.*,13.pp.70–72.
- [16] E. Zussman, A. Theron, AL. Yarin. 2003. Formation of nanofiber crossbars in electrospinning. *Appl. Phys. Lett.*,82.pp.973–975.
- [17] S.A. Theron, A.L. Yarin, E. Zussman, E. Kroll. 2005. Multiple jets in elctrospinning: experiment and modeling. *Polymer*, 46.pp . 2889–2899.
- [18] Z-M Huang, Y.-Z. Zhang, M. Kotak, S. Ramakrishna. 2003. A review on polymer nanofibers by electrospinning and their applications in nanocomposites. *Composites Science and Technology*, 63 .pp.2223–2253.
- [19] D. Emig, A. Klimmek, E. Raabe. *US Patent* 6395046. 2002.

-
- [20] D. Groitzsch, E. Fahrbach. *US patent* 4,618,524, 1986.
- [21] HL. Schreuder-Gibson, P. Gibson, K Senecal, M Sennett, J. Walker, W. Yeomans, et al. 2002. Protective textile materials based on electrospun nanofibers. *Journal of Advanced Materials*,34(3),pp. 44–55.
- [22] M.M. Bergshoef, G.J. Vancso. 1999. Transparent nanocomposites with ultrathin, electrospun nylon-4,6 fiber reinforcement. *Adv. Mater*, 11,pp.1362–1365.
- [23] Z. Ma, M. Kotaki, R. Inai, S. Ramakrishna. 2005. Potential of nanofiber matrix as tissue engineering scaffolds. *Tissue Eng*, 11 .pp.101.
- [24] C.Y. Xu, R. Inai, M. Kotaki, S. Ramakrishna. 2004 .Aligned biodegradable nanofibrous structure: a potential scaffold for blood vessel engineering. *Biomaterials*, 25 .pp. 877.
- [25] H. Yoshimoto, Y.M. Shin, H. Terai, J.P. Vacanti. 2003. A biodegradable nanofiber scaffold by electrospinning and its potential for bone tissue engineering. *Biomaterials*, 24 .pp. 2077.
- [26] M. Shin, O. Ishii, T. Sued, J.P. Vacanti. 2004. Contractile cardiac grafts using a novel nanofibrous mesh. *Biomaterials* ,25 .pp. 3717.
- [27] Z Ma, M. Kotaki, Thomas Yong, Wei He, S. Ramakrishna.2005 .Surface engineering of electrospun polyethylene terephthalate (PET) nanofibers towards development of a new material for blood vessel engineering. *Biomaterials*, 26 .pp.2527–2536.
- [28] HJ. Jin, S. Fridrikh, GC. Rutledge, D Kaplan. 2002. Electrospinning Bombyx mori silkwith poly(ethylene oxide). *Abstracts of Papers American Chemical Society*,224(1–2).pp408.
- [29] Y.K. Luu, K. Kim, B.S. Hsiao, B. Chu, M. Hadjiargyrou.2003. Development of a nanostructured DNA delivery scaffold via electrospinning of PLGA and PLA–PEG block copolymers, *J. Control. Release*, 89 .pp. 341.
- [30] G. Verreck, I. Chun, J. Rosenblatt, J. Peeters, A.V. Dijck, J. Mensch, M. Noppe, M.E. Brewster. 2003. Incorporation of drugs in an amorphous state into electrospun nanofibers composed of a waterinsoluble, nonbiodegradable polymer. *J. Control. Release*, 92 .pp.349.
- [31] PW. Gibson, HL. Schreuder-Gibson, D. Riven . 1999.Electrospun fiber mats: transport properties. *AIChE J* ,45(1).pp.190–195.
- [32] PW. Gibson, HL. Schreuder-Gibson, C. Pentheny. 1998. Electrospinning technology: direct application of tailorable ultrathin membranes. *J. of Coated Fabrics*,28,pp.63.
- [33] PW. Gibson, HL. Schreuder-Gibson, D. Rivin. 2001. Transport properties of porous membranes based on electrospun nanofibers. *Colloids and Surfaces A: Physicochemical and Engineering Aspects*,187,pp.469–481.
- [34] HL. Schreuder-Gibson, PW. Gibson, K Senecal, M. Sennett, J .Walker, W Yeomans, et al. 2002.Protective textile materials based on electrospun nanofibers. *Journal of Advanced Materials*.,34(3),pp.44–55.
- [35] ID Norris, MM Shaker, FK Ko, AG Macdiarmid. 2000.Electrostatic fabrication of ultrafine conducting fibers: polyaniline/polyethylene oxide blends. *Synthetic Metals*,114(2),pp.109–114.
- [36] C.M. Waters, T.J. Noakes, C. I. Pavery . *US patent*,5088807, 1992.
- [37] K.J. Senecal, L. Samuelson, M. Sennett, G.H. Schreuder. *US patent application publication* 0045547, 2001.

- [38] K.J. Senecal, DP. Ziegler, J. He, R. Mosurkal, H. Schreuder-Gibson, LA. 2002. Samuelson Photoelectric response from nanofibrous membranes. *Materials Research Society Symposium Proceedings*, 708.pp.285–9.
- [39] X. Wang, C. Drew, S.H. Lee, K.J. Senecal, J. Kumar, L.A. Samuelson. 2002. Electrospun nanofibrous membranes for highly sensitive optical sensors. *Nano Lett*, 11. pp.1273–1275.
- [40] B. Ding, J.H. Kim, Y. Miyazaki, S.M. Shiratori. 2004. Electrospun nanofibrous membranes coated quartz crystal microbalance as gas sensor for NH₃ detection, *Sens. Actuators B: Chem*, 101 .pp. 373–380.
- [41] P.I. Gouma. 2003. Nanostructured polymorphic oxides for advanced chemosensors. *Rev. Adv. Mater. Sci*, 5 .pp. 147–154.
- [42] K. Sawicka, P. Goum, S Simon. 2005. Electrospun biocomposite nanofibers for urea biosensing. *Sensors and Actuators B*, 108. pp. 585 – 588.
- [43] JM Deitzel, J Kleinmeyer, JK Hirvonen, et al. 2001. Controlled deposition of electrospun poly(ethylene oxide) fibers. *Polymer*,42.pp.8163–8170.
- [44] H Fong, DH. Reneker. 2001. Electrospinning and formation of nanofibers. In: Salem DR, editor. *Structure formation in polymeric fibers*. Munich: Hanser. pp. 225–246.
- [45] K. Fujihara,_, M. Kotak, S. Ramakrishn. 2005. Guided bone regeneration membrane made of polycaprolactone/calcium carbonate composite nano-fibers. *Biomaterials*, 26 .pp.4139– 4147.
- [46] X. Fang, DH. Reneker.1997. DNA fibers by electrospinning. *J. Macromolecular Sci. Phys.*, B36 .pp. 169–173.
- [47] GI. Taylor. 1969. Electrically driven jets. *Proc. R. Soc. London, Ser A* ,313.pp.453–475.
- [48] El-R. Kenawy , G. L. Bowlin , K. Mansfield , J. Layman , D. G. Simpsonc, E. H. Sanders., G. E. Wnek. 2002 . Release of tetracycline hydrochloride from electrospun poly(ethylene-co-vinylacetate), poly(lactic acid), and a blend. *Journal of Controlled Release*, 81 .pp. 57–64.
- [49] S. F. Fennessey, J. R.. Farris. 2004 . Fabrication of aligned and molecularly oriented electrospun polyacrylonitrile nanofibers and the mechanical behavior of their twisted yarns. *Polymer*, 45.pp. 4217– 4225.
- [50] S-H. Tan, R. Inai, M. Kotaki, S. Ramakrishna. 2005. Systematic parameter study for ultra-fine fiber fabrication viaelectrospinning process. *Polymer*, 46 .pp. 6128–6134.
- [51] H. Fong, I. Chun, D.H. Reneker. 1999. Beaded nanofibers formed during electrospinning. *Polymer*, 40 .pp.4585– 4592.
- [52] S. L. Shenoy, W. D. Bates, H. L. Frisch, G. E. Wnek. 2005.Role of chain entanglements on fiber formation during electrospinning of polymer solutions: good solvent, non-specific polymer–polymer interaction limit. *Polymer* ,46 .pp. 3372–3384.
- [53] H Fong, DH Reneker. 1999. Elastomeric nanofibers of styrene-butadiene-styrene triblockcopolymer. *J. Polym. Sci: Part B Polym. Phys.*,37(24).pp.3488–3493.
- [54] S. Kidoaki, K. Kwon, T. Matsuda.2005. Mesoscopic spatial designs of nano- and microfiber meshes fortissue-engineering matrix and scaffold based on newly devised multilayering and mixing electrospinning techniques. *Biomaterials*, 26 .pp. 37–46.
- [55] S.Y. Gu, J. Ren, G.J. Vancso .2005. Process optimization and empirical modeling for electrospun polyacrylonitrile (PAN) nanofiber precursor of carbon nanofibers. *European Polymer Journal*, xxx .pp.xxx–xxx.

-
- [56] CH. Zhang , X. Yuan , L. Wu , Y. Han, Jing Sheng. 2005. Study on morphology of electrospun poly(vinyl alcohol) mats. *European Polymer Journal* ,41 .pp. 423–432.
- [57] X. Geng, O-H. Kwon, J. Jang. 2005. Electrospinning of chitosan dissolved in concentrated acetic acid solution. *Biomaterials*, 26 .pp. 5427–5432.
- [58] A. Koski, K. Yim, S. Shivkumar. 2004. Effect of molecular weight on fibrous PVA produced by electrospinning. *Mater. Lett.*,58.pp.493–497.
- [59] JM Deitzel, J Kleinmeyer, D Harris, T. N. Beck. 2001. The effect of processing variables on the morphology of electrospun nanofibers and textiles. *Polymer*,42.pp.261–272.
- [60] Y. J. Ryu, Hak Yong Kim , K. H. Lee, H. C. Park , D. R. Lee.2003 . Transport properties of electrospun nylon 6 nonwoven mats. *European Polymer Journal* , 39 .pp. 1883–1889.
- [61] B. Kim, H. Park, S-H. Lee, W. M. Sigmund.2005 .Poly(acrylic acid) nanofibers by electrospinning. *Materials Letters* ,59.pp. 829–832.
- [62] T. Jarusuwannapoom , W. Hongrojjanawiwat, S Jitjaicham, L. Wannatong, M. Nithitanakul , C. Pattamaprom , P. Koombhongse , R. Rangkupan , P. Supaphol . 2005. Effect of solvents on electro-spinnability of polystyrene solutions and morphological appearance of resulting electrospun polystyrene fibers. *European Polymer Journal* , 41. pp. 409–421.
- [63] C.J. Buchko, L.C. Chen, Y. Shen, D.C. Martin. 1999. Processing and microstructural characterization of porous biocompatible protein polymer thin films. *Polymer*,40.pp.7397–407.
- [64] X.M. Moa, C.Y. Xub, M. Kotakib, S. Ramakrishna .2004.Electrospun P(LLA-CL) nanofiber: a biomimetic extracellular matrixfor smooth muscle cell and endothelial cell proliferation. *Biomaterials* ,25 .pp. 1883–1890.
- [65] A. F. Spivak and Y. A. Dzenis.1998.Asymptotic decay of radius of a weakly conductive viscous jet in an external electric field. *Appl. Phys. Lett*, 73.pp.3067.
- [66] D.H. Reneker, A.L. Yarin, H. Fong, S. Koombhongse. 2000. Bending instability of electrically charged liquid jets of polymer solutions in electrospinning, *J. Appl. Phys*, 87.pp. 4531–4547.
- [67] M. M. Hohman, M. Shin, G. Rutledge, and M. P. Brenner. 2001 .Electrospinning and electrically forced jets: I. Stability theory. *Phys. Fluids* 13.pp. 2201.
- [68] M. M. Hohman, M. Shin, G. Rutledge, and M. P. Brenner.2001.Electrospinning and electrically forced jets: II. *Applications.Phys. Fluids* 13.pp. 2221.
- [69] D. H. Reneker, A. L. Yarin, H. Fong, and S. Koombhongse. 2000.Bending instability of electrically charged liquid jets of polymer solutions in electrospinning. *J. Appl. Phys*, 87.pp. 4531.
- [70] A. L. Yarin, S. Koombhongse, and D. H. Reneker. 2001. Bending instability in electrospinning of nanofibers. *J. Appl. Phys.*, 89.pp.3018.
- [71] Y. M. Shin, M. M. Hohman, M. P. Brenner, and G. C. Rutledge. 2001. Electrospinning: A whipping fluid jet generates submicron polymer fibers’’ *Appl. Phys. Lett.*,78.pp. 1149.
- [72] J. G. Cook.1964. Handbook of Textile Fibers : I. *Natural Fibers*. Third Edition .Merrow publisher.
- [73] R. R. Franck.2001. *Silk, mohair,cashmere and other luxury fibres*. Woodhead Publishing.

-
- [74] D Kaplan, WW Adams, B Farmer, C Viney, editors. 1994. *Silk polymers: materials science and biotechnology*. Washington DC: ACS Symposium Series, p. 544.
- [75] B-M. Min., L. Jeong., Y.S. Nam., J-M. Kim, J. Y. Kim, W.H. Park .2004. Formation of silk fibroin matrices with different texture and its cellular response to normal human keratinocytes. *International Journal of Biological Macromolecules*, 34,pp.281–288.
- [76] N. Hojo,2000.Structure of Silk Yarn Part A. Biological and Physical Aspects. *Science Publisher* . USA.
- [77] S. Sukigara, M. Gandhi, J. Ayutsede, M. Micklus, F. Ko. 2003 .Regeneration of Bombyx mori silk by electrospinning: part 1:Processing Parameters and Geometric Properties. *Polymer*, 44,pp. 5721–5727.
- [78] S. Sukigara, M Gandhi, J. Ayutsede, M. Micklus, F. Ko. 2004 . Regeneration of Bombyx mori silk by electrospinning.Part 2. Process optimization and empirical modeling using response surface methodology. *Polymer*, 45 .pp. 3701–3708.
- [79] J. Ayutsede, M. Gandhi, S. Sukigara, M. Micklus, H-E. Chen,F. Ko. 2005. Regeneration of Bombyx mori silk by electrospinning. Part 3:characterization of electrospun nonwoven mat. *Polymer*, 46 .pp. 1625–1634.
- [80] E. Entchevaa, H. Biana, L. Yina, C-Y. Chunga, M. Farrella,Y. Kostovc.2004. Functional cardiac cell constructs on cellulose-based scaffolding. *Biomaterials*, 25 .pp. 5753 –5762.
- [81] S. O. Han, W. K. Son, J. H. Youk, T. S. Lee, W. H. Park,2005, Ultrafine porous fibers electrospun from cellulose triacetate. *Materials Letters*, xx .pp. xxx – xxx.
- [82] K. E. Park, S. Y. Jung, S. J. Lee, B-M Min, W. H. Park .2006 . Biomimetic nanofibrous scaffolds: Preparation and characterization of chitin/silk fibroin blend nanofibers. *International Journal of Biological Macromolecules* ,38 .pp. 165–173.

Chapter 11

EXPERIMENTAL STUDY ON APPLICATION OF WASTE RUBBER IN BITUMEN COMPOSITE

*A. K. Haghi**

University of Guilan, P. O. Box 3756, Rasht, Iran

ABSTRACT

This paper presents the result of laboratory tests carried out to study the relative performance of waste tire rubber in asphalt pavement. The result demonstrates that waste tire rubber reinforcement is the most advantageous pavement reinforcement technique for improvement of asphalt fatigue life.

INTRODUCTION

Transport vehicles are increasing in number as well as magnitude, and the use of super tires and different axle configurations is increasing too. The effects of these factors tend towards increased asphalt pavement deterioration, including fatigue, resulting in increased costs to maintain road networks at an adequate level [1-6]. The objective of this study is to evaluate the effects of adding rubber in the characteristics of bitumen composite. The rubbers in this study obtained from wasted tires. The wasted tires were crushed in a special cutting machine designed for this purpose in the laboratory. The size of rubbers in this study were in the ranges of 6-8 mm.

* Haghi@Guilan.ac.ir

EXPERIMENTAL

The aggregate gradation that used in this experimental work is shown in in table 1.

Table 1. Gradation of used aggregate

Percentage Passing	Sieve size mm
100	19
90-100	12.5
--	9.5
44-74	4.75
28-58	2.36
--	1.18
--	0.6
5-21	0.3
--	0.15
2-10	0.075

Table 2. Properties of bitumen used

Purity grade	Lose	Deflagration	Plasticity	Flow	Penetration	Density
	Weight		index		grade	
	(%)	0°C	(Cm)	0°C	mm/10	25°C
99	0.75	262	112	51	66	1.02

Tire Thread Characteristics

The high-modulus tire cords within waste rubber have desirable strength retention properties under long-term exposure to aggressive environment. Properties of this tire threads were shown in table 3.

Table 3. Tire thread properties

Fiber Properties	Nominal	Tenacity	Tenacity	Breaking	Elongation
	Denier			Load	at Break
	Tex	(cN/tex)	(gm/d)	(N)	(%)
Tire thread	1880	85	8	161	22

METHODOLOGY

The Indirect Tensile Stiffness Modulus (ITSM) Test

Samples tested under this experimental work are nominally with 100 mm diameter and 70 mm height for ITSM test. Before determination of stiffness modulus, the resilient modulus of samples were calculated (According to the ASTM D 4123)[7].

RESULT AND DISCUSSION

In Figures 1 and 2 the variation of tensile stress and tensile strain versus number of cycle for failure is shown for different specimens. It is clear that the tensile strain of reinforced samples decreased significantly. This can have positive effects on the fatigue life of specimen used.

From Figure 1 we can observe the variations of tensile stress versus number of cycle before fatigue cracking. As it can be seen obviously, the waste rubber reinforcement can increase the bearing stress significantly. In contrast, the non-reinforced sample experienced less cycles before failure. In view of the above, that reinforced sample can bear more stress than non-reinforced one. That means the waste tire reinforcement can enhance the fatigue life significantly. Meanwhile for certain percentage of bitumen, the fatigue life of reinforced sample is more reliable than normal asphaltic sample. These results are shown in figure 1. It can be concluded that the use of waste tire improved the fatigue life of asphaltic sample significantly.

In Figure 2 we can observe the variations of tensile strain versus number of cycle for failure. As it can be seen, waste tire reinforcement can decrease the tensile strain in contrast to non-reinforced sample. In certain bitumen percent, the tensile strain in reinforced sample is less than the tensile strain in non-reinforced specimen. It can be seen that the number of cycle for failure in reinforced sample is more than non-reinforced sample. Therefore, the reduction in fatigue cracks in reinforced specimen is expected. In samples with 5 and 6 percents of bitumen, the number of cycles for failure is increased significantly. It should be noted that with 5 percent of bitumen the application of waste rubber can cause a better cohesion between aggregates and bitumen. While using 4% bitumen the difference between tensile strain in reinforced specimen and non-reinforced sample is poor. This is because of percent reduction in the bitumen quantity. However, for 5 percent bitumen this difference is noticeable. Although the bitumen percent used is not optimum, therefore, the waste rubber reinforcement, lead to the decrease in tensile strain in contrast to non-reinforced sample. The result has shown in Figure 2.

Based on the results obtained in Figures 1 and 2, the fatigue characteristic among stress bearing and resistance against tensile strain, has been improved.

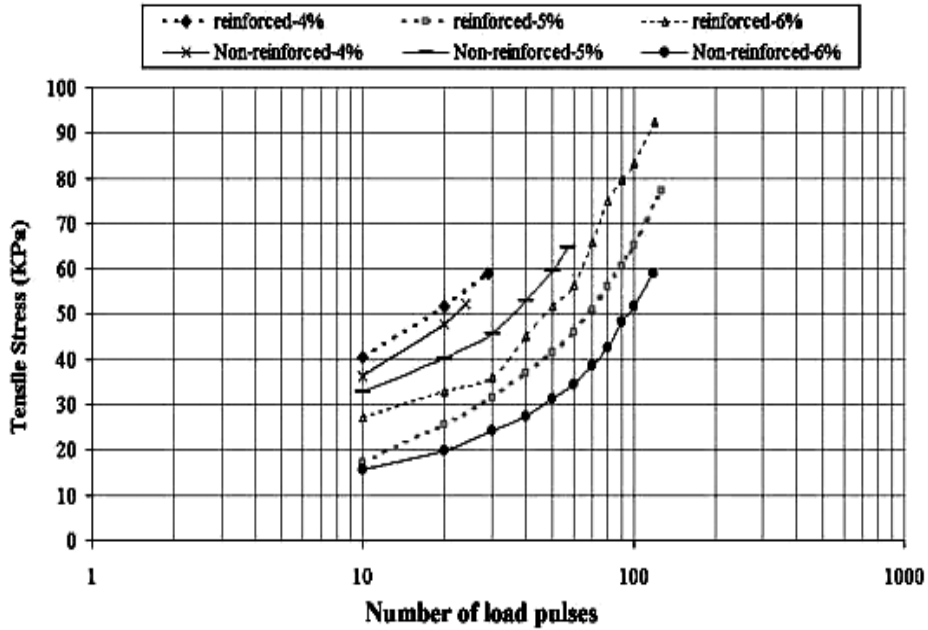


Figure 1. Tensile stress vs. number of load pulse.

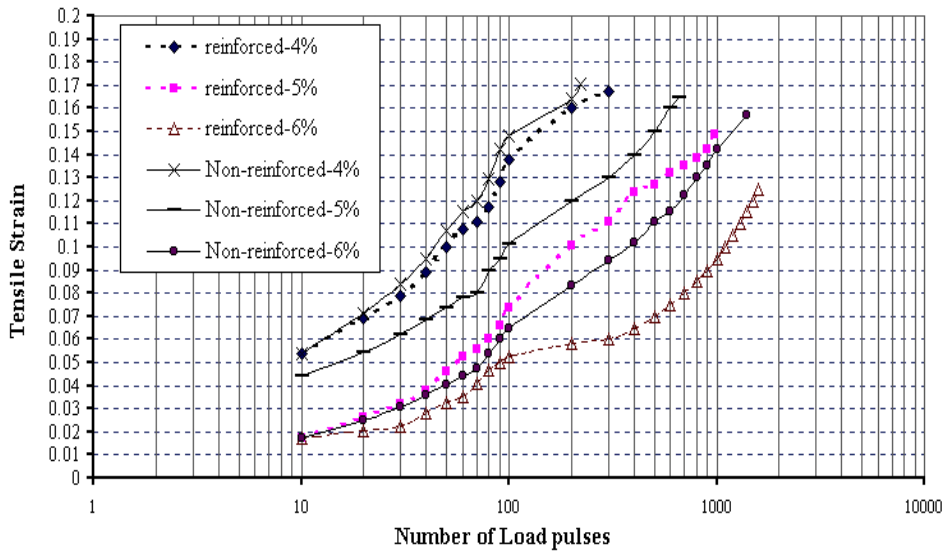


Figure 2. Tensile strain vs. number of load pulse.

Figure 3 indicate the stiffness modulus versus bitumen percent. As it can be seen clearly, the waste rubber reinforcement can improve the stiffness modulus, in contrast to non-reinforced samples. According to the experiments with certain bitumen percent, the value of stiffness modulus in reinforced specimen is more than the value of stiffness modulus in non-reinforced specimen, specially, when bitumen percent increased the cohesion between waste rubber, talus material and bitumen will increase, therefore, difference between stiffness

modulus at 6% bitumen in reinforced specimen and non- reinforced specimen will increase. For example, the difference between stiffness modulus at 6% bitumen in reinforced specimen and non- reinforced specimen is 60%.

In figure 4 we can observe the variations of stiffness modulus versus temperature at 6% bitumen. As it can be seen, the waste rubber reinforcement can cause better characters in asphaltic samples.

The waste rubber reinforcement can increase the stiffness modulus. It is clear that the reinforced sample can show a high stiffness than non-reinforced one.

As the temperature decreased, the cohesion between waste rubber, aggregates, material and bitumen increased. Therefore, by decreasing temperature, the stiffness modulus is decreased as well. Meanwhile, stiffness modulus in temperature of 25°C is more than 40°C. This different between stiffness modulus at 25°C and 40°C is about 53%.

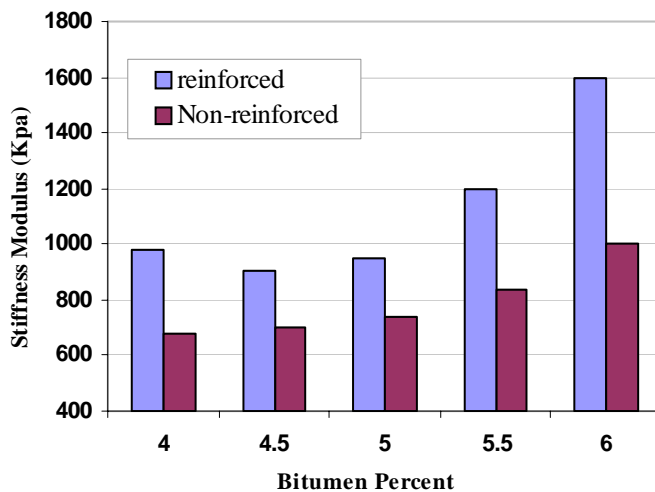


Figure 3. Stiffness modulus vs. bitumen percent.

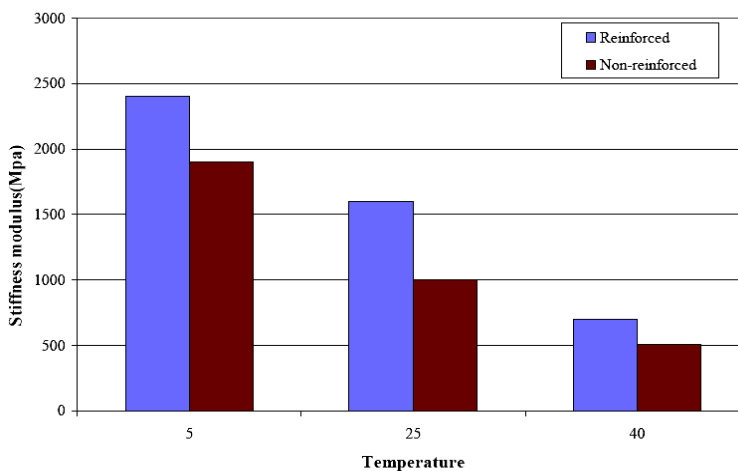


Figure 4. Stiffness modulus vs. temperature.

Figure 5 shows linear regression analysis of the ITFT result. As it can be seen obviously, regressions determine fatigue function for the asphalt mixtures. In figure 9 is shown that reinforced specimen's slope is more than nonreinforced specimens. Away from waste rubber reduction strain in reinforced specimens regression equation for reinforced specimen is $0.4273\varepsilon^{-0.1614}$ and for nonreinforced specimens is $0.2177\varepsilon^{-0.044}$.

In figure 6 we can observe the variations of fatigue life of composite versus stress. As it can be seen obviously, the waste rubber reinforcement can increase the final cycle in contrast to non-reinforced sample. In certain bitumen percent, the final cycle in reinforced sample is more than the final cycle in non-reinforced specimen. While using 4% bitumen the difference between final cycle in reinforced specimen and non-reinforced sample is poor. In samples with 5 and 6 percents of bitumen, the final cycle for failure is increased significantly. For 6 percent bitumen this difference is noticeable. This is because of the bitumen percent used is optimum.

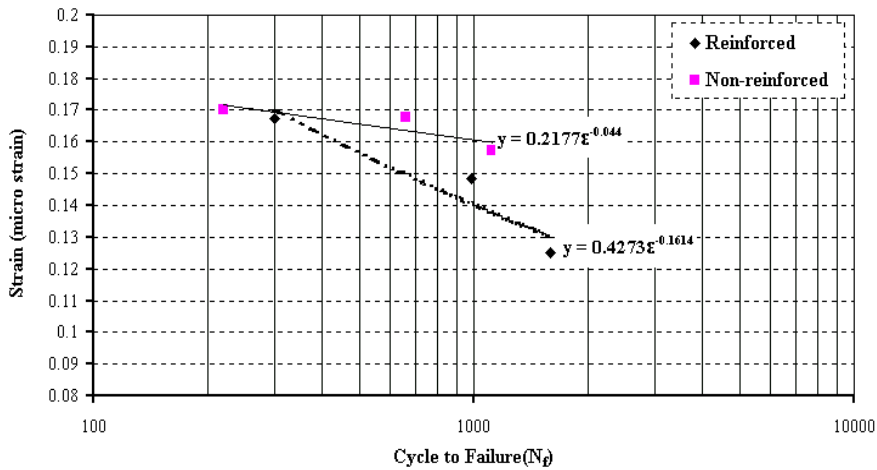


Figure 5. Strain vs. cycle to failure.

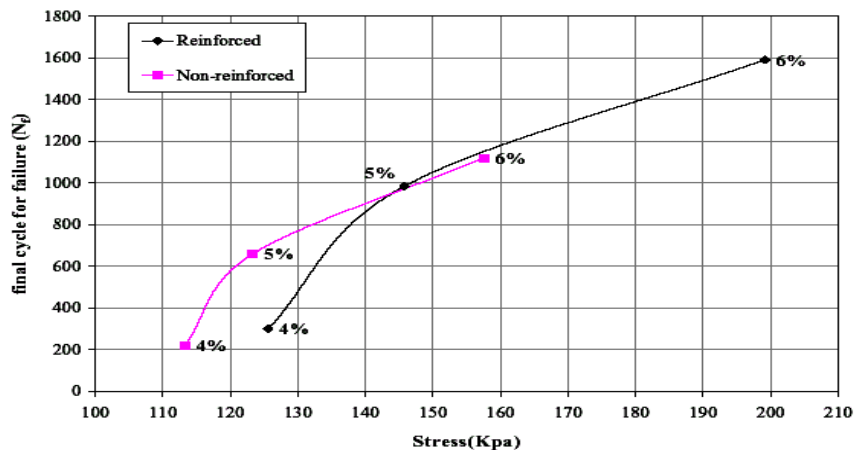


Figure 6. Fatigue life vs. stress.

In Figure 7 we can observe the variations of stiffness of creep at 100 second versus bitumen percent. As it can be seen, the waste rubber reinforcement can increase the stiffness of creep at 100 seconds in any percentage of bitumen. This improvement can be increased by increment in bitumen percent.

In Figure 8 the variation of percent axial strain versus number of seconds. It is clear that percent axial strain of reinforced samples in contrast to non-reinforced decreased significantly. In samples with 4 and 5 percents of bitumen, the difference between percent axial strain in reinforced and non-reinforced specimens is poor. But this difference in reinforced and non-reinforced samples with 6 percent is noticeable. From figure 8 we can observe that percent axial strain in reinforced sample with 6 percent of bitumen is the least.

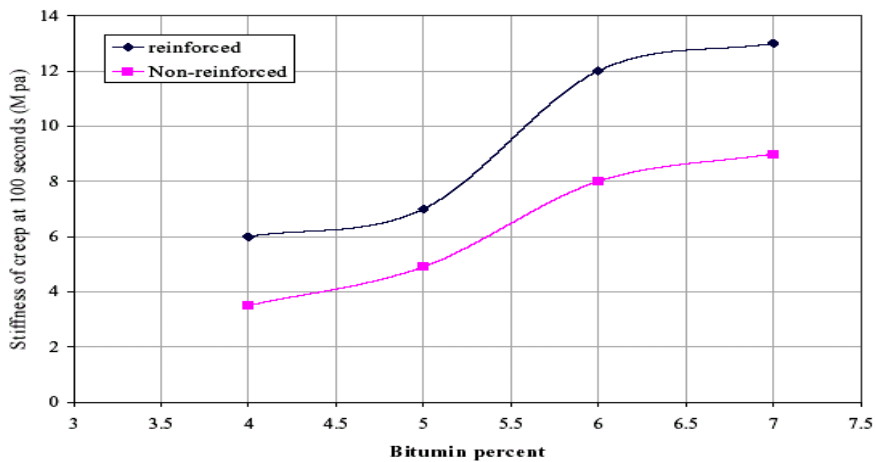


Figure 7. Stiffness of creep at 100 second vs. bitumen percent.

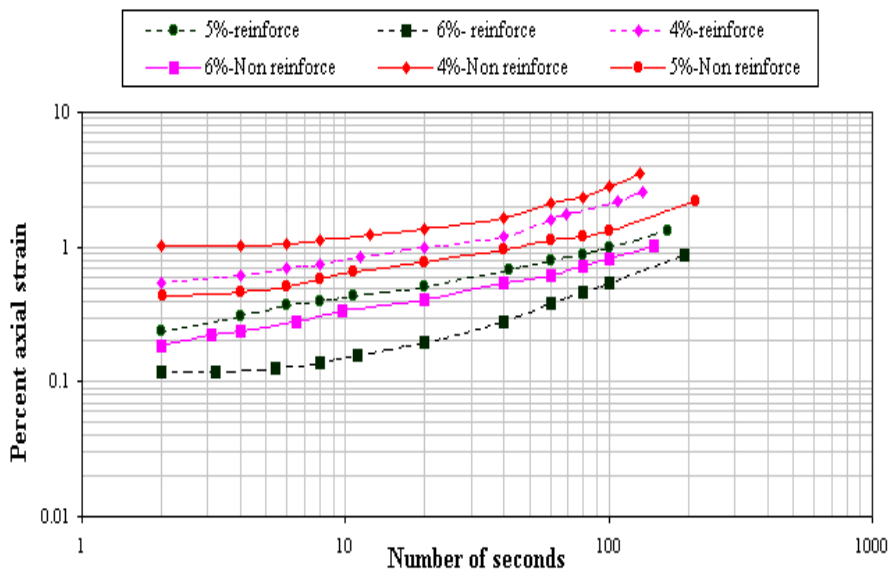


Figure 8. Percent axial strain vs. number of seconds.

According to this experimental work, the waste rubber reinforcement can obviously improved characters of asphaltic samples. As stability , creep tests indicated that reinforcement by waste rubber reduced their permanent deformation significantly, it means that waste rubber provides a strong composite for designing mixes to avert both pavement rutting and low temperature cracking in order to prolong road life.

CONCLUSION

The primary purpose of this project reported herein was to compare the behavior of the reinforced asphaltic sample with the normal asphaltic sample. Via the above test can be earn two important parameters as stiffness modulus and fatigue life in asphaltic specimen. In the Nottingham Asphalt Tester (NAT) system, applying a dynamic compressive load carries out the test and this loading can assist us in better analysis of asphaltic samples behavior. The software of NAT available the conditioning pulse for decreasing the probably error in this test. The five initial pulse of dynamic loading should be used in ITSM test for kept the materials response in the liner visco-elastic (LVE) range. The dynamic loading lead to tow type of deformation. The elastic deformation and the plastic deformation. In the ITFT the vertical deformation of specimen versus number of cycle for failure is determined. The improvement of fatigue character and capability in reinforced asphalt sample due to the fact that the loading surface in reinforced sample is perpendicular on tire cord mesh surface. Because if the loading surface was the parallel to the tire cord mesh surface, the capability of reinforced asphalt sample is increased.

The main conclusions achieved so far are the following:

- The stiffness modulus is a function of load, stress, horizontal deformation, percentage of bitumen and poisson ratio. The Poisson ratio's normally assumed to be 0.35 which is a representative value for most asphalt.
- In both reinforced and normal asphaltic samples, It can be seen that with increasing the bitumen percent , the stiffness modulus is increased but this increasing in reinforced samples is more than normal samples. This topic due to twin effects of bitumen and tire thread mesh.
- In ITFT the tensile strain in reinforced asphaltic samples is less than normal asphaltic samples, also with increasing bitumen percent , this strain is decreased. This topics due to this fact that the percentage of bitumen is optimal.
- In ITFT the capability of bearing the tensile stress in normal asphaltic samples is less than reinforced asphaltic samples, and this capability with increasing of bitumen percent is decreased.

The overall conclusion of this research indicates that the tire cord mesh reinforcement can have a positive effect on fatigue life.

REFERENCES

- [1] Medani. T.O., Molenaar. A.A.A., "*Estimation of Fatigue Characteristics of Asphalt Mixes Using Simple Tests*".
- [2] Markow, M.J., Hedrick, J.K., Brademeyer, B.D., and Abbo, E., "Analyzing the Interactions between Dynamic Vehicle Loads and Highway Pavements". *Transportation Research Record 1196*, TRB, National Research Council, Washington, D.C., pp. 161–169, 1988.
- [3] Finn, F., C. Saraf, R. Kulkarni, K. Nair, W. Smith, and A. Abdullah, "The Use of Distress Prediction Subsystems for the Design of pavement Structures", In Proc., 4th International Conference on the Structural Design of Asphalt Pavements, *Ann Arbor, Mich.*, Vol.1, 1977.
- [4] Shell Pavement Design Manual, "*Asphalt Pavement and Overlays for Road Traffic*", Shell International Petroleum Co. Ltd., London, U.K., 1978.
- [5] Shook, J.F., F. N. Finn, M. W. Witzak, and C. L. Monismith, "Thickness Design of Asphalt Pavements", The Asphalt Institute Method , In Proc., *5th International Conference on the Structural Design of Asphalt Pavements*, Delft, The Netherlands, Vol. 1, 1982, pp. 17-44.
- [6] Jucob.U. "Evaluation of fatigue cracking", *Transportation Research Record*, No.1570, 1998.
- [7] Annual Book of ASTM Standard, Road and Paving Materials; Vehicle- Pavement system, "*Standard Test Method for Indirect Tension Test for Resilient Modulus of Bituminous Mixtures*", D 4123-82, 2002.

Chapter 12

THERMODYNAMICS OF OSMOTIC PRESSURE OF POLYMERIC SOLUTIONS

Yu. G. Medvedevskikh¹, L. I. Bazylyak¹ and G. E. Zaikov²

¹Physical Chemistry of Combustible Minerals Department

L. M. Lytvynenko Institute of Physical–Organic Chemistry and Carbon Chemistry
National Academy of Sciences of Ukraine

²N. Emmanuel Institute of Biochemical Physics

Russian Academy of Sciences, 4 Kosygin Str., 117977, Moscow, RUSSIA

ABSTRACT

It was proposed the analysis of osmotic pressure for diluted, semi–diluted and concentrated polymeric solutions based on the taking into account a free energy of macromolecules conformation as a component of their chemical potential. It was shown, that only into diluted solutions a free energy of macromolecules conformation does not contribute into osmotic pressure and it is described by Vant–Goff’s equation. In a case of semi–diluted and concentrated solutions the contribution of the conformational component of chemical potential of macromolecules into osmotic pressure is dominant. Obtained expressions for the osmotic pressure in a case of semi–diluted and concentrated solutions are more general than proposed ones in the scaling method and self–consistent field method; generally they are in good agreement with the experimental data and don’t contain the empirical constants. It was discussed the special role of the critical concentration c^* of the polymeric chains intertwining. It was shown, that in this point a free energy of the conformation and also osmotic pressure were determined uniquely, whereas for their derivatives upon the macromolecules concentrations the jump is observed. On the basis of these peculiarities the concentration c^* is the critical point of the second order phase transition for the polymeric solutions. This in accordance with the de Gennes’ scaling theory application near c^* , although does not establish the criteria for the indexes of corresponding power functions estimation.

* E–mail: vfh@org.lviv.net

Keywords: *osmotic pressure, polymeric solutions, free energy of conformation.*

1. INTRODUCTION

Osmose plays an essential role in a wide technological and especially in biological systems represented by solutions of biopolymers. That is why understandable is interest of scientists to the problem of osmotic pressure of polymeric solutions which permits comparatively easy experimentally to determine the advantages and deficiencies of theoretical imaginations about thermodynamical properties of polymeric solutions.

Two main approaches for osmotic pressure of polymeric solutions theoretical description can be distinguished. First is *Flory–Huggins* method [1, 2], which afterwards has been determined as method of self-consistent field. In the initial variant the main attention has been paid into pair-wise interaction in the system “gaped monomeric links – molecules of solvent”. *Flory–Huggins* parameter χ was a measure of above-said pair-wise interaction and this limited application of presented method by field of concentrated solutions. In subsequent variants such method was extended on individual macromolecules into diluted solutions with taken into account the tie-up of chain links by *Gaussian* statistics [1].

For description of the osmotic pressure π of polymeric solutions the virial decomposition is used in the *Flory–Huggins* method

$$\pi = RT \frac{c}{N} \left(1 + A \frac{c}{N} \right) \quad (1)$$

in which c is the molar–volumetric concentration of monomeric links; N is the polymerization degree or length of a chain; A is the second virial coefficient which is the main object of analysis of multiple following variants of *Flory–Huggins* method.

It was discovered, that the expression (1) for the description of π into diluted and semi-diluted solutions required of different values of virial coefficient A . In particular, for the estimation of A in a field of diluted solutions it would be better to accept the whole conformation volume of macromolecule as excluded volume, that is R_F^3 , and in the field of semi-diluted solutions – the value $a^3(1 - d\chi)$ [3] where a is a length of a chain link and

$$R_f = aN^\nu \quad (2)$$

is the conformation radius of *Flory* ball with the index $\nu = 1/2$ or $3/5$.

Further development of the *Flory–Huggins* method in direction of taking into account the effects of far interaction, swelling of polymeric ball in “good” solvents [4, 5], difference of free volumes of polymer and solvent [6, 7] led to complication of expression for virial coefficient A and to growth of number of parameters needed for its numerical estimation, but weakly reflected on the possibility of equation (1) to describe the osmotic pressure of polymeric solutions in a wide range of concentrations.

It was admitted that the best variant for the diluted solutions is the *Vant–Goff* equation

$$\frac{\pi}{RT} = \frac{c}{N} \quad (3)$$

and for semi-diluted solutions – *Fixman* equation [8] or *Yamakawa* equation [9] differing only by the sense of virial coefficient B

$$\frac{\pi}{RT} = \frac{c}{N} \left[1 + B \left(\frac{c}{c^*} \right) \right] \quad (4)$$

here $c^* = N / N_A R_F^3$ is critical concentration of monomeric links corresponding to the start of the polymeric balls intertwining.

From the point of view [3, 10] the main deficiency of the self-consistent field method is fact, that it does not take into account the fluctuative properties of the polymeric solutions and correlations appearing due to the difference of the energies of pair-wise interaction into system monomeric links – solvent tie-up of links into chain. It is considered that these deficiencies somehow are eliminated by *Scaling* method [3] which is based on the principle of scaled invariance of polymeric solution properties as function of some characteristic parameters, for example length of chain N , relative concentration c/c^* and conformation radius R_F of *Flory* ball. Ideology of method conformably to polymer solutions was appeared from the assumption about the analogy of fluctuative behaviour of polymeric chains in semi-diluted solutions and magnetic in external field near the point of change of phase [11].

Analysis of osmotic pressure of semi-diluted polymeric solutions by *Scaling* method is based [3] on two positions. Accordingly to the first one it is assumed that the polymeric chain is in “good” solvent for which $\chi < 1/2$. This position is necessary in order to index ν in the expression (2) will be determined by the ratio

$$\nu = \frac{3}{(d+2)} \quad (5)$$

which is correct for swelling ball and gives the value $\nu = 3/5$, but not $\nu = 1/2$ for $d = 3$ -measured space.

The second position assumes that in semi-diluted solutions the polymeric chains are as much strong intertwined that the all thermodynamic values, in particular the osmotic pressure, achieve the limit (at $N \rightarrow \infty$) depending only on the concentration of monomeric links, but not on the chain length.

The following expression is initial for the determination of osmotic pressure of semi-diluted polymeric solutions accordingly to *Scaling* method:

$$\frac{\pi}{RT} = \frac{c}{N} f \left(\frac{c}{c^*} \right) \quad (6)$$

in which the dimensionless function $f(c/c^*)$ has two asymptotics. It is assumed for the diluted solution ($c/c^* \ll 1$), that $f(c/c^*) = 1$ or $f(c/c^*) = 1 + \text{const}(c/c^*)$, that leads respectively to the expressions (3) or (4).

Power law depentanizer $f(c/c^*) = \text{const}(c/c^*)^m$ is postulated for the semi-diluted solution ($c/c^* \gg 1$), in which the unknown index m accordingly to the second position of the *Scaling* method is from independence π on the length of a chain. This leads to the value $m = 1/(3\nu - 1)$, that is $m = 4/5$ for $d = 3$ -dimensional space. That is why the expression (6) is as follow

$$\frac{\pi}{RT} = \text{const} \cdot c^{9/4} \quad (7)$$

or, assuming $\varphi = a^3 c$ as volumetric part of polymer into solution

$$\frac{\pi}{RT} = \text{const}' \cdot \varphi^{9/4} \quad (8)$$

From the point of view [3] the experiments [12] confirm the correctness of the expression (8).

However, let note, that the assumption about independence of the osmotic pressure of semi-diluted solutions on the length of a chain is not physically definitely well-founded; per se it is equivalent to position that the system of strongly intertwined chains is thermodynamically equivalent to the system of gaped monomeric links of the same concentration. Therefore, both *Flory-Huggins* method and *Scaling* method do not take into account the conformation constituent of free energy of polymeric chains.

In presented work the analysis of osmotic pressure of the polymeric solutions has been done with taken into account the thermodynamics of conformation state of macromolecules following from the self-avoiding random walks statistics [13, 14].

II. STARTING POSITIONS

The following expression is stringent thermodynamical determination of the osmotic pressure

$$\pi = - \int_{\mu_s^0}^{\mu_s} d\mu_s / v_s \quad (9)$$

in which μ_s^0 and μ_s are chemical potentials of the solvent into standard and defined state respectively and v_s its partial-molar volume.

It follows from the *Gibbs-Durham* equation for two-component solution containing n_s moles of the solvent and n moles of macromolecules

$$d\mu_s = -\frac{n}{n_s} d\mu \quad (10)$$

where μ is the chemical potential of the macromolecules.

Since the polymeric chains unlike to the common molecules possess by free energy of the conformation F (or by negative entropy of conformation which is a measure of polymeric chains self-organization [13]), it should be included as an additional term in usual determination of chemical potential of component of the solution. Hence, we have for the macromolecules

$$\mu = \mu^0 + RT \ln \gamma c + F \quad (11)$$

here μ^0 is standard chemical potential of macromolecules; γ is an activity coefficient or coefficient of proportionality between the thermodynamic activity of macromolecules and their molar-volumetric concentration c .

Generally, the activity coefficient γ depends on the composition of solution. In the ranges of our narrow purposes of investigations of the macromolecules chemical potential conformation term influence on the osmotic pressure of polymeric solutions we will be neglect by the change of γ lying $\gamma \cong const$ in all range of the macromolecules concentrations into solution. This permits to write

$$d\mu = RT d \ln c + dF \quad (12)$$

Expressions (9) – (12) are initial for analysis of osmotic pressure of macromolecules solution into further presented partial variants.

III. DILUTED SOLUTIONS

Let determine the diluted solutions by two conditions

$$c \leq c^*, \quad (13)$$

$$n_s v_s \cong V \quad (14)$$

Here

$$c^* = 1 / N_A R_F^3 \quad (15)$$

is critical molar-volumetric concentration of macromolecules into solution corresponding to the start of polymeric chains conformation volumes intertwining; V is general volume of the solution.

Accordingly to [13] the conformation radius R_F of non-deformed *Flory* ball is described by the expressions (2) and (5) at $d = 3$. This dimensionality of real space will be kept further.

Free energy F of the conformation in calculation per one mole of macromolecules in general case of diluted solution is equal to [13]

$$F = \frac{5}{2} RTN^{1/5} / \lambda_v \quad (16)$$

Here $\lambda_v \leq 1$ is multiplicity of volumetric deformation of *Flory* ball. In diluted solutions this multiplicity is function only on the length of a chain and distinction of free energies of the states S_1 and S_2 of two neighbour monomeric chains. That is why in diluted solutions

$$dF = 0 \quad (17)$$

It follows that, the determination (9) takes the standard for the diluted solutions form

$$\pi = RT \int_0^c \frac{n}{V} d \ln c \quad (18)$$

that result ($n/V = c$) in the *Vant-Goff* equation

$$\pi = RTc \quad (19)$$

Hence, in the field of diluted both ideal ($\lambda_v = 1$) and real ($\lambda_v < 1$) solutions ($c \leq c^*$) the conformation component of the chemical potential of the macromolecules has not an influence on the osmotic pressure, and it is described by *Vant-Goff* equation.

IV. SEMI-DILUTED SOLUTIONS

In the given presented case the semi-diluted polymeric solutions determined by the conditions

$$c \geq c^* \quad (20)$$

$$n_s v_s \cong V \quad (21)$$

The last means that the volumetric part of macromolecules in solution is sufficiently little.

As it follows from [14] in the field of the chains intertwining the molar free energy of the conformation is linear function of relative concentration of macromolecules and is described by the following expression in approximation by deformation of m -ball in real solution

$$F = \frac{5}{2} RTN^{1/5} \left(\frac{c}{c^*} \right) \quad (22)$$

It follows that

$$dF = \frac{5}{2} RTN^{1/5} d \frac{c}{c^*} \quad (23)$$

With taken into account (10), (12), (21) and (23) the determination (9) for osmotic pressure assumes the form

$$\pi = RT \left[\int_0^c \frac{n}{V} d \ln c + \frac{5}{2} N^{1/5} \int_{c^*}^c \frac{n}{V} d \frac{c}{c^*} \right] \quad (24)$$

We will obtain after the integration

$$\pi = RTc \left[1 + \frac{5}{4} N^{1/5} \left(\frac{c}{c^*} - \frac{c^*}{c} \right) \right] c \geq c^* \quad (25)$$

The expression (25) is similar to the expression (4) but has more general character: it gives clear and simple determination of virial coefficient B and automatically is transferred into *Vant-Goff* equation accordingly to condition $c = c^*$.

The second term into square brackets (25) points out the relative contribution of the macromolecules conformation free energy into the osmotic pressure. This term is sufficiently significant: even at $c/c^* - c^*/c \approx 1$ and $N^{1/5} = 4$ its part exceeds 80 %. With the c/c^* and N increasing this contribution becomes dominant.

Accordingly to (19) the osmotic compressibility $\partial\pi/\partial c$ into diluted solutions does not depend on the concentration of macromolecules ($\partial\pi/\partial c = RT$); on the contrary, in semi-diluted solutions it becomes (as it follows from (25)) as linear function of relative concentration:

$$\partial\pi/\partial c = RT \left(1 + \frac{5}{2} N^{1/5} \frac{c}{c^*} \right) \quad (26)$$

V. CONCENTRATED SOLUTIONS

Let determine the concentrated polymeric solutions by the conditions

$$c \gg c^* \quad (27)$$

$$n_s v_s < V \quad (28)$$

that assumes a great volumetric concentration of macromolecules into solution.

Introducing the volumetric part φ of macromolecules into solution by the ratio

$$\varphi = v c \quad (29)$$

in which v is partial-molar volume of macromolecules. Attributive expression (9) with taken into account (10), (12) and (23) results in expression (30) by changing the $c = \varphi / v$, $c^* = \varphi^* / v$, $n_s v_s = V(1 - \varphi)$:

$$\pi = RT \frac{c}{N} \left(1 + A \frac{c}{N} \right) \quad (1)$$

$$\pi = RT \left[\int_0^{\varphi} \frac{d\varphi}{v(1-\varphi)} + \frac{5}{2} \frac{N^{1/5}}{\varphi^*} \int_{\varphi^*}^{\varphi} \frac{\varphi d\varphi}{v(1-\varphi)} \right] \quad (30)$$

In general case \bar{v} is complicated and independent function on solution composition. However, in narrow purposes of investigations the influence of macromolecules chemical potential conformation component on osmotic pressure we use the approximation $v = const$. Then after the integration of (30) we will obtain

$$\pi = -\frac{RT}{v} \left[\ln(1-\varphi) + \frac{5}{2} \frac{N^{1/5}}{\varphi^*} \left(\ln \frac{1-\varphi}{1-\varphi^*} + \varphi - \varphi^* \right) \right] \quad \varphi > \varphi^* \quad (31)$$

It follows that the osmotic compressibility $\partial \pi / \partial c = v \partial \pi / \partial \varphi$ will be equal to

$$\frac{\partial \pi}{\partial c} = \frac{RT}{1-\varphi} \left(1 + \frac{5}{2} N^{1/5} \frac{\varphi}{\varphi^*} \right), \quad \varphi > \varphi^* \quad (32)$$

Expressions (31) and (32) are more general than the previous ones (25) and (26) and easy transform in them accordingly to condition $\varphi^* \leq \varphi \ll 1$.

Taking into account, that φ^* is near to $N^{-4/5}$ upon order of value, we can assume, that $N^{1/5} / \varphi^* \gg 1$. Therefore, under condition $\varphi \gg \varphi^*$ for concentrated solutions the first additives in (31) and (32) can be neglected and we can obtain

$$\pi = -\frac{5}{2} \frac{RT}{v} \frac{N^{1/5}}{\varphi^*} [\ln(1-\varphi) + \varphi] \quad (33)$$

$$\frac{\partial \pi}{\partial c} = \frac{5}{2} RT \frac{N^{1/5}}{\varphi^*} \frac{\varphi}{1-\varphi} \quad (34)$$

This means, that in concentrated solutions π and $\partial \pi / \partial c$ is wholly determined by the conformation component of chemical potential of macromolecules.

Let write other form (33) assigning the condition $\varphi^* \leq \varphi \ll 1$. Then factorizing $\ln(1-\varphi)$ in exponential series we will obtain

$$\pi = \frac{5}{2} \frac{RT}{v} \frac{N^{1/5}}{\varphi^*} \left(\frac{\varphi^2}{2} + \frac{\varphi^3}{3} + \dots \right) \quad (35)$$

As we can see, the eq. (35) is analogue of the scaling expression (8) at evident determination of $const'$ in the last one.

In that way, the thermodynamic approach with the use of conformational term of chemical potential of macromolecules permitted to obtain the expressions for osmotic pressure of semi-diluted and concentrated solutions in more general form than proposed ones in the methods of self-consistent field and scaling. It was shown, that only the osmotic pressure of semi-diluted solutions does not depend on free energy of the macromolecules conformation whereas the contribution of the last one into the osmotic pressure of semi-diluted and concentrated solutions is prelevant.

VI. CONCLUSION

Let draw attention on the dependence of the osmotic pressure on the length of a chain. If formally to lay that $v = v_m N$, where v_m is a partial-molar volume of the chain's links, then we will obtain $\varphi^* = (v_m / N_A a^3) N^{-4/5}$. Therefore, the expression (33) can be written in the form

$$\pi = -\frac{5}{2} \frac{RT}{v_m} \frac{N_A a^3}{v_m} [\ln(1-\varphi) + \varphi] \quad (36)$$

which shows the independence of π on N in obvious elevation.

However, for this it was necessary to turn into the parameter v_m of the chain's links, to their tie-up, and the concentration of polymer to express by volumetric part, which is general for the macromolecules and their links. The contrary situation can be observed into diluted solutions: at using the molar-volumetric concentration of *links*, the *Vant-Goff* equation in the form (3) indicates on the dependence of π on N , whereas at using the molar-volumetric concentration of *macromolecules* the same *Vant-Goff* equation in the form (19), on the contrary, indicates on the independence of π on N . Since the macromolecule (but not its

links) is a component of the solution, from the thermodynamic point of view, the expression (19) is more correct form of the *Vant–Goff* equation writing.

Under this connection let mark that the position about an independence of the osmotic pressure of polymeric solutions into concentrated field of the strongly intertwined chains used in the scaling method is successful upon the result (8) in the presented concrete case, but can not be by general principle spreading on the all thermodynamic visualizations of polymeric solutions. For instance, free energy of the macromolecules conformation accordingly to (22) is function not only on the concentration, but also on the length of a chain at any choice of the method for the concentration expression.

That fact the scaling method and presented thermodynamic approach from seeming opposite positions lead to practically the same result in the form (8) and (35) can be named as “*mysterious incident*” if it were not two circumstances. First is exactly free energy of the conformation makes the main contribution into the osmotic pressure of the semi–diluted and concentrated solutions. The second is the peculiarity of the point $c = c^*$.

As we can see from the expressions (19) and (25), the osmotic pressure of the solution in the point $c = c^*$ has the same value $\pi = RTc^*$ independently on the move $c \rightarrow c^*$ from below ($c^* > c \rightarrow c^*$) or from above ($c^* < c \rightarrow c^*$). On the contrary, the osmotic compressibility in the point $c = c^*$ has two values: first is $\partial\pi/\partial c = RT$ at approach zone $c \rightarrow c^*$ from below, the second accordingly to (26) $\partial\pi/\partial c = RT\left(1 + \frac{5}{2}N^{1/5}\right)$ at approach zone $c \rightarrow c^*$ from above.

The reason of this is the analogous behaviour of free energy of the conformation F and its derivative $\partial F/\partial c$. In accordance with the (16) and (22) in the point $c = c^*$ the value $F = \frac{5}{2}RTN^{1/5}$ is uniquely independently on a fact from which side to approach into c^* . On the contrary, the derivative $\partial F/\partial c$ in the point $c = c^*$ has two values: first is $\partial F/\partial c = 0$ at move $c \rightarrow c^*$ from below, the second is $\partial F/\partial c = \frac{5}{2}RTN^{1/5}/c^*$ at move $c \rightarrow c^*$ from above. Hence, in the point $c = c^*$ the derivative $\partial F/\partial c$ has a jump, consequence of which is also the jump of $\partial\pi/\partial c$.

Since free energy of the conformation $F = -TS$, where S is the entropy of the conformation, it follows, that at given external parameters P and T neither free energy of conformation F nor it's the first derivative upon temperature S do not change in the point $c = c^*$, testifying only the hump; but their derivatives upon the concentration test the jump.

On the basis of these features the point $c = c^*$ is the critical one for the change of phase of the second kind for polymeric solutions. In view of this, the analogy between the magnetic behaviour near the critical temperature of the change of phase and polymeric solution behaviour near the critical concentration $c = c^*$ of the change of phase noting by *Des Cloizeaux* [11] permits to use the scaling correlations, however does not determine the criteria of the corresponding power functions [15] indexes estimation.

REFERENCES

- [1] Flory P. J. *Principles of Polymer Chemistry* // New York: Cornell Univ. Press, 1953, 594 p.
- [2] Huggins M. L. *Physical Chemistry of Polymers* // New York: Interscience, 1958, 175 p.
- [3] De Gennes *Scaling ideas in Physics of Polymers* // Moscow: Myr, 1982, 368 p.
- [4] Zimm B. H., Stockmayer W. H., Fixman M. Excluded Volume in Polymer Chains // *J. Chem. Phys.*, 1953, 21 (10), p. 1716–1723.
- [5] Zimm B. H., Stockmayer W. H. Dimensions of Chain Molecules Containing Branches and Rings // *J. Chem. Phys.*, 1949, 17 (3), p. 1301–1314.
- [6] Prigogine I. *The Molecular Theory of Solutions* // New York: Interscience, 1959, 479 p.
- [7] Patterson D. Role of Free Volume Changes in Polymer Solutions Thermodynamics // *J. Polym. Sci. C*, 1968, 16, p. 3379–3389.
- [8] Fixman M. // *J. Chem. Phys.*, 1960, 33 (2), p. 370–381.
- [9] Yamakawa H. // *J. Chem. Phys.*, 1965, 43 (4), p. 1334–1344.
- [10] Grossberg A. Yu., Khokhlov A. R. *Statistical Physics of Macromolecules* // Moscow: Nauka, 1989, 344 p.
- [11] Des Cloizeaux // *J. Phys. (France)*, 1976, 37 (5), p. 431–434.
- [12] Okano K., Wada E., Taru Y., Hiramatsu H. // *Rep. Prog. Polym. Sci. Japan*, 17, 141 (1974).
- [13] Medvedevskikh Yu. G. // *Condensed Matter Physics*, 2001, v. 4, № 2 (26), p. p. 209, 219.
- [14] Medvedevskikh Yu. G. *Conformation and deformation of linear macromolecules in concentrated solutions and melts in the self-avoiding random walks statistics (see paper in presented book)*.
- [15] Marck N. H., Parrinello M. *Collective Effects in Solids and Liquids* // Adam Hilder Ltd, Bristol, 1982.

Chapter 13

EXPERIMENTAL SURVEY ON A POLYMERIC STABILIZER MATERIAL

A. K. Haghi*

The University of Guilan, P. O. Box 3756, Rasht, Iran

ABSTRACT

While lime is most commonly used as stabilizing agent for clayey sands but this stability can be significantly improved with composition of lime/ polyamide 66 strips. Lime reacts chemically with fine grained material through a process termed cation exchange. The lime creates a surplus of Ca^{++} cations which tend to replace monovalent cation. This cation exchange process results in the clayey sand becoming much less susceptible to moisture (*i.e.* more stable in terms of volume change). Polyamide 66 does not react chemically with the composite materials being stabilized but increase the sand particles reinforcement. Hence, two broad areas of stabilization mechanisms are presented in this work; chemical and mechanical stabilization clayey sand composite. Polyamide 66 is an engineering plastic being used with distinguished role on this category of polymers due to its high chemical and mechanical resistance. In this paper, the mechanisms involved in sand stabilization, the methodologies applied, the evaluation criteria, and the resulting data have been appraised and interpreted.

INTRODUCTION

Polyamide-66 (PA66) is a semi-crystalline polymer (poly(hexamethylene adipamide)) synthesized by the polycondensation of diamine and diacid. The numbers "66" indicate how many ($—CH_2—$) units occur in the diacid and the diamine groups. Polyamide (PA) is a well-known material with different commercial names, e.g. Nylon[™] by DuPont, Stanyl[™] by DSM, etc. Polyamides are complex engineering polymers used for a wide range of industrial applications in bulk and fibrous forms. PA66 fibers are used in the moorings of ships, in

* Haghi@Guilan.ac.ir

ropes, straps, belting and as tire reinforcement. This indicates the high strength capability of these types of fibers in aggressive environment and no changes in their physical and mechanical characteristics is expected with respect to time. Because highway and airport pavement layers are subjected to a complex interaction of loading, the design process involves many variables, which are difficult to quantify. Although a great deal of pavement research has been conducted through the years, a direct mathematical solution capable of determining required pavement layer thickness and material types has not achieved. For this reason, pavement design procedures contain assumptions and simplifications that allow the engineer to design a pavement layer with reasonable confidence that it will perform adequately for its design life. Hence, the theory and design criteria need to be periodically reviewed and modified as necessary to correct deficiencies. Based on the recent studies reported by A. A. Kadi *et al* [1] Optimum design is, however, required for the desired properties to be obtained.

Meanwhile, based on another study reported by A. B. Moustafa *et al* [2], sandy, silty, loamy, clayey, and sandy-loamy soils were impregnated with three types of binding materials, namely, urea formaldehyde, phenol formaldehyde, and sodium silicate. Ammonium chloride, hexamethylene tetramine, and sodium fluorosilicate were used as catalysts for the previously mentioned substances, respectively. Some physico-mechanical tests were carried out with the stabilized soils and different parameters affecting the strength, absorption and durability of stabilized soils were studied [3].

There are a number of specialized stabilizers for which there is little technical information or test data. These stabilizers are sold under trade names. These products are only useful in stabilizing fine-grained soils [4].

The aim of this work is to study the effect of polyamide strips on engineering properties of lime stabilized clayey sands.

Polymeric stabilizer materials are a subset of a much larger recent development in civil engineering. ASTM has defined a geosynthetic as a planar product manufactured from polymeric materials used with soil, rock, or other geotechnical-related material as part of a civil engineering system. A geotextile is a permeable geosynthetic made of textile materials.

BACKGROUND

Plastics, invented towards the end of 18 century and after the World War II, used as alternative to natural sources and materials, has become an indispensable part of human life. The use of plastics is increasing due to their easy formability, light weight and resistance to various chemical materials. Polyamide composite materials have received much interest for highway and airport applications over the last century. Among the available thermoplastic polymers, polyamide (PA) is considered a good candidate as thermoplastic composite matrix, mainly due to its low cost and easy handling. Typically, PA 66 absorbs 4-5% moisture. The migration of moisture uniquely optimized by PA 66 strengthens the mixture in the contact zone of the fiber, potentially at a much higher level than polypropylene-based fiber, which is hydrophobic. This theorized strength gain at the interface of PA 66 and mixture could then increase the bond between the two materials. This potential increase in mechanical bond can be verified by reported results from various tests[5]. PA 66 strips can provides an isotropic

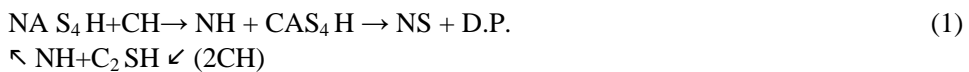
reinforcement that proactively inhibits cracking and adds long-term durability [6]. PA 66 is the strongest aliphatic nylon, and offers good abrasion resistance when compared to PA 6. Better low temperature toughness than Acetal, PBT, or PA 6 and has good fatigue resistance.

In recent years polymer geotextiles have been proposed to improve the performance of paved and unpaved roadways and to reduce base course thickness. Existing literature shows that laboratory and analytical studies performed in the past have shown promising results, however, conflicting and sometimes inconclusive results have been reported with regards the degree of improvement provided by polymer geotextiles. One of the principal application of polymer geotextiles in road pavements has been as a separator between the base course or subbase and subgrade. The main purpose of the granular base is to dissipate the stress imposed by vehicles on the underlying soil to a safe level and thereby control the life of the pavement. At the absence of a polymer geotextile, intermixing of the base and subgrade (base contamination) may occur under the influence of traffic loading due to the pumping of fines from the subgrade into the base course. The intermixing between two dissimilar material causes a net reduction of base course thickness and weakening of that layer [1].

Lime, as a stabilizing agent, is used in various forms and purity. The Most commonly used types are hydrated high-calcium lime, hydrated dolomitic lime, quicklime, and dolomitic quicklime. The availability of calcium from these stabilizers varies due to their composition and solubility. In order to properly stabilize a clayey sand, they should be able to offer an adequate supply of calcium. In the presence of magnesium (dolomitic lime), the calcium availability for unit weight is reduced and, thereby, should be compensated by a higher dosage. As magnesium is high in pH conditions forms $Mg(OH)_2$, the likelihood of magnesium participating in clayey sand stabilization process is low. As the inherent characteristics of clayey sand to be stabilized are virtually fixed, the amount of stabilizer necessary to achieve a desired level of stabilization becomes the primary parameter.

Admixes to the soil in stabilization process compound with the minerals and soil grains, and may lead to generation of new chemical mix with different properties in comparison with the primary properties of soil. Lime as an ordinary stabilizer compounds with soil in the form of quick-lime (CaO) or hydrated lime (Ca(OH)₂) can improve soil physical properties [7].

It should be noted that lime reacts with clay particles. This leads to strength increase by pozzolanic and carbonation cementation processes. Cation exchange and pozzolanic reactions result in strength increase. The level of reactivity and hence strength gained in soil-lime mixtures depends on the level of pozzolanic product created. The chemical reaction between soil and lime can be presented as below:



where:

- S= SiO₂
- H= H₂O
- A= Al₂O₃
- C= CaO
- N= Na₂O

D. P. = Degradation Product: Silicate is gradually reacted and consumed where calsum-aluminate and alumina are provided. The PA 66 fibers used in this study obtained from LG Company have desirable strength retention properties under long-term exposure to aggressive environment (e.g., seawater, alkalis, and acids). These fibers have reasonable thermal stability, retaining a high percentage of room temperature properties at elevated temperature. Their creep properties compare favorably with those of other organic fibers (Table 1). These fibers can be incorporated in clayey sand at relatively low volume fractions (below 0.3 percent) which is basically used to control shrinkage cracking. They are chemically inert and very stable in the alkaline environment and have a hydrophobic surface and thus do not absorb part of the mixing water. They are currently manufactured in a variety of geometries and configurations; they can be produced as monofilaments, collated fibrillated fiber bundles, and continuous films. The PA 66 strips can be dispersed in clayey sands rather conveniently and also provides a better mechanical bonding to the mixture. In this research, we examine if the addition of PA strips may leads to improvement in the resistance of composite.

Table 1. PA 66 characteristics

Characteristic	Min	Max
Density	62	1.15
Tensile strength [MPa]	62	82
Compressive strength [MPa]	46	86
Water absorption (24 hours) [%]	1.4	1.5
L/D (Length /Diameter)	24:1	-
Critical Length [mm]	-	20

Aims of the Project

When a site is selected for constructing a new pavement or rehabilitating an old pavement, the in-place materials may be used as they naturally occur. The materials may also be removed and replaced with higher quality materials, or they may be modified in some manner to provide qualities that are appropriate. When the soils are modified, it is referred to as stabilization. The reasons for stabilizing soils include improving engineering properties such as strength. The main objective of this study is to:

- Stabilize clayey sand within reasonable time, and
- Modifying the engineering properties of clayey sand using polyamide strips.

EXPERIMENTAL

Sand samples were stabilized by hydrated lime with 70 to 80% pure degree and 0.1 weight percent of polyamide strips. The specimens were mixed with lime in dry state and then water added gradually. The short parallel polyamide strips were located in the diagonal direction. Water content of specimens had been determined by modified proctor compaction

test according to AASHTO guideline. All samples were then compacted in 5 layers in standard uniaxial test and indirect tensile test according to ASTM-D 5102 and ASTM-D 3967, respectively. They were also compacted in order to reach to relative density of 90 to 95 percent. The cylindrical samples for compressive and tensile tests that were built had a dimension of 10cm high and 5cm diameter. The loading in the tensile strength test was directed toward the longitudinal axis of specimen and was perpendicular to PA strips.

After 24 hours curing in laboratory open condition, at 23 °C, they were taken out from molds and placed in an oven in constant temperature at 45 °C, to increase the rate of curing, in humid condition to allow chemical reactions to take place. After 48 hours curing, samples were tested. Three samples were prepared and cured for each test in this manner.

The samples were then reinforced by polyamide 66 strips (Table 1), prepared in the same way as non-reinforced samples and cured.

RESULTS

Two important parameters can be considered and discussed, when polyamide 66 as reinforcing fibers is used in lime stabilized clayey sand samples; namely compressive and tensile strength. In essence, in soil stabilization one of the most important factors that should be considered is the modification of tensile strength. Because, as a general rule, soils like other construction materials such as concrete and asphalt mixtures has low tensile strength.

In view of the above, an increase in the tensile strength of specimens can be observed when specimens are reinforced with polyamide 66 strips. Herein, the higher the clay content the higher the tensile strength. Meanwhile, as it is shown in Figure1, increase in tensile strength is more important for reinforced specimens.

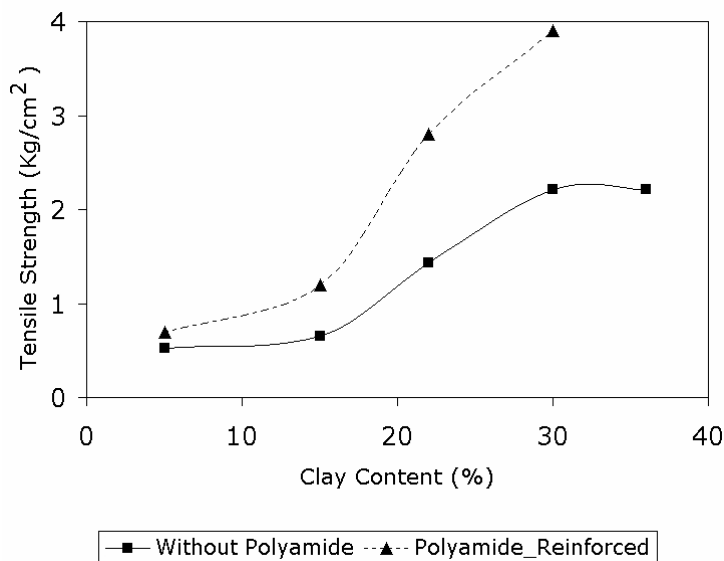


Figure 1. Tensile Strength Variation versus Clay Content (With and without polymeric reinforcement).

Therefore, more than 100 percent increase in tensile strength of specimens is obtainable by using polyamide 66 strips as reinforcing fibers in the samples. This is a significant improvement.

Figure 2 illustrates the stress-strain variations for stabilized specimens containing 15, 22 and 30 % clay.

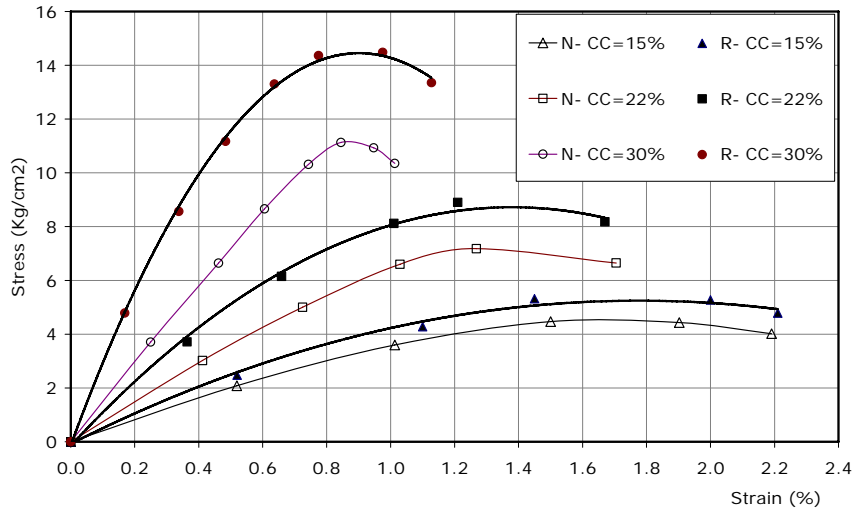


Figure 2. Stress-Strain variation for 15, 22 and 30 % Clay Content N(Non-Reinforced), R(Polyamide-Reinforced).

In our previous studies [2,3], we have shown that for lime-stabilized clayey sand, a parabolic behavior for the stress- strain curve is expected. Hence, for our polyamide reinforced materials, a similar behavior can be observed. This is presented in equation 2 for stabilized specimens containing 15% lime:

$$\sigma = -1.65\varepsilon^2 + 5.87\varepsilon \quad (2)$$

where:

$$\sigma = \text{Stress (Kg/cm}^2\text{)}$$

$$\varepsilon = \text{Strain (\%)}$$

Note: In this equation, coefficient of correlation (R^2) is 0.993 for specimens containing 22% clay.

It is observed that polyamide-reinforced specimen behaves in similar way and shows a parabola stress- strain curve presented by equation 3:

$$\sigma = -4.53\varepsilon^2 + 12.55\varepsilon \quad (3)$$

Note: In equation 2, coefficient of correlation (R^2) is 0.996.

Table 2. Stress-strain relationships

Clay content	Stress-Strain Eq.	R ²
15	$\sigma = -1.65\varepsilon^2 + 5.87\varepsilon$	0.993
22	$\sigma = -4.53\varepsilon^2 + 12.55\varepsilon$	0.996
30	$\sigma = -17.66\varepsilon^2 + 31.93\varepsilon$	0.999
$\sigma = \text{Stress (Kg/cm}^2\text{)}$		
$\varepsilon = \text{Strain (\%)}$		

Similar behavior can be observed for specimens stabilized with 30% clay.

Consequently, the similar parabolic stress- strain explains the behavior of polyamide-reinforced sample as follow:

$$\sigma = -17.66\varepsilon^2 + 31.93\varepsilon \quad (4)$$

Note: In this equation coefficient of correlation (R²) is 0.999.

Based on the variation of stress-strain presented in Figure 2 and in Table 2, it is clear that the higher the clay content, the higher the compressive strength. Meanwhile, the compressive strength of specimens reinforced with polyamide 66 strips is higher than the others. As shown in these figures, compressive strength can even be raised up to 25% when polyamide 66 strips as reinforcing agent is used.

In general, most clayey sands can be successfully stabilized with lime [2]. However, the addition of polyamide 66 strips can significantly improve the engineering properties of stabilized clayey sand and moderates the cracks propagation. A typical cracks distribution in a polymeric reinforced specimen in tension as well as in compression is shown in Figures 3 and 4 respectively. The overall results of this study indicate that lime/polyamide stabilizer composite is performing adequately.

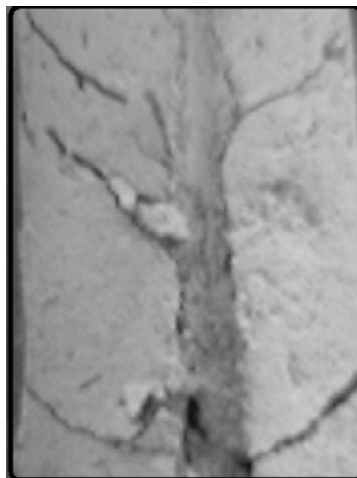


Figure 3. A typical cracks patterns in a polymeric reinforced specimen in the indirect tensile test.

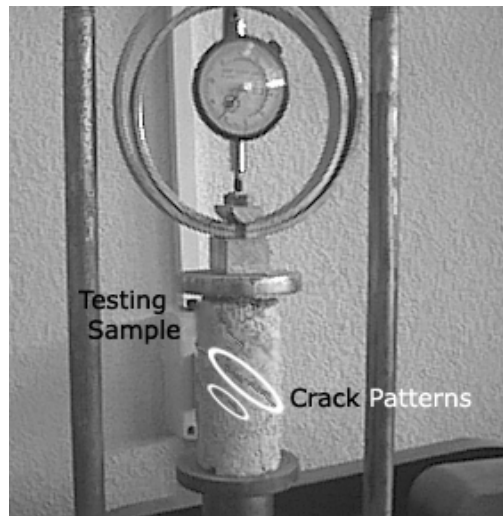


Figure 4. A typical cracks patterns in a polymeric reinforced specimen in the unconfined compressive test.

DISCUSSION

As it was mentioned earlier, there are a number of specialized stabilizers for which there is little technical information or test data. These stabilizers are sold under trade names. These products are only useful in stabilizing fine-grained soils. ASTM D 4609, American Society for Testing and Materials, provides guidance in application of these materials in terms of strength [7].

There is no doubt that lime migration usually occurs in the context of diffusion of clayey sand in the presence of stabilizers. Conceptually, the parameters that control this phenomenon should be those associated with the diffusion process. It is also clear that lime migration refers primarily to the migration of Ca^{2+} into the layer structure of clay; it will be equally applicable to any stabilizer that supplies calcium. The extent to which this takes place depends, primarily, on the chemical potential (concentration gradient of calcium) between the core (reaction front) and the outer surface (pore). The amount of stabilizer determines the supply of calcium, the most necessary component for stabilization, and calcium may be supplied from various sources. Therefore, lime migration, in principle, will not be associated solely with the addition of lime as a stabilizer. In view of the above, in order to be able to improve the stabilization criteria, we are suggesting the application of polyamide in our mixture, which seems to be more reliable than any other stabilizers that have been reported before. That means, the presence of polyamide fiber as an admixture can greatly influence the engineering properties and stabilization of clayey sand. This can be achieved in normal construction operations in the field.

When lime is added to clayey sand for modification of its engineering properties, it is called lime-modified clayey sand. Now in this study, when polyamide fiber is used for the same purpose, it should be termed differently. Our resulting material is referred to as “reinforced

clayey-sand". In this case, the criterion is based upon durability and the strength. It provides a durable pavement base with sufficient strength to help traffic loads.

CONCLUSIONS

From the observations made and tests conducted, the following general conclusions can be made:

- (1) The strength and stiffness of the clayey sand is well improved using the lime/polymeric stabilizer.
- (2) The cracking patterns observed were at minimum. This revealed that the stiffness of the mixture is significantly improved.
- (3) The variation of stress-strain in the mix design indicates that the lime/polymeric-stabilizer can be used in heavy-duty pavements.
- (4) Based on the variation of tensile strength obtained, the durability of the lime/polymeric-stabilizer can be improved significantly.
- (5) The results indicate that the lime/polyamide can be a good candidate for stabilization of clayey sand.

REFERENCES

- [1] Abdellatif Ait-Kadi, Brahim Brahimi, Mosto Bousmina, 2004, Polymer blends for enhanced asphalt binders, *Polymer engineering and science*, Volume 36, issue 12, pp 1724-1733.
- [2] B. Moustafa¹, A. R. Bazaraa², A. R. Nour El Din, 2003, Soil stabilization by polymeric materials, *Angewandte Makromolekulare Chemie*, Volume 97, Issue 1, pp 1-12.
- [3] Rollings, M.P., and Rollings, R. S., 1966, *Geotechnical Materials in Construction*, McGrawHill, N. Y.
- [4] Boardman, D. I., Glendinning, S. and Rogers, C.D.F., 2001, Development of Stabilization and Solidification in Lime-Clay Mixes, *Gèotechnique*, vol. LI, No. 6, August 2001, pp. 533-544.
- [5] Ingles, O. G. and Metcalf, J. B., 1972, *Soil Stabilization, Principles and Practice*, John Wiley and Sons, 369 p.
- [6] Tabtabaei, A., 1982, Application of Lime Stabilized Geomaterials in Road Construction, *Technical Journal of Tehran University*, No. 44, pp. 47-58.
- [7] American Society for Testing and Materials, 1994, Standard Guide for Evaluating Effectiveness of Chemicals for Soil Stabilization, *D 4609-94 Annual Book of Standards*, Vol. 04, 08, PA, USA.

Chapter 14

POLYMERS IN ELECTRONIC DEVICES: NEW TRENDS AND ACHIEVEMENTS

*M. Ziabari, F. Raeesi and A. K. Haghi**

The University of Guilan, P. O. Box 3756, Rasht, Iran

ABSTRACT

An organic polymer that possesses the electrical, magnetic and optical properties by doping/de-doping process commonly associated with a conventional polymer is termed an Intrinsically Conducting Polymer (ICP) more commonly known as synthetic metals. In this paper, the application of ICPs in different types of sensors, transistors, and display devices are reviewed. Although, there are a lot of applications for ICPs, we are focusing mainly on these more interesting ones. The emphasis of this study is on major development in above mentioned field over the last 5-10 years.

1. INTRODUCTION

Today, the polymer-based transistors would be expected to be superior to conventional inorganic transistors. Moreover, the difficult process of constructing the inorganic transistors can be replaced by a simple technology involving organic ICPs. ICPs are best suited for electrochromic display devices (ECDs). They show different colors depending on the oxidation-reduction state. The function of a sensor is to provide information on our physical, chemical and biological environment. ICPs can be used for constructing different type of sensors such as biosensors, gas sensors, humidity sensors and ion sensors.

Since their discovery in 1970s ICPs have impacted different fields of industry. One of these emerging fields is microelectronics which is of great importance in manufacturing different kinds of electrical devices. The discovery of conducting polymers has been regarded as so important that it was recognized with the 2000 Nobel prize in chemistry.

* Corresponding author E-Mail: Haghi@Guilan.ac.ir

The emphasis in electronic technology is to make better, faster and smaller electronic devices for application in modern life. Almost all electronic devices are fabricated from semiconductor silicon. Organic materials such as proteins, pigments and ICPs have been considered as alternatives for carrying out the same functions that are presently being performed by conventional semiconductors. Among these materials, ICPs have attracted most attention for possible applications in molecular electronics (ME) because of their unique properties and versatility. These ME materials differ from conventional polymers. The presence of an extended π -conjugation in polymer, confers the required mobility to changes that are created on the polymer backbone (by the process of doping) and make them electrically conducting. π electrons are delocalized across the molecule, leading to the semiconducting or conductive characteristics of a conjugated system.

The first conducting polymer was trans-polyacetylene which was doped with bromine and was produced at 1970s. Soon other conjugated polymers such as poly (p-phenylene), polypyrrole (PPy), polyethylene dioxythiophene (PEDOT) and polyaniline (PANI) and their derivatives which are stable and processable were synthesized. The molecular structures of a few ICPs are shown in Figure 1.

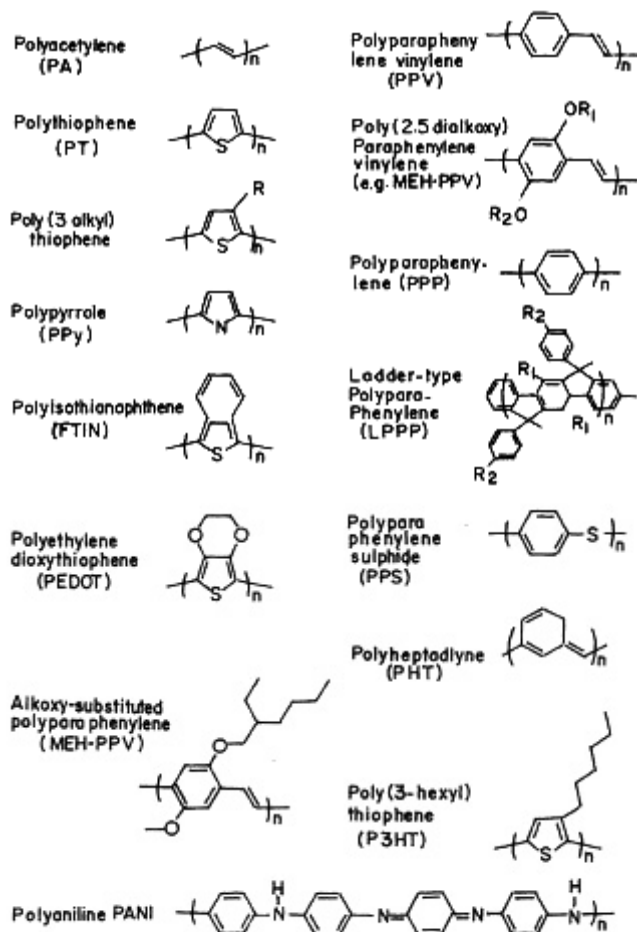


Figure 1. Structures of a few ICPs.

The conductivity of these polymers can be tuned from insulating regime to superconducting regime, by chemical modification, by the degree and nature of doping. Besides these, polymers offer the advantages of lightweight, flexibility, corrosion-resistivity, high chemical inertness, electrical insulation, and the ease of processing. Another advantages lie in the fact that these materials possess specific advantages such as high packing density, possibility of controlling shape and electronic properties by chemical modification. However there are several problems associated with these materials, namely reproducibility and stability. Therefore ICPs also referred to as “synthetic metals” are promising materials for ME devices such as light-emitting diodes (LEDs), thin-film transistors (FETs), sensors and electrochromic display devices (ECDs) [1,2,3,4,10, 13,17,18].

2. TRANSISTORS

Organic thin film transistors (OTFTs) have a potential as the active matrix driving element for many electronic devices such as flexible paper-like displays, biological plastic chips or low-cost identification tags, whose driving elements may not be achieved from conventional inorganic materials and processing technologies [8]. In general, OTFTs utilize a thin film of organic semiconducting material as the active layer of the transistor. Two electrodes (“source” and “drain”) in contact with the organic semiconductor are used to apply a source–drain voltage and measure the source–drain current that flows through the organic semiconductor, while a third electrode (“gate”) is used to modulate the magnitude of the source–drain current. The gate can be used to switch the transistor “on” (high source–drain current) and “off” (negligible source–drain current). Depending on the organic semiconducting material used as the active layer, the mobile charge carriers can either be electrons (n-type material) or holes (p-type material) [6].

OTFTs can be roughly classified into two primary categories: organic field-effect transistors (OFETs) and organic electrochemical transistors (OECTs). Figure 2 shows the schematic cross section of an OEFT and an OECT. In OFETs, the source–drain current is modulated by field-effect doping, where the charge carrier density in the organic semiconductor is controlled by the gate electrode via an electric field applied across an insulating layer (gate dielectric). In OECTs the source–drain current is modulated by electrochemical doping or de-doping, where the change in conductivity of the organic semiconductor is mediated by ions from an adjacent electrolyte. OECTs exhibit much lower operating voltages than OFETs, but due to the movement of ions involved in OECTs, their switching times are considerably slower (on the scale of seconds or longer) than those for OFETs (on the scale of milliseconds or shorter).

Classical (inorganic) field effect transistors (FETs) operate by the principle that the conductivity of an (inorganic) semiconductor, which is connected to an electrical circuit by a “source” terminal and a “drain” terminal attached to opposite ends of the active semiconductor, can be increased or decreased by the presence of an electric field which is supplied by an electrically conducting “gate” electrode. The gate electrode is not attached directly to the source or drain electrodes. The electric field associated with a given positive or negative potential applied to the gate electrode passes through a nonconducting material “dielectric” that separates the source/drain electrode material from the gate electrode. The

change in conductivity of the active semiconducting source/drain material is, in effect, modified by the “through space” electric field effect [5].

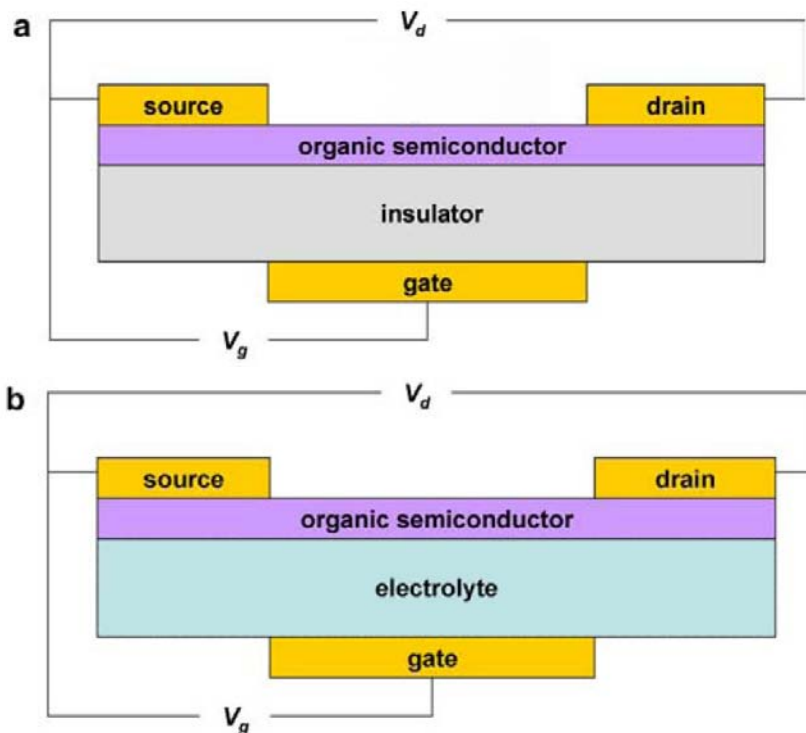


Figure 2. (a) Schematic cross section of an organic field-effect transistor (OFET). (b) Schematic cross section of an organic electrochemical transistor (OECT). The applied source–drain voltage V_d and gate voltage V_g are also shown.

In contrast to the small molecules, polymers can be processed easily from solution and therefore are useful for applications on flexible plastic substrates and in multilayer device configurations. However, solution-processed polymer films are inherently more disordered than in case of molecular FETs. It can be concluded from the above results that conjugated polymer based FETs are much cheaper than Si based device. However, the slow response and limited lifetime of the device restrict them to replace current Si technology. Nevertheless, the possibility of making flexible and flat panel with conjugated polymers open a new area of large-area low-cost plastic electronics [10].

One of the important parameters deciding the performance of FETs is the mobility. Charge carrier mobilities in ICP based FETs are found to be around 10^{-5} $\text{Cm}^2/\text{V.s}$ depending on the applied voltage and nature of the gate insulator. These values are significantly lower than that of inorganic semiconductor device in which mobilities are in the range of 0.1-1 $\text{Cm}^2/\text{V.s}$. In an FET, the interface of the gate insulator and organic semiconductor layer plays an important role in charge transport. Electrical characteristics of the FETs are estimated by observing the change of the relationship between source-drain current (I_{SD}) and voltage (V_{SD}) upon sweeping gate voltage (V_G). From the I_{SD} - V_{SD} and I_{SD} - V_G relationships of FETs, the turn-off gate voltage, on/off ratio (defined as the current ratio of $I_{on,max}$ to $I_{off,min}$), the trans

conductance (g_m , defined as the slope of the plot of I_{SD} versus V_G) and the response rate of the FETs to the electric field can be obtained [8-10].

The polymer-based transistor would be expected to be superior to conventional inorganic transistors. Furthermore, the sophisticated technology required for constructing the inorganic transistors can be replaced by a simpler technology involving ICPs. Rani and Santhanam [9] constructed a Polycarbazole-based electrochemical transistor. Since this polymer has a high redox potential compared to the other polymers, a transistor made of polycarbazole would be expected to have better transfer and saturation characteristics. The transistor was fabricated using Pt-coated glass electrodes, polycarbazole was deposited on both Pt electrodes. One half of the polycarbazole-deposited Pt plate was used as the source and the other half as the drain. The transistor designed for their study is shown in Figure 3. Remarkable features of the polycarbazole transistor include the low hysteresis of the device in scanning forward and reverse directions of the drain voltage and the maximum positive voltage needed for the saturation of the drain current.

During the last decade, various types of inorganic-organic hybrid FET devices have been reported. In the hybrid FETs, the electrodes and the dielectric layer were formed using inorganic materials, which are same as those used for conventional inorganic FETs, while the active channel was formed using organic semiconducting materials such as pentacene, perylene and various oligomers. Nevertheless, the hybrid OFETs are hardly able to be employed in low-cost, large area and flexible display, because they require complicated manufacturing processes and high-cost special equipments to evaporate each component of the device at the elevated temperatures. The processes for All-polymer FETs are expected to give rise to many advantages in manufacturing the active matrix driving element for large area display panel with mechanical flexibility and optical transparency. Since the All-polymer FETs composed of only polymeric materials, the devices could be fabricated by using a simple and low-cost process at room temperature and possessed fairly high optical transmittance and mechanical flexibility. We, therefore, consider the All-polymer FETs may be applicable to an active matrix driving element for the flexible and transparent electronic systems [5,8].

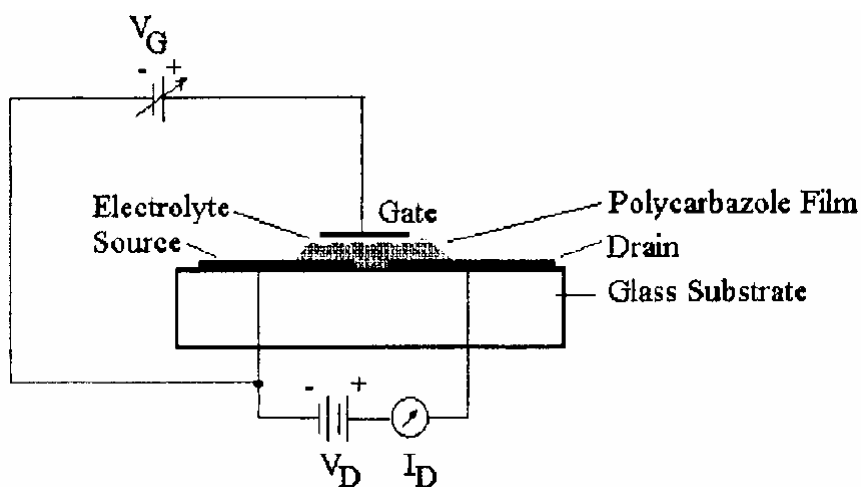


Figure 3. Schematic diagram for the characterisation of the device.

Lu et al. [5] fabricated an all polymer FET type (metallic polymer)–insulator–(metallic polymer) (PIPFET) by line patterning technique which involves no printing of a ICP and which uses a localized, as distinct from a global, gate electrode. A hybrid FET device is also described in which a commercial micrometer is used as the adjustable gate electrode to controllably vary the thickness of the dielectric material. Figure 4 shows their fabricated FET device. They reported a curious effect whereby an electric field apparently greatly affects the conductivity of an organic polymer, PEDOT, doped to the metallic conducting regime when it is used in an All-polymer field effect transistor configuration. It has been postulated that a doped ICP consists of metallic “islands” surrounded by lowly conducting “beaches” as shown in Figure 5. The field changes the conductivity of the semiconducting beaches but not that of the metallic islands, hence the field changes the extent of electrical percolation between the metallic islands, and therefore changes the bulk conductivity of the material.

Pinto et al. [7] have proposed a technique called electrospinning to electrostatically lay down the active semiconducting polymer on substrates. Since electrospinning can be used in the controlled assembly of parallel, periodic fiber arrays, this technology is attractive for fabricating low-cost logic and switching circuits based on ICPs. Figure 6 shows the basic elements of the electrospinning apparatus. FET behavior in doped electrospun PANi/PEO nanofibers was observed. Saturation channel currents were observed at surprisingly low source-drain voltages. Reducing or eliminating the PEO content in the fiber enhanced device parameters.

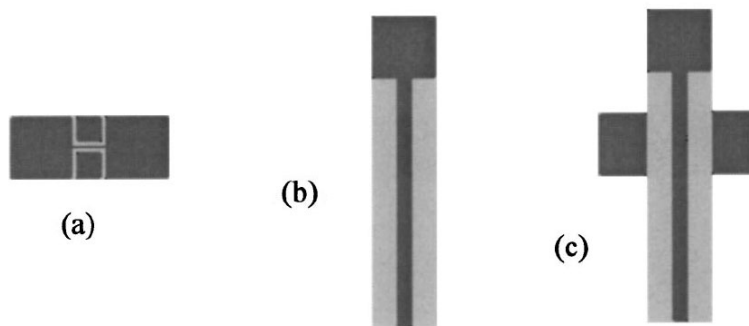


Figure 4. (a) indicates the source-drain electrode (b) the gate electrode coated with PEDOT (c) the fabricated device made by superposition of b on a.

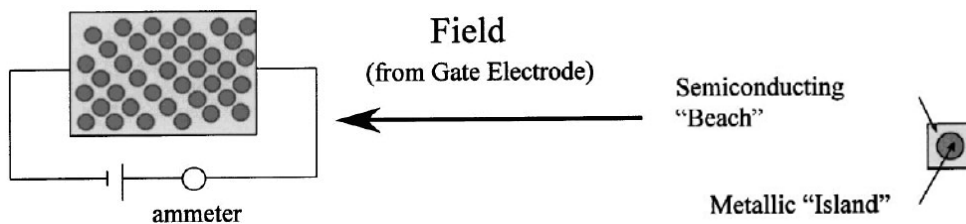


Figure 5. Percolation field effect in doped ICPs. Metallic islands separated by beaches of non- or lowly conducting (semiconducting) polymer.

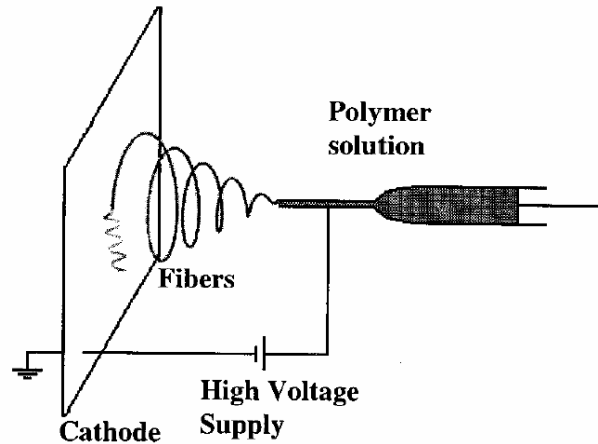


Figure 6. Schematic showing the main components of an electrospinning apparatus.

Lee et al. [8] reported a novel photolithographic method to fabricate the flexible All-polymer FET with optical transparency, where all components are formed from the polymeric materials. Active channel and all three electrodes were formed on a flexible polymer substrate using the simple photolithographic patterning technique of the electrically conducting PEDOT or PPy. Transparent photocrosslinkable polymers such as PVCN or Epoxy/MAA polymer were used as the dielectric layer. Fig 7. shows the structure of the All-polymer FET. These FET devices exhibited relatively longer response times (order of minute) than those of the conventional inorganic FETs, The source-drain current of the FETs decreased with increase of the positive gate voltage, implying the p-type FETs worked in the depletion mode.

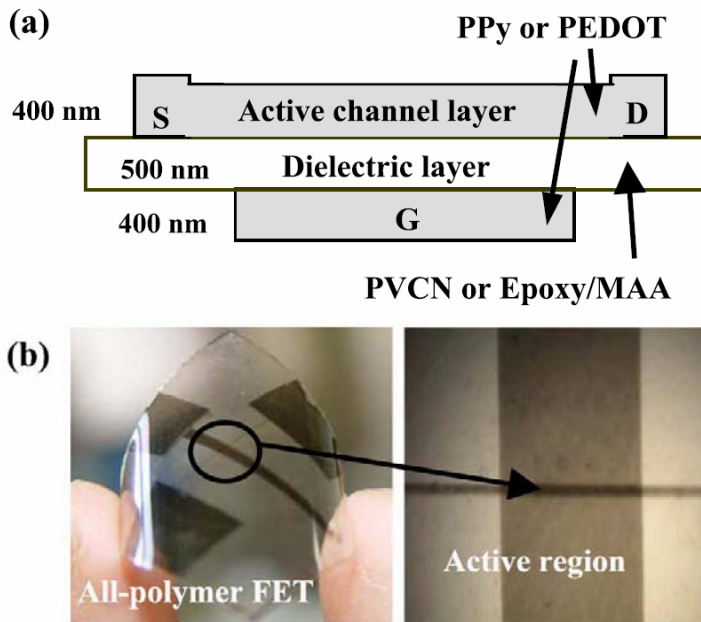


Figure 7. Schematic structure of the flexible All-polymer FET with optical transparency.

Doped and de-doped nanotubes and nanowires of PPy, PANi and PEDOT were synthesized by the electrochemical polymerization method, using Al_2O_3 nanoporous templated after Kim et al. [11]. The electrical and optical properties of the nanotubes and nanowires were controlled through various synthetic conditions such as doping level, dopant and template dissolving solvent. It was observed that the nano-systems were transformed from a conducting state to a semiconducting or insulating state through the process of de-doping with the treatment of NaOH as a solvent. From the gate dependence of I-V characteristic curves for the systems, it was clear that charge carriers were p-type. Therefore, these nanotubes and nanowires could be used in the fabrication of polymer-based transistors.

3. DISPLAY DEVICES

One important application of ICPs is electrochromism. The absorption and emission spectra of certain dyes may be shifted by hundreds of angstroms upon application of a strong electric field. This effect is called “electrochromism”. In other words, Electrochromism is the property of a material where its color is changed by an electrochemical redox reaction. An electrochromic material is the one that changes color in a persistent but reversible manner by an electrochemical reaction and the phenomenon is called electrochromism. Electrochromism is the reversible and visible change in transmittance and/or reflectance that is associated with an electrochemically induced oxidation–reduction reaction. The color change is commonly between a transparent (“bleached”) state and a colored state, or between two colored states. These color changes are directly related to the conductivity changes of the polymer and so are affected by a small electric current at low dc potentials of the order of a fraction of volts to a few volts. An electrochromic device is essentially a rechargeable battery in which the electrochromic electrode is separated by a suitable solid or liquid electrolyte from a charge balancing counter electrode, and the color changes occur by charging and discharging the electrochemical cell with applied potential of a few volts. Figure 8 illustrates an electrochromic device configuration. An electrochromic device is composed as follows: glass/transparent conductor (ITO)/electrochromic layer (WO_3)/ion conduction layer (PPy, electrolyte)/ion storage layer (V_2O_5)/transparent conductor (ITO)/glass [12,14,15].

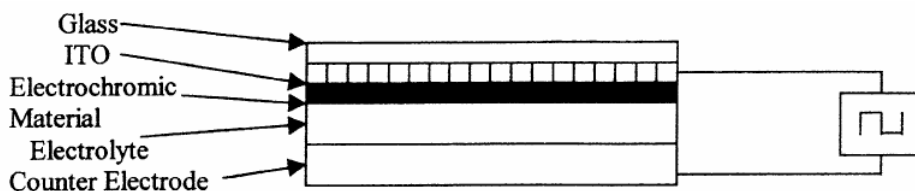


Figure 8. Schematic diagram of the ECD.

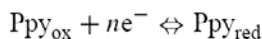
In the recent years, ICPs have gained a lot of attention for ECDs. This is due to the fact that all electroactive and ICPs are potentially electrochromic materials, and are more processable than inorganic electrochromic materials and offer the advantage of a high degree of color tailorability. Furthermore, we can tune the optical properties of these materials by controlled doping and/or dedoping. ECD is comparable in properties with that of LCD with

the added advantages that it can be made into different colors without the addition of external dye or window, does not depend upon the viewing angle and can be easily prepared in the form of large area windows. Widespread applications of ECDs depend on reducing costs, increasing device lifetime and overcoming the problem of ECD degradation. Table 1 gives a comparison between inorganic and polymeric electrochromic materials [15].

Table 1. Comparison between inorganic and polymeric electrochromic materials

Property	Inorganic materials	Polymers
Method of preparation	Needs sophisticated techniques such as vacuum evaporation, spray pyrolysis, sputtering, etc.	The material can be easily prepared by simple chemical, electrochemical polymerization and the films can be obtained by simple techniques such as dip-coating, spin coating, etc.
Processibility of the materials	The materials are poor in processibility	The materials can be processed very easily
Cost for making the final product (device)	High as compared to the polymer based devices	Low cost as compared to the inorganic materials
Colors obtainable	Limited number of colors are available from a given material	Colors depends on the doping percentage, choice of the monomer, operating potential, etc. Hence, large number of colors are available with the polymeric materials
Contrast	Contrast is moderate	Very high contrast can be obtained
Switching time (ms)	10–750	10–120
Lifetime	10^3 – 10^5	10^4 – 10^6 cycles

PPy film is blue-violet in doped (oxidized) state. Electrochemical reduction yields the yellow-green undoped form. The schematic of the doping/dedoping process can be given as



The electrochromism of PPy is unlikely to be exploited, mainly due to the degradation of the film on repetitive color switching.

The electrical and electrochromic properties of PANi depend not only on its oxidation state but also on its protonation state, and hence the pH value of the electrolyte used. As shown in Figure 1 PANi exhibits electrochromic behavior. Electrochromic behavior of PANi is shown in Figure 9. As demonstrated, small change in the pH of the solution and/or potential could create color and conductivity changes. PANi is green in the oxidized state and is transparent yellow in the reduced states. It has violet color in very acidic and yellow brownish in very basic media [14-16].

Prakash et al. [16] constructed a portable electrochromic display window using a PANi coated SnO₂ glass plate and AlCl₃ melt. The potential excursions from 0 to 1.0 V produced sharp color changes on the electrode from colorless to green, suggesting that surface activity is helpful for electrochromic display. It exhibited a fast response time (10ms) and a long cycle life (1000) [16]. A composite of two conducting polymers, PANi and PPy, could result in much improved physical properties with respect to their applications in electrochromic devices. Although PANi composite materials have unique photo/chromic properties they have their specific problems with respect to their reproducibility and reusability. Problems exist due to the dynamic nature of these polymers thereby preventing their successful application as novel display devices. Using the structure shown in Figure 10 a conducting PANi was polymerized on the top of a Pt electrode previously coated with PPy. By measuring the

conductivity of the polymer we are able to predict the color of the polymer and vice versa [14].

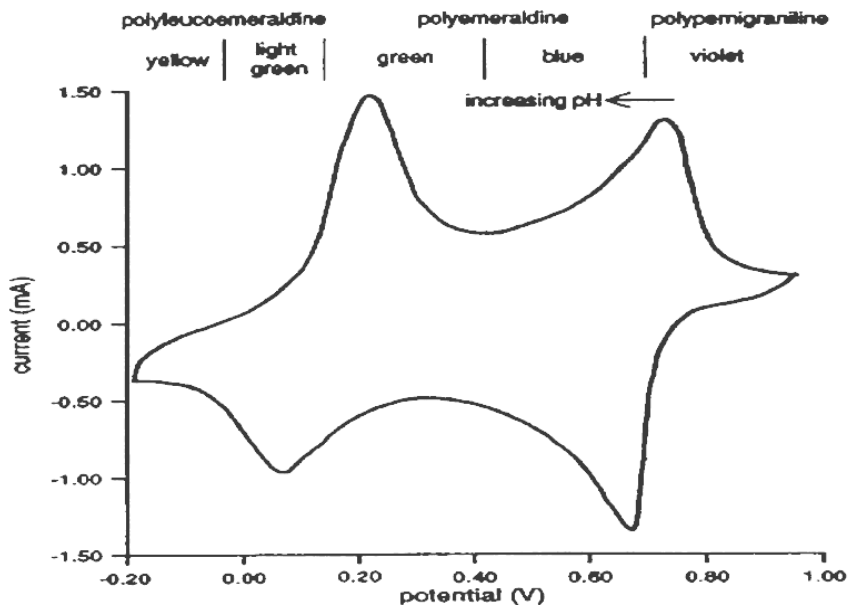


Figure 9. Multicolor performance of conducting PANi at different oxidation/reduction states.

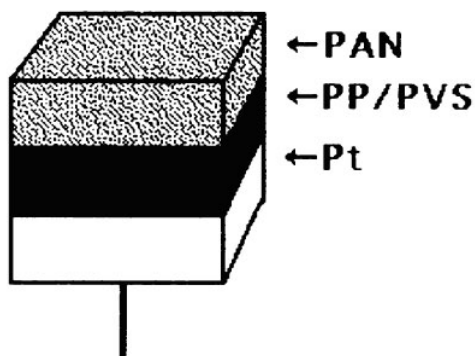


Figure 10. A polymeric composite electrode. PAN (Polyaniline), PP (polypyrrole) and Pt (Platinum).

It was thought that by combining the PPy and PANi with Prussian blue (PB) not only the adhesion of PB could be improved but also this combination would exhibit a wide range of electrochromic colors. Somani et al. [18] studied the electrochromic response of PPy/PB and PANi/PB composite films in different electrolytes by depositing the PB films on top of conducting PPy and PANi films, all prepared by electrochemical methods. They concluded that the use of PB on PPy and PANi not only yields high contrast but also extends the electrochromic response to a wider region of the visible spectrum, thus working as a sensitizer for improving the electrochromic response of the conducting PPy and PANi. It was noted that during electrochromic cycling, PPy changed its color from dark greenish blue (in

oxidized state) to pale brown/yellow and PB from blue to bleached transparent white state (when reduced). On the other hand, PPy/PB film changed its color from bluish green (in oxidized state) to pale brown (in the reduced state).

Lee et al. [12] described the assembly method of a solid-state electrochromic device using organic conductive polymer as the active material and a transition metal oxides the electrochromic layer. The electrochromic films (WO_3 , V_2O_5) prepared by sol-gel spin-coating and the vacuum evaporation process. The PPy films were coated by electropolymerization in a pyrrole solution. The polymer product obtained by electro-oxidizing the pyrrole monomer depended on the fabrication conditions used during the electropolymerization, for example, the potential employed for the deposition, the temperature, the solvent and the counter ion present in the pyrrole-containing solution.

Most of the so-called “all plastic” electrochromic devices described in the literature comprise not only plastic components, but also inorganic compounds as one of the electrochromic materials. In order to assemble an all-plastic and flexible electrochromic device it is necessary to improve the mechanical properties of the ICPs used as electrochromic materials. This problem can be overcome by mixing the ICPs with thermoplastics or elastomers to produce polymeric blends which show the electrochromic properties of the ICPs associated with the mechanical properties of common polymers. Another attempt has been made to use an electrochromic device for time–temperature integration. Such a device could be used for “smart” labeling of frozen good. An electrochromic window (EW) is an ECD which allows electrochemically driven modulations of light transmission and reflections. Such electrochromic optical switching device is usually called as “smart window”. It can be used for a variety of applications where the optical modulation effect can be used significantly [15].

ICP thin films were used as driving electrodes for polymer-Dispersed Liquid-Crystals (PDLC) display devices. Liquid-crystalline–based display devices, which are commonly made of a liquid-crystal compound sandwiched between two substrates coated with a conducting layer of indium tin oxide (ITO), whose substitution with ICP electrodes could improve the optical and mechanical properties of the display devices. On the way to all-organic displays, PDLC sandwiched between two plastic substrates coated with ICP layers are promising devices for paper-like displays for electronic books which require flexibility, lightness, and low-power consumption. The electro-optical characteristics (transmission properties, drive voltages and switching times) of the PDLC devices depend on the nature of the ICP substrate used [13].

Kawase et al. [17] fabricated All-polymer thin film transistors by inkjet printing technique. They used these transistors as active-matrix backplane for information displays. This field has been dominated by amorphous Si TFTs and large liquid crystal displays with an amorphous Si TFT active matrix backplane have been manufactured at a reasonable cost. An organic TFT is expected to reduce the cost even more, and to be applied to flexible displays based on a plastic substrate. The TFT characteristics required for active-matrix displays are (1) sufficient drain current, (2) low off current, (3) low gate leakage current through an insulator, (4) small gate overlap capacitance and (5) uniform characteristics.

4. BIOSENSORS

The estimation of metabolites such as glucose, urea, cholesterol and lactate in whole blood is of central importance in clinical diagnostics. A biosensor is a device having a biological sensing element either intimately connected to or integrated within a transducer. The aim is to produce a digital electronic signal, which is proportional to the concentration of a specific chemical or set of chemicals. A general schematic of a biosensor is shown in Figure 11.

A transducer converts the biochemical signal to an electronic signal. The transducer of an electrical device responds in a way that a signal can be electronically amplified, stored and displayed. Biocomponents function as biochemical transducers. This biocomponent can be enzymes, tissues, bacteria, yeast, antibodies/antigens liposomes and organelles. Most of the biological molecules such as enzymes, receptors, antibodies, cells etc. have to be fixed in a suitable matrix. The activity of immobilized molecules depends upon surface area, porosity, hydrophilic character of immobilizing matrix, reaction conditions and the methodology chosen for immobilization. ICPs have attracted much interest as a suitable matrix of enzymes, ICPs are used to enhance speed, sensitivity and versatility of biosensors in diagnostics to measure vital analytes.

Another advantage offered by ICPs is that the electrochemical synthesis allows the direct deposition of the polymer on the electrode surface, while simultaneously trapping the protein molecules. It is thus possible to control the spatial distribution of the immobilized enzymes, the film thickness and modulate the enzyme activity by changing the state of the polymer. Because of these ICPs have been used in the fabrication of biosensors in various fields such as: Health care, immuno sensors, DNA sensors, environmental monitoring, and food analysis.

An example for showing this importance is that the largest group of direct electron-transfer biosensors is based on coimmobilization of the enzyme in an ICP, namely PPy and PANi. [19,20,23,24] In a recent work by Qu et al. biosensors for choline were developed using layer by layer assembled functionalized MWNT, and PANi multilayer film. By using the conducting polymer of PANi, the biosensor immobilized abundant CNTs stably and achieved the aim of antiinterference [33]. A. Ramanaviciene et al. has synthesized nanostructured (molecularly imprinted) conducting polymer, PPy and applied it in design of chemical sensor sensitive to caffeine [27].

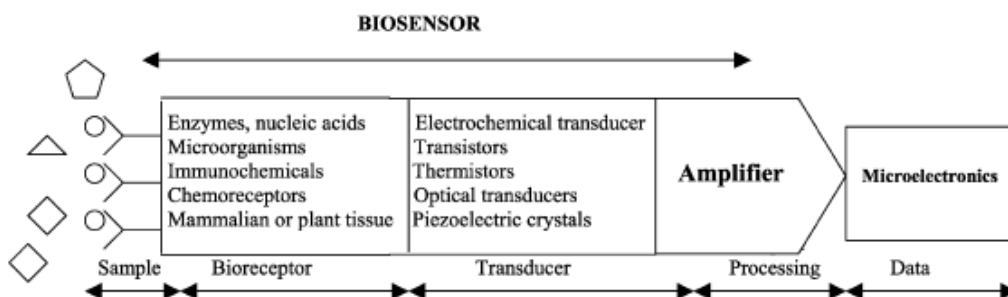


Figure 11. Schematic diagram of a biosensor.

In the field of environmental works W. Bourgeois et al. developed a sensor array based measurement system for continuous monitoring of water and waste water. They tested an on-

line measurement system that incorporated an array of ICPs for continuous analysis both in laboratory, and in field [21]. Other types of sensors: The emission of gaseous pollutants has become a serious environmental concern. Sensors are needed to detect and measure the concentration of such gaseous pollutants. ICPs showed promising applications for sensing gases having acid-base or oxidizing characteristics. ICP composites with other polymers such as PVC, PMMA, etc. polymers with active functional groups and SPEs are also used to detect such gases [19,20].

Z. Opilski et al. investigated on optical interferometric structures that can be applied in toxic gas sensors. The sensor head consists of PANi and nafion layers deposited on the face of the telecommunication optical fiber [31]. Humidity sensors are useful for the detection of the relative humidity (RH) in various environments. Polymer composites and modified polymers with hydrophilic properties have been used in humidity sensor devices. Suri et al. prepared nanocomposite pellets of iron oxide and PPy for humidity and gas sensing by a simultaneous gelation and polymerization process. This resulted in the formation of a mixed iron oxide phase for lower PPy concentration, stabilizing to a single cubic iron oxide phase at higher PPy concentrations, sensitivity to humidity increased with increasing PPy concentration [19].

Scott T. McGovern et al. constructed micro-humidity sensors from polyester-insulated platinum wire substrate to have a thickness of no more than 150 μm . These electrodes were dip-coated in ICP. Two processable PANi blends were developed with polyvinyl alcohol (PVA) and a butyl acrylate/vinyl acetate copolymer. The sensors showed high sensitivity, low resistance, and good reversibility without hysteresis [29]. Razat Nohria et al. have deposited SPANi using layer by layer and spin coating techniques for humidity sensing application. The layer by layer assembled sensors showed better sensing performance in terms of response time, sensitivity and repeatability as compared to the spin coated sensors [30]. M.F Mabrook et al. used inkjet-printed films of the conductive polymer PPy for vapor sensing at room temperature [28].

Other important type of sensors are ion sensors generally, ion sensors have been developed taking the polymer as the conductive system/component, or as a matrix for the conducting system. When such systems come in contact with analytes to be sensed, some ionic exchange/interaction occurs, which in turn is transmitted as an electronic signal for display. Ion sensors find wide applications in medical, environmental and industrial analysis. They are also used in measuring the hardness of water. Ion-selective chemical transduction is based on ion selectivity conveyed by ionophore ion-exchange agents, charged carriers and neutral carriers doped in polymeric membranes.

A new Ca^{2+} -selective PANi based membrane has been developed for all-solid-state sensor applications. PANi is used as the membrane matrix, which transforms the ionic response to an electronic signal [19,24]. Tom Lindfors et al. used PPy as a component in all-solid-state ion sensors. PPy(DBSA) modified electrodes showed good reproducible cationic response to Ca^{2+} with the sensitivity of 27.2 ± 0.2 mV decade⁻¹ which remained practically constant over 10 d. The standard potential, however, was found to drift 70 mV over the same time period [26].

Yung-Chen Luo et al. prepared amperometric ammonium ion sensor based on PANi-poly(styrene sulfonate-co-maleic acid) composite conducting polymeric electrode. Two kinds of PANi- PSSMA composite films were prepared and their ammonium ion-sensing were studied. PANi- PSSMA(I) was prepared by incorporating PSSMA anions into a

PANi/Au/Al₂O₃ plate was used to prepare another composite electrode of PANi-PSSMA(II)/Au/Al₂O₃. Compared with PANi-PSSMA(I), PANi-PSSMA(II) exhibited sensitivity to ammonium ion due to its fibrous morphology and high porosity [34].

CONCLUSION

ICPs have attracted much attention in recent years because of the large number of possible applications in various electronic devices such as in sensors, light emitting diodes (LEDs), organic thin film transistors (OTFTs), electrochromic display devices (ECDs). It is even said that ICPs can be considered as alternatives for carrying out the same functions that are presently being performed by conventional polymers. Their conductivity, besides retaining the main properties of an organic polymer such as strength and low density and packed structure can make them a good choice for future works. OTFTs have a potential as the active matrix driving element for many electronic devices such as flexible paper-like displays, biological plastic chips or low-cost identification tags, whose driving elements may not be achieved from conventional inorganic materials and processing technologies. Conjugated polymer based FETs are much cheaper than Si based device. In the recent years, ICPs have gained a lot of attention for ECDs. This is due to the fact that all electroactive and ICPs are potentially electrochromic materials, and are more processable than inorganic electrochromic materials and offer the advantage of a high degree of color tailorability. Conductive polymers enhance speed, sensitivity and versatility of sensors and they have an increasing use in producing more reliable sensors.

REFERENCES

- [1] http://www.findarticles.com/p/articles/mi_m1200/is_20_163/ai_102696929.
- [2] A. G. Macdiarmid, *Angew.chem.int.ed.* 2001,40,2581-2590.
- [3] N. hall, *CHEM.COMMUN.*2003.
- [4] S. Ramakrishnan. *RESONANCE*. November 1997.
- [5] J. Lu, N. J. Pinto and A. G. MacDiarmid, *J. Applied Physics*, Vol. 92, No. 10, 15 November 2002.
- [6] J. T. Mabeck and G. G. Malliaras. *J. Anal Bioanal Chem* 384 (2006) 343–353.
- [7] N. J. Pinto, A. T. Johnson, A. G. MacDiarmid, C. H. Mueller, N. Theofylaktos, D. C. Robinson, and F. A. Miranda. *J. Applied Physics*, Vol. 83, No. 20, 17 November 2003.
- [8] M. S. Lee, H. S. Kang, H. S. Kang, J. Joo, A. J. Epstein and J. Y. Lee. *J. Thin Solid Films* 477 (2005) 169– 173.
- [9] V. Rani and K.S.V. Santhanam, *J. Solid State Electrochem* 2 (1998) 99-101.
- [10] V. Saxena and B.D. Malhotra, *J. Current Applied Physics* 3 (2003) 293–305.
- [11] B. H. Kim, D. H. Park, J. Joo, S. G. Yu and S. H. Lee, *J. Synthetic Metals* 150 (2005) 279–284.
- [12] D. S. Lee, D. D. Lee, H. R. Hwang, J. H. Paik, J. S. Huh, J. O. Lim and J. J. Lee, *J. Material Science: Materials in Electronics* 12 (2001) 41-44.

-
- [13] F. Roussel, R. Chan-Yu-King and J. M. Buisine, *The European Physical Journal E* 11, 293–300 (2003).
- [14] A. Talaie, J. Y. Lee, Y. K. Lee, J. Jang, J. A. Romagnoli, T. Taguchi and E. Maeder, *J. Thin Solid Films* 363 (2000) 163-166.
- [15] P. R. Somani and S. Radhakrishnan, *J. Materials Chemistry and Physics* 77 (2002) 117–133
- [16] R. Prakash and K. S. V. Santhanam, *J. Solid State Electrochem* 2 (1998) 123-125.
- [17] T. Kawase, T. Shimoda, C. Newsome, H. Siringhaus and R. H. Friend, *J. Thin Solid Films* 438–439 (2003) 279–287.
- [18] P. Somani, A. B. Mandale and S. Radhakrishnan, *Acta Materialia* 48 (2000) 2859-2871.
- [19] B. Adhikari, S. Majumdar/*Prog. Polym. Sci.* 29(2004)699-766.
- [20] E. Bakker, *Anal. chem.* 2004, 76, 3285-3298.
- [21] W. Bourgeois, P. Hogben, A. Pike, R. M. Stuetz, *Sensors and Actuators B* 88(2003)312-319.
- [22] <http://www.nsti.org/publ/MSM2001/175.pdf>
- [23] M. Gerard et al./*Biosensors and Bioelectronics* 17(2002)345-359.
- [24] M. Trojanowicz, *Microchim. Acta* 143, 75-91(2003).
- [25] <http://homepage.ntlworld.com/colin.pratt/applcp.pdf>.
- [26] T. Lindfors, J. Bobacka, A. Lewnstrom and A. Ivaska, *Electrochimica Acta*, vol. 43, no. 23, pp. 3503-3509, 1998.
- [27] A. Ramanaviciene, A. Finkelsteinas, A. Ramanavicius, *Materials Science*. vol. 10, no. 1 (2004).
- [28] M. F. Mabrook, C. Pearson, M. C. Petty/*sensors and actuators B* 115(2006)597-551.
- [29] S. T. McGovern, G. M. Spinks, G. G. Wallace, *Sensors and Actuators B* 107(2005)657-665.
- [30] R. Nohira, Ranjeek K. Khillan, Yi Su, Rohit Dikshit, Yuri Lvov, Kody Varahramyan. *Sensors and Actuators B* 114(2006)218-222.
- [31] Z. Opilski, T. Pustelney, E. Maciak, M. Bednorz, A. Stoarczyk, M. Jadamiec. *Bull. Poli. Acad. Sci. Tec. Sci.* vol 53, no 2, 2005.
- [32] M. Matsuguchi, A. Okamoto, Y. Sakai, *Sensors and Actuators B* 94(2003)46-52.
- [33] F. Qu, M. Yang, J. Jiang, G. Shen, R. Yu. *Analytical Biochemistry* 344(2005)108-114.
- [34] Y. C. Luo, J. S. Do, *Sensors and Actuators B* 115(2006)102-108.

Chapter 15

**SELECTIVE ETHYLBENZENE OXIDATION INTO
 α -PHENYLETHYLHYDROPEROXIDE WITH DIOXYGEN
IN THE PRESENCE OF TRIPLE CATALYTIC SYSTEMS
INCLUDING BIS (ACETYLACETONATE) Ni(II) AND
ADDITIVES OF ELECTRON-DONOR COMPOUND L^2
AND PHENOL AS EXO LIGANDS**

L. I. Matienko and L. A. Mosolova*

Emanuel Institute of Biochemical Physics,
Russian Academy of Sciences,
4 Kosygin str., Moscow, 119991 Russia

ABSTRACT

The economically acceptable method of co-production of propylene oxide and styrene monomers with the use of α -phenylethylhydroperoxide (PEH) provides high cleanness of initial hydroperoxide, which is produced by the ethylbenzene oxidation with dioxygen or air in the presence of initiator or catalyst. This article is devoted to phenomena we discovered i.e. synergetic effects of increase in the selectivity (S_{PEH}) and the maximum PEH concentration as well as the conversion degree (C) of ethylbenzene oxidation with dioxygen into α -phenylethylhydroperoxide (PEH) (at the selectivity $S_{PEH} = 85-90\%$) in the presence of three – component catalytic systems. These triple systems include the nickel (II) bis (acetylacetonate) ($Ni(II)(acac)_2$) and the additives of two exo ligands – modifiers: electron-donor compound L^2 and phenol. The values of conversion degree and PEH yield we reach by applying those triple systems exceed parameters analogous to above ones in the presence of binary systems $\{Ni(II)(acac)_2+L^2\}$, that we proposed and optimized, and known catalysts of ethylbenzene oxidation into PEH. The mechanism of control of the selective ethylbenzene oxidation into PEH by triple catalytic systems is discussed.

* E-mail:matienko@sky.chph.ras.ru

Keywords: *monomers propylene oxide and styrene, selective oxidation, dioxygen, ethylbenzene, α -phenylethylhydroperoxide, nickel (II) bis (acetylacetonate), N-methylpyrrolidon-2, HMPA, MSt (M=Na, K), PhOH.*

1. INTRODUCTION

In spite of theoretical interest the problem of selective oxidation of alkylarens (ethylbenzene and cumene) with dioxygen in ROOH, primary products of RH oxidation, is of current importance from practical point of view in connection with ROOH use in large-tonnage productions such as production of monomers propylene oxide and styrene (α -phenylethylhydroperoxide (PEH)), or phenol and acetone (cumyl hydroperoxide) [1]. Propylene oxide is produced by epoxidation of propylene with PEH, which is in turn produced by oxidation of ethylbenzene in the presence of initiator or catalyst [1]. The by-product of the epoxidation, methyl phenyl carbinol (MPC), is later dehydrated to yield the monomer styrene. The selectivity ethylbenzene oxidation into PEH in the presence of the majority of the known catalytic systems is not higher than 90% and at the very small RH conversion degree (≤ 5 -10%) [2-6]. We proposed for the first time the method of control of the selectivity and the conversion degree of the ethylbenzene and cumene oxidations into corresponding ROOH in the presence of nickel complexes with different electron-donor ligands – modifiers [7-12]. This method allows carrying out the selective oxidation of ethylbenzene and cumene into corresponding ROOH with the high selectivity $S_{\text{ROOH}}(\geq 90\%)$, the conversion degree C ($\sim 19\%$ for ethylbenzene [12] and $\sim 45\%$ for cumene [8]) and also ROOH yield, that higher than the corresponding parameters in the industrial processes [1] and in the known catalytic oxidations. Thus, in our processes, the oxidations into ROOH are carried out through the only stage unlike of the industrial two stages of oxidations of ethylbenzene and cumene [1]. On the basis of the established mechanism of control of Ni(II)(acac)₂ catalytic activity by monodentate ligands-modifiers L^2 in ethylbenzene oxidation, we proposed the optimization methods of selective ethylbenzene oxidation into α -phenylethylhydroperoxide. These extraordinary methods include the use of macrocycle polyesters (18-crown-6) or quaternary ammonium salts R₄NBr (Me₄NBr) as exo ligands-modifiers L^2 [11, 12]. But those methods have one essential defect – the transformation of the catalytic active complexes into inactive particles in the course of oxidation that results in the sharp decrease of S_{PEH} .

One of the most effective methods of control of selective ethylbenzene oxidation into α -phenylethylhydroperoxide with dioxygen may be the application of the third component of catalytic system – phenol (PhOH) along with Ni(II)(acac)₂ and the additives of electron-donor compounds (ligands) L^2 . PhOH is the product of ethylbenzene oxidation, catalyzed by Ni(II)(acac)₂. We established previously that the sharp decrease of rate and selectivity of ethylbenzene oxidation into PEH, catalyzed by Ni(II)(acac)₂, at the initial stages of oxidation is connected with formation of complex Ni(II)(acac)₂·PhOH that was an effective inhibitor of the ethylbenzene oxidation: under the action of Ni(II)(acac)₂·PhOH, heterolytic decomposition of PEH into PhOH and acetaldehyde took place, and also Ni(II)(acac)₂·PhOH terminated the chains of oxidation reacting with RO₂[•] - radicals [13,14]. The method of

control of selective ethylbenzene oxidation into PEH with the use of triple systems $\{\text{Ni(II)(acac)}_2 + \text{L}^2 + \text{PhOH}\}$ is considered in this article.

2. EXPERIMENTAL

Ethylbenzene (RH) oxidation was studied at 120°C in glass bubbling-type reactor in the presence of Ni(II)(acac)_2 and additives of L^2 ($\text{L}^2 = \text{N-methylpyrrolidone-2 (MP)}$, $\text{HMPA MSt (M=Na, Li)}$) and PhOH . The selectivity S_{PEH} and RH conversion degree C of ethylbenzene into PEH oxidation were determined using the formulas: $S_{\text{PEH}} = [\text{PEH}] / \Delta[\text{RH}] \cdot 100\%$ and

$$C = \Delta[\text{RH}] / [\text{RH}]_0 \cdot 100\%.$$

Analysis of Oxidation Products

α -Phenylethylhydroperoxide was analyzed by iodometry. By-products (P), including methylphenylcarbinol (MPC) acetophenone (AP), and phenol (PhOH), as well as the RH content in the process were examined by GLC [6-11]. The $[\text{PhOH}]$ in the products of ethylbenzene oxidation was determined as $\{[\text{PhOH}] - [\text{PhOH}]^0\}$, $[\text{PhOH}]$ – the concentration of phenol in probes examined by GLC, $[\text{PhOH}]^0$ – the concentration of phenol added into reaction.

The overall rate of the process was determined from the rate of accumulation of all oxidation products. A correlation between RH consumption and product accumulation was established: $\Delta[\text{RH}] = [\text{PEH}] + [\text{P}] + [\text{PhOH}]$, where $\text{P} = \text{AP} + \text{MPC}$.

The overall reaction rate of reaction (w) and the rates of product accumulation (w_p) were determined with accuracy of $\pm 0.5 - 5\%$ [10]. The catalytic ethylbenzene oxidation with dioxygen was carried out in the O_2 – solution two phase systems under kinetic control.

The order in which PEH, AP, and MPC formed was determined from the time dependence of product accumulation rate rations at $t \rightarrow 0$. The variation of these rations with time was evaluated by graphic differentiation [17].

3. RESULTS AND DISCUSSION

We observed a significant increase in parameters of the selective ethylbenzene oxidation: conversion degree C ($S_{\text{PEH}} = 85-90\%$) (Figure 1, Table 1) and $[\text{PEH}]^{\text{max}}$ (Figure 3, Table 1), - in the presence of triple systems $\{\text{Ni(II)(acac)}_2 + \text{L}^2 + \text{PhOH}\}$ ($\text{L}^2 = \text{MP}$, $\text{HMPA MSt (M=Na, Li)}$) as compared with the catalysis by binary system $\{\text{Ni(II)(acac)}_2 + \text{L}^2\}$. In this case the value of S_{PEH} is high (about 85-90%) both at the beginning of the reaction and at the significant depth of the process unlike the catalysis by $\{\text{Ni(II)(acac)}_2 + \text{L}^2\}$. In the latter case, the dependence of S_{PEH} on C has a well-defined extremum. For example, in the case of $\{\text{Ni(II)(acac)}_2 + \text{MP}\}$ $S_{\text{PEH}}^{\text{max}} = 85 - 87\%$ at $C \sim 8 - 10\%$ (Figure 1, Table 1).

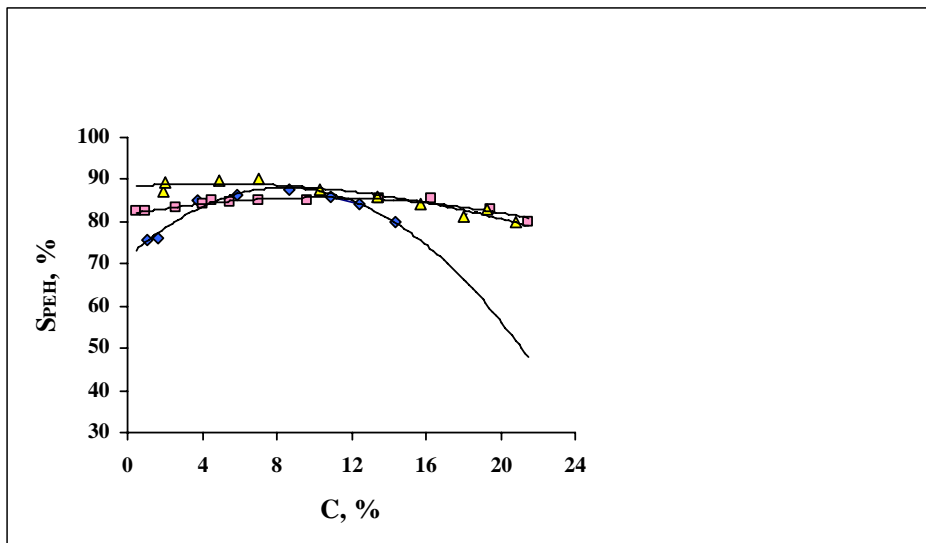


Figure 1. Dependence of S_{PEH} on C in reaction of ethylbenzene oxidation catalyzed by binary system $\{\text{Ni(II)(acac)}_2 + \text{MP}\}$ (◆) and two triple systems $\{\text{Ni(II)(acac)}_2 + \text{MP} + \text{PhOH}\}$ with $[\text{PhOH}] = 3 \cdot 10^{-3} \text{ mol l}^{-1}$ (◻) or $4.6 \cdot 10^{-4} \text{ mol l}^{-1}$ (Δ) and $[\text{Ni(II)(acac)}_2] = \text{const} = 3 \cdot 10^{-3} \text{ mol l}^{-1}$, and $[\text{MP}] = \text{const} = 7 \cdot 10^{-2} \text{ mol l}^{-1}$, 120°C .

Table 1. The values of parameters of, $C_{S \geq 80\%}$, $[\text{PEH}]^{\text{max}}$, $\tilde{S} \cdot C$ in reactions of ethylbenzene oxidation in the presence of triple catalytic systems $\{\text{Ni(II)(acac)}_2 + \text{L}^2 + \text{PhOH}\}$. $[\text{Ni(II)(acac)}_2] = 3.0 \cdot 10^{-3} \text{ mol l}^{-1}$, 120°C

L^2 ($[\text{L}^2]$, mol l^{-1})	$[\text{PhOH}]$, mol l^{-1}	$\tilde{S} \cdot C \cdot 10^{-2} (\%, \%)$	C (%)	$[\text{PEH}]^{\text{max}}$ (% mass)
NaSt ($3.0 \cdot 10^{-3}$)	$3.0 \cdot 10^{-3}$	30.1	>35.0	27
NaSt ($3.0 \cdot 10^{-3}$)	—	10.9	14.2	16
LiSt ($3.5 \cdot 10^{-3}$)	$1.0 \cdot 10^{-3}$	20.6	24.0	26.0
LiSt ($3.5 \cdot 10^{-3}$)	—	14.4	18.0	19.0
HMFA ($2.0 \cdot 10^{-2}$)	$1.0 \cdot 10^{-3}$	16.2	19.0	20.0
HMFA ($2.0 \cdot 10^{-2}$)	—	11.1	14.0	17.5
MII ($7.0 \cdot 10^{-2}$)	$3.0 \cdot 10^{-3}$	17.5	21.0	21.0
MII ($7.0 \cdot 10^{-2}$)	$4.6 \cdot 10^{-4}$	18.1	21.0	21.0
MII ($7.0 \cdot 10^{-2}$)	—	11.9	12.2	17.5

As is evident, phenomenal results were obtained in the case of application of system, including NaSt as L^2 $\{\text{Ni(II)(acac)}_2 (3.0 \cdot 10^{-3} \text{ mol l}^{-1}) + \text{NaSt} (3.0 \cdot 10^{-3} \text{ mol l}^{-1}) + \text{PhOH} (3.0 \cdot 10^{-3} \text{ mol l}^{-1})\}$ (Table 1). Parameter $C > 35\%$ at the $S_{PEH}^{\text{max}} = 85-87\%$. Concentration $[\text{PEH}]^{\text{max}} = 1.6-1.8 \text{ mol l}^{-1}$ (~27 mass %), that is higher than $[\text{PEH}]^{\text{max}}$ for all binary catalytic

systems $\{\text{Ni(II)(acac)}_2 + \text{L}^2\}$ studied by us earlier and also the most effective triple catalytic systems $\{\text{Ni(II)(acac)}_2 + \text{L}^2 + \text{PhOH}\}$. Parameter $\tilde{S} \cdot C$ (see below) $\sim 30.1 \cdot 10^2$ (%,%) is much higher, than in the case the other triple systems and the most active binary systems [12]. The data presented in Table 1 are protected by patent RU No.2237050. Registration date is 11.2.2004; the authors are L.I. Matienko, L.A. Mosolova, patent holder is Emanuel Institute of Biochemical Physics, Russian Academy of Sciences.

For estimation of efficiency of selective ethylbenzene oxidation into α -phenylethylhydroperoxide in the presence of triple systems we proposed to use parameter $\tilde{S} \cdot C$ [15]. \tilde{S} is averaged selectivity of oxidation into PEH characterizing change of S in the course of oxidation from S^0 at the beginning of reaction to some S^{lim} conditional value chosen as a standard $S^0 < S \leq S^{\text{lim}}$. For comparable by value systems selectivity as S^{lim} was selected the value $S^{\text{lim}} = 80\%$ approximately equal to selectivity of non-catalyzed ethylbenzene oxidation into PEH at initial stages of reaction. C – conversion degree at $S = S^{\text{lim}}$. We established that efficiency of catalytic system $\{\text{M(L}^1)_2 + \text{L}^2\}$ ($\text{M}=\text{Ni(II)}$, $\text{L}^1=\text{acac}^-$, $\text{L}^2= \text{MSt}$ ($\text{M}=\text{Na, Li}$) N -methylpyrrolidone-2, HMPA) estimated by the value of parameter $\tilde{S} \cdot C$ was significantly increased in the presence of PhOH.

Mechanism of selective ethylbenzene oxidation into α -phenylethylhydroperoxide in the presence of triple systems is demonstrated here on the example of $\{\text{Ni(II)(acac)}_2 + \text{MP} + \text{PhOH}\}$ system. While investigating dependence of parameter $\tilde{S} \cdot C$ on $[\text{MP}]$ in oxidation reaction in the presence of $\{\text{Ni(II)(acac)}_2 + \text{MP} + \text{PhOH}\}$ at $[\text{Ni(II)(acac)}_2]=\text{const}=3 \cdot 10^{-3}$ mol l^{-1} and $[\text{PhOH}]=\text{const}=3 \cdot 10^{-3}$ mol l^{-1} (120°C) it turned out that dependence is extreme (Table 2).

Table 2. Parameter $\tilde{S} \cdot C \cdot 10^{-2}$ (%,%) versus $[\text{MP}]$ in the ethylbenzene oxidation upon catalysis by the system $\{\text{Ni(II)(acac)}_2 + \text{L}^2 + \text{PhOH}\}$ ($\text{L}^2=\text{MP}$), $[\text{Ni(II)(acac)}_2]=[\text{PhOH}]=\text{const}=3 \cdot 10^{-3}$ mol l^{-1} , 120°C

$[\text{MP}], \text{mol l}^{-1}$	$\tilde{S} \cdot C \cdot 10^{-2}(\%,\%)$
0	0
$0.3 \cdot 10^{-2}$	0.29
$3.0 \cdot 10^{-2}$	11.30
$7.0 \cdot 10^{-2}$	17.50
$21.0 \cdot 10^{-2}$	11.20
$20.0 \cdot 10^{-2}$ *	11.00

* $[\text{PhOH}]=0$.

Table 3. Dependence of $\tilde{S} \cdot C \cdot 10^{-2}$ (%,%) on $[\text{Ni(II)(acac)}_2]$ in reaction of ethylbenzene oxidation catalyzed by $\{\text{Ni(II)(acac)}_2 + \text{MP} + \text{PhOH}\}$. $[\text{PhOH}]=\text{const}=3 \cdot 10^{-3}$ mol l^{-1} , $[\text{MP}]=\text{const}=7 \cdot 10^{-2}$ mol l^{-1} , 120°C

$[\text{Ni(II)(acac)}_2], \text{mol l}^{-1}$	$\tilde{S} \cdot C \cdot 10^{-2}(\%,\%)$
$1.0 \cdot 10^{-3}$	15.41
$3.0 \cdot 10^{-3}$	17.47
$5.0 \cdot 10^{-3}$	12.65

Maximum value of $\tilde{S}\cdot C$ is reached at $[MP] = 7 \cdot 10^{-2} \text{ mol l}^{-1}$ ($\tilde{S}^{\max}=85-87\%$). Concentration $[MP] = 7 \cdot 10^{-2} \text{ mol l}^{-1}$ corresponds to formation of complexes of Ni(II)(acac)_2 with MP of structure 1:1 (in the absence of PhOH) [29]. It is characteristic that the value $(\tilde{S}\cdot C)^{\max} = 17.5 \cdot 10^2 (\%,\%)$ exceeds value $\tilde{S}\cdot C$ for complexes $\text{Ni(II)(acac)}_2\cdot\text{MP}$ ($11.9 \cdot 10^2 (\%,\%)$) and coordinated saturated complexes $\text{Ni(II)(acac)}_2\cdot 2\text{MP}$. Observing significant synergetic effect of parameter $\tilde{S}\cdot C$ increase under catalysis by $\{\text{Ni(II)(acac)}_2 + \text{L}^2\}$ in the presence of inhibitor phenol may be explained by unusual catalytic activity of formed triple complexes $\text{Ni(II)(acac)}_2\cdot(\text{L}^2)\cdot(\text{PhOH})$ [16]. This presumption is confirmed by dependences of $\tilde{S}\cdot C$ on $[\text{Ni(II)(acac)}_2]$ at $[\text{PhOH}]=\text{const}=3 \cdot 10^{-3} \text{ mol l}^{-1}$ and $[\text{MP}]=\text{const}=7 \cdot 10^{-2} \text{ mol l}^{-1}$ ($(\tilde{S}\cdot C)^{\max}=17.47 \cdot 10^2 (\%,\%)$ at $[\text{Ni(II)(acac)}_2]=3 \cdot 10^{-3} \text{ mol l}^{-1}$) (Table 3), and also of $\tilde{S}\cdot C$ on $[\text{PhOH}]$ at $[\text{Ni(II)(acac)}_2]=\text{const}=3 \cdot 10^{-3} \text{ mol l}^{-1}$ and $[\text{MP}]=\text{const}=7 \cdot 10^{-2} \text{ mol l}^{-1}$. In the latter case $\tilde{S}\cdot C$ reaches the extremum ($\tilde{S}\cdot C)^{\max}=17.5$ and $(\tilde{S}\cdot C)^{\max}=18.12 \cdot 10^2 (\%,\%)$ at two $[\text{PhOH}]$ concentrations differing by an order of magnitude : $[\text{PhOH}] = 3 \cdot 10^{-3}$ and $4.6 \cdot 10^{-4} \text{ mol l}^{-1}$ accordingly (Figure 1, 2)

Obtained data (Figure 1, 2) testify on the fact that in both these cases selective ethylbenzene oxidation into PEH is connected with formation in the course of oxidation of catalytically active complexes with composition 1:1:1. The confirmation of triple complexes of composition 1:1:1 formation in the process came from the comparison of kinetics of accumulation of the products of ethylbenzene oxidation catalyzed by two triple systems $\{\text{Ni(II)(acac)}_2(3 \cdot 10^{-3} \text{ mol l}^{-1}) + \text{MP}(7 \cdot 10^{-2} \text{ mol l}^{-1}) + \text{PhOH}\}$ at $[\text{PhOH}] = 3 \cdot 10^{-3}$ or $[\text{PhOH}] = 4.6 \cdot 10^{-4} \text{ mol l}^{-1}$. The some differences observed at the initial stages of two reactions are caused obviously by the different initial conditions of triple complexes $\text{Ni(II)(acac)}_2\cdot(\text{L}^2)\cdot(\text{PhOH})$ formation in the course of catalytic ethylbenzene oxidation in these cases.

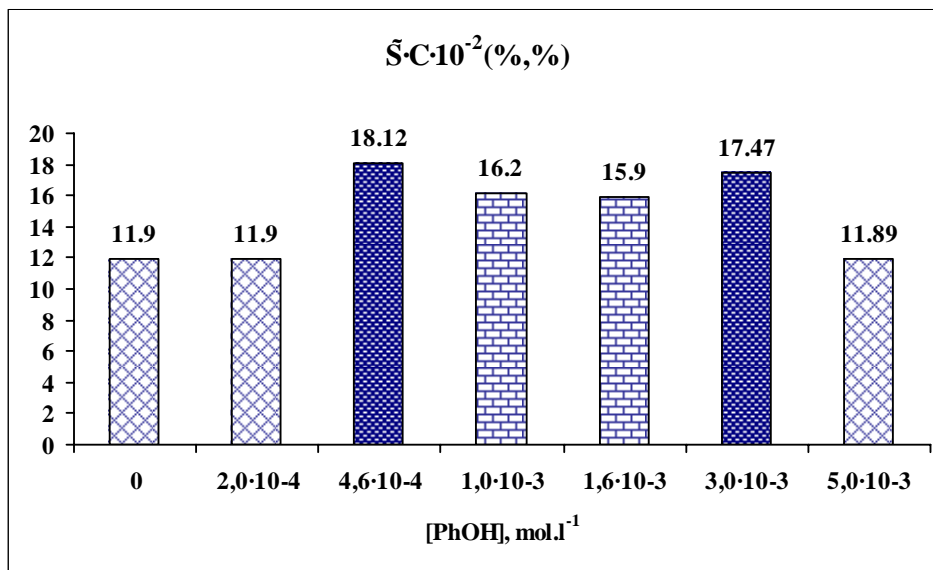


Figure 2. Dependence of parameter $\tilde{S}\cdot C \cdot 10^{-2} (\%,\%)$ on $[\text{PhOH}]$ in reaction of ethylbenzene oxidation catalyzed by $\{\text{Ni(II)(acac)}_2 + \text{MP} + \text{PhOH}\}$. $[\text{Ni(II)(acac)}_2] = \text{const} = 3 \cdot 10^{-3} \text{ mol l}^{-1}$, $[\text{MP}] = \text{const} = 7 \cdot 10^{-2} \text{ mol l}^{-1}$. 120°C .

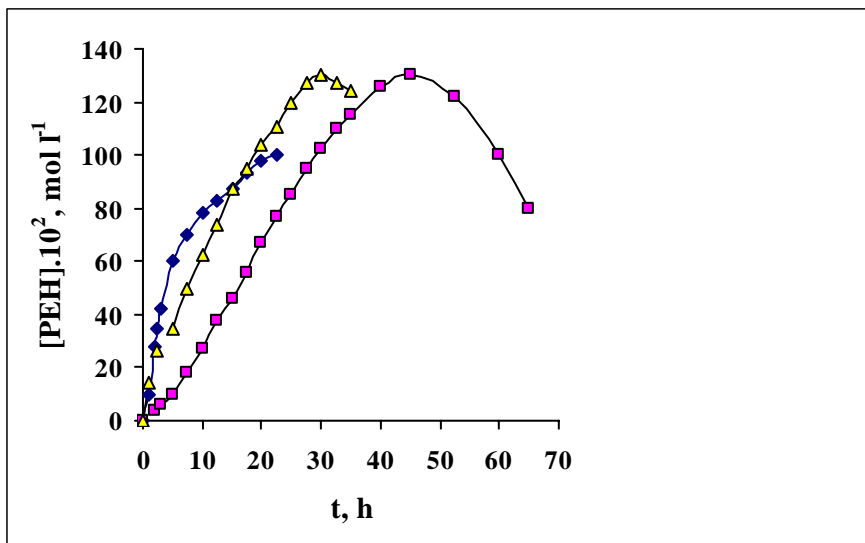


Figure 3. Kinetics of accumulation of PEH in reaction of ethylbenzene oxidation catalyzed by binary system $\{\text{Ni(II)(acac)}_2+\text{MP}\}$ (\blacklozenge) and two triple systems $\{\text{Ni(II)(acac)}_2 + \text{M} + \text{PhOH}\}$ with variable values of $[\text{PhOH}] = 3 \cdot 10^{-3} \text{ mol l}^{-1}$ (\square) or $4.6 \cdot 10^{-4} \text{ mol l}^{-1}$ (\triangle) and $[\text{Ni(II)(acac)}_2] = \text{const} = 3 \cdot 10^{-3} \text{ mol l}^{-1}$, and $[\text{MP}] = \text{const} = 7 \cdot 10^{-2} \text{ mol l}^{-1}$. 120°C .

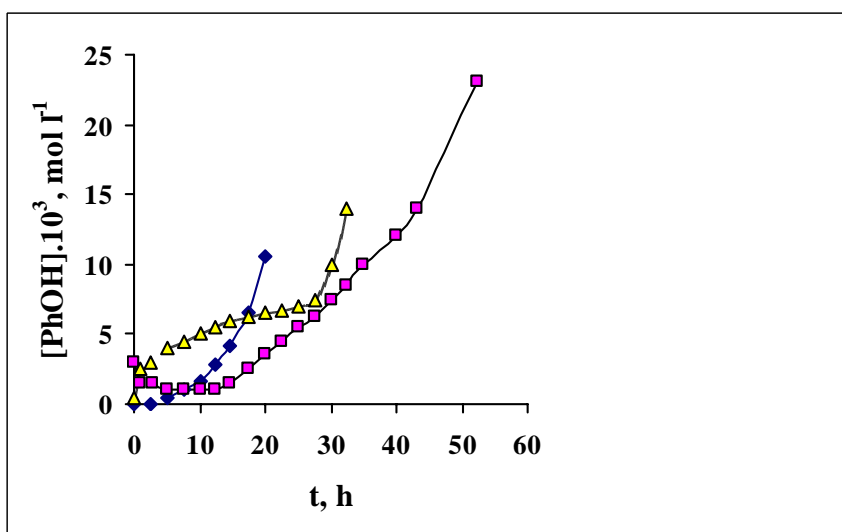


Figure 4. Kinetics of accumulation of PhOH in reaction of ethylbenzene oxidation catalyzed by binary system $\{\text{Ni(II)(acac)}_2+\text{MP}\}$ (\blacklozenge) and two triple systems $\{\text{Ni(II)(acac)}_2 + \text{MP} + \text{PhOH}\}$ with variable values of $[\text{PhOH}] = 3 \cdot 10^{-3} \text{ M}$ (\square) or $4.6 \cdot 10^{-4} \text{ M}$ (\triangle) and $[\text{Ni(II)(acac)}_2] = \text{const} = 3 \cdot 10^{-3} \text{ mol l}^{-1}$, and $[\text{MP}] = \text{const} = 7 \cdot 10^{-2} \text{ mol l}^{-1}$. 120°C .

At catalysis by triple system $\{\text{Ni(II)(acac)}_2+\text{MP}+\text{PhOH}\}$ with small $[\text{PhOH}] = 4.6 \cdot 10^{-4} \text{ mol l}^{-1}$ the increase in values of the initial rates of PEH (Figure3) (and of AP and MPC also) accumulation may be due to the formation of complexes of structure $(\text{Ni(II)(acac)}_2)_m \cdot (\text{L}^2)_n \cdot (\text{PhOH})_q$. The fast increase in the concentration of PhOH right up to

$[\text{PhOH}] = (3\text{--}5) \cdot 10^{-3} \text{ mol l}^{-1}$ (at $t=0\text{--}5 \text{ h}$) is observed. $[\text{PhOH}] = (3\text{--}5) \cdot 10^{-3} \text{ mol l}^{-1} \sim$ corresponds to $[\text{PhOH}]$ for the first combination $\{\text{Ni(II)(acac)}_2 (3.0 \cdot 10^{-3} \text{ mol l}^{-1}) + \text{MP} (7.0 \cdot 10^{-2} \text{ mol l}^{-1}) + \text{PhOH} (3.0 \cdot 10^{-3} \text{ mol l}^{-1})\}$ and to the formation of complexes of structure $[\text{M(L}^1)_2 \cdot (\text{L}^2) \cdot (\text{PhOH})]$ (Figure 4). Then at 8 – 30 h the concentration of PhOH increased slowly up to $[\text{PhOH}] \sim 7.5 \cdot 10^{-3} \text{ mol l}^{-1}$. The increase in the rate of PhOH accumulation at the beginning of the process may be due to the function of PhOH as acid that becomes stronger because of outer sphere coordination of PhOH with nickel complex $\text{Ni(II)(acac)}_2 \cdot \text{MP}$ [17], and this effect favors to heterolysis of PEH with the formation of phenol. This supposition is confirmed by the following facts. So the accumulation of PhOH, but not the consumption, at the maximum initial rate $w_{\text{PhOH}}^0 = w_{\text{PhOH}}^{\text{max}}$ is observed upon addition of PhOH ($3.0 \cdot 10^{-3} \text{ mol l}^{-1}$) into the reaction of ethylbenzene oxidation catalyzed by coordinated saturated complexes $\text{Ni(II)(acac)}_2 \cdot 2\text{MP}$ ($[\text{Ni(II)(acac)}_2] = 3.0 \cdot 10^{-3} \text{ mol l}^{-1}$, $[\text{MP}] = 2.1 \cdot 10^{-1} \text{ mol l}^{-1}$) (Figure 5, (Table 2)), and also in the case of the ethylbenzene oxidation catalyzed by binary system $\{\text{Ni(II)(acac)}_2(3.0 \cdot 10^{-3} \text{ mol l}^{-1}) + \text{PhOH}(4.6 \cdot 10^{-4} \text{ mol l}^{-1})\}$ at $[\text{MP}] = 0$ (unpublished data).

The observed catalytic effect in the presence of $\{\text{Ni(II)(acac)}_2(3.0 \cdot 10^{-3} \text{ mol l}^{-1}) + \text{MP}(7.0 \cdot 10^{-2} \text{ mol l}^{-1}) + \text{PhOH}(4.6 \cdot 10^{-4} \text{ mol l}^{-1})\}$ (Figure 1,3) are not caused by the action of binary systems $\{\text{Ni(II)(acac)}_2(3.0 \cdot 10^{-3} \text{ mol l}^{-1}) + \text{PhOH}(4.6 \cdot 10^{-4} \text{ mol l}^{-1})\}$ or $\{\text{MP}(7.0 \cdot 10^{-2} \text{ mol l}^{-1}) + \text{PhOH}(4.6 \cdot 10^{-4} \text{ mol l}^{-1})\}$. Actually, in the reaction of ethylbenzene oxidation in the presence of system $\{\text{Ni(II)(acac)}_2(3.0 \cdot 10^{-3} \text{ mol l}^{-1}) + \text{PhOH}(4.6 \cdot 10^{-4} \text{ mol l}^{-1})\}$, the maximum selectivity only $S_{\text{PEH}}^{\text{max}}=75\%$ at very small $C \leq 2\%$, and then at $C > 2\%$ S_{PEH} fast decreases. In the presence of system $\{\text{MP}(7.0 \cdot 10^{-2} \text{ mol l}^{-1}) + \text{PhOH}(4.6 \cdot 10^{-4} \text{ mol l}^{-1})\}$ the oxidation proceeds as in the absence of additives of PhOH, and that is practically non-catalyzed oxidation.

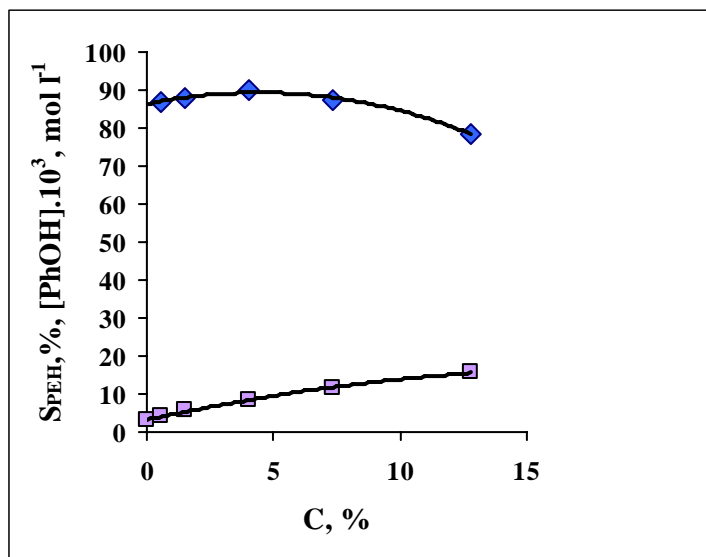


Figure 5. The dependences of S_{PEH} (◇) and $[\text{PhOH}]$ (□) on C in reaction of ethylbenzene oxidation in the presence of triple system $\{\text{Ni(II)(acac)}_2 (3.0 \cdot 10^{-3} \text{ mol l}^{-1}) + \text{MP} (2.1 \cdot 10^{-1} \text{ mol l}^{-1}) + \text{PhOH} (3.0 \cdot 10^{-3} \text{ mol l}^{-1})\}$. 120°C .

In the case of the combination $\{\text{MP}(7.0 \cdot 10^{-2} \text{ mol l}^{-1}) + \text{PhOH}(3.0 \cdot 10^{-3} \text{ mol l}^{-1})\}$ (value of $[\text{PhOH}]$ is 10 times higher) the maximum selectivity $S_{\text{PEH}}^{\text{max}} \approx 85\%$ at the initial stages of the process, and then S_{PEH} fast decreases.

The consumption of PhOH at the beginning of the process in the presence of the catalytic system $\{\text{Ni(II)(acac)}_2 (3.0 \cdot 10^{-3} \text{ mol l}^{-1}) + \text{MP} (7.0 \cdot 10^{-2} \text{ mol l}^{-1}) + \text{PhOH} (3.0 \cdot 10^{-3} \text{ mol l}^{-1})\}$ with $[\text{PhOH}] = 3.0 \cdot 10^{-3} \text{ mol l}^{-1}$ (Figure4) may be due to the formation of the triple complexes $\text{Ni(II)(acac)}_2 \cdot (\text{L}^2) \cdot (\text{PhOH})$ and least of all due to consumption of PhOH as inhibitor in the reaction of chain termination, $\text{PhOH} + \text{RO}_2^\bullet \rightarrow$. Actually the rate of PhOH consumption is unchanged in fact over a wide range of MP concentrations $[\text{MP}] = (0.3 - 7.0) \cdot 10^{-2} \text{ mol l}^{-1}$. We established previously that the rate of RO_2^\bullet - radicals formation in the ethylbenzene oxidation catalyzed by $\text{Ni(II)(acac)}_2 (3.0 \cdot 10^{-3} \text{ mol l}^{-1})$ upon of additives of MP increased significantly due to increase in activity of the formed complexes $\text{Ni(II)(acac)}_2 \cdot \text{MII}$ at the stages of chain initiation (O_2 activation) and homolytic decomposition of PEH [7].

Similarity of phenomenology of ethylbenzene oxidation in the presence of $\{\text{Ni(II)(acac)}_2 (3.0 \cdot 10^{-3} \text{ mol l}^{-1}) + \text{MP} (7.0 \cdot 10^{-2} \text{ mol l}^{-1}) + \text{PhOH} (3.0 \cdot 10^{-3} \text{ mol l}^{-1})\}$ and $\{\text{Ni(II)(acac)}_2 (3.0 \cdot 10^{-3} \text{ mol l}^{-1}) + \text{NaSt} (3.0 \cdot 10^{-3} \text{ mol l}^{-1}) + \text{PhOH} (3.0 \cdot 10^{-3} \text{ mol l}^{-1})\}$ allows assuming analogous mechanism of selective catalysis realizing by triple complexes formed in the course of oxidations. Also, the parallel formation of PEH and side products AP and MPC is established in these two cases: $w_{\text{P}}/w_{\text{PEH}} \neq 0$ at $t \rightarrow 0$ ($\text{P} = \text{AP}$ or MPC) and $w_{\text{AP}}/w_{\text{MPC}} \neq 0$ at $t \rightarrow 0$ at the beginning of reaction and in developed reaction of ethylbenzene oxidation catalyzed by $\{\text{Ni(II)(acac)}_2 + \text{L}^2 + \text{PhOH}\}$ ($\text{L}^2 = \text{NaSt}, \text{MP}$). Increase in S_{PEH} during the catalysis by complexes $\text{Ni(II)(acac)}_2 \cdot \text{L}^2 \cdot \text{PhOH}$ ($\text{L}^2 = \text{NaSt}, \text{MP}$) in comparison with non-catalyzed oxidation is connected with the change of direction of the formation of side products AP and MPC (AP and MPC are not formed from PEH, as it takes place in non-catalyzed oxidation) and also with hindering of heterolytic decomposition of PEH.

CONCLUSION

Thus, in this article we discuss phenomenon that we discovered i.e.: the considerable increase in the efficiency of selective ethylbenzene oxidation reaction into α -phenylethylhydroperoxide with dioxygen in the presence of triple systems $\{\text{Ni(II)(acac)}_2 + \text{L}^2 + \text{PhOH}\}$, estimated by parameters $\tilde{S} \cdot C$, the conversion degree C (at $S_{\text{PEH}} \sim 85\text{-}90\%$), and the hydroperoxide contents ($[\text{PEH}]^{\text{max}}$), in comparison with catalysis by binary systems $\{\text{Ni(II)(acac)}_2 + \text{L}^2\}$. The obtained synergetic effects of increase in those parameters is caused by the formation of catalytic active triple complexes $\text{Ni(II)(acac)}_2 \cdot \text{L}^2 \cdot \text{PhOH}$. The advantage of the triple systems consists in the fact that the formed *in situ* complexes $\text{Ni(II)(acac)}_2 \cdot \text{L}^2 \cdot \text{PhOH}$ are active for a long time, and are not transformed in the course of the process into inactive particles. Thus, the application of triple systems, including Ni(II)(acac)_2 , electron donor ligand L^2 and PhOH, as homogeneous catalysts is one of the most effective methods of control of selective ethylbenzene oxidation by dioxygen into PEH.

The interesting phenomenon was established. Depending on the ligand surrounding of nickel ion, the PhOH becomes both effective as a deactivating ligand and as an effective activating ligand. In the absence of the exo ligand L^2 the coordination of PhOH to Ni(II)(acac)_2 is favorable to heterolytic decomposition of PEH and inhibition of the

ethylbenzene oxidation. In the presence of the exo ligand L^2 the formed triple $Ni(II)(acac)_2 \cdot L^2 \cdot PhOH$ complexes, that include PhOH, are the effective catalysts of the selective ethylbenzene oxidation into α -phenylethylhydroperoxide with molecular O_2 .

REFERENCES

- [1] K. Weissermel, H.-J. Arpe, *Industrial Organic Chemistry*, 3rd ed., transl. by C.R. Lindley. New York, VCH, 1997, 427 pp.
- [2] N.M. Emanuel, *Uspekhi khimii*, Vol. 47, N 8, pp. 1329-1396, 1978 (in Russian).
- [3] N.M. Emanuel, D. Gal, *Ethylbenzene oxidation. Model reaction*, Moscow, Nauka, 1984, 375 pp. (in Russian).
- [4] Yu.D. Norikov, E.A. Blyumberg, L.V. Salukvadze, *Problemy kinetiki i kataliza*, Moscow, *Nauka*, Vol. 16, pp.150-165, 1975 (in Russian).
- [5] M.V. Nesterov, V.A. Ivanov, V.M. Potekhin, V.A. Proskuryakov, M.Yu. Lysukhin, *Zh. Prikl. Khimii*, Vol. 52, N 7, pp. 1585-1589, 1979 (in Russian).
- [6] P.P. Toribio, J.M. Campos-Martin, J.L.G. Fierro, *J. Mol. Catal. A: Chem.*, Vol. 227, pp. 101-105, 2005.
- [7] L.A. Mosolova L.I. Matienko, *Neftekhimiya*, Vol. 25, N 4, pp. 540-545, 1985 (in Russian).
- [8] L.A. Mosolova, L.I. Matienko, I.P. Skibida, *Kinetika i kataliz*, Vol. 29, N 5, pp. 1078-1083, 1988 (in Russian).
- [9] L.A. Mosolova, L.I. Matienko, I.P. Skibida, *Kinetika i kataliz*, Vol. 28, N 2, pp. 479-484, 1987 (in Russian).
- [10] L.A. Mosolova, L.I. Matienko, I.P. Skibida, *Kinetika i kataliz*, Vol. 28, N 2, pp. 484-488, 1987 (in Russian).
- [11] L.A. Mosolova, L.I. Matienko, I.P. Skibida, *Izv. AN SSSR, Ser. Khim.*, N 8, pp. 1406-1412, 1994 (in Russian).
- [12] L.A. Mosolova, L.I. Matienko, I.P. Skibida, *Izv. AN SSSR, Ser. Khim.*, N 8, pp. 1412-1417, 1994 (in Russian).
- [13] L.I. Matienko, Z.K. Maizus, *Kinetika i kataliz*, Vol. 15, N 2, pp. 317-322, 1974 (in Russian).
- [14] L.A. Mosolova, L.I. Matienko, Z.K. Maizus, E.M. Brin, *Kinetika i kataliz*, Vol. 21, N 3, pp. 657-660, 1980 (in Russian).
- [15] L.I. Matienko, L.A. Mosolova, *Izv. AN SSSR, Ser. Khim.*, N 4, pp. 689-693, 1997 (in Russian).
- [16] V.A. Golodov, *Russ. Khim. Zh.*, Vol. 44, N 3, pp 45-57, 2000 (in Russian).
- [17] V. Gutmann. *Coord. Chem. Revs.*, Vol.8, N 1, pp.225-255, 1976.

Chapter 16

APPLICATION OF POLYPROPYLENE FIBER AND RECYCLED GLASS IN COMPONENT OF CEMENT- BASED COMPOSITE

*A. Sadrmomtazi and A. K. Haghi**

The University of Guilan, P. O. Box 3756, Rasht, Iran

ABSTRACT

A modern lifestyle, alongside the advancement of technology has led to an increase in the amount and type of waste being generated, leading to a waste disposal crisis. This study tackles the problem of the waste that is generated from carpet and glass. In order to dispose of or at least reduce the accumulation of certain kinds of waste, it has been suggested to reuse some of these waste materials to substitute a percentage of the primary materials used in the ordinary Portland cement concrete.

Fiber-reinforced cement-based materials have found increasing applications in residential housing construction. Currently, fiber-cement composite products can be largely found in nonstructural housing components, including siding and roofing materials. Advantages associated with fibers include widespread availability from renewable sources, high fiber tensile strength, high fiber modulus of elasticity, relatively low cost, and well-developed technology to extract the fibers. Fiber-cement composite products for residential housing have been generally limited to exterior applications, such as siding, and roofing. Their exterior use has been limited in the industry due to degradation to ambient wetting and drying. Thus, these components must be currently maintained by painting to avoid moisture problems. Key points of this investigation are to evaluate the application of Polypropylene fibers in a cement-based composite containing recycled glass. This current study concentrates on those waste materials to be used as substitutes for conventional materials, mainly aggregates, in ordinary Portland cement concrete (OPC) mixes.

* Corresponding author e-mail: Haghi@Guilan.ac.ir

1. INTRODUCTION AND OVERVIEW

While portland cement concrete is the most widely used manufactured material, plain concrete, mortars, and cement pastes are brittle, possess low tensile strength, and exhibit low tensile strains prior to failure. These shortcomings have been traditionally overcome by embedding within the cement-based material some other material with greater tensile strength. Today, fiber-cement composites can be found in products such as extruded non-pressure pipes and non-structural building materials, mainly thin-sheet products. Perhaps the most widely known are fiber-cement siding materials, which have been called “tomorrow’s growth product”

Because of the large amount of fibrous materials generated each year and the potential for significant benefit, a broad range of research has been conducted to convert the fibrous materials into useful products. The main intent of this chapter is to determine the technical feasibility of utilizing Geofibers for properties improvement of glass-concrete composites. The results are indicative of strong potentials for application of geofiber for the reinforcement of glass-concrete (“glasscrete”) composites. Meanwhile, using waste glass in this geofiber composite would contribute to cleaning the environment. Utilization of waste glass and reducing the landfilling can demonstrate the cost effectiveness of this project. This approach could have significant impact to the use of large amount waste glass and improve the performance of glass cement composites.

In general, waste glass produced can be sorted out as:

- building/automobile windows and doors;
- glassware and bottles;
- television tubes and light bulbs;
- others such as mirror and clock covers.

Among them, the first two are the major sources. Several domestic glass manufacturers have attempted to recycle the glass waste.

Waste recycling has become increasingly important for western society over the past few years. The European desire to increase recycling of glass, particularly that of glass bottles, has led to a large collect system in containers and a target of 75% of the collected glass (2.2 million tons) recycled by the year 2005 in France [1]. Nevertheless, there will still be 5% of collected glass (0.1 to 0.15 million tons) that is not recycled and must be disposed of, as glass can only be melted down after the removal of non-ferrous metals and other contaminants, which are mixed with the smallest glass fragments [2]. For the long period of disposal, it is predicted that the waste glass will corrode very slowly by contact with groundwater, and certain quantities of radionuclides will be released from the glass. Therefore, the waste glass corrosion and associated radionuclide release for the long-term are one of the most important phenomena to be evaluated for safety assessment of the disposal system [1].

Glass is a thermodynamically metastable, highly viscous liquid phase. When glass is placed in aqueous environments, various reactions, such as ion exchange, hydrolysis and transformation to more stable phases, occur simultaneously, and the effects of these reactions are generally referred to as “corrosion”. However, the glass corrosion allows the release of

radionuclides from glass, and the glass corrosion and associated radionuclide release for the long-term must be evaluated sufficiently [3].

Geofiber reinforcement is used nowadays in many applications. Geofiber reinforced concrete is also well understood. The use of geofiber as reinforcement for cementitious composites, however, is a relatively new field for which some detailed research is needed.

Concrete, the composite material consisting of aggregate held together by a hydraulic cementing agent, has been known to ancient civilizations. In spite of its worldwide popularity, the proliferation of concrete has been a mixed blessing [3]. If mixed or placed improperly or maintained inadequately, concrete structures can deteriorate prematurely and thereby contribute to the problems referred to generally as our “crumbling infrastructure”. Also the indiscriminate use of concrete without concern for esthetic appearance has led to the partially deserved reputation of concrete as being ugly. More significantly, the increased worldwide concern about environmental issues and the need to change our way of life for the sake of sustainable development has led to the identification of the concrete industry as a major user and abuser of natural resources and energy and as an important contributor to the release of greenhouse gases. These issues pose formidable challenges for the concrete industry for years to come. The construction community as well as the public at large will demand increased emphasis on environmentally friendly high-performance building materials at affordable cost. This implies not only excellent mechanical properties but durability as well. Fortunately, concrete materials science has emerged as a tool well suited to face these issues [4].

The introduction and development of advanced composite material opened the door to new and innovative application in civil and structural engineering. Key points of this investigation are to evaluate the application of geofiber in glass-concrete composites and:

- 1) To convert glass waste into useful product.
- 2) To consume glass wastes; this would otherwise go to landfill.
- 3) To protect the environment from being heavily contaminated

2. BACKGROUND

Since ancient times, natural fibers have been used to reinforce brittle materials. For example, thousands of years ago, Egyptians began using straw and horsehair to reinforce and improve the properties of mud bricks. In more recent times, large-scale commercial use of asbestos fibers in a cement paste matrix began with the invention of the Hatschek process in 1898. However primarily due to health hazards associated with asbestos fibers, alternate fiber types have been investigated and introduced throughout the 1960's and 1970's.

The use of composite materials has increased significantly during the recent years. A composite material usually consists of two materials with physically separable phases. In a polymeric composite the first phase is some kind of polymer material (called binder material or matrix) which surrounds the second phase (reinforcement). The reinforcement may be platelets, particles or fibers (long or short). Usually this second phase is added to improve stiffness, strength and toughness of the matrix material. Since the polymeric matrix has low density, composites based on these materials often show excellent specific properties. Long fibers that is oriented in the direction of loading offer the most efficient load transfer. This is

because the ineffective fiber length (the distance at the ends of the fiber with less efficient load transfer) is short compared to the whole fiber length. A fiber is considered long when its length to diameter ratio is higher than 100. Popular fibers are glass-, carbon- and aramide fibers which are all synthetic. Another group of fibers that often qualifies as long fibers are the natural fibers. When we talk about natural fiber composites we mean a composite material that is reinforced with fibers from natural or renewable resources, in contrast to for example carbon fibers that have to be synthesized (with crude oil as origin). Natural geofibers may come from plants, animals or minerals. The use of natural geofibers and natural fiber composites are certainly not new to mankind. Bricks made from clay reinforced with straws have been used for thousands of years as building material. Textiles and ropes made from flax and hemp have been around for very long time and are still used today. Paper and cotton sheets impregnated with phenol- or melamine-formaldehyde resin were introduced in the early 1900 for electronic purposes.

For the last decades concrete producers have made wide use of waste or by-product materials in concrete [1,2]. Proper replacement of these materials in concrete would have two major significant: improving fresh and hardened properties of concrete and minimizing the environmental pollutions due to solid waste disposal.

Glass is one of the materials produced in many forms such as containers, windows, light bulbs, etc which all have a limited life. Glass is an inert material that could be recycled many times but in many countries waste glass are sent to landfill and stockpile. Since the glass is not a biodegradable material in landfill so there is a strong need to utilize waste glass. For solving the disposal of large amount of waste glass, reuse in concrete industry may be the most feasible application [2-6].

Waste glass can be used as partial replacement of coarse aggregate, fine aggregate, cementitious materials or ultra fine filler in concrete, depending on its chemical composition and particle size. Previous efforts have been made shown that replacement of glass as a part of coarse aggregate was not satisfactory because of chemical reaction between the alkali in the cement and the silica in the glass [7]. This strongly expansive alkali-silica reaction (ASR) creates a gel, which swells in the presence of moisture, causes cracking and unacceptable damage of the concrete. Recent studies have shown that if the waste glass finely ground, could be used in mortars and concrete as a very fine addition without introducing problems concerning ASR. In fact, a general conclusion of literatures shows that if the waste glass is finely ground under $75\mu\text{m}$, ASR does not occur and mortar durability is guaranteed because of its pozzolanic properties. Also on a market price basis, it would be much more profitable to use the glass in powder form as cement replacement to make a value added composite cement.

Glass is a non-metallic inorganic material made by sintering selected raw materials comprising silicate and other minor oxides as shown in Table 1. By cooling the molten glass on mold beds sheet glass of desirable sizes is formed. A conventional glass is rather brittle, easily broken by a small impact. This physical property has been used to crush the waste glass to form desirable particles for mixing purpose. In general, broken glass has a specific gravity of 2.5, a bulk unit weight of 1.3–1.4 tons per cubic meter, and a water absorption rate of 0.3–0.4 wt%. It has high volumetric stability under a temperature up to $700\text{ }^{\circ}\text{C}$. Its thermal expansion coefficient and softening point are $8.8\text{--}9.2\times 10^{-6}\text{ cm/cm/}^{\circ}\text{C}$ and $718\text{--}738\text{ }^{\circ}\text{C}$, respectively.

Table 1. Typical composition of glass used in this research

Oxide	Weight (%)
SiO ₂	70.87–72.83
Na ₂ O	12.40–13.67
CaO	8.84–10.47
Al ₂ O ₃	1.47–2.43
K ₂ O	0.79–1.17
SO ₂	0.20–0.26
MgO	0.11–3.91
Fe ₂ O ₃	0.03–0.37
TiO ₂	0.01–0.04

In developing concrete products with crushed waste glass aggregate, the economics is controlled by the price the product can fetch on the open market. Commodity products, by definition, are characterized by low values, which exert strong pressures on the production and manufacturing technology [5]. The value added by the glass is marginal to nonexistent in those cases. But by utilizing the special properties of glass, chemical, physical, or esthetic, novel products can be developed, for which the prices fetched in the open market are much less exposed to competitive pressures.

What makes glass such a special ingredient for concrete becomes apparent by summarizing its special properties:

- Because it has basically zero water absorption, it is one of the most durable materials known to man. With the current emphasis on durability of high-performance concrete, it is only natural to rely on extremely durable ingredients.
- The excellent hardness of glass gives the concrete an abrasion resistance that can be reached only with few natural stone aggregates.
- For a number of reasons, glass aggregate improves the flow properties of fresh concrete so that very high strengths can be obtained even without the use of superplasticizers [6].
- The esthetic potential of color-sorted post-consumer glass, not to mention specialty glass, has barely been explored at all and offers numerous novel applications for design professionals.
- Very finely ground glass has pozzolanic properties and therefore can serve both as partial cement replacement and filler [7].

This study is limited to application of unwanted materials such as carpet wastes and recycled glass in cement-based composites.

3. EXPERIMENTAL APPROACH

The term glass comprises several chemical varieties including binary alkali-silicate glass, boro-silicate glass, and ternary soda-lime silicate glass. Most of the packaging glass which is the subject of this paper is of the soda-lime silicate variety. It is manufactured in various colours, mostly green, amber and clear, but waste glass after being collected from the domestic waste stream is of a mixed colour. Research on the use of crushed glass as a partial replacement for aggregate dates back many decades [1]. Major tests carried out in this program followed the ACI standard procedures. Figure 1 gives the general flow chart of the test programs.

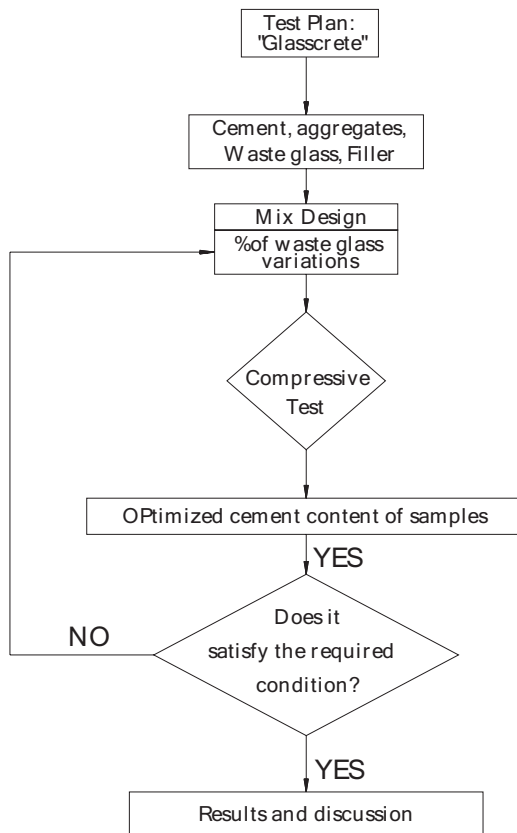


Figure 1. Test Flow Chart for GeoFiber™ composite.

3.1. Material Specification

Clean flat glass and waste carpet fibers were used in this study. The chemical composition of the glass was analyzed using an X-ray microprobe analyzer and listed in Table 2 together with that of silica fume and rice husk ash for comparison.

In accordance to ASTM C618, the glass satisfies the basic chemical requirements for a pozzolanic material. However, it does not meet the optional requirement for the alkali content because of high percentage of Na_2O .

To satisfy the physical requirements for fineness, the glass has to be ground to pass a 45 μ m sieve. This was accomplished by crushing and grinding of glass in the laboratory, and by sieving the ground glass to the desired particle size. To study particle size effect, two different ground glasses were used:

- Type I: ground glass having particles passing a #80 sieve (180 μ m);
- Type II: ground glass having particles passing a #200 sieve (75 μ m).

According to ASTM C618, the 180 μ m and 75 μ m glass did not qualify as a pozzolan due to the coarse particle size. The purpose of this study was to examine if the coarse ground glass could still be a pozzolan. The particle size distribution for two types of ground glass, silica fume, rice husk ash and ordinary Portland cement were studied using laser particle size analysis and listed in Table 3. Results indicate that glass type I and II respectively have 42% and 70% fine particles smaller than 45 μ m would have pozzolanic behaviour according to ASTM C618. The particle shapes of all materials were analyzed using the scanning electronic microscope is shown in Figure 2.

The high-modulus Geofiber™ obtained from industrial sectors has desirable strength retention properties under long-term exposure to aggressive environment. Properties of this Geofiber™ are shown in table.

Fiber Properties	Nominal	Tenacity		Breaking	Elongation
	Denier	Tenacity	Tenacity	Load	at Break
	Tex	(cN/tex)	(gm/d)	(N)	(%)
GeoFiber	1880	85	8	161	22

Table 2. Chemical composition of glass, silica fume and rice husk ash used in this study (by weight percent)

	Glass	Silica fume	Rice husk ash
SiO_2	72.50	91.1	92.15
Al_2O_3	1.06	1.55	0.41
Fe_2O_3	0.36	2.00	0.21
CaO	8.00	2.24	0.41
MgO	4.18	0.60	0.45
Na_2O	13.1	-	0.08
K_2O	0.26	-	2.31
CL	0.05	-	-
SO_3	0.18	0.45	-
$L.O.I$	-	2.10	-

Table 3. Laser particle size analysis of materials in cement-based composites (by percentage)

Particle size (μm)	Cement	Glass I	Glass II	Silica fume	Rice husk ash
4.5	14.95	4.69	7.81	42.67	24.63
5.5	18.42	5.98	9.96	51.15	29.88
6.5	21.75	7.30	12.16	58.37	34.63
7.5	24.93	8.64	14.40	64.48	38.93
9	29.42	10.66	17.70	71.98	44.68
11	34.90	13.29	22.15	79.50	51.25
13	39.82	15.82	26.63	84.75	56.80
15.5	45.24	18.78	31.30	88.98	62.61
18.5	50.82	22.00	36.66	91.83	68.38
21.5	55.59	24.89	41.48	93.38	73.21
25	60.41	27.93	46.55	94.47	78.00
30	66.27	31.85	53.03	95.52	83.67
37.5	73.50	37.18	61.96	96.71	90.08
45	79.35	42.09	70.15	97.63	94.35
42.5	84.05	46.72	77.86	98.24	96.92
62.5	88.89	52.60	87.66	98.75	98.67
75	93.31	59.74	100.00	99.20	99.55
90	96.82	67.91	100.00	99.64	99.91
105	98.72	75.21	100.00	99.88	100.00
125	99.68	83.22	100.00	99.97	100.00
150	100.00	90.57	100.00	100.00	100.00
180	100.00	100.00	100.00	100.00	100.00
Av. particle size (μm)	27.17	76.90		7.38	15.83
Scatter Module	0.96	1.04		0.92	0.97

3.2. Mix Design

Compressive strength test were conducted to study the strength development of composite cement paste containing the ground waste glass at early age. The cement replacement by the ground waste glass was 10%, 20%, 30% and 40% by total weight. The composite cement paste containing ground waste glass were compared to the cement having the same percent replacement by silica fume and rice husk ash as well as to the control specimen without any mineral additives. The five batches were defined as follows:

- Ordinary Portland cement paste: no mineral additives
- Waste glass type I: 10%, 20%, 30% and 40% by weight of the Portland cement replaced by waste glass type I
- Waste glass type II: 10%, 20%, 30% and 40% by weight of the Portland cement replaced by waste glass type II
- Silica fume: 10%, 20%, 30% and 40% by weight of the Portland cement replaced by waste silica fume

- Rice husk ash: 10%, 20%, 30% and 40% by weight of the Portland cement replaced by husk rice ash.

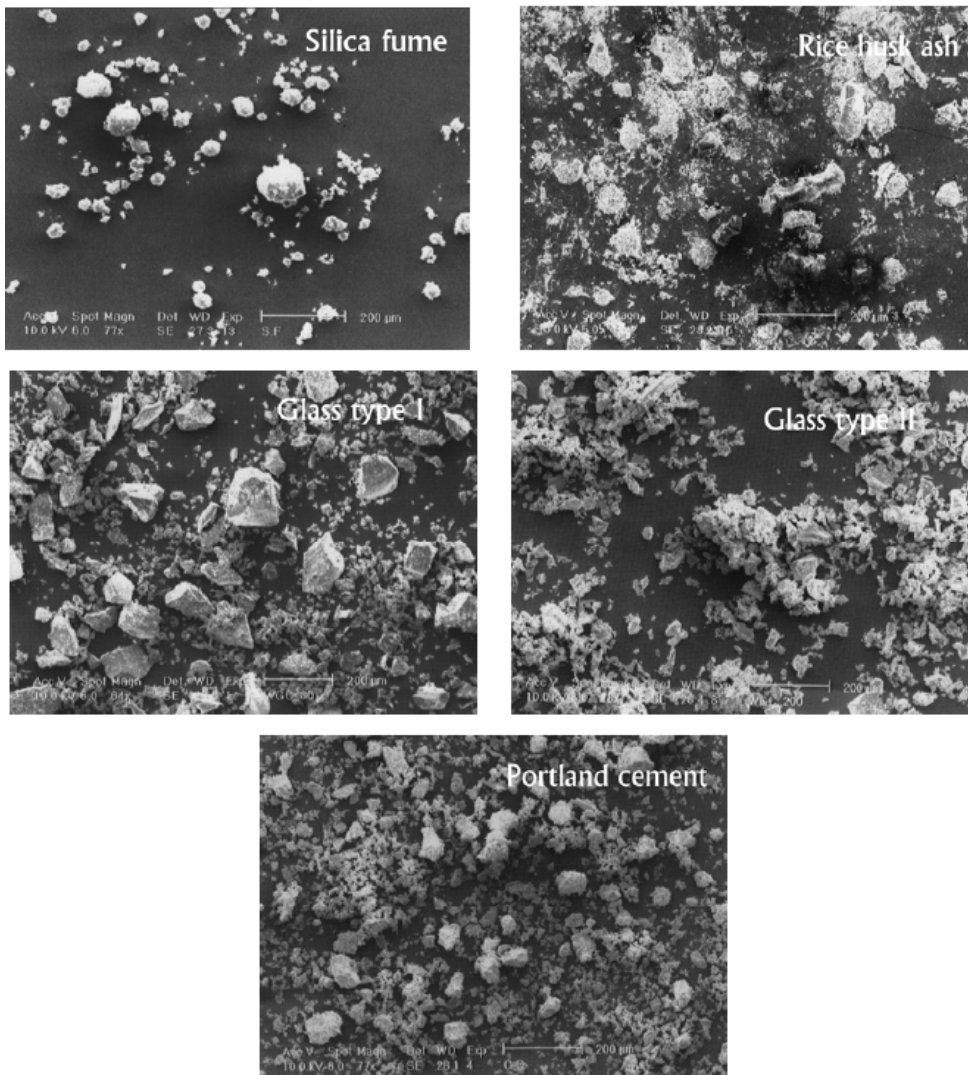


Figure 2. Particle size and shape of ground waste glass type I, type II, silica fume, rice husk ash and ordinary Portland cement.

Figure 1 shows the laboratory flow chart for "GeoFiber™ composite. The cement paste was mixed in a paste mixer and the water to cementitious ratio for achieving the suitable workability was selected according to Table 4. To evaluate the strength development of composite cements at the age of 3,7,14 and 28 days for each batches four $20 \times 40 \text{ mm}$ cylindrical specimens were cast. 24 hours after casting, the specimens were demolded and cured in water at 20°C . As shown in this table the glass needs lower water to cementitious ratio because of low water absorption.

Table.4. Water/cement ratio for various mixtures

	Percentage of replacement			
	10%	20%	30%	40%
	Water/Cement ratio			
Glass Type I	26	26	26	26
Glass Type II	26	26	26	26
Silica fume	28	30	32	34
Rice husk ash	29	31	33	35
Portland cement (Control)	Water/Cement = 26%			

4. RESULTS AND DISCUSSION

The compressive strength of the composite cements in comparison with control specimens are shown in Figure 3.

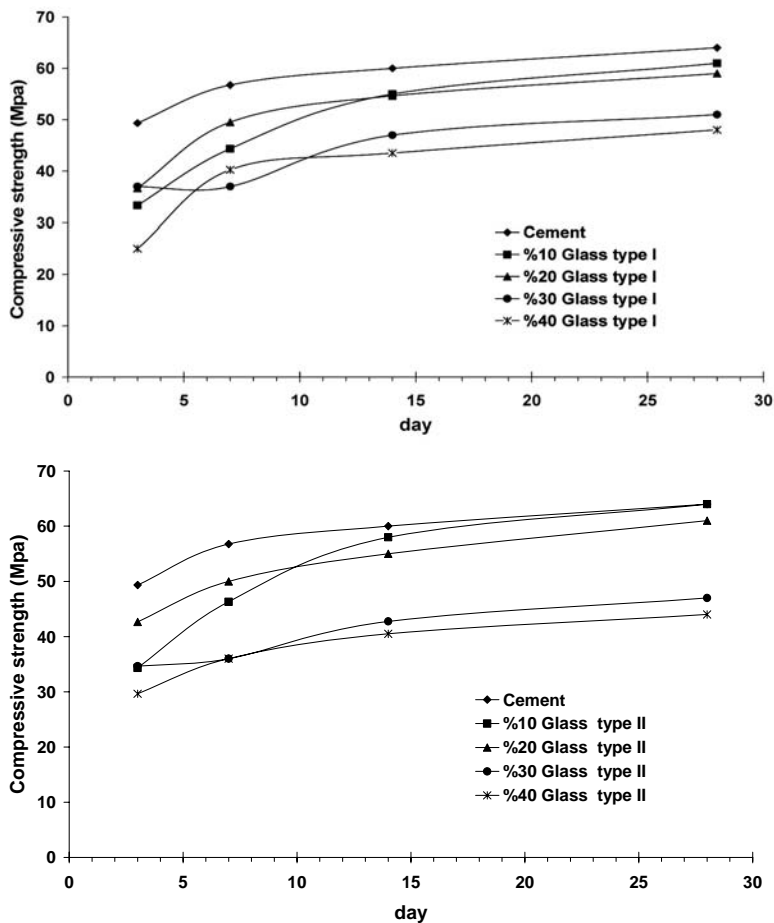


Figure 3. Continued on next page.

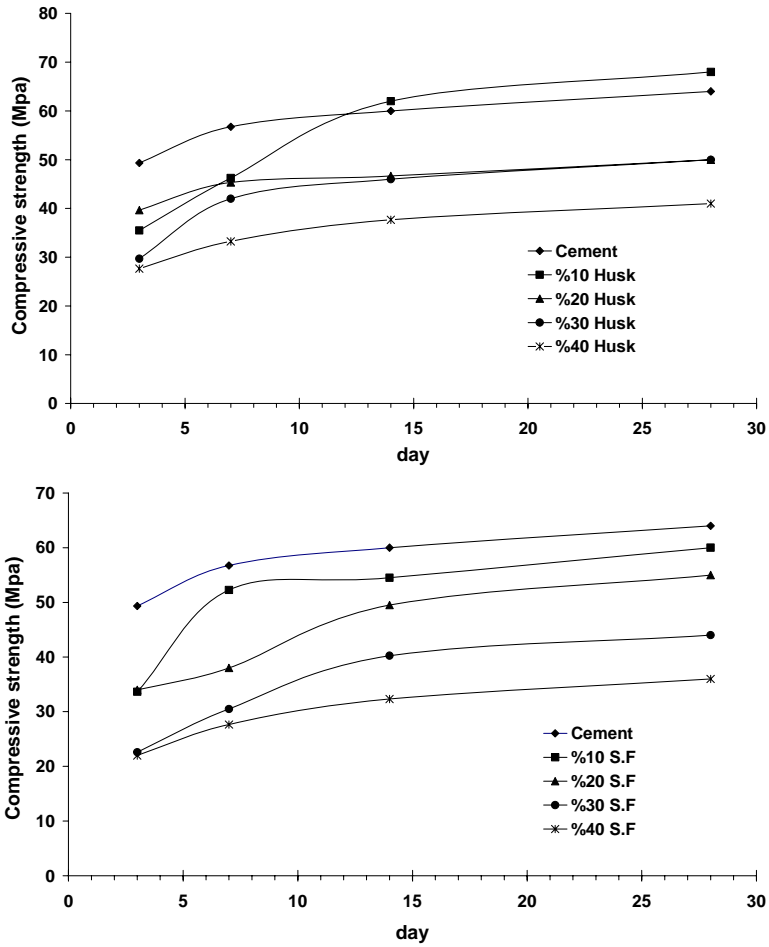


Figure 3. Compressive strength of cement-based composites.

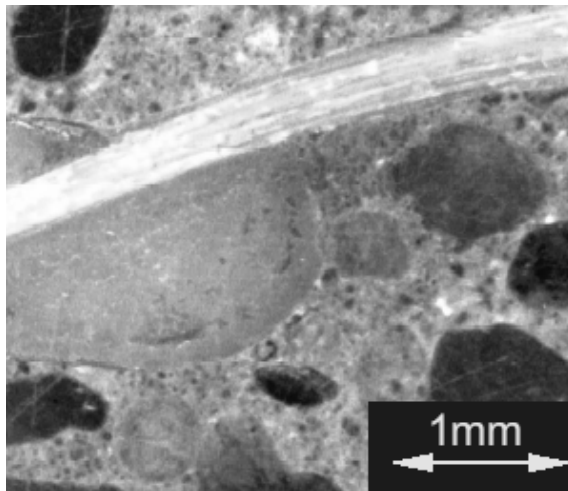


Figure 4. Geofiber™ in cement-based composite.

Result of all tests in Figure 2 shows that increasing the amount of replacement from 10% to 40%, decrease the compressive strength of composite cements. However, the highest compressive strength has seen in rice husk ash with 10% replacement but by increasing the amount of replacement its strength decreases sharply in comparison with other composite cements. This principle is also seen in silica fume specimens.

It seems that there exists a competition in strength development between 10% replacement of waste glass with different particle size. The effect of glass particle size on the compressive strength shows that the smaller size of ground glass leads to a higher compressive strength. Also results indicate that compressive strength of glass type II which has particle size of smaller than $75\mu\text{m}$, have reached the control specimen strength after 14 days. So, it is clear that the glass of type II between others exhibits a pozzolanic behaviour and it's the best choice for producing "Glasscrete" which is the aim of authors future work. Geofiber™ used in all the samples,

Effect of Fiber Volume Fraction

The properties of fiber cement-based composites are largely controlled by the manufacturing process. During manufacturing, different parameters, such as fiber content, the properties of the matrix (i.e., water-to-cement ratio, sand-to-cement ratio), the molding pressure, and the curing method, can be varied to achieve the desired properties in the composite.

Effect of Curing Conditions

Curing conditions play an important role in the composite behavior, which has been attributed primarily to the influence of curing on the matrix properties. Two curing methods that are generally used in fiber cement composites are air/moist curing (normal pressure and temperature) and autoclave curing (high pressure and temperature).

Effect of Fiber Type

Some contradictory results have been reported concerning the effect of the fiber type on the mechanical performance of fiber cement composites (i.e. enhancements in flexural toughness).

Effect of Fiber Moisture State

Due to their hygroscopic nature, fiber-cement composites are sensitive to moisture changes in the material itself and in the ambient environment. In the wet state, it is believed that the bond between the fiber and cement matrix is weakened. Therefore, fiber pull out is the dominant mode of failure for the wood fibers. On the other hand, in the dry state, the bond strength is increased. The potential for fiber/matrix debonding and microcracking at the interface during wet/dry cycling of composites is dependent upon (among other factors) the dimensional stability of the fiber reinforcement in response to moisture fluctuations.

Composite Durability: Wet/Dry Cycling

Changes in the fiber and fiber/cement interfacial region due to environmental interactions can affect the long-term performance of cement-based composites reinforced with natural fibers. A significant mechanism of changes in composite properties is pulp fiber degradation

as a result of environmental interactions or changes in the fibers itself due to its presence in the strongly alkaline matrix. There appears to be two related mechanisms which lead to composite degradation during wet/dry cycling: (1) the degree of fiber-cement bonding and (2) fiber mineralization.

Effect of Fiber Drying History

The fiber drying history has been shown by Mohr *et al.* (2003a) to have little effect on wet/dry cycling durability. Flexural strength and toughness were similar over the range of wet/dry cycles investigated. Thus, fiber swelling/shrinking does not seem to play any direct role in composite degradation.

Effect of Matrix Composition

Efforts to improve the durability of fiber-reinforced cement materials to wet/dry cycling have largely concentrated on the addition of supplementary cementing materials. The use of artificial pozzolans has been shown to delay or minimize composite degradation by lowering the pore solution pH, reacting with calcium hydroxide to produce C-S-H, and refining the pore structure, all of which are thought to minimize the mineralization and subsequent embrittlement of fibers with a cement matrix. Silica fume, used at relatively large amounts (i.e., 30% or greater replacement of cement by weight) appears to significantly minimize composite degradation due to wet/dry cycling. Silica fume replacements can reduce the pore water pH.

Despite improvements in composite durability with certain cement replacements, little is known as to the mechanism of improved durability. That is, does the cement pore solution play a significant role, or does the permeability of the composite? Or are durability improvements based on a combination of the two? Also, how is cement hydration altered by lowering the pore solution pH? These questions must be answered before establishing any criteria or recommendations for improving pulp fiber-cement composite durability.

5. CONCLUDING REMARKS

Local recycling pressures are providing an impetus to examine the use of unconventional materials in construction such as waste glass in Portland cement. Storage or reuse conditions of waste are still currently defined on a regulatory or technical basis which does not take into account the impact of the waste deposit on the environment, due to lack of technical data in this domain. One of the objectives was to develop mixes of relatively low reactivity containing glass, Geofiber™, pozzolanic materials and various admixtures. It should be noted that with the large number of variables, the detection of unfavorable components prior to excessive long-term testing is essential. The work led to the development of reliable novel composite replacing traditional cement mixtures. It can serve as a valuable composite in the development of new concrete products. The results of this study confirm the advantage "glascrete" containing Geofiber™ over concrete that contains only regular components.

Following a normal growth in population, the amount and type of waste materials have increased accordingly. Many of the non-decaying waste materials will remain in the environment for hundreds, perhaps thousands of years. The non-decaying waste materials

cause a waste disposal crisis, thereby contributing to the environmental problems. The problem of waste accumulation exists worldwide, especially in the densely populated areas. Most of these materials are left as stockpiles, landfill material or illegally dumped in selected areas.

The tests carried out in this study were primarily designed to provide an indication of relative advantages of the use of a number of recycled materials, carpet and glass wastes. This would provide an overview of the reuse of waste materials in the construction industry. The purpose of present study was to protect environment by saving more landfills, to increase the cement plant capacity by using more beneficial additives.

The data presented in this paper show that there is a great potential for the utilization of Geofiber™ in cement-based composites. It is considered this utilization would provide much greater opportunities for value adding and cost recovery as it could be used as a replacement for expensive materials.

A smaller particle size of glass results in a higher compressive strength in cement paste. Results show that the best percentage of waste glass replacement in cement paste is 10% by weight. The use of ground waste glass as a replacement in cement seems feasible. This laboratory study shows the first step toward producing concrete with mixture of waste glass and Geofiber™.

Nevertheless, waste utilization is an attractive alternative to disposal cost and potential pollution problems are reduced or even eliminated along with the achievement of resource conservation. There are million tons of waste glass is land filled each year around the world.

In addition to recycling glass by its use in cement-based composites, glass aggregates can be used aesthetically in this composite, which can give a shiny clean finishing effect on the surface of the cement product.

Because cement-based materials are well-known insulators, another avenue for further research and product development is the strategic use of fiber-cement composites for sound and heat insulation. Such products might be composed wholly of fiber-cement (likely aerated) or where fiber cement is just one component in an insulating panel or member.

REFERENCES

- [1] P.K. Mehta, O.E. Gjørv, "Properties of Portland cement concrete containing fly ash and condensed silica fume", *Cement and Concrete Research*, 12(1982), 587–595.
- [2] C. Polley, S.M. Cramer, R.V. Cruz, "Potential for using waste glass in Portland cement concrete", *Journal Materials in Civil Engineering*, ASCE, 10 (4), (1998), 210–219.
- [3] Y. Shao, T. Lefort, S. Moras, D. Rodriguez, "Studies on concrete containing ground waste glass", *Cement and Concrete Research*, 30(2000), 91-100.
- [4] A. Shayan, A. Xu, "Value-added utilization of waste glass in concrete", *cement and concrete research*, 34(2004), 81-89.
- [5] V. Corinaldesi, G. Gnappi, G. Moriconi, A. Montenero, "Reuse of ground waste glass as aggregate for mortars", *Waste Management*, 25(2005), 197-201.
- [6] C.H. Chen, R. Huang, J.K. Wu, C.C. Yang, "Waste E-glass particles in cementitious mixtures", *Cement and Concrete Research*, 36(2006), 449-456.

-
- [7] C. Meyer, S. Baxter, W. Jin, "Alkali-silica reaction in concrete with waste glass as aggregate", *Materials for a New Millennium, Proceedings of ASCE Materials Engineering Conference*, Washington D.C., (1996), 1388–1394.

Chapter 17

A NEW APPROACH FOR PREDICTION OF FAILURE IN UNIDIRECTIONAL GLASS/EPOXY COMPOSITES

*A. Farjad Bastani, H. Haftchenary, K. Mohammadi and
A. K. Haghi **

The University of Guilan, P.O. Box 3756 , Rasht, Iran

ABSTRACT

The present paper aims to assess damage in UD GRP composites of various off-axis angles under axial loads. Damage analysis presented in this paper is drastically influenced by void content of the material and it assumes that there should be a direct relationship between the failure of composite material and its void content.

The proposed analysis is a very helpful tool for designers dealing with unidirectional off-axis composites.

Keywords: *GRP Composites, Off-axis angles, Loading level, void content, statistical analysis.*

INTRODUCTION

Fibre reinforced plastic (FRP) composites are gaining a wide recognition as an alternative to the traditional metallic materials in a variety of applications. As a result a reasonable step is to understand the mechanics of composites and provide the designers and industry with the knowledge based on reliable data stemmed from extensive research.

Voids are among the most common manufacturing induced defects in composites [1-2]. They are formed primarily due to the entrapment of air during the formulation of the resin system, in resin rich areas, and due to moisture absorbed during the material storing and

* Corresponding author e-mail: Haghi@Guilan.ac.ir

processing [3-4]. Also, chemical reactions and inadequate values of temperature and pressure or tearing in the vacuum bag during cure cycle contribute to their formation. Moreover, in service conditions may contribute to their growth [3]. It is well known that voids have detrimental effects on the strength of composite laminates [3, 5]. In general, they decrease the static strength and fatigue life of composite laminates and cause a greater susceptibility to water penetration and environmental conditions. The influence is more pronounced in the interlaminar shear strength [3-4, 6-7], compressive strength [8], and bending strength that are associated with matrix dominated mechanical properties. It has also been experimentally observed that voids may cause a dramatic decrease in fatigue life despite having only a moderate influence on the static strength [9].

There are a wide variety of parameters that induce voids in composites. Effect of these parameters on mechanical properties of composite is the subject of so many researches [10-15]. Furthermore, induced voids affect the fatigue behaviour of composite materials product [16, 17].

OBJECTIVES OF THE PROJECT

The present paper examines damage evolution of monotonically loaded UD GRP composites. Experiments were set to monitor damage progress as tensile loads applied to the composite specimens with various off-axis angles. A number of ASTM D3039 test specimens were manufactured in 7 different off-axis angles and monotonically loaded at 5 loading levels using a Hounsfield HS-100KS tensile testing machine. Tensile tests were accompanied with SEM observations of composite specimens along and perpendicular to the fibre direction to estimate voids formation rate and voids propagation as a source of damage in polymeric composites.

A statistical analysis based on General Linear Model (GLM) was developed to analyse the influence of loading and off-axis angle on damage of composite laminates. The void content in the composite specimens acted as stress raiser resulting in cracks initiation, propagation and failure as tensile loads progressively applied. Analysis of Variance (ANOVA) was performed for void contents to check the statistical differences caused by the experimental errors.

A three-dimensional map of void content against load and off-axis angle was constructed to depict the influence of loading level and off-axis angle on micro-cracks initiated on the vicinity of voids in the GRP specimens. Utilizing this map it is possible to optimize angle/load combination for minimum damage in designing reliable structures using GRP composites.

EXPERIMENTAL PROCEDURE

Several methods to design experiments have been considered for cost-effectiveness of experiments [18-25]. In this study, the "General Full Factorial Design" was chosen, because of high scattered data which is normal in composite materials. This design considers all possible situations and the number of tests is calculated by Eq. (1):

$$\prod_{i=1}^N x_i = \text{Total number of tests} \quad (1)$$

where

$x_i = i^{\text{th}}$ factor

$N =$ Number of factors

According to Eq. (1), seven monotonic tests with various off-axis angles of 0° , 15° , 30° , 45° , 60° , 75° and 90° and at five different loading levels of “Untested, PT1, PT2, PT3 and FULL” were performed. Multiplying it by five replicates and two views of SEM photography, 350 different tests have been performed.

Tensile test specimens have been fabricated based on ASTM D 3039 for off-axis angles. The materials chosen for fiber and matrix were E-Glass UD-weaves and ML-506 Epoxy resin, respectively. UD-weave fiber lay-up and test specimen geometry are shown in Figure 1 and Figure 2:

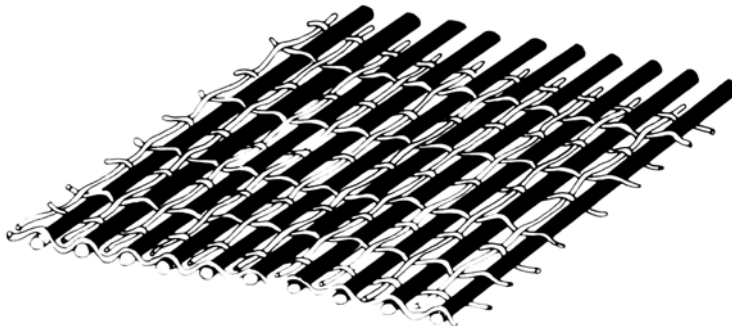
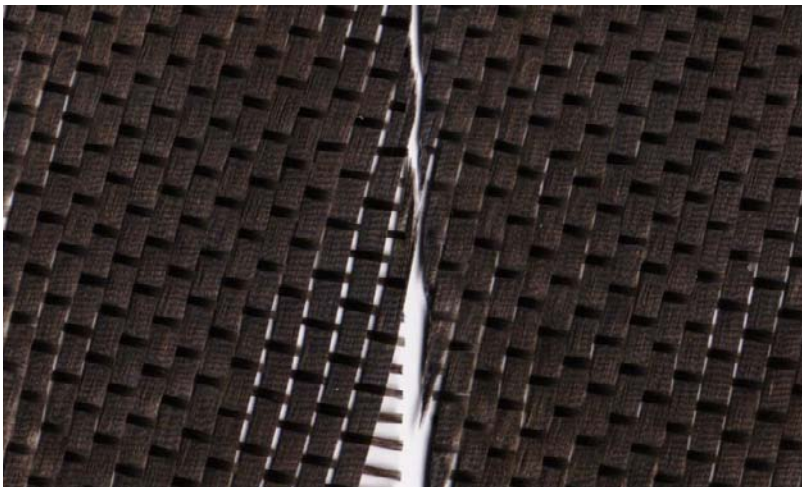


Figure 1. UD-weave form of the fibers.

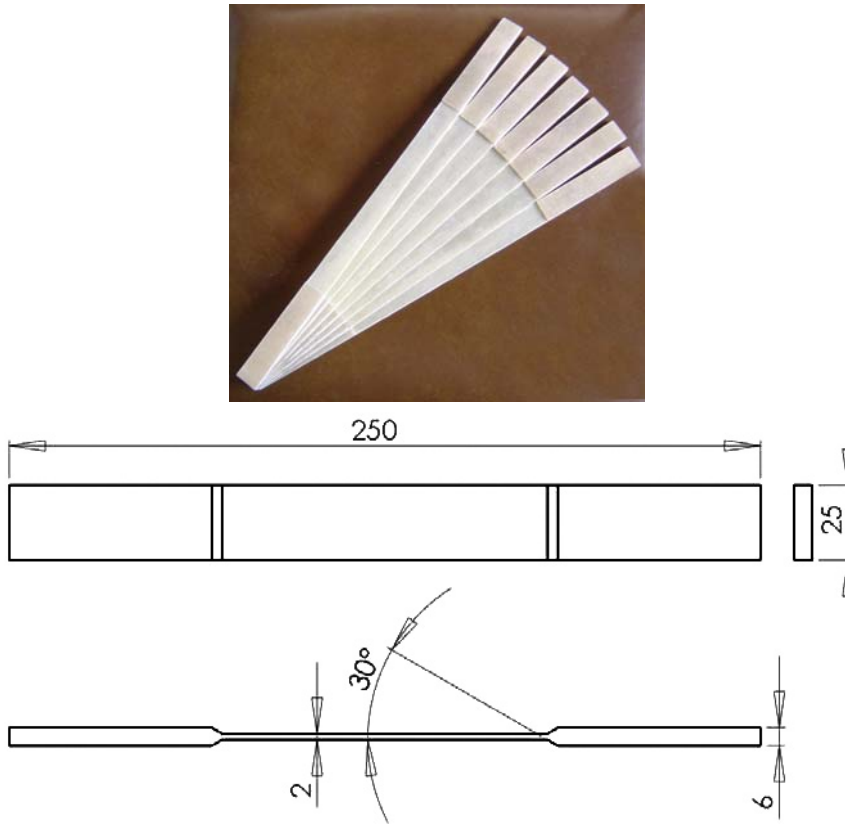


Figure 2. Test coupons according to ASTM D 3039.

Three specimens from each off-axis angle were loaded under tensile load up to full failure, using Hounsfield HS-100KS universal machine. To specify the loading levels the stress-strain curves presented in Figure 3 were used. Figure 3 presents stress-strain diagram of a UD GRP composite axially loaded making an off-axis angle of 30 degrees with fibre direction. Two distinct points, first kink and second kink, marked on this graph were taken to be the threshold of a major damage in material. The first load level was untested samples (1). The next loading level was chosen to be between zero and at a point shown by a black arrow on the graph, (2). The third level, is taken to be between the points shown by the first and second arrows (3), and the fourth load level taken at mid point between the second arrow and the final failure load (4). Finally, the last sample was taken at the failure load (5).

The loaded specimens were sectioned at two perpendicular directions as shown in Figure 4. The specimens were then mounted in cold mount, polished with 12 grades of sandpaper and gold-coated to be prepared for SEM photography.

It is virtually impossible to detect all of the voids by taking photographs; therefore, a few samples have been prepared and presented here. With a confidence interval of 95%, 10 photos for each section have been taken. For a good balance of accuracy and reliability, 150X magnification factor was found to be a good zoom factor. To measure the damage induced in the specimen, the area of voids should be calculated and divided by whole area of the photo.

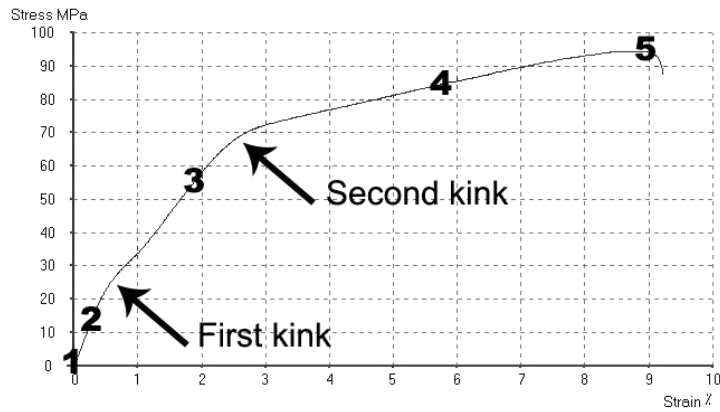


Figure 3. Typical stress strain curve for 30° GRP specimen.

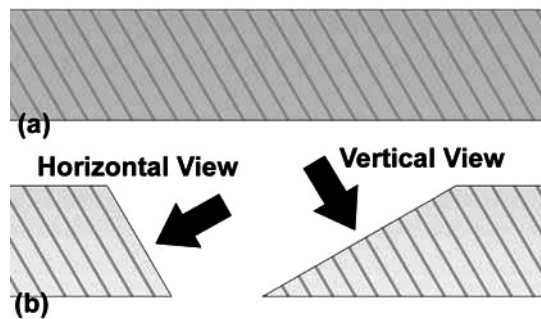


Figure 4. Section schematic views for a 60° specimen. (a) Un-sectioned and loaded specimen and (b) Two perpendicular views for SEM.

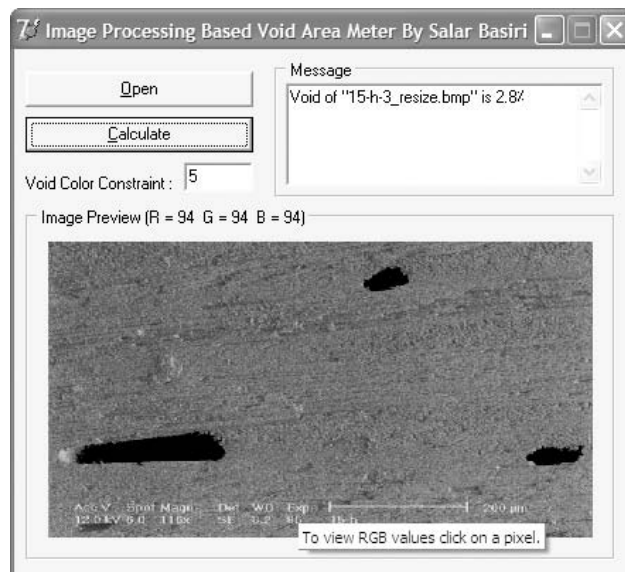


Figure 5. A screenshot of VoidScan software.

To do this calculation a Borland Delphi program based on image processing techniques, named as VoidScan [26], has been developed to evaluate the percentage of void in each photo. The screenshot of the software is shown in Figure 5.

GENERAL LINEAR MODEL

In most engineering problems, the response depends on several regressors. Multi-linear regression is a straightforward expansion of simple linear regression to more than one regressor. Essentially, model estimation, model testing and prediction all follow the same basic procedure. Often engineering phenomenon can be modeled as a linear combination of several regressors. It is intended here to model the void content of composite test specimens in terms of these factors:

- The angle between loading direction and fibers direction (off-axis angle)
- The amount of load introduced to the specimen

A possible model for this situation is

$$y_i = \beta_0 + \beta_1 x_{i1} + \beta_2 x_{i2} + \varepsilon_i \quad (2)$$

where

y_i is the void content of the specimen

x_{i1} is the off-axis angle

x_{i2} is the load applied to specimen

β_0 is the y-intercept.

β_1 is the slope or coefficient associated with the off-axis angle.

β_2 is the slope or coefficient associated with the load.

ε_i is a random error.

Just as in simple linear regression it is assumed that the random errors are independent of mean zero and variance σ^2 . Under these assumptions, the expected value of the response for the i^{th} set of conditions for the regressors is:

$$E[y] = \beta_0 + \beta_1 x_{i1} + \beta_2 x_{i2}. \quad (3)$$

In the multiple regression setting, care should be exercised with interpretation of the coefficients, namely, β 's. The coefficient, β_j , represents the expected change in the response for a one-unit change in x_j given that all the other regressors are held constant! [25] In this

work a complete control over all two regressors were achieved. As a result, it was possible to change one regressor while holding the others constant.

Just like simple linear regression model, the method of least squares was used to estimate the coefficients.

b_0, b_1, \dots, b_k are the corresponding estimates of the coefficients, and \hat{y}_i is the predicted value for the response of the i^{th} set of conditions for the regressors. Thus:

$$\hat{y}_i = b_0 + b_1 x_{i1} + b_2 x_{i2} \quad (4)$$

Defining the sum of squares of the residuals by

$$SS_{res} = \sum_{i=1}^n (y_i - \hat{y}_i)^2 \quad (5)$$

We call b_0, b_1, \dots, b_k the least squares estimates if they minimize SS_{res} . From calculus, we find these estimates by taking the partial derivatives of SS_{res} with respect to each parameter and setting them to zero, which produces the following k+1 equations in k+1 unknowns (k=2):

$$\begin{aligned} \frac{\partial}{\partial b_0} \sum_{i=1}^n [y_i - (b_0 + b_1 x_{i1} + b_2 x_{i2})]^2 &= 0 \\ \frac{\partial}{\partial b_1} \sum_{i=1}^n [y_i - (b_0 + b_1 x_{i1} + b_2 x_{i2})]^2 &= 0 \end{aligned} \quad (6)$$

These derivatives result in “normal” equations:

$$\begin{aligned} nb_0 + b_1 \sum_{i=1}^n x_{i1} + b_2 \sum_{i=1}^n x_{i2} &= \sum_{i=1}^n y_i \\ b_0 \sum_{i=1}^n x_{i1} + b_1 \sum_{i=1}^n x_{i1}^2 + b_2 \sum_{i=1}^n x_{i1} x_{i2} &= \sum_{i=1}^n x_{i1} y_i \\ b_0 \sum_{i=1}^n x_{i2} + b_1 \sum_{i=1}^n x_{i1} x_{i2} + b_2 \sum_{i=1}^n x_{i2}^2 &= \sum_{i=1}^n x_{i2} y_i \end{aligned} \quad (7)$$

RESULTS AND DISCUSSION

Void content for any pair of load-angle data, produces one value, therefore, normality and homogeneity of all 5 replicates should be verified to report a mean value. Boxplot, Anderson-

Darling normality test [27], probability plot and cumulative distribution function (CDF) are criteria that could be used to check the normality of the data [25, 27 and 28].

Probability plot is presented here to verify the correctness of data. In probability plots the vertical scale on the graph resembles the vertical scale found on normal probability distribution. The horizontal axis is a linear scale. The line forms an estimate of the cumulative distribution function (CDF) for the population from which data are drawn. An example for PT1 series is shown in Figure 6.

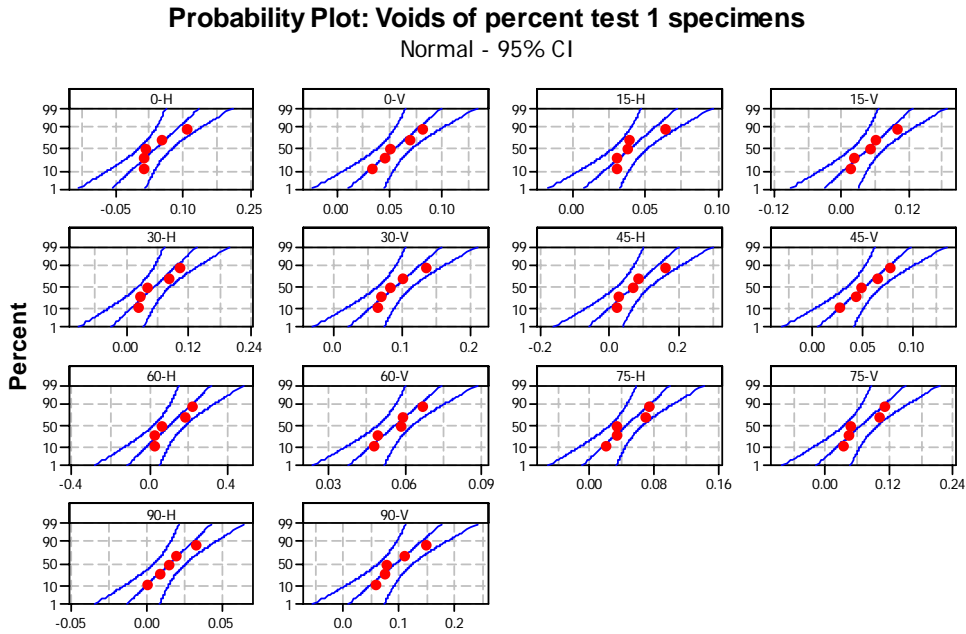


Figure 6. Probability plot of voids for PT1 specimens with 95% confidence interval.

As it is clearly shown in Figure 6, there were no data outside the upper and lower bound of 95% confidence interval with a normal distribution, so the data could be used for modeling purposes.

The normal distribution plays a very important role in the science of statistical inferences. Moreover, many phenomena generate random variables with probability distribution that are very well approximated by a normal distribution. The formula for the normal probability distribution is shown in Eq. (8):

$$f(x) = \frac{1}{\sigma\sqrt{2\pi}} e^{-\frac{1}{2}\left(\frac{x-\mu}{\sigma}\right)^2} \quad (8)$$

where

μ =Mean of the normal random variable x

σ =Standard deviation

π =3.1416...

e =2.71828...

DATA PRESENTATION

When there are three variables – two affecting one – “3D Surface Plot” is used to evaluate relationships between three variables at once. A 3D surface plot has three axes. In addition, 3D Surface Plot uses interpolation to produce a continuous surface (surface plot) or grid (wireframe plot) of z-values that fits the data. [25]

Contour Plot may be a better method to show 3D data. In a contour plot, the values for two variables are represented on the x- and y-axes, while the values for a third variable are represented by shaded regions, called contours. A contour plot is like a topographical map in which x-, y-, and z-values are plotted instead of longitude, latitude, and altitude. 3D wireframe plot and Contour plot of horizontal sections is shown in Figure 7.

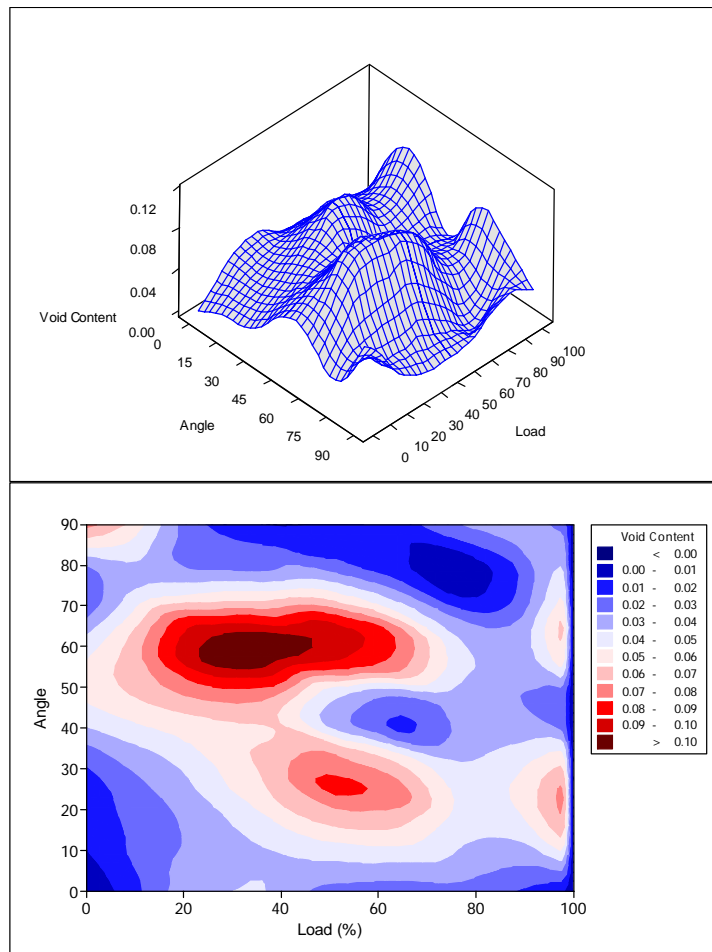


Figure 7. 3D wireframe plot and Contour plot of damage vs. angle and load for horizontal sections.

GLM RESULTS

Solving set of Eq. (7) we can find value's of coefficients. Results are tabulated in Table. (1).

Table 1. General linear model coefficients and p-values

Term	Coefficients	Standard error coefficient	T-test value	P-Value
Constant	0.043334	0.002699	16.06	0.000
<i>Loading</i>				
FULL	0.009509	0.005417	1.76	0.081
PT1	0.008466	0.005393	1.57	0.119
PT2	0.003694	0.005393	0.69	0.494
PT3	-0.01142	0.005393	-2.12	0.036
<i>Angle</i>				
0	-0.009294	0.006604	-1.41	0.162
15	0.001666	0.006604	0.25	0.801
30	0.007786	0.006604	1.18	0.240
45	-0.002394	0.006740	-0.36	0.723
60	0.023266	0.006512	3.57	0.000
75	-0.009294	0.006604	-1.41	0.162

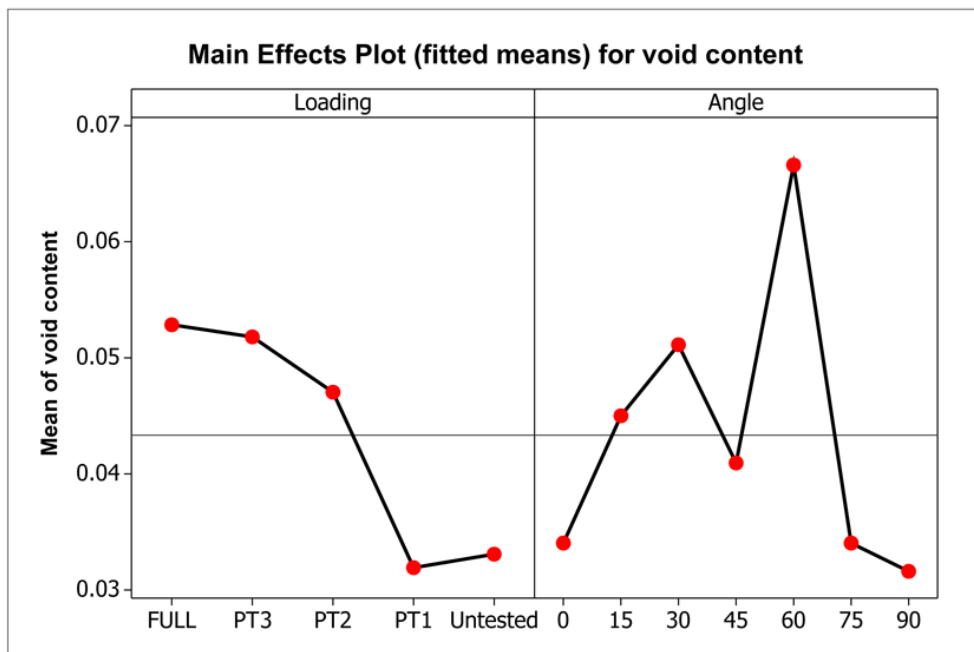


Figure 8. Main effects plot for horizontal sections.

Main Effects Plot is used to plot data when there are multiple factors. The points in the plot are the means of the response variable at the various levels of each factor, with a reference line drawn at the grand mean of the response data.

As shown in Figure 8 the relationship between the loading and the void content is successfully proven. When we trace the curve from untested situation to full loading (horizontal axis), the void content (vertical axis) increases from its minimum to the maximum level, gradually. So it is possible to prognoses the failure of material by means of its void content. Void content could be calculated with GLM equation, i.e. Eq. (4).

Right side of Figure 8 shows the significance of 60° angle in void content propagation which has also been found in Figure 7.

CONCLUSION

A new approach to predict the failure of UD GRP composites has been developed in this paper. The direct relationship between the void propagation and failure of composite material has been successfully achieved. The effect of off-axis angle and loading level on void content was then mathematically described.

The proposed analysis is a very helpful tool for designers dealing with unidirectional off-axis composites. By referring to this model a decision can be reached on the off-axis angle and load condition, with a certain safety factor before fracture of the specimen. It could be concluded that the void propagation has a critical value in 60° and designer should exercise special care when designing a UD composite structure under 60° angle between load direction and fiber orientation. The probability of material fracture then could be calculated from the GLM model provided here.

To derive a practical approach from this project, the void measurement tests should be performed using non-destructive techniques (NDT), to predict the failure of material before the fracture.

REFERENCES

- [1] Michelle Leali Costa, Sergio Frascino M. de Almeida, Mirabel Cerqueira Rezende, The influence of porosity on the interlaminar shear strength of carbon/epoxy and carbon/bismaleimide fabric laminates, *Composites Science and Technology* 61 (2001), pp. 2101–2108.
- [2] Strong AB. *Fundamentals of composites manufacturing: materials, method and applications*. SME: Dearborn, 1989.
- [3] Stone DE, Clark B. Ultrasonic attenuation as a measure of void content in carbon-fibre Reinforced Plastics. *Non Destructive Testing* 1975; July: 137–45.
- [4] Jeong H. Effects of Voids on the Mechanical Strength Ultrasonic attenuation of laminated composites. *J. Comp. Mater.* 1997; 31(3):276–92.
- [5] Savage G. *Carbon-carbon composites* 1993 Chapman and Hall London.

-
- [6] Bowles KJ, Frimpong S. Voids effects on the interlaminar shear strength of unidirectional graphite-fiber-reinforced composites. *J. Comp. Mater.* 1992; 26 10:1487–509.
- [7] Almeida SFM, Santacreu ACM. Environmental effects in composite laminates with voids. *Polym. and Polym. Comp.* 1995;3(3):193–204.
- [8] Suarez JC, Molleda F, Guemes A. Void content in carbon fiber/epoxy resin composites and its effects on compressive properties. In: *Miravete A, editor. Proceedings of ninth international conference on composite materials* (vol VI Madrid). Spain, ICCM-9: Woodhead Publishing Limited, 1993. p. 589–96.
- [9] Almeida SFM, Nogueira Neto ZS. Effects of void content on the strength of composite laminates. *Comp. Struct.* 1994; 28:139–48.
- [10] Ling Liu , Bo-Ming Zhang, Dian-Fu Wang, Zhan-Jun Wu, Effects of cure cycles on void content and mechanical properties of composite laminates, *Composite Structures* 73 (2006), pp. 303–309.
- [11] Youssef K. Hamidi, Levent Aktas, M. Cengiz Altan, Three-dimensional features of void morphology in resin transfer molded composites, *Composites Science and Technology* 65 (2005), pp. 1306–1320.
- [12] Hansong Huang, Ramesh Talreja, Effects of void geometry on elastic properties of unidirectional fiber reinforced composites, *Composites Science and Technology* 65 (2005) pp. 1964–1981.
- [13] M. Sakaguchi, A. Nakai, H. Hamada, N. Takeda, The mechanical properties of unidirectional thermoplastic composites manufactured by a micro-braiding technique, *Composites Science and Technology* 60 (2000), pp. 717-722.
- [14] K.-H. Im, D.K. Hsu, H. Jeong, Material property variations and defects of carbon/carbon brake disks monitored by ultrasonic methods, *Composites: Part B* 31 (2000), pp. 707-713.
- [15] M.D. Wakeman, T.A. Cain, C.D. Rudd, R. Brooks, A.C. Long, Compression moulding of glass and polypropylene composites for optimised macro- and micro-mechanical properties II. *Glass-mat-reinforced thermoplastics*.
- [16] M.N. Bureau , J. Denault, Fatigue resistance of continuous glass fiber/polypropylene composites: consolidation dependence, *Composites Science and Technology* 64 (2004), pp. 1785–1794.
- [17] A.R. Chambers , J.S. Earl, C.A. Squires, M.A. Suhot, The effect of voids on the flexural fatigue performance of unidirectional carbon fibre composites developed for wind turbine applications, *International Journal of Fatigue* 28 (2006), pp. 1389–1398.
- [18] G.E.P. Box, W.G. Hunter, and J.S. Hunter (1978). *Statistics for Experimenters. An Introduction to Design, Data Analysis, and Model Building*. New York: John Wiley and Sons.
- [19] R.V. Lenth (1989). "Quick and Easy Analysis of Unreplicated Factorials," *Technometrics*, 31, 469-473.
- [20] D.C. Montgomery (1991). *Design and Analysis of Experiments*, Third Edition, John Wiley and Sons.
- [21] Nair, V.N., and Pregibon, D. (1988). "Analyzing Dispersion Effects From Replicated Factorial Experiments", *Technometrics*, 30, pp.247-257.
- [22] Pan, G. (1999). "The Impact of Unidentified Location Effects on Dispersion-Effects Identification from Unreplicated Factorial Designs," *Technometrics*, 41, 313-326.

-
- [23] R.L. Plackett and J.P. Burman (1946). "The Design of Optimum Multifactorial Experiments," *Biometrika*, 34, 255-272.
 - [24] G. Taguchi, "*Introduction to quality engineering*", Asian Productivity organization, Tokyo, 1990.
 - [25] MiniTAB 14 *User's Manual*. MiniTAB Inc. 2003.
 - [26] Salar Basiri, VoidScan software, 2006.
 - [27] R.B. D'Agostino and M.A. Stephens, Eds. (1986). *Goodness-of-Fit Techniques*, Marcel Dekker.
 - [28] T.A. Ryan, Jr. and B.L. Joiner (1976). "*Normal Probability Plots and Tests for Normality*," Technical Report, Statistics Department, The Pennsylvania State University. (Available from Minitab Inc.)

Chapter 18

PROPERTIES OF POLYMER NANOCOMPOSITES BASED ON ORGANOMODIFIED Na^+ -MONTMORILLONITE

A. Y. Bedanokov, A. K. Mikitaev, V. A. Borisov and
M. A. Mikitaev*

Karpov Institute of Physical Chemistry,
Moscow, 105064, Russia, Vorontsovo pole st., 10

1. METHODS OF SYNTHESIZING POLYMER NANOCOMPOSITES BASED ON POLYETHYLENETEREPHTHALATE

One of the most important engineering plastics used in many branches of industry are polyalkyleneterephthalates. In this group polyethyleneterephthalate (PET) is of prime interest. Increase in the volume of producing PET is due to it's application in processing tare, fibers, films, construction details. High thermal stability, deformation-tensile and barrier properties of PET have particular meaning in this applications. These properties may be obtained by introducing layered silicates in polymer matrix.

Polymer materials, modified with layered silicate nanoparticles, have some significant advantages. For example, introducing Na^+ -montmorillonite into polymer matrix increases initial modulus, tensile strength, thermal stability and fire resistance, reduces gas permeability rate of material.

We are studying opportunities of manufacturing nanocomposite polymer materials in process of two-phase polyethyleneterephthalat synthesis and in process of melt blending using organically modified (organomodified) layered silicates based on Na^+ -montmorillonite. Polyethyleneterephthalat properties depending on it's nature and amount of organomodified layered silicate introduced into polymer matrix are in research. In the course of explorations for the first time were obtained nanocomposites via two declared methods using montmorillonite from bentonite clay of the Gerpegezh field (Russia, KBR).

* E-mail: azamat2@mail.ru

Forming of exfoliate structure with higher amount of organomodified layered silicate was determined in the process of synthesizing polyethyleneterephthalate compared to it's amount in process of melt blending.

Small-angle XRD analysis confirms allocating of organomodified layered silicate in composite on nanometer-thick level.

It is shown that using organomodified layered silicate based on russian produced montmorillonite with amount of organomodifier up to 25%, improved physical properties may be achieved, up to such properties of commercial organoclays (Bentonite-128, Bentonite-160) containing up to 35% of modifier. We determined the correlation between thermal properties and containing of nanomer particles in polyethyleneterephthalate. For the first time it was demonstrated that nanocomposites based on polyethyleneterephthalate and layered silicates have higher rate and degree of crystallinity.

2. POLYMER LAYERED SILICATE NANOCOMPOSITE STRUCTURE

Special attention in studying nanocomposite properties usually attracts to allocation of organomodified layered silicates on polymer matrix which plays important part due to depending of this properties on allocation.

One of the main methods of researching organomodified layered silicates allocation in nanocomposite is X-Ray diffraction method (XRD). Figure1 shows XRD patterns of nalchikit, nalchikit-M (organomodified nalchikit) and polyethyleneterephthalate containing different amount of nalchikit-M.

As it is seen from Figure1, there is a peak characteristic at region $2\Theta = 7,0^\circ$ ($d = 1,19$ nm) for nalchikit, peak characteristic at $2\Theta = 3,5^\circ$ ($d = 2,47$ nm) for nalchikit-M. In the course of introducing up to 5%wt of nalchikit-M to polyethyleneterephthalate polymer matrix there is no peak. It indicates about intercalation of clay leaves to separate silicate layers. Diffraction patterns exhibit full clay exfoliation.

Increase in nalchikit-M content to 7 wt% results in a peak on diffraction graph in the region $2\theta=6^\circ$, it's intensity is very low. Peak intensity maximum corresponds to $d=1,76$ nm. It suggests that in prepared composite areas with full nalchikit-M exfoliation coexists with areas with partially ordered layered packages. Further increase in nalchikit-M content to 10 wt% results in appearance of high intensity peak in the region $2\theta=6^\circ$. This peak appearance confirms presence of layered silicate as agglomeration.

Dependency of interplanar distance on organomodified layered silicate content in composites, produced via two-stage melt polycondensation using bentonite-128 and bentonite-160 as nanomer additive is the same as in composites produced using nalchikit-M (Figure2).

For nanocomposites produced via melt blending, formation of mixed type composite occurs already at 5 wt% of layered silicate in polyethyleneterephthalate. X-ray diffraction analysis patterns are shown on Figure3.

Obtained results, apparently, indicate on existence of threshold concentration that organomodified layered silicate can distribute at nanometer level in such polymer, with forming of nanocomposite of exfoliate structure.

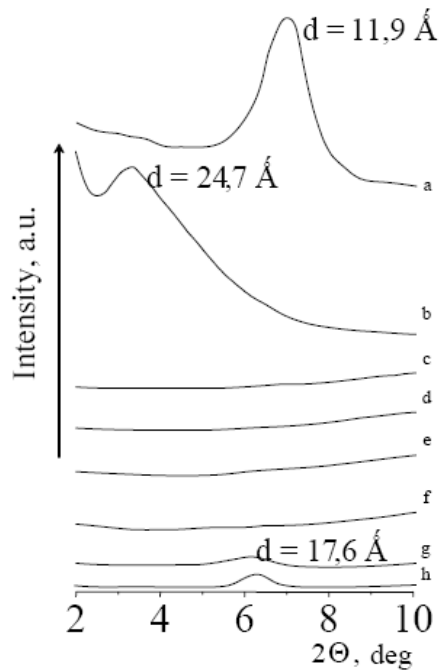


Figure 1. XRD patterns: a – nalchikit; b – nalchikit-M; polyethyleneterephthalate, produced via synthesis with nalchikit-M containing: c – 0%; d – 1%; e – 3%; f – 5%; g – 7%; h – 10%.

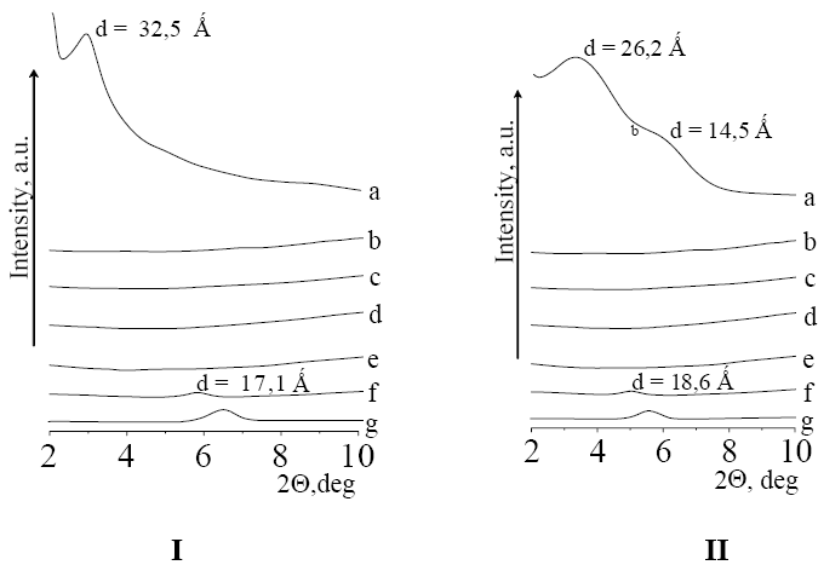


Figure 2. XRD patterns:

I: a – bentonite-128; polyethyleneterephthalate, produced via synthesis with bentonite-128 containing: b – 0%; c – 1%; d – 3%; e – 5%; f – 7%; g – 10%.

II: a – bentonite-160; polyethyleneterephthalate, produced via synthesis with bentonite-160 containing: b – 0%; c – 1%; d – 3%; e – 5%; f – 7%; g – 10%.

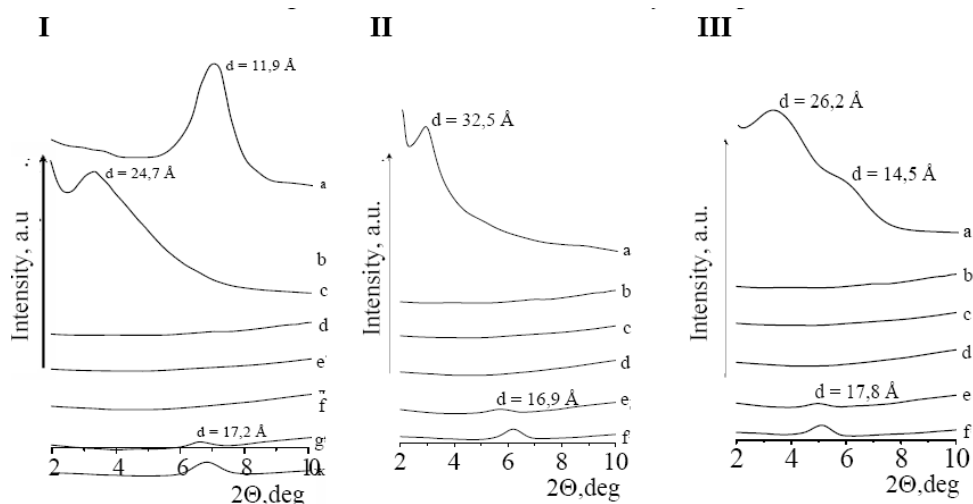


Figure 3. XRD patterns:

I: a – nalchikit; b – nalchikit-M; polyethyleneterephthalate, produced via melt blending with nalchikit-M containing: c – 0%; d – 1%; e – 3%; f – 5%; g – 7%.

II: a – bentonite-128; polyethyleneterephthalate, produced via melt blending with bentonite-128 containing: b – 0%; c – 1%; d – 3%; e – 5%; f – 7%.

III: a – bentonite-160; polyethyleneterephthalate, produced via melt blending with bentonite-160 containing: b – 0%; c – 1%; d – 3%; e – 5%; f – 7%.

However, threshold concentration of organomodified layered silicate is a few higher at processing on oligomer formation stage rather than in process of melt blending. It can be explained by expanding distance between silicate plates (interlayer space - gallery) in the synthesis process mainly as a result of penetration of growing polymer chains in a space between layers.

3. PHYSICAL-MECHANICAL PROPERTIES OF POLYETHYLENETEREPHTHALATE/LAYERED SILICATE NANOCOMPOSITES

Some physical-mechanical properties of nanocomposites produced by *in situ* method, and also produced via melt blending polyethyleneterephthalate with organomodified montmorillonite (nalchikit-M), educed from bentonite clay of Gerpegezh field (Russia, KBR) and from commercial clay bentonite-128.

Measurement results are shown in Table 1.

As it is seen from table 1 that the larger is the organomodified layered silicate content the higher are ultimate strength and initial modulus. It can be due to orientation of polymer chains in silicate layers. Percent elongation at break for all composites was equal to 4-8%.

Table 1. Some properties of polyethyleneterephthalate and nanocomposites based on it, produced via synthesis (*in situ*)

Composite		Properties	
		Ultimate strength, MPa	Initial modulus, GPa
PET + nalchikit-M	0	65	3,00
	1	73	3,52
	3	85	3,81
	5	94	3,98
	7	87	4,15
	10	78	4,26
% увеличения		12 to 44 %	17 to 42 %
PET + bentonite-128	1	71	3,48
	3	84	3,82
	5	93	4,01
	7	88	4,17
	10	80	4,23
% увеличения		9 to 31 %	16 to 41%

4. THERMAL PROPERTIES OF POLYMER NANOCOMPOSITES

Introducing organomodified layered silicates into polymer matrix, it brings to polymer thermal stability change.

To estimate thermal stability of obtained polyethylene-terephthalate/layered silicate nanocomposites the following well-known methods were used: thermal gravimetric analysis (TGA), differential scanning calorimetry (DSC) and melt thermal stability coefficient determination. Results of thermal stability research for polyethyleneterephthalate/layered silicate are shown in Table 2.

Table 2. Molten polyethyleneterephthalate/layered silicate thermal stability, 255 °C and 2,16 kg

Composite	MFI ₅ , ^{*)} g/10 min	MFI ₁₅ , ^{**)} g/10 min	MFI ₃₀ , ^{**)} g/10 min	K _{15/5} ^{****)}	K _{30/5} ^{*****)}
PET	35	44	62	1,26	1,77
PET + 1 % nalchikit-M	34	35	33	1,02	0,97
PET + 3 % nalchikit-M	37	33	41	0,9	1,11

Table 2. (Continued)

Composite	MFI ₅ , ^{*)} g/10 min	MFI ₁₅ , ^{**)} g/10 min	MFI ₃₀ , ^{***)} g/10 min	K _{15/5} ^{****)}	K _{30/5} ^{*****)}
PET + 5% nalchikit-M	32	39	34	1,21	1,06
PET + 7% nalchikit-M	38	43	50	1,13	1,32
PET + 10% nalchikit-M	42	49	61	1,16	1,45

^{*)} - MFI value after 5-min exposition in device chamber;

^{**)} - MFI value after 15-min exposition in device chamber;

^{***)} - MFI value after 30-min exposition in device chamber;

^{****)} - $K_{15/5}$ – MFI₁₅ to MFI₅ ratio;

^{*****)} - $K_{30/5}$ – MFI₃₀ to MFI₅ ratio.

There are two explanations of increased melt PET thermal stability when organomodified layered silicates are introduced. On the one hand the increased PET thermal stability is connected with barrier properties of layered silicate itself. On the other - layered silicate plate can participate as a binding bridge between two polymer macromolecules, which can fix end-groups and decrease their hydrolytic activity.

Results on thermal gravimetric analysis (TGA) are shown in Figure 4 and Table 3.

Table 3. Thermal gravimetry analysis data* for polyethyleneterephthalate and nanocomposites based on it, produced via synthesis

Nalchikit-M, wt %	Destruction temperature, °C	Coke residue value at 600°C, %
0	380	1
1	398	8
3	400	19
5	400	24
7	394	26
10	390	20

*on air.

It was found basing on TGA data that initial destruction temperature raises for all prepared nanocomposites containing up to 5%. In contrast to original PET all nanocomposites decompose producing coke residue, which number increases with higher content of layered silicate. Nanocomposite presence indicates on more complex behavior of nanocomposite thermodestruction process. It is likely that the layered silicate addition is an initiator of coking as a result of barrier effects to volatile products, formed in process of thermal destruction and other processes, concerned with change of macromolecular chains entropy in near-surface nanocomposite layers.

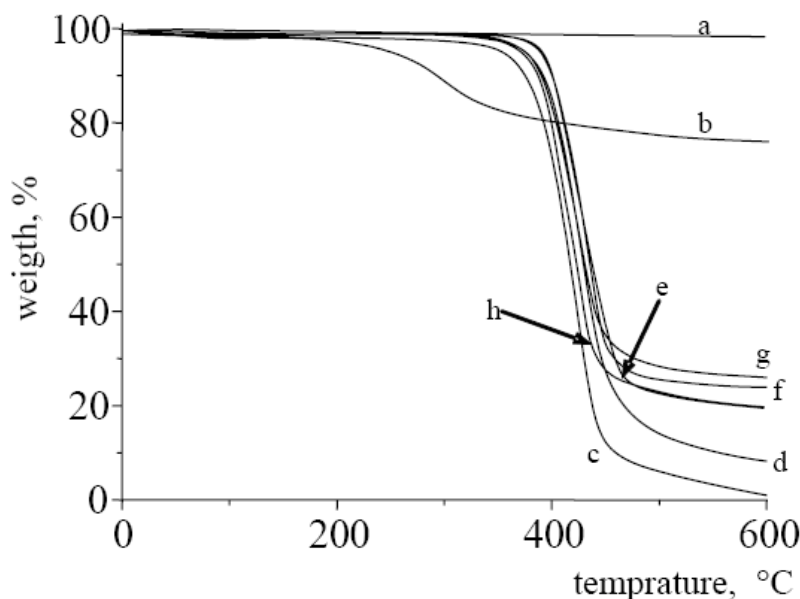


Figure 4. Thermogravimetric analysis curves (on air, 20 °C/min):

a – nalchikit; b – nalchikit-M; c – polyethyleneterephthalate; nanocomposites produced via synthesis with nalchikit-M containing: d – 1%; e – 3%; f – 5%, g – 7%, h – 10%.

DSK data demonstrate raise of PET crystallinity rate in the presence of nano-particles. It is confirmed by calculations of crystallization half-time at melt freezing. Crystallization half-time ($t_{1/2}$) for nanocomposites is always lower than pristine PET. Nanocomposite containing 5% of nalchikit-M has the lowest $t_{1/2}$ (1,35 min) and its crystallinity rate (2,25 min) is 1,67 times higher than pristine PET.

Also it is discovered that initial crystallization temperature of nanocomposites is higher (204-207°C) than polyethyleneterephthalate (190°C). In turn, nanocomposites melting temperature is lower than PET melting temperature. Melting temperature lowering can be explained by reduced crystallite sizes. Narrowing of melting peak width indicates on more narrow lay-out in crystallite sizes in polyethyleneterephthalate nanocomposites. The ΔH_m value for all nanocomposites is higher than for polyethyleneterephthalate (42 joule/g) and raises at nalchikit-M content increase. It means that PET crystallinity rate raises in the presence of nalchikit-M.

CONCLUSION

Experimental results obtained allow to mark a promise of this research direction. Developing new polymer composite materials based on natural layered silicates and polyethyleneterephthalate - the most needed polymer material - gives opportunity to modify PET properties and therefore expand the field of its application.

INDEX

A

- absorption spectra, 66, 67, 68, 69
access, 66, 73
accuracy, 23, 52, 58, 197, 224
acetic acid, 11, 145
acetone, 196
acetophenone, 197
acetylcholine, 11, 12
acetylcholinesterase, 17
achievement, 8, 218
acid, 6, 11, 13, 17, 84, 130, 132, 133, 134, 191, 202
acrylate, 191
acrylic acid, 145
activation, 34, 42, 43, 44, 101, 203
activation energy, 101
active oxygen, 8
active radicals, 6
actuators, 193
additives, 164, 195, 196, 197, 202, 203, 212, 218
adhesion, 141, 188
age, 4, 212, 213
ageing, 76
agent, 8, 169, 171, 175, 207
aggregates, vii, 49, 50, 51, 52, 54, 55, 149, 151, 205, 209, 218
aging, 4, 16, 17
agriculture, 83
alanine, 129, 130, 131
albumin, 84
alcohol, 145
alcohols, 72
aldehydes, 1, 30, 32
algorithm, 68
alkenes, 29
alternative, 7, 58, 170, 218, 221
alternatives, 180, 192
ambient air, 112, 127
amines, 10
amino acid, 84, 129, 131
ammonium, 191
animals, 2, 4, 7, 13, 208
anion, 6, 10, 86
anisotropy, 22, 50, 51, 52, 54
annihilation, 36
ANOVA, 222
anthracycline, 8
anti-apoptotic, 76
antibiotic, 8
anticholinesterase, 12
anti-inflammatory, 76
antimetabolites, 8
antioxidant, 2, 3, 4, 5, 6, 7, 8, 10, 11, 12, 13, 16, 17, 75
antioxidants, vii, 1, 2, 3, 4, 5, 6, 7, 8, 11, 13, 15, 16
antitumor, 3, 8, 9, 10, 14, 16
antitumor agent, 4, 8, 9, 10
apoptosis, 76
argon, 66
argument, 5
Arrhenius parameters, 32
arteriosclerosis, 75, 76
asbestos, 207
ash, 210, 211, 212, 213, 214, 216, 218
assessment, 43, 206
assumptions, 170, 226
asthma, 75, 76
asymptotics, 160
atoms, 20, 34, 35, 39, 58, 59, 60, 61, 92, 94
attachment, 141
attacks, 34
automation, 99
availability, 171, 205
azidothymidine, 10, 11

B

bacteria, 190
band gap, 57, 62
BAO, 5, 6
base pair, 66, 67, 70, 73
basis set, 26
behavior, 57, 61, 62, 73, 154, 174, 175, 184, 187, 216, 240
bending, 96, 112, 114, 126, 222
benzene, 119
benzopyrene, 3
bias, 57
bile, 76, 81
bile duct, 76, 81
biliary cirrhosis, 76, 81
bilirubin, 76, 77, 81
biliverdin, 75, 77, 82
biliverdin reductase, 76, 77, 82
binding, 10, 66, 68, 70, 73, 76, 86, 170, 240
bioantioxidant, 5, 12
bioantioxidants, 3, 4, 5, 11, 17
biochemistry, 5, 8, 17
biocompatibility, 141
biodegradability, 141
biodegradable, 141, 143, 208
biological activity, vii, 3, 4, 8, 11, 16
biological systems, 12, 158
biologically active compounds, 10
biomacromolecules, 66
biomass, 85
biomedical applications, 113, 141
biophysics, 5
biopolymer, 2, 65, 66, 68, 70, 72, 73
biosensors, 179, 190
biosynthesis, vii, 15, 85, 86, 87
biotechnology, 146
bitumen, vii, 147, 148, 149, 150, 151, 152, 153, 154
blends, 143, 177, 191
blood, 17, 143, 190
bonding, 66, 172, 217
bonds, 7, 20, 33, 34, 45, 46, 58
brain, 12, 13, 16, 17, 76
Brazil, 62
breakdown, 75
bromine, 180
buffer, 50, 66, 67, 68, 69, 70, 71, 72, 77, 86
bulk materials, 97
butadiene, 144
butadiene-styrene, 144

C

Ca²⁺, 76
cabbage, viii
caffeine, 190
calcium, 144, 171, 176, 217
calcium carbonate, 144
calculus, 227
calorimetry, 43
candidates, 113
capacitance, 94, 189
capillary, 113, 120, 122
carbon, 12, 39, 57, 58, 59, 75, 82, 130, 131, 144, 208, 231, 232
carbon atoms, 58, 130
carbon monoxide, 75, 82
carbon nanotubes, 57
carbonyl groups, 28
carboxylic acids, 11
carcinogen, 3
carcinogenesis, 3
carrier, 181, 182
cashmere, 145
cast, 130, 213
casting, 213
catalysis, 197, 199, 200, 201, 203
catalyst, 58, 195, 196
catalysts, 170, 195, 204
catalytic activity, 89, 196, 200
catalytic effect, 202
catalytic system, 195, 196, 198, 199, 203
cation, 25, 169
cattle, 4
cDNA, 69, 70, 71
cell, 1, 2, 4, 5, 6, 8, 11, 12, 13, 50, 66, 75, 84, 86, 87, 88, 141, 145, 146, 186
cell culture, 5
cell membranes, 11, 12
cell metabolism, 4, 5, 6, 12, 13
cellulose, 21, 23, 26, 128, 132, 140, 146
cellulose triacetate, 146
cellulose xanthate, 140
ceramics, 92
certificate, 15, 16
chalcogenides, 57
charge density, 111, 118, 123, 125, 127
chemical bonds, 20
chemical composition, 208, 210
chemical properties, 57
chemical reactions, 173, 222
chemical vapor deposition, 57
chemiluminescence, 3
chemotherapy, 8, 16

- chicken, 67, 84
children, vii
Chinese, vii
chirality, 59, 61
chitin, 146
chloride, 84, 118, 170
chlorobenzene, 119
chloroform, 21, 119
cholesterol, 13, 17, 190
chromatography, 89, 90
classes, 4, 58, 128
classification, 128
cleaning, 206
clone, 87, 88, 89
C-N, 30, 58, 59, 60
coatings, 93, 94
cobalt, 82, 84
cocoon, 128, 129
cognitive function, 12
cohesion, 149, 150, 151
coke, 240
collagen, 141
community, 207
compatibility, 107
competition, 42, 43, 45, 124, 216
components, vii, 2, 3, 6, 7, 8, 9, 10, 26, 67, 68, 69,
71, 73, 77, 100, 112, 113, 127, 185, 189, 205, 217
composites, vii, 21, 22, 23, 25, 50, 108, 191, 206,
207, 209, 212, 215, 216, 218, 221, 222, 231, 232,
236, 238
composition, 1, 2, 4, 7, 12, 17, 30, 57, 77, 129, 161,
164, 169, 171, 200, 209, 211
compounds, vii, 2, 3, 4, 5, 7, 8, 10, 11, 12, 16, 19,
31, 57, 58, 66, 83, 90, 171, 189, 196
compressibility, 163, 164, 166
concentrates, 205
concentration, 3, 6, 7, 21, 22, 23, 25, 50, 51, 52, 55,
67, 68, 70, 71, 76, 77, 78, 79, 81, 84, 87, 115,
116, 117, 118, 120, 122, 123, 125, 133, 134, 135,
136, 137, 138, 140, 157, 158, 159, 160, 161, 162,
163, 164, 165, 166, 176, 190, 191, 195, 197, 201,
236, 238
concrete, 166, 173, 205, 206, 207, 208, 209, 217,
218, 219
conditioning, 154
conduction, 93, 100, 101, 186
conductivity, 96, 98, 100, 101, 102, 112, 116, 117,
118, 120, 124, 125, 126, 181, 184, 186, 187, 188,
192
conductor, 57, 186
confidence, 170, 224, 228
confidence interval, 224, 228
configuration, 94, 184, 186
conformity, 4
conjugated bilirubin, 76
conjugated dienes, 30
conjugation, 180
conservation, 101, 126, 218
consolidation, 232
constant rate, 107
construction, 173, 176, 205, 207, 217, 218, 235
consumption, 6, 7, 189, 197, 202, 203
contaminants, 206
contamination, 171
control, 23, 78, 80, 81, 83, 92, 93, 123, 171, 172,
176, 190, 195, 196, 197, 203, 212, 214, 216, 227
convergence, 38
conversion, 19, 21, 22, 25, 26, 27, 28, 29, 195, 196,
197, 199, 203
cooling, 208
copolymers, 143
correlation, 3, 12, 34, 50, 174, 175, 197, 236
correlation function, 34
correlations, 159, 166
corrosion, 181, 206
cosmic rays, 96
cost effectiveness, 206
costs, 100, 147, 187
cotton, 128, 129, 208
couples, 126
coupling, 126
covalent bond, 92
creep, 153, 154, 172
creep tests, 154
crystallinity, 241
critical value, 114, 122, 231
crude oil, 208
crystal structure, 22
crystalline, 129, 131, 169, 189
crystallinity, 241
crystallization, 241
crystals, 119
CTA, 140, 141
cultivation, 87, 88
cultivation conditions, 88
culture, 141
cumulative distribution function, 228
curing, 2, 3, 4, 92, 173, 216
current ratio, 182
CVD, 58
cycles, 149, 217, 232
cycling, 188, 216, 217
cytochrome, 82
cytomegalovirus, 11
cytoprotectant, 81
cytotoxic, 8, 79

D

death, 2, 11
 decay, 2, 67, 68, 70, 71, 73, 145
 decomposition, 1, 2, 25, 28, 32, 72, 140, 158, 196, 203
 decontamination, 83
 defects, 7, 221, 232
 deficiency, 5, 159
 definition, 5, 209
 deformation, 126, 154, 162, 167, 235
 degradation, 90, 187, 205, 216, 217
 degree of crystallinity, 236
 degumming, 139
 delivery, 122, 143
 demand, 207
 density, 26, 34, 35, 61, 92, 100, 101, 102, 104, 118, 123, 173, 181, 192, 207
 density functional theory, 26
 deposition, 57, 116, 144, 189, 190
 derivatives, 3, 8, 9, 10, 11, 16, 83, 140, 157, 166, 180, 227
 designers, 221, 231
 desire, 206
 destruction, 22, 240
 detachment, 34, 41
 detection, 28, 67, 75, 76, 144, 191, 217
 deviation, 37, 51, 228
 DFT, 35, 36, 38
 dialysis, 132
 dichloroethane, 119
 dielectric constant, 97, 98, 112, 120, 127
 dielectric materials, 92
 dielectric permeability, 21, 114
 dielectric permittivity, 72
 dielectric strength, 116
 dielectrics, 92, 98
 dienes, 29, 45, 46
 differential scanning, 239
 differential scanning calorimetry, 239
 differentiation, 141, 197
 diffraction, 236
 diffusion, 50, 71, 72, 73, 101, 176
 diffusion process, 176
 diffusivity, 101, 105
 dimensionality, 162
 dimer, 19, 21
 dimethylformamide, 119
 dipole, 50, 51, 92
 direct measure, 43
 disappointment, 107
 disorder, 12
 displacement, 54

dissociation, 71
 distribution, 50, 51, 92, 98, 116, 120, 121, 140, 175, 190, 211, 228
 DMF, 119
 DNA, vii, 2, 4, 8, 10, 11, 65, 66, 67, 68, 69, 70, 71, 72, 73, 90, 143, 144, 190
 doors, 206
 doping, 179, 180, 181, 186, 187
 dosage, 171
 double bonds, 20
 double helix, 66, 70, 73
 drug release, 113
 drugs, 7, 12, 14, 143
 drying, 77, 92, 93, 94, 102, 103, 106, 107, 108, 205, 217
 DSC, 239
 DSM, 169
 durability, 170, 171, 177, 207, 208, 209, 217
 dyeing, 93
 dyes, vii, 65, 66, 67, 68, 69, 70, 71, 72, 73, 93, 94, 186

E

E.coli, 84, 85, 86, 87, 88, 89, 90
 economics, 209
 education, vii
 egg, 84
 elaboration, 83
 elastic deformation, 154
 elasticity, 115, 205
 elastomers, 29, 189
 electric charge, 126
 electric current, 120, 142, 186
 electric field, 92, 97, 100, 111, 112, 113, 114, 116, 120, 126, 127, 133, 134, 135, 136, 137, 138, 141, 145, 181, 183, 184, 186
 electrical conductivity, 115, 118, 123, 125, 126
 electrical properties, 116
 electricity, 112, 127
 electrochemical reaction, 186
 electrochromic films, 189
 electrodes, 181, 183, 185, 189, 191
 electrolyte, 181, 186, 187
 electromagnetic, 91, 92, 93, 96, 97, 99, 100
 electromagnetic wave, 99
 electromagnetic waves, 99
 electron, vii, 17, 19, 20, 26, 42, 43, 49, 50, 70, 92, 96, 119, 190, 195, 196, 203
 electron pairs, 42
 electronic structure, 58, 61
 electronic systems, 183
 electrons, 37, 91, 94, 96, 180, 181

electrophoresis, 84, 89
 electrospinning, 112, 113, 114, 116, 118, 120, 122,
 124, 126, 129, 131, 132, 135, 137, 138, 139, 140,
 141, 142, 143, 144, 145, 146, 184, 185
 elongation, 70, 117, 118, 120, 125, 238
 emission, 186, 191
 emitters, 94
 encoding, vii, 83, 84, 86, 90
 endothermic, 26
 energy, 20, 26, 28, 33, 34, 35, 36, 38, 39, 41, 42, 43,
 58, 60, 61, 66, 70, 71, 91, 92, 93, 94, 96, 97, 98,
 99, 101, 107, 108, 117, 157, 162, 166, 207
 energy consumption, 26, 93
 energy transfer, 70, 71, 99
 entanglements, 117, 135, 144
 entrapment, 221
 entropy, 44, 161, 166, 240
 environment, 83, 100, 103, 106, 148, 170, 172, 179,
 206, 207, 211, 216, 217, 218
 environmental conditions, 222
 environmental issues, 207
 enzymatic activity, 81, 86
 enzyme, 12, 75, 78, 79, 81, 82, 83, 86, 90, 190
 enzymes, 4, 5, 6, 7, 190
 epoxy, 231, 232
 EPR, 13, 19, 21, 22, 23, 28, 50
 equilibrium, 20, 22, 51, 106, 114
 equipment, 93
 erythrocyte membranes, 17
 erythrocytes, 12
 ESR, 30, 50
 ester, 11, 21
 ethers, 11
 ethylene, 32, 33, 34, 36, 38, 39, 40, 42, 43, 45, 143,
 144
 ethylene oxide, 143, 144
 evaporation, 21, 103, 105, 123, 140, 189
 evolution, 222
 excitation, 66
 exercise, 231
 experimental condition, 103
 experimental design, 137
 exposure, 2, 7, 21, 22, 23, 24, 25, 28, 29, 30, 148,
 172, 211
 extinction, 67
 extracellular matrix, 145

F

fabric, 93, 94, 231
 fabrication, 143, 144, 186, 189, 190
 failure, 99, 149, 152, 154, 206, 216, 221, 222, 224,
 231

fat, 1, 2
 fatigue, 147, 149, 152, 154, 155, 171, 222, 232
 Fermi level, 61
 ferrite, 99
 ferritin, 75
 ferrofluids, 50
 ferromagnetic, vii, 51
 ferromagnets, 51
 fiber bundles, 172
 fiber content, 216
 fibers, 104, 111, 112, 113, 115, 116, 118, 119, 120,
 122, 123, 125, 128, 130, 132, 133, 134, 135, 137,
 139, 140, 141, 142, 143, 144, 145, 146, 169, 172,
 205, 207, 210, 216, 217, 223, 226, 235
 fibroblasts, 141
 filament, 57, 129
 film, 52, 53, 129, 130, 181, 187, 189, 190, 192
 film thickness, 190
 films, 50, 52, 53, 54, 130, 172, 188, 189, 191, 235
 fire resistance, 235
 fixation, 11
 flexibility, 113, 181, 183, 189
 fluctuations, 216
 fluid, 94, 112, 113, 114, 120, 126, 145
 fluorescence, 17, 66, 83, 86, 90
 fluorine, 84
 focusing, 179
 food, 2, 79, 81, 91, 92, 190
 food industry, 2
 formaldehyde, 34, 170, 208
 formamide, 26, 27
 France, vii, 167, 206
 free energy, 117, 157, 158, 160, 161, 162, 163, 165,
 166
 free radicals, 2, 5, 7, 12, 34
 free volume, 158
 free will, viii
 free-radical, 2, 3, 5, 6, 8
 freezing, 241
 friction, 92
 fusion, 83, 84

G

gas phase, 20, 22, 25, 32
 gas sensors, 179, 191
 gases, 58, 191
 Gaussian, 26, 30, 35, 43, 47, 158
 gel, 21, 84, 208
 gelation, 191
 gene, 6, 76, 81, 82, 84, 86
 gene expression, 6, 76, 81, 82
 generation, 17, 20, 21, 26, 28, 30, 171

- Germany, 86
gerontology, 4
Gibbs energy, 43, 44
gland, 128, 132
glass, 108, 140, 183, 186, 187, 197, 205, 206, 207, 208, 209, 210, 211, 212, 213, 216, 217, 218, 219, 232
glasses, 211
glucose, 77, 140, 190
glutathione, 76
glycine, 129, 130
gold, 224
grades, 224
grains, 171
graph, 36, 78, 79, 224, 228, 236
graphite, 57, 232
gravimetric analysis, 239, 240
gravitational constant, 104
gravity, 94, 112
greenhouse gases, 207
groundwater, 206
groups, 19, 20, 21, 23, 25, 26, 27, 28, 29, 30, 45, 92, 115, 125, 126, 128, 169, 191, 240
growing polymer chain, 238
growth, 3, 4, 58, 140, 141, 158, 206, 217, 222
guidance, 1, 176
homeostasis, 12, 13
homogeneity, 227
homogeneous catalyst, 203
homolytic, 203
Honda, 16, 47
host, 84, 93
hot spots, 92
households, 91
housing, 205
human immunodeficiency virus, 11
human organisms, 15
humidity, 105, 179, 191
Hungary, 67
hybrid, vii, 7, 8, 10, 11, 12, 183, 184
hydrocarbons, 34, 45
hydrogen, 20, 130
hydrogen atoms, 20
hydrogen bonds, 130
hydrolysis, 83, 86, 89, 206
hydroxide, 217
hyperbilirubinemia, 76, 81
hyperfine interaction, 24
hyperplasia, 3, 81
hypothesis, 1, 2
hypoxia, 76
hysteresis, 183

H	I
----------	----------

- halogen, 10, 34
hardness, 191, 209
hazards, 207
health, 207
heart attack, 18
heat, 91, 92, 93, 96, 97, 98, 99, 100, 101, 102, 103, 105, 108, 129, 218
heat capacity, 101, 102
heat transfer, 93, 99
heating, 91, 92, 93, 94, 97, 98, 99, 100, 101, 103, 108
heating rate, 93
heavy metals, 76
height, 149
heme, vii, 75, 77, 78, 79, 81, 82
heme degradation, 75, 76
heme oxygenase, vii, 77, 78, 79, 81, 82
hemp, 128, 208
hexagonal lattice, 58
hexane, 119
higher quality, 172
histone, 90
HO-1, 75, 76, 81
HO-2, 76
identification, 55, 181, 192, 207
image analysis, 132
images, 87, 115, 118, 119, 140, 141
immobilization, 190
immobilized enzymes, 190
immunodeficiency, 11
in situ, 137, 203, 238, 239
in transition, 7
in vitro, 2, 5, 8, 12
in vivo, 3, 5, 8, 12, 66, 82, 90
independence, 160, 165, 166
independent variable, 106
indication, 139, 218
indices, 6, 12, 58
indium, 189
inducer, 79
inducible enzyme, 76
induction, 1, 33, 38, 44, 75, 76, 81, 82, 87, 88, 89
inductor, 84, 85
industrial application, 91, 98, 169
industrial sectors, 211
industry, 49, 93, 179, 205, 207, 208, 218, 221, 235
inflammation, 76
infrastructure, 207

inhibition, 11, 12, 203
 inhibitor, 196, 200, 203
 initial reagents, 33
 initial state, 7, 26
 initiation, 19, 20, 28, 203, 222
 instability, 92, 112, 126, 142, 145
 insulation, 181, 218
 insulators, 92, 96, 218
 integration, 22, 23, 163, 164, 189
 intensity, 50, 83, 113, 236
 interaction, vii, 6, 8, 20, 21, 26, 27, 34, 40, 50, 51,
 52, 66, 92, 100, 135, 144, 158, 159, 170, 191
 interaction effect, 135
 interactions, 11, 12, 21, 26, 29, 50, 67, 91, 216
 interface, 170, 182, 216
 internet, 55
 introns, 76
 inversion, 100
 ionic conduction, 98, 120
 ions, 30, 76, 181
 IR, 21, 28, 29, 130
 IR spectra, 21, 28, 29, 130
 IR spectroscopy, 21
 Iran, 91, 109, 111, 147, 169, 179, 205, 221
 iron, 75, 76, 191
 irradiation, 1, 2, 3, 98, 107
 ischemia, 75, 76
 isobutylene, 30
 isolation, 5, 84
 isophthalic acid, 21
 isotope, 34

J

Japan, 63, 66, 167

K

keratinocytes, 141, 146
 ketones, 1, 30
 killing, 77
 kinetic model, 68
 kinetics, 2, 31, 67, 68, 70, 71, 73, 87, 103, 200

L

labeling, 189
 lactic acid, 144
 laminated composites, 231
 land, 218
 landfills, 218
 laser ablation, 57

leakage, 99, 189
 leukemia, 10
 lifestyle, 205
 lifetime, 182, 187
 ligand, 8, 10, 84, 203
 ligands, 66, 195, 196
 light emitting diode, 192
 light transmission, 189
 light-emitting diodes, 181
 likelihood, 94, 171
 linear dependence, 71, 92
 linear function, 162, 163
 linear macromolecule, 167
 linear model, 230
 links, 158, 159, 160, 165
 lipid metabolism, 12
 lipid peroxidation, 4, 7, 12, 13
 lipids, 1, 2, 3, 4, 5, 6, 7, 12, 15
 liposomes, 190
 liquid phase, 20, 45, 206
 liquids, 93
 Lithuania, 84
 liver, vii, 1, 76, 77, 81, 82
 localization, 65
 low temperatures, 30, 32
 lumen, 128
 lung, 76
 lung disease, 76
 lying, 161
 lysozyme, 84, 86

M

machinery, 97
 macromolecular chains, 240
 macromolecules, 11, 12, 19, 20, 27, 29, 157, 158,
 160, 161, 162, 163, 164, 165, 166, 240
 macrophages, 82
 magnesium, 171
 magnet, 52
 magnetic field, 49, 53, 96
 magnetic moment, 50, 52, 54
 magnetic particles, 55
 magnetic properties, 49
 magnetic resonance, vii, 49, 50, 55
 magnetization, 49, 50, 52, 53, 54, 55
 malignant growth, 14
 malignant tumors, 8
 manufacturing, 94, 112, 179, 183, 209, 216, 221,
 231, 235
 market, 208, 209
 MAS, 131
 material surface, 93

- materials science, 146, 207
 matrix, 50, 54, 65, 92, 130, 131, 132, 140, 143, 144, 170, 181, 183, 189, 190, 191, 192, 207, 216, 217, 222, 223
 measurement, 67, 79, 98, 190, 231
 mechanical behavior, 144
 mechanical properties, 57, 189, 207, 222, 232
 media, 50, 52, 113, 187
 medicine, 49, 55
 MEK, 119
 melamine, 208
 melt, 113, 187, 235, 236, 238, 239, 240, 241
 melting, 241
 melting temperature, 241
 melts, 167
 membranes, 1, 4, 7, 12, 13, 143
 memory, 12
 Merck, 21, 77
 Mercury, 82
 metabolism, 4, 5, 6, 7, 76
 metabolites, 190
 metals, 96, 179, 181, 206
 methanol, 67, 72, 130
 methyl group, 73
 methyl groups, 73
 MFI, 239, 240
 mice, 10, 13
 microelectronics, 179
 micrometer, 112, 184
 microorganisms, 7
 microscope, 86, 87, 119
 microsomes, 77, 78, 79, 80
 microstructure, 58, 108
 microstructures, 57
 microviscosity, 13
 microwave, 91, 92, 93, 94, 95, 96, 97, 98, 99, 100, 101, 102, 103, 104, 107, 108
 microwave heating, 92, 93, 94, 97, 99, 100, 103, 108
 microwave radiation, 92, 97
 microwaves, 91, 92, 93, 95, 96, 97, 99, 100, 101, 103, 107
 migration, 94, 98, 103, 170, 176
 military, 113
 minerals, 171, 208
 MIP, 44
 mixing, 77, 144, 172, 189, 208
 mobility, 52, 54, 180, 182
 modeling, 108, 142, 144, 146, 228
 models, 3, 10, 12
 moderates, 175
 modified polymers, 191
 modulus, 148, 149, 150, 151, 154, 205, 211, 235, 238, 239
 moisture, 92, 93, 98, 101, 102, 103, 129, 169, 170, 205, 208, 216, 221
 moisture content, 92, 93, 98, 101, 102, 103
 molar volume, 160, 164, 165
 mold, 208
 mole, 86, 162
 molecular mass, 87, 88
 molecular mobility, 22
 molecular oxygen, 34, 41
 molecular structure, 180
 molecular weight, 84, 88, 89, 114, 115, 116, 117, 123, 125, 126, 145
 molecules, 5, 7, 8, 10, 11, 30, 65, 66, 67, 68, 70, 72, 73, 91, 92, 158, 161, 182, 190
 momentum, 126, 127
 monomer, 189, 196
 monomers, 195, 196
 monotherapy, 7
 morphology, 115, 117, 118, 119, 120, 121, 123, 124, 125, 133, 134, 135, 140, 145, 192, 232
 Moscow, viii, 1, 13, 19, 31, 49, 55, 57, 65, 82, 83, 84, 90, 157, 167, 195, 204, 235
 motion, 30, 50, 98, 103
 moulding, 232
 movement, 92, 181
 multiple factors, 231
 multiple regression, 136, 137, 226
 multiple regression analysis, 136, 137
 multiplicity, 82, 162
 multiwalled carbon nanotubes, 58

N

- Na⁺, vi, 235
 NaCl, 86, 117, 118, 119
 nafion, 191
 nanocomposites, 142, 143, 235, 236, 238, 239, 240, 241
 nanofibers, vii, 112, 113, 118, 119, 120, 122, 124, 130, 131, 132, 133, 135, 141, 142, 143, 144, 145, 146, 184
 nanofibrous membranes, 144
 nanomaterials, 57
 nanometer, 236
 nanometers, 111, 112
 nanoparticles, vii, 49, 50, 51, 52, 54, 55, 235
 nanostructures, 55
 nanotube, 57, 58
 nanotubes, vii, 57, 58, 59, 60, 61, 186
 nanowires, 186
 National Research Council, 155
 NATO, 90
 natural resources, 207

nausea, 8
 neglect, 50, 161
 negligence, 6
 nerve, 13
 nerve fibers, 13
 Netherlands, 155
 neurons, 17
 neutrons, 94
 New Jersey, 74
 New York, 29, 30, 46, 83, 167, 204, 232
 nickel, 195, 196, 202, 203
 nitrate, 10, 19, 20, 21, 29, 140
 nitric acid, 26
 nitric oxide, 19, 20, 26, 29, 81
 nitric oxide synthase, 81
 nitrides, 57
 nitrobenzene, 119
 nitrogen, vii, 11, 12, 19, 20, 21, 22, 25, 26, 27, 28, 29, 30, 58, 59
 nitrogen dioxide, 19, 20, 21, 22, 25, 26, 27, 28, 29, 30
 nitrogen oxides, vii, 29
 nitroso compounds, 20
 nitrosoamides, 30
 nitroxyl, 8, 10, 11, 16, 30, 65, 66, 69, 71, 72, 73
 nitroxyl radicals, 8, 10, 30
 NMR, 130, 131
 N-N, 58
 Nobel Prize, 1
 noise, 96
 normal distribution, 228
 nucleation, 140
 nuclei, 94
 nucleotide sequence, 84
 nucleus, 76, 94

O

observations, 177, 222
 oil, 1
 olefins, 20, 32, 44, 45, 46
 oligomers, 183
 one dimension, 106
 operon, 86
 optical fiber, 191
 optical properties, 179, 186
 optimization, 26, 35, 38, 58, 68, 144, 146, 196
 optimization method, 196
 optoelectronic devices, 113
 organ, 4
 organic compounds, vii, 46
 organic fibers, 172
 organic solvent, 72, 129

organic solvents, 72, 130
 organism, 4, 5, 7
 organization, 161, 233
 orientation, 34, 49, 52, 53, 54, 55, 96, 231, 238
 orthoaminoazotoluene, 3
 oscillation, 43
 osmotic pressure, 157, 158, 159, 160, 161, 162, 163, 164, 165, 166
 ototoxicity, 8
 oxidation, vii, 1, 2, 5, 7, 8, 10, 12, 13, 30, 34, 179, 186, 187, 188, 195, 196, 197, 198, 199, 200, 201, 202, 203, 204
 oxidation products, 1, 7, 197
 oxidative damage, 75
 oxidative stress, 12, 13, 16, 76, 82
 oxides, 32, 57, 144, 189, 208
 oxidizability, 4, 7
 oximes, 20
 oxygen, 34, 39, 41, 65, 66, 67, 73
 ozonation, 44, 45, 46
 ozone, vii, 31, 32, 33, 34, 36, 37, 38, 39, 40, 41, 42, 43, 44, 45, 46
 ozonides, 32
 ozonolysis, 34

P

PAA, 118, 119
 packaging, 210
 PAN, 120, 142, 144, 188
 parameter, 58, 124, 125, 137, 144, 158, 165, 171, 199, 200, 227
 partial differential equations, 106
 particles, 21, 22, 50, 51, 52, 55, 94, 119, 169, 171, 196, 203, 207, 208, 211, 218, 236, 241
 pathophysiology, 16
 pathways, 5, 7, 26, 35, 42, 43, 44, 45, 46
 patterning, 184, 185
 PCR, 84
 PEP, 39
 peptides, 17
 percolation, 184
 permeability, 76, 82, 100, 104, 105, 217, 235
 permeation, 12
 permit, 5, 73
 permittivity, 97, 100
 peroxidation, 7
 peroxide, 32, 34
 peroxide radical, 32, 34
 peroxides, 5
 peroxyxynitrite, 20
 perylene, 183
 pesticides, 83, 90

- PET, 143, 235, 239, 240, 241
pH, 50, 66, 67, 72, 77, 81, 83, 84, 86, 90, 171, 187, 217
phage, 86
pharmacology, 8
phenol, 11, 13, 78, 82, 170, 195, 196, 197, 200, 202, 208
phenomenology, 203
PhOH, 196, 197, 198, 199, 200, 201, 202, 203
phospholipids, 17
phosphorous, 90
photochemiluminescence, 3
photographs, 116, 140, 224
photolysis, 66, 67, 70, 71
physical properties, 58, 171, 187, 236
physical-mechanical properties, 238
physicochemical properties, 2
physics, 94
pigments, 180
plants, 7, 128, 208
plasma, 16
plasmid, 84, 86, 90
plastic deformation, 154
plastics, 98, 170, 235
platelets, 207
platinum, 8, 10, 16, 191
PMMA, 191
Poisson ratio, 154
polarity, 21, 71, 72, 114
polarization, 98
pollutants, 191
pollution, 218
poly(methyl methacrylate), 21
polyacrylamide, 84, 90
polyamide, 19, 169, 170, 172, 173, 174, 175, 176, 177
polyamide fiber, 176
polyamides, 19, 20, 25, 29, 30
polycarbonate, 21
polycondensation, 21, 169, 236
polyesters, 196
polyethyleneterephthalate, 235, 236, 237, 238, 239, 240, 241
polymer, vii, 52, 54, 111, 112, 113, 114, 115, 116, 117, 118, 120, 122, 123, 125, 126, 133, 134, 140, 142, 143, 144, 145, 158, 159, 160, 165, 169, 171, 179, 180, 182, 183, 184, 185, 186, 188, 189, 190, 191, 192, 207, 235, 236, 238, 239, 240, 241
polymer chains, 238
polymer composite material, 241
polymer film, 52, 54, 182
polymer films, 52, 54, 182
polymer materials, vii, 235
polymer matrix, 235, 236, 239
polymer solutions, 112, 140, 142, 144, 145, 159
polymeric blends, 189
polymeric chains, 157, 159, 160, 161
polymeric composites, 222
polymeric materials, 170, 177, 183, 185
polymeric membranes, 191
polymerization, 158, 186, 191
polymerization process, 191
polymers, vii, 19, 20, 21, 23, 25, 26, 28, 29, 30, 34, 101, 116, 124, 141, 146, 169, 170, 179, 180, 181, 182, 183, 185, 187, 189, 191, 192
polypeptide, 90, 132
polypeptides, 130
polypropylene, 170, 232
polystyrene, 119, 145
polyurethane, 142
polyvinyl alcohol, 191
polyvinylpyrrolidone, 19, 20, 50
poor, 100, 129, 149, 152, 153
population, 217, 228
porosity, 104, 112, 190, 192, 231
potential energy, 34, 39, 46
poultry, 4
power, viii, 12, 50, 97, 100, 102, 103, 104, 126, 157, 166, 189
precipitation, 50
prediction, 93, 97, 226
pressure, 21, 42, 67, 103, 105, 106, 112, 127, 157, 165, 206, 216, 222
prices, 209
primary products, 196
probability, 20, 228, 231
probability distribution, 228
probe, 98
processing variables, 145
producers, 208
production, 112, 195, 196, 209
productivity, 120
program, 26, 35, 42, 43, 44, 58, 210, 226
proliferation, 4, 145, 207
propagation, 175, 222, 231
prophylactic, 3
proportionality, 161
propylene, 195, 196
protein, 2, 5, 75, 76, 78, 79, 81, 83, 84, 87, 88, 89, 90, 128, 145, 190
protein folding, 83
proteins, 2, 4, 6, 7, 82, 83, 89, 128, 130, 180
protons, 28, 94
pulse, 66, 150, 154
purification, 84, 85
PVA, 117, 118, 119, 121, 123, 124, 145, 191

PVC, 191
PVP, 20, 21, 22, 23, 24, 25, 28, 50, 52, 53, 54

Q

quantum chemical calculations, 42
quantum chemistry, 32, 46
quantum yields, 65
quantum-chemical calculations, 24, 44, 45
quartz, 21, 50, 144
quaternary ammonium, 196

R

radiation, 1, 2, 4, 13, 14, 76, 91, 92, 96, 98, 100
Radiation, 14, 91, 108
radiation damage, 14
radical formation, 75
radical mechanism, 28, 29
radical reactions, 2, 3, 5, 6, 8, 19, 28, 29
radio, 91, 97
radionuclides, 206, 207
radius, 111, 114, 145, 158, 159, 162
Raman spectra, 139
Raman spectroscopy, 139
random errors, 226
random walk, 160, 167
range, 22, 45, 46, 50, 71, 84, 92, 94, 97, 112, 115,
120, 139, 140, 141, 154, 158, 161, 169, 182, 188,
203, 206, 217
raw materials, 208
reactant, 58
reactants, 72
reaction mechanism, 32
reaction rate, 6, 42, 43, 44, 46, 197
reaction rate constants, 6, 42, 43, 44
reactivity, 20, 28, 171, 217
reading, 86
reagents, 33, 34, 38, 41
real time, 50
receptors, 6, 7, 190
recognition, 86, 90, 221
recombination, 20
recovery, 10, 218
recycling, 206, 217, 218
reduction, 7, 8, 10, 112, 141, 149, 152, 171, 179,
186, 187, 188
refining, 217
reflection, 129
regenerated cellulose, 132
regeneration, 144
regression, 103, 152, 226

regression analysis, 152
regression equation, 152
regulation, 4, 5, 7, 12, 13, 82
reinforcement, 143, 147, 149, 150, 151, 152, 153,
154, 169, 170, 171, 173, 206, 207, 216
reinforcing fibers, 173, 174
relationship, 135, 136, 137, 142, 182, 221, 231
relationships, 7, 11, 12, 175, 182, 229
relaxation, 7, 67, 92
relaxation times, 92
reliability, 224
remediation, 93
reparation, 4
replication, 86
reproduction, 11
reputation, 207
residuals, 227
residues, 131
resistance, 8, 94, 129, 149, 169, 170, 172, 191, 209,
232
resources, 208
response time, 185, 187, 191
retention, 148, 172, 211
returns, 3
reusability, 187
rheology, 126
ribosome, 86
rice, 210, 211, 212, 213, 216
rice husk, 210, 211, 212, 213, 216
risk, 17
RNA, 11, 86
Romania, 108
ROOH, 196
room temperature, 21, 22, 51, 67, 140, 172, 183, 191
rotational mobility, 50
rubber, vii, 92, 147, 148, 149, 150, 151, 152, 153,
154
rubbers, 147
Russia, vii, viii, 1, 19, 31, 49, 57, 65, 83, 84, 86, 157,
195, 235, 238

S

safety, 99, 140, 206, 231
salt, 117
salts, 50, 196
sample, 21, 52, 53, 54, 92, 98, 99, 100, 101, 103,
130, 149, 151, 152, 153, 154, 175, 224
saturated fat, 13
saturated hydrocarbons, 34
saturation, 50, 55, 104, 107, 183
savings, 93, 107
scaling, 142, 157, 165, 166

- scaling law, 142
scanning electronic microscope, 211
school, 2
second virial coefficient, 158
selectivity, 100, 191, 195, 196, 197, 199, 202, 203
SEM micrographs, 122, 135
semiconductor, 61, 62, 180, 181, 182
semiconductors, 62, 180
senile dementia, 17
sensing, 190, 191
sensitivity, 12, 190, 191, 192
sensors, 144, 179, 181, 190, 191, 192, 193
separation, 51, 140, 141
series, 120, 165, 228
serine, 129, 130
SFT, 108
shade, 94
shape, 33, 35, 39, 50, 51, 52, 54, 113, 114, 115, 116, 140, 181, 213
shear, 222, 231, 232
shear strength, 222, 231, 232
shoot, 111
signaling pathway, 82
signals, 67, 70
silica, 21, 208, 210, 211, 212, 213, 216, 218, 219
silicon, 180
silk, 128, 129, 130, 131, 132, 133, 134, 137, 138, 139, 146
silver, 10
simple linear regression, 226, 227
simulation, 44, 50, 55
sintering, 208
SiO₂, 21, 22, 23, 24, 57, 171, 209
skin, 129
smooth muscle, 145
society, 13, 108, 206
sodium, 10, 118, 170
software, 154, 225, 226, 233
soil, 170, 171, 173
sol-gel, 189
solid phase, 22
solid polymers, 21
solid waste, 208
solidification, 132
solubility, 171
solvent, 21, 71, 72, 76, 114, 116, 120, 124, 134, 140, 144, 158, 159, 160, 186, 189
solvents, 7, 67, 116, 119, 124, 125, 130, 141, 145, 158
sorption, 102, 105
Spain, 57, 232
species, 8, 98, 130
specific gravity, 208
specific surface, 112
specificity, 36
spectroscopy, 17, 55, 86, 130
spectrum, 5, 11, 22, 28, 52, 67, 77, 83, 91, 96, 130, 188
speed, 190, 192
spin, 13, 17, 20, 29, 30, 33, 36, 41, 71, 189, 191
spindle, 115, 116, 124
spleen, 76
stability, 36, 58, 154, 169, 181, 208, 216, 239, 240
stabilization, 38, 50, 169, 171, 172, 173, 176, 177
stabilizers, 170, 171, 176
stable radicals, 19, 20, 21, 22, 23
stages, 3, 5, 16, 26, 27, 28, 32, 126, 129, 132, 196, 199, 200, 203
standard deviation, 50, 133
stasis, 76, 81
statistical analysis, 221, 222
statistical inference, 228
statistics, 158, 160, 167
stem cells, 141
stomatitis, 11
storage, 186
strain, 84, 90, 149, 150, 152, 153, 154, 174, 175, 177, 224, 225
strength, 20, 34, 95, 97, 100, 118, 120, 148, 170, 171, 172, 173, 175, 176, 177, 192, 206, 207, 211, 212, 213, 214, 215, 216, 217, 218, 222, 232, 238, 239
stress, 16, 76, 112, 122, 124, 127, 132, 149, 150, 152, 154, 171, 174, 175, 177, 222, 224, 225
stress-strain curves, 224
stretching, 28, 126
styrene, 144, 191, 195, 196
substitutes, 205
substitution, 58, 189
substitution reaction, 58
substrates, 182, 184, 189
sucrose, 77
superoxide, 6
supply, 140, 171, 176
surface area, 112, 113, 124, 190
surface tension, 111, 112, 113, 114, 115, 116, 117, 123, 127
surplus, 169
survival, 10
survival rate, 10
susceptibility, 222
suspensions, 50
sustainable development, 207
Sweden, 84
swelling, 158, 159, 217
switching, 181, 184, 187, 189

Switzerland, 85
 SWNTs, 57
 symptom, 12
 synthesis, 4, 5, 7, 8, 11, 14, 31, 57, 84, 90, 190, 235, 237, 238, 239, 240, 241
 systems, 5, 6, 7, 12, 33, 49, 50, 55, 94, 100, 112, 186, 191, 195, 197, 198, 199, 200, 201, 202, 203

T

targets, 7, 8
 technology, 31, 91, 93, 107, 108, 112, 142, 143, 179, 180, 182, 183, 184, 205, 209
 television, 206
 TEM, 9
 temperature, 22, 49, 50, 51, 52, 54, 55, 58, 84, 91, 92, 93, 96, 98, 100, 101, 103, 132, 151, 154, 166, 171, 172, 173, 189, 208, 216, 222, 240, 241
 tensile strength, 113, 173, 174, 177, 205, 206, 235
 tensile stress, 149, 154
 tension, 113, 116, 124, 175
 test data, 170, 176
 tetrahydrofuran, 119
 textiles, 145
 TFE, 43, 44, 46
 TGA, 239, 240
 theory, 42, 51, 52, 103, 123, 126, 145, 170
 therapeutic agents, 12
 therapeutic approaches, 16
 therapy, 6, 7, 12, 13
 thermal decomposition, 21
 thermal destruction, 240
 thermal expansion, 208
 thermal properties, 92, 236
 thermal stability, 22, 172, 235, 239, 240
 thermodestruction, 240
 thermodynamic parameters, 35
 thermodynamics, 160
 thermoplastics, 140, 189, 232
 thiocarbocyanine, vii, 65, 66, 67, 68
 thin films, 145, 189
 threshold, 224, 236, 238
 time, 3, 4, 5, 6, 7, 8, 10, 26, 87, 92, 93, 97, 101, 102, 103, 107, 130, 170, 172, 189, 191, 196, 197, 203, 208, 235, 236, 241
 tin, 189
 tin oxide, 189
 tissue, 113, 141, 143
 TNF, 76
 tocopherol, 2, 5, 6
 tocopherols, 15
 toluene, 120
 total energy, 36, 38, 41

toxic effect, 2, 3
 toxic products, 1, 2
 toxicity, 1, 2, 8, 10
 Toyota, 47
 trade, 170, 176
 traffic, 171, 177
 transcription, 86
 transducer, 76, 190
 transduction, 191
 transformation, 85, 196, 206
 transformations, 26
 transistor, 181, 182, 183, 184
 transition, 3, 34, 38, 41, 129, 130, 157, 189
 transition metal, 189
 translation, 86
 transmission, 12, 91, 99, 189
 transparency, 183, 185
 transport, 108, 120, 126, 143, 182
 transport processes, 108
 trend, 4
 tumor, 3, 10
 tumor cells, 3
 tumor growth, 3
 tumors, 3, 16

U

Ukraine, 157
 uniform, 92, 97, 98, 118, 125, 126, 134, 189
 urea, 144, 170, 190
 users, 91
 UV, 3, 66, 86, 87

V

vacuum, 66, 91, 189, 222
 valence, 2, 5, 36
 validity, 36
 values, 11, 35, 39, 43, 44, 54, 67, 71, 72, 73, 81, 101, 102, 133, 138, 158, 159, 166, 182, 195, 198, 201, 209, 222, 229, 230
 vapor, 57, 191
 variable, 21, 201, 228, 229, 231
 variables, 35, 39, 100, 116, 117, 120, 137, 170, 217, 228, 229
 variance, 135, 226
 variation, 54, 94, 149, 153, 174, 175, 177, 197
 vascular diseases, 16
 vector, 58, 84
 vehicles, 147, 171
 velocity, 50, 97, 105, 111
 versatility, 6, 180, 190, 192

vibration, 142
viruses, 11
viscosity, 7, 12, 50, 67, 68, 70, 72, 112, 115, 116,
117, 118, 124, 125, 126, 134, 135
vitamins, 3
VSD, 182

W

war, 92
waste disposal, 205, 218
waste water, 190
water absorption, 208, 209
water vapor, 102
wear, 129
web, 111, 113
weight ratio, 24
wetting, 129, 205
White House, vii
wind, 232

windows, 187, 206, 208
wood, 92, 216
wool, 102, 128, 129
World War I, 170
writing, 166

X

xenon, 66
X-ray diffraction, 236
XRD, 236, 237, 238

Y

yarn, 97
yeast, 84, 190
yield, 8, 19, 21, 23, 25, 28, 36, 65, 67, 72, 83, 107,
129, 195, 196